2-3-2016 12:00 AM

Piezoelectric Device for Measuring Shear Wave Velocity of Soils and Evaluation of Low and High Strain Shear Modulus

Saeed Ahmad
The University of Western Ontario

Supervisor
M. Hesham El Naggar
The University of Western Ontario

Graduate Program in Civil and Environmental Engineering
A thesis submitted in partial fulfillment of the requirements for the degree in Doctor of Philosophy

Abstract

The shear wave velocity (V_s) and shear modulus (G) are important parameters that are required when dealing with a variety of geotechnical problems covering a wide range of shear strain in a soil medium. Different laboratory tests can be used to measure V_s and G such as resonant column, bender element and cyclic triaxial tests. However, these tests have several limitations in terms of stiffness of the test specimens and range of shear strain that can be applied to them. The importance of V_s in geotechnical engineering and the shortcomings of existing testing devices for its measurement have motivated this research. Innovative piezoelectric ring actuators (PRA) devices were fabricated and were incorporated in oedometer and triaxial apparatuses to measure V_s for different types of soils.

The PRA device incorporated in a conventional oedometer apparatus facilitated measuring V_s simultaneously with 1D consolidation testing of sand and clays. The performance of the developed PRA setup was evaluated and verified through comparing measured V_s of Ottawa sand with results available in the literature and those obtained from bender element testing. Effects of initial state/void ratio, applied pressure, mean particle size, along with percentage of non-plastic fines on V_s of Ottawa sand were investigated using the PRA setup. Cohesive soils (natural and reconstituted) were tested in oedometer and static triaxial tests. The results from oedometer, static triaxial along with V_s measurements were utilized to produce useful correlations for V_s with some standard soil parameters such as soil compressibility index, C_c, and undrained shear strength, S_u. In addition, the measured small strain stiffness ($E_{dynamic}$), large strain static triaxial stiffness (E_{static}) and oedometric stiffness ($E_{oedometer}$) were used to establish the range of dynamic to static stiffness ratios $E_{dynamic}/E_{oedometer}$, and $E_{dynamic}/E_{static}$.

The PRA device incorporated in the cyclic triaxial apparatus was employed to test six different sensitive and in-sensitive cohesive soils. V_s and G were measured using the cyclic triaxial test and the PRA device at different strain amplitudes. The results were utilized to produce dimensionless correlations for V_s and G for cohesive soils. The measured V_s using the PRA device incorporated in a conventional triaxial apparatus along with the developed correlations can then be utilized to reliably estimate the shear modulus reduction curve of cohesive soils without performing cyclic triaxial tests.

Keywords

Piezoelectric ring actuators, shear wave velocity, low-strain shear modulus, dynamic shear modulus, stiffness, oedometer, cyclic triaxial, static triaxial, cohesive soils, sands, empirical correlations.

Co-Authorship Statement

This thesis is prepared in accordance with the regulation for an integrated article format thesis stipulated by the school of graduate and post graduate studies at Western University. All the laboratory testing, interpretation of results and writing of the draft and the final thesis were carried out by the candidate himself, under the supervision of Dr. M. Hesham El Naggar. The supervisor's contribution consisted of providing advice throughout the research program, and reviewing the draft and the final thesis and results from this research. The results of all the laboratory tests presented will be used in journals and conferences publications, which will be coauthored with Dr. Hesham El Naggar.

The results of the tests presented in Chapter three will be submitted as journal paper. The paper will be co-authored with Dr. Hesham El Naggar and Dr. Deyab Gamal El-Dean. The candidate did all the laboratory work, interpretation of results and writing of the draft. The co-authors provided advice on this work, reviewed the draft and the results.

The results of the tests presented in Chapter four and five will be submitted as a journal papers. These papers will be co-authored by Dr. Hesham El Naggar, Dr. Aly Ahmed and Dr. Deyab Gamal El-Dean. The candidate did all the laboratory work, interpretation of results and writing of the draft. The co-authors provided advice on this work, reviewed the draft and the results.

Some of the results presented in Chapter 4 regarding the Kaolinite-Silt soil are published as a conference paper. The candidate is the first author of this work and is co-authored by Dr. Ahmed Alnuaim and Dr. Hesham El Naggar. The candidate did all the laboratory work, interpretation of results and most of the writing of the paper. The co-author Dr. Ahmed Alnuaim prepared and provided the tested sample and did the writing part in the said conference paper regarding the sample preparation. The co-author Dr. Hesham El Naggar provided advice on this work, reviewed the draft and the results.

Dedication

Dedicated to my beloved parents. My father **JAMIL AHMAD** (late) & my mother **RUKHSANA ANJUM** for their endless love, endless support and endless encouragement. They favored me over themselves and have given me all what they could. “My Lord! Bestow on them Your Mercy as they did bring me up when I was small”. They are people behind all my achievements and success in life. I owe them every single thing I achieved in life. I really love them and I am so short of words to express my sincere and deepest gratitude to them.

Dedicated to my beautiful wife **SAMAN MUNIR**. She brought me all the happiness and joy ever since she came to my life. I really love her and thank her for all the support and encouragement she gave me. I am very grateful to here for her patience she has shown since we are away from each other for almost two years due to my PhD Studies.

To my sister **Farah Ahmad**, my brothers; **YASIR AHMAD**, **JAWAD AHMAD** and **WAJAHAT AHMAD** and their wives. To my beautiful nephews **MUHAMMAD HASEEB AHMAD** and **MUHAMMAD QASIM AHMAD**.

Also to all my in-laws especially to my father-in-law **MUNIR AHMED** and my mother-in-law **AZRA MUNIR**.

Acknowledgments

“My Lord, enable me to be grateful for Your favor which You have bestowed upon me and upon my parents and to do righteousness of which You approve. And admit me by Your mercy into [the ranks of] Your righteous servants.”

First and foremost, praise and thanks go to my Creator and Provider (Allah) the most beneficent, the most merciful for his uncounted blessings on me. "Glory be to You, we have no knowledge except what You have taught us. Verily, it is You, the All-Knower, the All-Wise.".

There are so many people that I would like to thank for helping me throughout this long journey and making this work possible. First of all, I would like to thank **Prof. Hesham El Naggar** from the core of my heart for his guidance and excellent supervision. I am very grateful to him for his faith in my work and my efforts. My deepest gratitude to him for his moral and financial support throughout this long journey. Dr. El Naggar has been a role model, a fatherly figure, a great influence, a wonderful teacher, an inspiration and above all an excellent human.

Additional heaps of thanks go out to **Dr. Aly Ahmed** for his guidance, encouragement and support. I really admire his care and his kindness. I am very thankful to him for his compassion and treating me like a younger brother.

I am also very grateful to Dr. Deyab Gamal El-Dean for his advice and guidance.

I would like to express my sincere thanks to all my teachers and faculty especially Prof. Tim Newson and the staff of Civil and Environmental Engineering Department here at Western University, and also to all my teachers, friends and colleagues back in Pakistan.

I would also like to extend great thanks to fellow graduate students, and all my friends specially Erol Tas and Saleem Shaikh for their sincere friendship and encouragement throughout this long journey.

I would like to thank Clayton Cook and Gary Snyders from University Machine Services, Eugen Porter from the Electronic Shop for their help.

I am also thankful to Syed F. Hosain, Technical Account Manager at Testforce Systems for his help during the purchasing process of the electronic equipment for this research.

I am also thankful to all the lab technicians at Western University and the entire Geotechnical Research Center (GRC), especially Cynthia Quintus.

I am thankful to University of Engineering and Technology, Peshawar, Pakistan for their initial financial support during the first few terms of my PhD studies.

Finally, I am thankful to everyone else I've met in Western University that provided their assistance and support to me over the time I was here.

Table of Contents

List of Tables

List of Figures

Chapter 1

1 Introduction

1.1 General

The intensity of seismic shaking depends heavily on the response of soils to applied cyclic loading, which is primarily controlled by their mechanical properties. The seismic provisions of the National Building Code of Canada (NBCC, 2010) have been revised to update the seismic hazard at different locations in Canada. One of the basic inputs to predict the ground motion parameters is the classification of soils and rocks in terms of their shear wave velocity similar to soil classes defined by the National Earthquake Hazard Reduction Program (NEHRP), USA. These soil classes are chiefly based on the measured weighted average of shear wave velocity of a site from the surface to a depth of 30m (V_{s30}) (Hunter and Motezedian, 2006). This V_{s30} can utilized for developing regional/site-specific ground-shaking hazard maps. The shear wave velocity is also a main input of many quantitative earthquake engineering design and analysis methods. Furthermore, it is an essential soil property for characterizing site-response for evaluation of seismic hazard associated with important projects.

1.2 Importance of Dynamic Soil Properties in Geotechnical Engineering

There are numerous types of geotechnical engineering problems related to dynamic loading, e.g. wave propagation in elastic media, machine vibrations, seismic response and liquefaction etc. For many geotechnical engineering problems related to the wave propagation effects, the soil experiences low levels of strains while those involving the stability of masses of soil, large strains are induced in the soil. The response of soils under dynamic loading is controlled by the ***dynamic soil properties***. The properties themselves are not dynamic and are applicable to a host of non-dynamic problems. The soil properties that influence the wave propagation and other low-strain dynamic loading include the stiffness (shear wave velocity, V_s, or shear modulus, G_{max}), damping ratio (ξ), Poisson's ratio (ν) and density (ρ). Stiffness and damping are the more important while

the importance of Poisson's ratio and density is not the same as stiffness and damping (Kramer, 1996).

Dynamic soil properties, especially the stiffness (V_s or G_{max}) and damping, are extremely important parameters that are required when dealing with a variety of soil related problems. They are utilized in applications involving the analysis of foundation vibrations due to blasting, machine vibrations and dynamic structural analysis of the superstructures as well as dynamic soil-structure interactions problems involving traffic vibrations (Luna and Jadi, 2000). They also play a key role in determining the response of foundations and structures to earthquake, wind and wave loads (Humar 2005). The soil stiffness parameters (V_s or G_{max}) are needed for the seismic zonation, evaluation of liquefaction potential, performing site response analysis and predicting the ground motion. They can also be used in the assessment of soil settlement analyses and to determine the soil history i.e. the preconsolidation pressure and OCR (Yoon et al. 2011, Lee et al. 2008).

The primary consolidation time can be assessed with the evolution of shear wave velocity and the slope of the resistance-log time curve (Lee et al. 2008). Robertson et al. (1995) proposed the values of normalized shear-wave velocity to evaluate the in-situ state of cohesionless soils. This helped in identifying the boundary between contracting (loose) or dilatant (dense) sands. Shear wave velocity is a key soil property defining the state parameters of sandy soils. An indirect relationship between friction angle, void ratio, and shear wave velocity for sandy soils has been developed by Cha and Cho (2007), thus presenting an alternate method of estimating the shear strength of sandy soils through the shear wave velocity measurements. Fioravante et al. (1998) has used Shear wave velocity to estimate the coefficient of the earth pressure at rest (K_o). Both vertical and lateral variations in shear wave velocity are often used in 1D and 2D analyses of soil deposits and stress deformation analyses that provide key input for seismic design (Hunter and Crow, 2012). Shear wave velocity was also used as a tool to evaluate stress-induced anisotropy and inherent soil anisotropy (Lee et al. 2008); Pennington et al. (1997); Yamashita and Suzuki (2001); Kuwano and Jardine (2002); Zeng and Grolewski (2005); Ismail and Rammah (2006).

Comparing the measured field and lab V_s values can indicate the level of the sample disturbance for undisturbed cohesive soil specimens. It can also be used to indicate the level of disturbances in a variety of lab specimens themselves. Shear wave velocity has been used to assess the sample

disturbance of granular/cohesionless soil. It is a sensitive measurement to detect changes in void ratio and soil structure due to freezing and thawing. Shear wave velocity measurements can be used to detect sample disturbance due to freezing and thawing of cohesionless soils (Sasithar et al., 1994). It was also used to evaluate the influence of fines on the assessment of liquefaction (Liu and Mitchell, 2006).

The most important factors that affect the dynamic behavior of soils can be divided into two main groups: First, external parameters such as path, magnitude, rate, and duration of stress/strain; second, the characteristics of the material itself, such as soil type, size and shape of soil particles, and void ratio (Moayerian, 2012). The shear-wave velocity of sand is also controlled primarily by the effective confining stresses and void ratio.

The soil stiffness (V_s or G_{max}) has been correlated well with other soil parameters including:

- Applied effective stress
- Void ratio
- fabric
- Undrained shear strength
- Degree of compaction/consolidation
- Mass density/Unit weight
- Relative density (sands)
- Compression index

1.3 Laboratory Techniques used for Measurements of Dynamic Soil Properties

Different laboratory tests can be used to measure the dynamic soil properties. The laboratory tests employed to measure G_{max} include: resonant column (RC) test (Khan et al., 2008), ultrasonic pulse test (Khan et al., 2011) and the piezoelectric bender element (BE) test (Dyvik and Madshus, 1985).

The RC and BE are the common and popular tests used to measure, V_s, while there are some concerns associated with them. The RC test is relatively expensive and involves dedicated and typically expensive device that requires time consuming specimen preparation and may require

extensive calibration depending upon the type of device. On the other hand, BE test has its own shortcomings. Gamal El-Dean (2007) showed that BE tests can lead to highly unreliable and erroneous results. Ismail and Rammah (2005) listed the limitations of using bender elements in measuring V_s. These include: bender elements penetrate through soil samples causing disturbance for undisturbed and cemented soils; they require filling the holes made in soil with coupling material like epoxy or gypsum; they may experience short circuiting and loss of signal due to failure of epoxy coating on the elements; they induce high stresses in the conical zone adjacent to conventional platens of the triaxial apparatus; they can't be used in harsh environments (e.g. electrokinetic treatment); and depolarization at high voltages due to their small thickness.

Measuring the soil shear wave velocity at high strains can provide a reliable means for evaluating the variation of soil shear modulus with the strain level. However, the available testing techniques do not readily allow that. Instead, the soil stiffness at high strains is evaluated by subjecting the soil to cycles of shear strain and evaluating the secant shear modulus from the resulting hysteretic loops. This process comes with its many challenges as well. Hence, there is a need for developing a device that will allow accurate and reliable direct measurement of the shear wave velocity at high levels of shear strain.

1.4 Research Objectives and Scope of Work

The present research attempts to review the issues and shortcomings of the current laboratory testing techniques that are used to measure the shear wave velocity of soils. In addition, it reviews the correlations between the shear wave velocity and basic soil properties. The outcome of these reviews has motivated adopting a new laboratory technique that was pioneered at University of Sherbrooke [Université de Sherbrooke] for measurement of soil shear wave velocity (e.g. Gamal El Dean, 2007). This technique involved developing piezoelectric ring actuators (PRA) device incorporated in an oedometer for measuring the soil shear wave velocity. In the current study, two PRA devices were developed at The University of Western Ontario with significant modifications to the original design proposed by Gamal El Dean (2007); one was incorporated in an oedometer and another was incorporated in a triaxial cell.

This study has several objectives as described in the following. The first objective is to optimize the design of the PRA device to ensure the most effective, reliable and economical configuration. This included selection of the material type, shape and size (diameter and height) of the used piezoceramic elements as well as the associated electronic components (i.e. function generator to produce exciting signal, power amplifier, high performance PCI based data acquisition system, cables and connectors, etc.). It also involved developing a computer program in order to view, capture, save, and process the input and output signals from the developed device. Finally, the design of the fabricated devices was refined to facilitate incorporating them in an oedometer and triaxial devices.

The second objective is to rigorously evaluate the performance of the fabricated PRA setups by testing a variety of soils including cohesionless (sand) and cohesive (clay) soil samples. The measured shear wave velocity using the fabricated PRA devices are compared with the published literature for well documented soils in order to verify the performance of the developed devices. In addition, the measured V_s values are compared with those measured using the conventional bender elements.

The third objective is to measure V_s for a variety of soils (sand and clays), and establish and verify useful empirical correlations between V_s and other basic soil parameters such as void ratio, effective stress, compression index and undrained shear strength.

Finally, the PRA device incorporated in triaxial cell is used to accurately evaluate the effect of shear strain (γ) level on soil stiffness. The results obtained from the fabricated PRA setup are then used to correlate values of V_s for cohesive soils measured at different shear strain levels with shear modulus reduction curves in order to enable the development of shear modulus reduction curves using V_s measurements during conventional triaxial tests (i.e. without conducting cyclic loading). This involves measuring the dynamic properties of natural and re-constituted cohesive soils subjected to different levels of shear strain. The secant shear modulus, G, values are determined from the hysteresis loops during cyclic shearing, while the shear wave velocity is measured at the same shear strain amplitude using the PRA device. The results are then utilized to correlate the measured shear wave velocity at very low strains Vs_{max} as well as at high strains, Vs, to the secant soil shear modulus, G, at different strain levels as well as very low strain shear modulus G_{max}.

1.5 Thesis Outline

This thesis is divided into six chapters. This section provides a brief the contents of each chapter.

Chapter 1 presents and highlights the importance of the shear wave velocity in the field of geotechnical engineering. It presents the many applications of shear wave velocity emphasizing its utility in numerous aspects of geotechnical engineering. It also discusses briefly the limitations of the conventional resonant column and bender element tests. It also presents the objectives and scope of work of the present study. Finally it presents the original contributions from the current study.

Chapter 2 reviews the existing field and laboratory techniques that are used for measuring the shear wave velocity of soils. A special emphasis is placed on the pulse techniques and the most important interpretation methods used in pulse tests to determine shear wave velocity from the tests results. In addition, Chapter 2 reviews the existing literature on empirical correlations (using data from lab and field testing) for estimating shear wave velocity from other soil properties.

Chapter 3 presents the details of the fabrication of the setup for the oedometer test and the modifications of the fabricated PRA to overcome some of the practical challenges faced as well as the interpretation techniques used to analyze the signals travel time. It also discusses the simultaneous oedometer testing and V_s measurements of Ottawa sand. The effects of applied pressure, particle size and fines on the shear wave velocity of the tested Ottawa sand are then evaluated, and comparisons are made with the published literature as well as those obtained using conventional bender elements. Finally, Chapter 3 presents some useful empirical correlations to estimate the low strain stiffness of Ottawa sand.

Chapter 4 presents the results of the comprehensive V_s measurements and oedometer testing of various natural and reconstituted cohesive soils. It investigates the variations of soil V_s and G_{max} with the effective vertical and mean stresses. The results are then compared with the relevant published literature to verify the performance of the PRA device incorporated in the triaxial cell. It also presents some useful empirical correlations for V_s of cohesive soils with basic soil properties. In addition, the undrained shear strength of the tested soils was obtained from static triaxial tests (isotropically consolidated undrained). Finally, Chapter 4 presents some correlations between the

soil shear wave velocity and its static stiffness obtained from the oedometer testing and static triaxial testing.

Chapter 5 describes the fabrication of the PRA device incorporated in the cyclic triaxial apparatus and provides the shear wave velocity measurements for various cohesive soils using the fabricated device. The results from the PRA setup are compared with those obtained from the PRA incorporated in the oedometer to verify the performance of both devices. In addition, the shear wave velocity is measured at different levels of shear strain and is correlated to the shear modulus, G, for the tested sensitive and non-sensitive (natural undisturbed and reconstituted) soils. These correlations can be used to estimate the shear stiffness and hence modulus reduction curves at different high strain amplitudes using the measured V_s at these strain amplitudes, hence eliminating the need for cyclic triaxial tests.

Chapter 6 summarizes the main outputs and conclusions of the present studies. It also presents the recommendations and suggested Improvements for future development of PRA device. Finally, considering the potential of the PRA setup, some future researches are recommended.

1.6 Thesis Original Contributions

In this study, innovative piezoelectric ring actuators devices were manufactured and incorporated in oedometer and triaxial devices to facilitate the measurement of soil shear wave velocity at different levels of confining pressure and shear strain amplitudes. To the author's knowledge, it is the first time the PRA device is incorporated in in triaxial device and utilized to measure soil shear wave velocity at different shear strain amplitudes. The following contributions are claimed as original contributions of this thesis.

1. The correlations of G_{max} of the tested cohesive soils with the static stiffness values obtained from oedometer tests as well as isotropically consolidated undrained (CIU) triaxial tests are original. The stiffness ratio ($G_{dynamic}/G_{static}$) was evaluated for the tested soil specimens. In addition, the stiffness ratios E_{dyn}/E_{oed}, $E_{dynamic}/E_{static}$, E_{stat}/E_{oed} were evaluated for the tested soils. These correlations allow prediction of dynamic shear modulus from the more readily available oedometer and conventional triaxial test results.

2. The correlations of G_{max} with the undrained shear strength (S_u) of the tested soil are original. These correlations can be used to estimate the soil stiffness knowing its undrained shear strength.
3. The variation of dynamic stiffness of the artificial clay manufactured by mixing kaolin (K) and silt (S) was evaluated for the first time. This artificial clay, referred to as K-S soil, is widely used in laboratory and centrifuge studies.
4. The fabricated PRA device incorporated in the triaxial cell facilitated, for the first time, accurate measurement of *Vs*, and hence G, at high levels of strain, which can eliminate the challenges associated with evaluating the secant shear modulus from hysteretic loops.
5. Based on measured V_s and G values at different levels of strain, dimensionless empirical correlations are proposed to correlate shear wave velocity at different shear strain level, V_s, normalized by Vs_{max} at very low strain to the shear modulus reduction curve, G/G_{max}. The measured V_s at different strain levels, along with the proposed correlations, can then be used to evaluate the shear modulus reduction curve of the soil without the need to perform cyclic triaxial testing. This approach has the potential to provide reasonable estimate of the shear modulus reduction curve using the conventional triaxial cell when the more expensive cyclic triaxial cell is not available.
6. Empirical correlations are provided to evaluate V_s or G_{max} using a simple mechanical property of soil (i.e. compression index, C_c).

References

Cha, M. and Cho, G., (2007). "Shear strength estimation of sandy soils using shear wave velocity." *Geotechnical Testing Journal*, 30(6), 484-495.

E.S. Bang, J.H. Kim (2009). "Evaluation of shear wave velocity distribution map using SPT-uphole tomography method." *In Proceedings of the 17th International Conference on Soil Mechanics and Geotechnical Engineering, Alexandria, Egypt*. 953–956.

Fioravante, V., Jamiolkowski, M., Presti, D.L., Manfredini, G. and Pedroni, S., (1998). "Assessment of the coefficient of the earth pressure at rest from shear wave velocity measurements." *Geotechnique*, 48(5), 657-666.

Gamal El-Dean, D., (2007). Development of a new piezo-electric pulse testing device and soil characterization using shear waves (Doctoral dissertation, These de doctorat en genie civil, Université de Sherbrooke).

Humar, L. 2005. Dynamics of Structures (2nd Edition). New York: Taylor & Francis.

Hunter, J.A. and Motezedian, D., (2006). "Shear wave velocity measurements for soft soil earthquake response evaluation in the eastern Ottawa region, Ontario, Canada". *In 19th EEGS Symposium on the Application of Geophysics to Engineering and Environmental Problems.*

Hunter, J.A., Crow, H.L., Arsenault, J.L., Atukorala, U., Best, M.E., Campos, D., Candy, C., Chouinard, L., Claprood, M., Dutrisac, H. and Fleming, J., (2012). "Shear wave velocity measurement guidelines for Canadian seismic site characterization in soil and rock." *Geological Survey of Canada*, Open File, 7078, p.227.

Ismail, M. A. & Rammah, K. I. (2006). "A New Setup for Measuring Go during Laboratory Compaction." *ASTM Geotechnical Testing Journal*, 29(4), 1-9.

Kang, X., Bate, B. and Ge, L., (2014). "Characterization of Shear Wave Velocity and Its Anisotropy in Uniform Granular Materials." *In Geo-Congress 2014 Technical Papers@ Geo-characterization and Modeling for Sustainability*, 2029-2041. ASCE.

Khan, Z. H.; Cascante, G.; El Naggar, M. H. and Lai, C. G., (2008). "Measurement of Frequency-Dependent Dynamic Properties of Soils Using the Resonant-Column Device" *Journal of Geotechnical and Geoenvironmental Engineering, ASCE,* 134(9), 1319-1326.

Khan, Z., Cascante, G., and El-Naggar, H. (2011). "Dynamic properties of cemented sands using the ultrasonic waves." *Canadian Geotechnical Journal*, 48(1): 1–15

Kuwano, R. and Jardine, R.J., (2002). "On the applicability of cross-anisotropic elasticity to granular materials at very small strains." *Géotechnique*, 52 (10), 727-749.

Lee, C., Lee, J.S., Lee, W. and Cho, T.H., (2008). "Experiment setup for shear wave and electrical resistance measurements in an oedometer." *Geotechnical Testing Journal*, 31(2), 149-156.

Liu, N. and Mitchell, J.K., (2006). "Influence of nonplastic fines on shear wave velocity-based assessment of liquefaction." *Journal of Geotechnical and Geoenvironmental Engineering*, 132(8), 1091-1097.

Luna, R. and Jadi, H., (2000), "Determination of dynamic soil properties using geophysical methods." In Proceedings of the first international conference on the application of geophysical and ndt methodologies to transportation facilities and infrastructure, St. Louis, MO, 1-15.

Moayerian, S., (2012). "Effect of Loading Frequency on Dynamic Properties of Soils Using Resonant Column." Master Thesis. University of Waterloo.

Pennington, D.S., Nash, D.F.T. and Lings, M.L., (1997). "Anisotropy of G0 shear stiffness in Gault Clay." Géotechnique, 47(3), 391-398.

Robertson, P.K., Sasitharan, S., Cunning, J.C. and Sego, D.C., (1995). "Shear-wave velocity to evaluate in-situ state of Ottawa sand." *Journal of Geotechnical Engineering*, 121(3), 262-273.

Roesler, S.K. (1979). "Anisotropic shear modulus due to stress anisotropy." *ASCE, Journal of the Geotechnical Engineering Division,* 105(7), 871–880.

Sasitharan, S., Robertson, P.K. and Sego, D.C., (1994). "Sample disturbance from shear wave velocity measurements." *Canadian Geotechnical Journal*, 31(1), 119-124.

Yamashita, S. and Suzuki, T. (2001). "Small strain stiffness on anisotropic consolidated state of sands by bender elements and cyclic loading tests." Proc. of 15th International Conference on Soil Mechanics and Geotechnical Engineering, Istanbul, Vol 1, 325-328.

Yoon, H.K., Lee, C., Kim, H.K. and Lee, J.S., (2011). "Evaluation of preconsolidation stress by shear wave velocity". *Smart Structures and Systems*, 7(4), 275-287.

Zeng, X. and Grolewski, B., (2005). "Measurement of G_{max} and estimation of K_o of saturated clay using bender elements in an oedometer." Geotechnical Testing Journal, 28(3), 264-274.

Chapter 2

2 Literature Review

2.1 Introduction

This chapter reviews the conventional methods for the determination of shear wave velocity in laboratory and in-situ as well as their limitations. In addition, the concept of piezoelectricity and the physical and mechanical properties of piezoelectric materials are also presented. The different interpretation techniques used for the signal analysis to determine the shear wave velocity arrival time are presented and discussed. The shortcomings of conventional soil laboratory tests utilized for V_s or G_{max} measurements are discussed, along with the possible remedies to overcome these shortcomings using the fabricated device, which will also clarify the objectives of this research. Empirical correlations for the prediction of V_s and G_{max} with basic soil properties are also discussed. In addition, some correlations relating V_s and G_{max} with field tests such Standard Penetration Test (SPT) and Cone Penetration Test (CPT) indices are also presented.

2.2 Piezoelectricity and Piezoelectric Materials

All pulse based laboratory testing techniques such as bender elements, bender-extender and shear-plate transducers that are employed to measure shear and compression wave velocities, utilize piezoelectric materials in some form or shape. Hence, understanding the concept of piezoelectricity and piezoelectric materials is essential.

Piezoelectricity is the electricity/electric charge produced by mechanical pressure on certain crystals (notably quartz or Rochelle salt); alternatively, electrostatic stress produces a change in the linear dimensions of the crystal. When certain crystalline minerals are subjected to a mechanical force, the crystals become electrically polarized. Applied tension and compression generate voltages of opposite polarity, and in proportion to the applied force. Such behavior is known as the piezoelectric effect. Mechanical compression or tension on a poled piezoelectric ceramic element changes the dipole moment, creating a voltage output. In addition, if these voltage generating crystals are exposed to an electric field, they elongate or shorten (in proportion to the

strength of the field) depending upon the polarity of the applied electric field. Such behavior is known as the inverse piezoelectric effect.

Compression parallel to the polarization direction (or tension perpendicular to it) generates voltage of the same polarity as the polarization/poling voltage, while compression perpendicular to the polarization direction (or tension parallel to it) generates a voltage with polarity opposite to that of the poling voltage. These actions are generator actions (i.e. conversion of mechanical energy of compression or tension into electrical energy) by the ceramic elements. Applied stress and the generated voltage (or field strength) by the piezoelectric ceramic element are linearly proportional up to a material-specific stress. The same holds for the applied voltage and generated strain.

On the other hand, when the polarity of the applied voltage is similar as the applied poling voltage of a ceramic element, the element will elongate and its diameter will reduce. If the applied voltage polarity is opposite to that of the polarization voltage, the element will shorten and broaden. In case of the applied voltage being alternating, the element will elongate and shorten in cyclic manner, at the frequency of the applied voltage. This is motor action, i.e. electrical energy is converted into mechanical energy. The motor and generator actions (or the piezoelectric effect and the inverse piezoelectric effect) of the piezoelectric ceramic elements are the key properties in the development of the bender elements as well as the piezoelectric ring actuators that are used for measuring the shear wave velocity of soils in the present study.

The output voltages, movements, and forces from piezoelectric are quite small in magnitude. For example, a typical disc of piezoelectric ceramic will increase or decrease in thickness by only a small fraction of a millimeter. Piezoelectric materials have been adapted in an impressive range of applications. They are used in sensing applications, such as in force or displacement sensors. For example, they are used in the car's airbag sensors. The inverse piezoelectric effect is used in actuation applications, such as in motors and devices that precisely control positioning, and in generating sonic and ultrasonic signals.

Metal oxide-based and synthetic piezoelectric ceramics are usually physically strong and chemically inactive, and are comparatively low-cost to fabricate. The structure/composition, shape, and dimensions of a piezo ceramic element can easily be tailored depending upon the requirements

of a specific application. Ceramics fabricated from formulations of lead zirconate / lead titanate (PZT) have revealed a greater sensitivity and can be operated at higher temperatures, as compared to ceramics of other compositions, and thus they are the most widely used piezoelectric ceramics nowadays.

2.2.1 Selected Piezoelectric Transducer and its Properties

PZT or "lead zirconate titanate" is a metallic oxide based piezoelectric ceramic transducer having wall-electrodes and polarized in the radial direction. The piezo ceramic rings used in this study are made of "lead zirconate titanate – APC 850 manufactured by APC International Ltd., USA. The rings are coated with a very thin film of silver from inside and outside to serve as electrodes. They operate on the transversal piezo effect. When an electric voltage is applied between the outer and inner diameter of a thin-walled tube, it contracts/expands axially and radially. The physical and mechanical properties of APC 850 are summarized in Table.2-1.

In general, APC 850 is a soft ceramic preferred to use for low-power resonance or non-resonance devices. This material is used for low power devices giving high coupling and high charge sensitivity. APC 850 ceramic has high dielectric constant, high coupling, and high charge sensitivity, high density with a fine grain structure, a high Curie point, and a clean, noise-free frequency response. It produces a clean, noise-free frequency response as reported by the manufacturer.

The behavior of ceramics is characterized by some specific parameters. The piezoelectric constants **d** and **g** (d = piezoelectric charge constant and g = piezoelectric voltage constant) define the ceramics quality for transmitter and receiver functions, respectively. The coupling coefficient **k** shows the piezoceramic transducer's efficiency in converting the applied electrical energy into a mechanical movement and vice versa.

Table 2-1: Physical & mechanical properties of the piezoelectric material (APC 850) APC international: (https://www.americanpiezo.com/)

APC Material 850 Navy Type Equivalent: Navy II		
Piezoelectric Coefficients	***Symbol***	***Value***
Relative Dielectric Constant	K^T	1900
Dielectric Dissipation Factor (Dielectric Loss (%)*	tan δ	≤ 2.00
Curie Point (°C)**	T_c	360
Electromechanical Coupling Factor	K_P	0.63
	k_{33}	0.72
	k_{31}	0.36
	k_{15}	0.68
Piezoelectric Charge Constant (10^{-12} C/N or 10^{-12} m/V)	d_{33}	400
	$-d_{31}$	175
	d_{15}	590
Piezoelectric Voltage Constant (10^{-3} Vm/N or 10^{-3} m^2/C)	g_{33}	24.8
	$-g_{31}$	12.4
	g_{15}	36.0
Young's Modulus (10^{10} N/m^2)	Y^E_{11}	6.3
	Y^E_{33}	5.4
Frequency Constants (Hz*m or m/s)	N_L (longitudinal)	1500
	N_T (thickness)	2040
	N_P (planar)	1980
Density (g/cm^3)	ρ	7.6
Mechanical Quality Factor	Q_m	80
Electrode thickness (μm)	t_e	6-12

* At 1 kHz, low field
** Maximum operating temperature = Curie point/2
*** Maximum voltage: 5-7 VAC /mil for APC 850

In Table. 2-1, the mechanical quality factor (**Q_m**) indicates the mechanical losses of energy. Higher the values of **d**, **g**, and **k**, the better the material is. The factor **Q_m** should be as low as possible for a rapid decay of transducer vibrations after the initial excitation.

Electromechanical coupling factor, **k**, is an indicator of the effectiveness with which a piezoelectric material converts electrical energy into mechanical energy or mechanical energy into electrical energy. The different values of **k** used for the identifications of the piezoelectric material are presented as follows:

$\mathbf{k_{33}}$ = Coupling factor/coefficient for electric field in direction 3 (parallel to direction in which ceramic element is polarized) and longitudinal vibrations in direction 3.

$\mathbf{k_{31}}$ = Coupling factor/coefficient for electric field in direction 3 and longitudinal vibrations in direction 1.

$\mathbf{k_{15}}$ = Coupling factor/coefficient for the thickness shear oscillation of a plate.

$\mathbf{k_P}$ = Coupling factor/coefficient for radial oscillation (planar) of a round disk.

The Curie point $\mathbf{T_c}$ is related to maximum operating temperature for the piezoelectric material. The maximum operating temperature is half of the Curie point i.e. Curie point/2. If a piezoelectric ceramic material is heated to its Curie point $\mathbf{T_c}$, the domains will become disordered and the material will be depolarized.

The permittivity **ε** or the relative dielectric coefficient $\mathbf{K^T}$ is the ratio of the absolute permittivity of the ceramic material and the permittivity in vacuum (ε_o = 8.85 × 10-12 F/m), where the absolute permittivity is a measure of the polarizability in the electrical field. The dependency of the dielectric coefficient from the orientation of the electric field and the dielectric displacement is symbolized by the corresponding indices.

The dielectric loss **tan δ** is the ratio of the effective series resistance to the effective reactance. It is the tangent of the loss angle.

Piezoelectric charge coefficient, also known as piezoelectric deformation coefficient or piezo modulus, d_{ij} is the ratio of induced electric charge to applied mechanical stress or of achievable mechanical stress to the applied electric field applied. For piezo actuators, the piezo modulus is also referred to as deformation coefficient. ***OR*** the piezoelectric charge constant, d, is the

polarization generated per unit of mechanical stress (T) applied to a piezoelectric material or, alternatively, is the mechanical strain (S) experienced by a piezoelectric material per unit of electric field applied. The first subscript “i" to d_{ij} indicates the direction of polarization generated in the material when the electric field, E, is zero or, alternatively, is the direction of the applied field strength. The second subscript “j” is the direction of the applied stress or the induced strain, respectively. Because the strain induced in a piezoelectric material by an applied electric field is the product of the value for the electric field and the value d, d is an important indicator of a material's suitability for strain-dependent (actuator) applications. (APC international)

d_{33} = strain produced per unit of applied electrical field in V/m or charge density in C/m^2 per unit of pressure in N/m^2, each in the polarization direction

d_{31} = induced polarization in direction 3 (parallel to polarization direction) per unit stress applied in direction 1 (perpendicular to direction in which ceramic element is polarized) or induced strain in direction 1 per unit electric field applied in direction 3

d_{15} = induced polarization in direction 1 (perpendicular to direction in which ceramic element is polarized) per unit shear stress applied about direction 2 (direction 2 perpendicular to direction in which ceramic element is polarized) or the induced shear strain about direction 2 per unit electric field applied in direction 1

The piezoelectric voltage coefficient **g** is the ratio of the electric field strength **E** to the effective mechanical stress **T**. Dividing the respective piezoelectric charge coefficient dij by the corresponding permittivity gives the corresponding **g_{ij}** coefficient. ***OR*** The piezoelectric voltage constant, g, is the electric field generated by a piezoelectric material per unit of mechanical stress applied or, alternatively, is the mechanical strain experienced by a piezoelectric material per unit of electric displacement applied. The first subscript to g i.e. “i" indicates the direction of the electric field generated in the material, or the direction of the applied electric displacement. The second subscript “j” is the direction of the applied stress or the induced strain, respectively. Because the strength of the induced electric field produced by a piezoelectric material in response to an applied physical stress is the product of the value for the applied stress and the value for g, g is important for assessing a material's suitability for sensing (sensor) applications. (APC international).

g_{33} = induced electric field in direction 3 (parallel to direction in which ceramic element is polarized) per unit stress applied in direction 3 or induced strain in direction 3 per unit electric displacement applied in direction 3.

g_{31} = induced electric field in direction 3 (parallel to direction in which ceramic element is polarized) per unit stress applied in direction 1 (perpendicular to direction in which ceramic element is polarized) or induced strain in direction 1 per unit electric displacement applied in direction 3.

g_{15} = induced electric field in direction 1 (perpendicular to direction in which ceramic element is polarized) per unit shear stress applied about direction 2 (direction 2 perpendicular to direction in which ceramic element is polarized) or induced shear strain about direction 2 per unit electric displacement applied in direction 1.

The mechanical quality factor **Q_m** characterizes the "sharpness of resonance" of a piezoelectric body.

The frequency constants/coefficient **N** describes the relationship between the geometrical dimension A of a body and the corresponding (series) resonant frequency. The indices designate the corresponding direction of oscillation, A = dimension, $N = f_s \times A$). When an unrestrained piezoelectric ceramic element is exposed to a high frequency alternating electric field, an impedance minimum, the planar or radial resonance frequency, coincides with the series resonance frequency, f_s. The relationship between the radial mode resonance frequency constant, N_P, and the diameter of the ceramic element, D_Φ, is expressed by: $N_P = f_s D_\Phi$. At higher resonance, another impedance minimum, the axial resonance frequency, is encountered. The thickness mode frequency constant, N_T, is related to the thickness of the ceramic element, h, by: $N_T = f_s h$. A third frequency constant, the longitudinal mode frequency constant, is related to the length of the element: $N_L = f_s l$

2.2.2 Applied Shear/Radial Strains from the Piezoceramic Rings

Radial displacement is a result of the superposition of decrease/increase in wall thickness and the tangential extension/contraction. Hence, the radial strain of an unrestrained piezo ceramic ring under the applied voltage *V* can be calculated as follows (Gamal El-Dean, 2007)

$$\gamma_{Radial} = \frac{\Delta r}{r} \tag{2.1}$$

$$\gamma_{Radial} = \frac{d_{31} V}{t} \tag{2.2}$$

where, *t* is the wall thickness of the piezo ($t = 0.5 * [D_o - D_i]$), *V* is the applied voltage and d_{31} is the piezoelectric charge coefficient or piezoelectric deformation coefficient or piezo modulus as discussed earlier.

It is important to mention that Gamal El-Dean, (2007) reported that no exact equations are available to compute strains for the piezo rings as all the equations reported by the author are applicable and valid for a cylinder of H (height) >> r (radius) i.e. H/r = 5 to 10. The ring actuators have a height, H = 3.5 mm. The outer diameter of the used piezo ring is 44 mm. Thus, the ratio of H/r is less than 5, so this equation is just an approximation for the strain calculations and, therefore, further investigation is needed to derive the exact deformation equations for these piezoceramic rings.

Soils are assumed to behave as linear elastic material at shear strains below 10^{-3} %. Using this value as a limiting strain γ_{radial} in Eq.2.2 along with the values of t = 3 mm and d_{31} from Table.2-1, the limiting voltage was calculated a found to be around 175 V. This voltage is much higher than the voltage applied in conventional bender element tests. Almost all the tests conducted during the present study were performed at an input voltage of 50 - 100 V. The applied voltages ensured the tests were performed by keeping soil in the linear-elastic ranges hence providing the true measurement of shear wave velocity V_s and hence maximum shear modulus G_{max}.

Another important point to highlight is the boundary condition of the piezo rings. The limiting voltage is determined assuming the ring to be unrestrained. The piezo rings as an entire PRA setup are assumed to present a stiffer response. To reach the value of the limiting radial/shear-strain, a higher displacement will be required and since the physical and mechanical properties of piezo rings cannot be altered, it can only happen at the cost of increasing the input voltage, therefore input voltages even higher than 175 V may be safely applied.

Increasing the input voltage has another concern i.e. depolarization. Exposure to a strong electric field, of polarity opposite that of the polarizing field, can depolarize a piezoelectric material. The degree of depolarization depends on the type/grade of material, the exposure time, the temperature, and other factors, but fields of 200-500 V/mm (APC international) or greater typically have a significant depolarizing effect. An alternating current will have a depolarizing effect during each half cycle in which polarity is opposite that of the polarizing field.

Using the lower end of this input voltage range it can be safely said that the used piezos can take a very high input voltage without depolarization thanks to thickness of the rings. Such high input voltages cannot be applied to the bender elements since they are quite thin and can easily get depolarized due to high input voltages.

Polarization is the initiation of the piezoelectricity in ceramics and is obtained by applying voltage between a pair of electrode faces. The deformation of the polarized ceramic element depends on the following: ceramic shape and composition, direction of the poling axis, and location of the applied electrical field. Generally, ceramics can be polarized to generate (or to sense) compression or shear waves (Brignoli et al. 1996). However, spurious motions always seem to be present. For instance, a ceramic element that mainly produces shear displacements will also generate small compressive displacements. This result is further amplified by the finite nature of the S-wave source, which also contributes to the creation of compression wave energy (Sanchez-Salinero 1986).

2.3 Laboratory Techniques Used for Measuring Dynamic Soil Properties

The lab techniques for measuring dynamic soil properties can be divided into two broad categories namely.

- Low-Strain Laboratory Tests
- High-Strain Laboratory Tests

2.3.1 Low-Strain Tests

2.3.1.1 Bender Elements

Bender elements comprise of two-layers of piezo-ceramic plates cross-sectionally polarized. Each plate consists of two conductive outer electrodes, two piezoceramic sheets, and a conductive center shim of brass or stainless steel plate as shown in Fig.2-1 (a). The electrodes are usually nickel or silver deposits. Shirley and Hampton (1978) and Shirley (1978) pioneered the use of bender elements for geotechnical testing. Later, Dyvik and Madshus (1985) conducted extensive testing and demonstrated good agreement between G_{max} measured with bender elements and the resonant column technique. However, there are several difficulties associated with bender element installations, including electrical crosstalk due to electromagnetic coupling through the soil, mixed radiation of both P- and S-waves, near field effects, and uncertain detection of first arrivals. These will be addressed in details in the next sections.

Depending upon the orientation of the polarization, bender elements can be classified into two types: series [Fig. 2-1 (A) & (b)] and parallel [Fig. 2-1 (B) & (c)]. The same direction orientation is parallel bender element while the opposite direction orientation is a series bender element. When the two ends of the bender elements are polarized in the same direction in such a way that the voltage is applied or measured at each side individually is a parallel type bender element. Parallel bender elements are preferred as a source or emitter since for the same applied voltage, the parallel-type connection provides twice the displacement of the series-type connection. When two ends of the bender elements are polarized in the opposite direction is called a series bender element. Since

in the series type of electrical connection the total voltage is the sum of the individual voltages, this type of configuration is preferred as a receiver bender element.

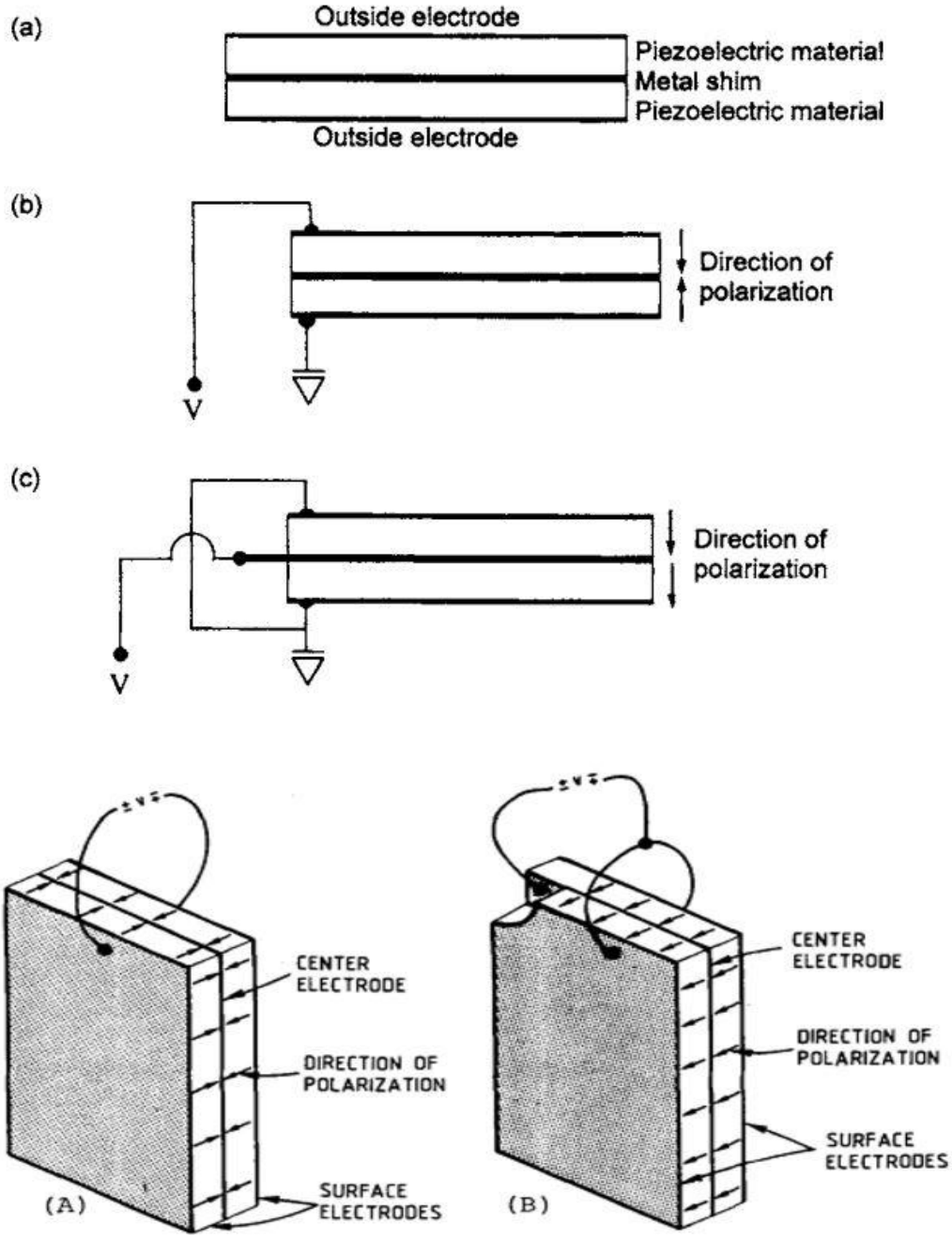

Figure 2-1. Series and Parallel Bender element Configuration (Dyvik and Madshus, 1985)

(a) Definition of bender element: (A) & (b) Series configuration: (B) & (c) Parallel configuration

When a voltage is applied between the two ends of the bender elements, the polarization of the ceramic material and the type of electrical connections causes the extension of one end and the contraction of the other. The net movement is a bending displacement and it is due to this reason they are called bender elements. When implanted properly into a soil, this bending displacement produces a perturbation with strong shear wave content. (Camacho-Tauta et al., 2012). A typical bender element setup is shown in Fig. 2-2.

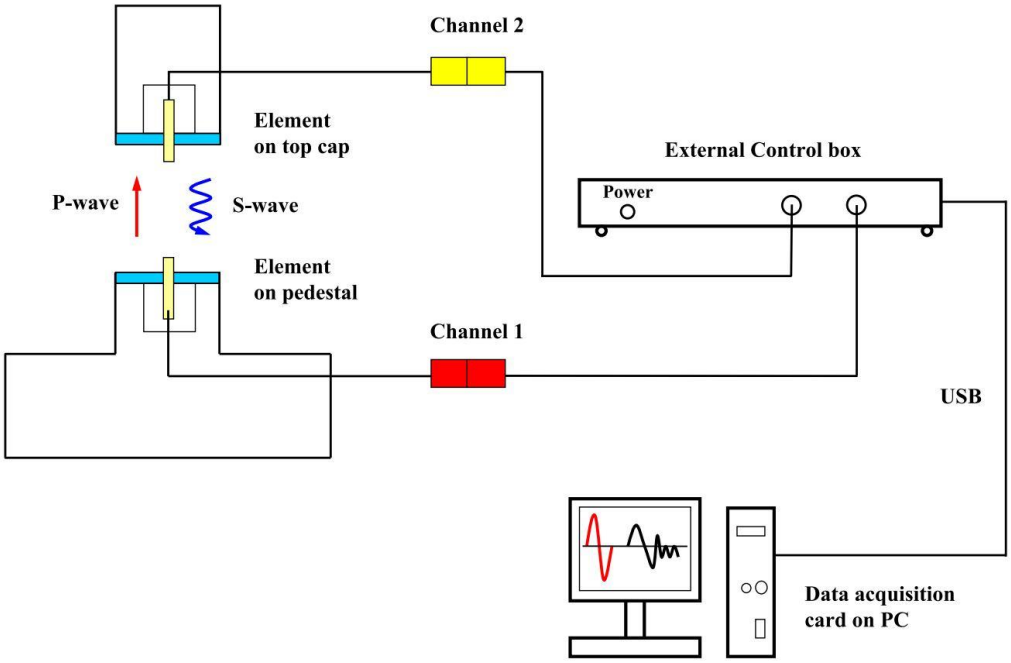

Figure 2-2. A typical bender element setup (Gu et al., 2013)

Initially, the step signal (square wave with very low frequency) or square signal was used to excite the BE transmitter for two main reasons. Firstly, the starting time can be easily defined with such input signals, and secondly due to the fact that the sudden change produces a significant perturbation. The fact that the step signal produces an output composed of all frequencies or simply it consists of infinite number of frequencies creates issues due to the highly dispersive nature of the soil. In highly dispersive medium like soils, each frequency component travels with its own speed hence creating problems in using frequency domain analysis technique to estimate the arrival time. Over the course of many years, researchers have consistently shown preference for a sine pulse as it consists of only one fundamental frequency.

2.3.1.2 Shear-plate transducers

Several researchers used disk shaped piezo-ceramic transducers to measure seismic wave velocities in laboratory soil specimens (Brignoli et al., 1996; Ismail and Rammah, 2006; and Suwal and Kuwano, 2013). The advantages of using such a technique is that small strain stiffnesses can be measured using elastic waves on the specimens that can be tested in a non-destructive manner in the course of other testing procedures (e.g. triaxial tests). Unlike bender elements, they do not need to penetrate through the soil sample and hence do not cause any damage to the sample and are well suited for undisturbed stiff soil samples, cemented soils and soils with large aggregates. Another advantage is that it is possible to make a direct comparison between the field and laboratory values.

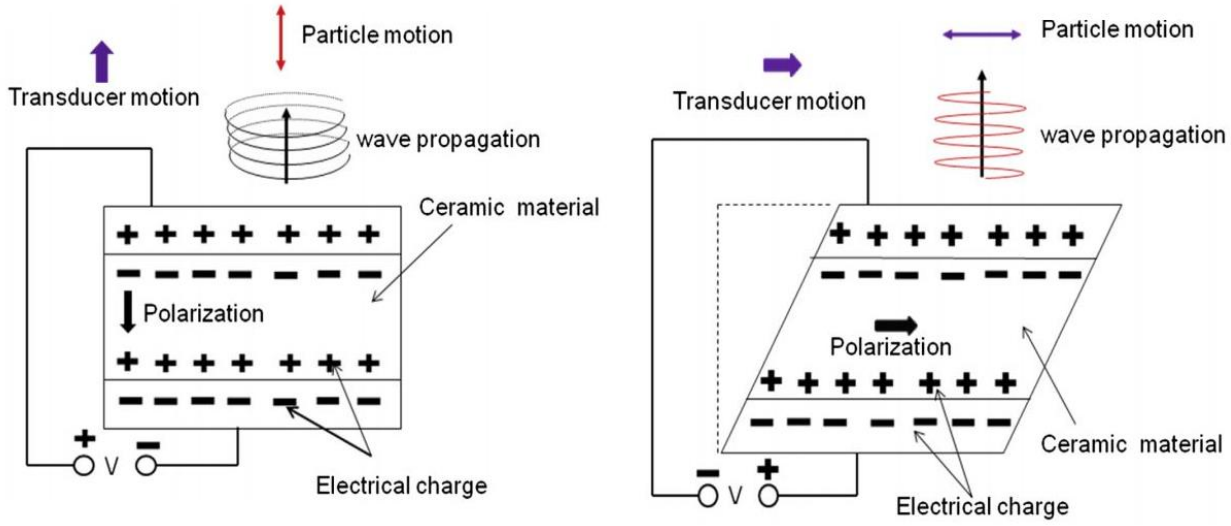

Figure 2-3. P-type (left) and S-type (right) disk transducers (Suwal and Kuwano, 2013)

Fig.2-3 shows a schematic of both the P-type (left) and the S-type (right) piezo disk shape piezo elements used by Suwal and Kuwano (2013). The P-type element is polarized in the longitudinal direction, which is perpendicular to that direction of the electrode. Such an element generates a longitudinal compression wave under the applied electric field/voltage. On the contrary, the S-type element is polarized direction parallel to that of the electrode (in the transverse direction), creating a shear wave upon in an application of the applied voltage.

Suwal and Kuwano (2013) used the trigger accelerometer method (Ahn Dan and Koseki, 2002) for measuring the propagated waves in the specimen. In the trigger accelerometer technique, a pair of triggers is firmly installed on the top cap, which is excited according to the function set on the function generator. A pair of accelerometers is fixed on the surface of the specimen as schematically shown in Fig.2-4.

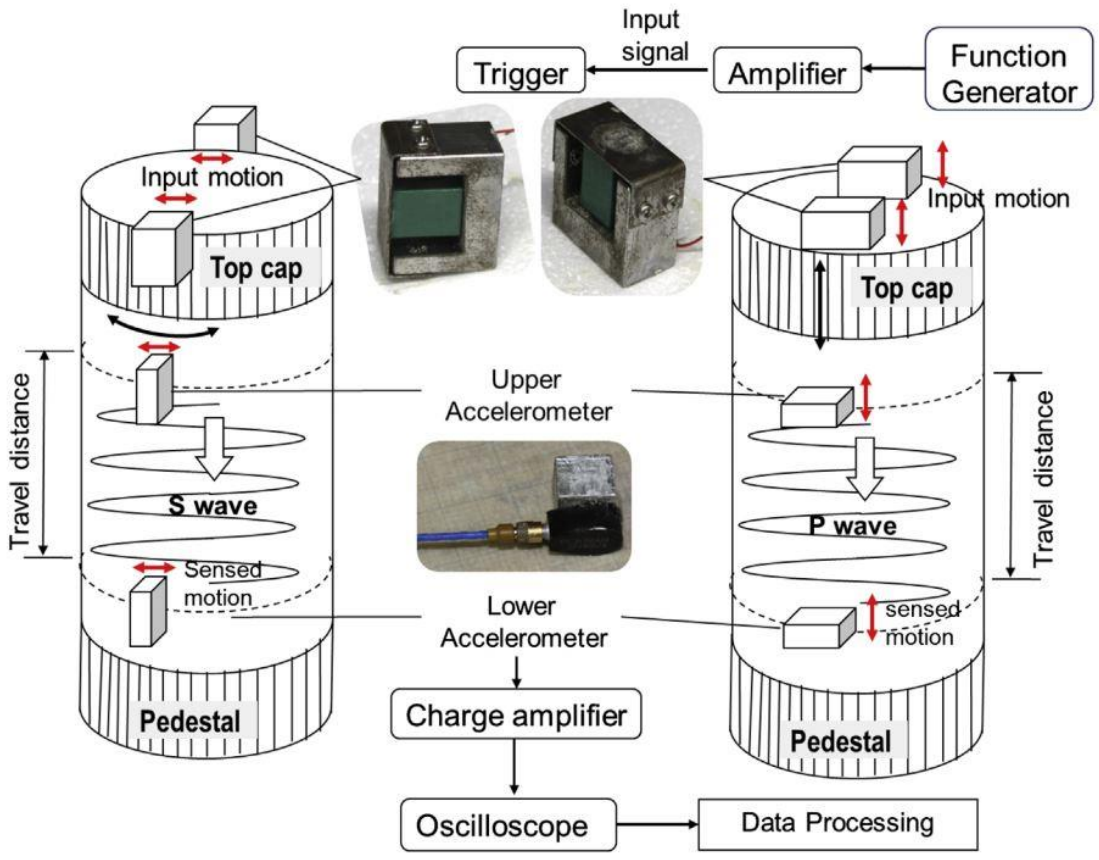

Figure 2-4. Trigger accelerometer method. P-type piezo element (right) and S-type piezo element (left) (Suwal and Kuwano, 2013)

Suwal and Kuwano, (2013) used the P-type elements with the diameter = 20 mm, and thickness = 2 mm) while their S-type transducer's diameter = 20 mm, and thickness = 5 mm. They also used a third type of elements called the PS-type element, which can emit and receive both compression and shear waves. They created PS-type element by firmly amalgamating P-type and S-type elements in epoxy resin. All the three types of the elements with their dimensions are shown in Fig.2-5.

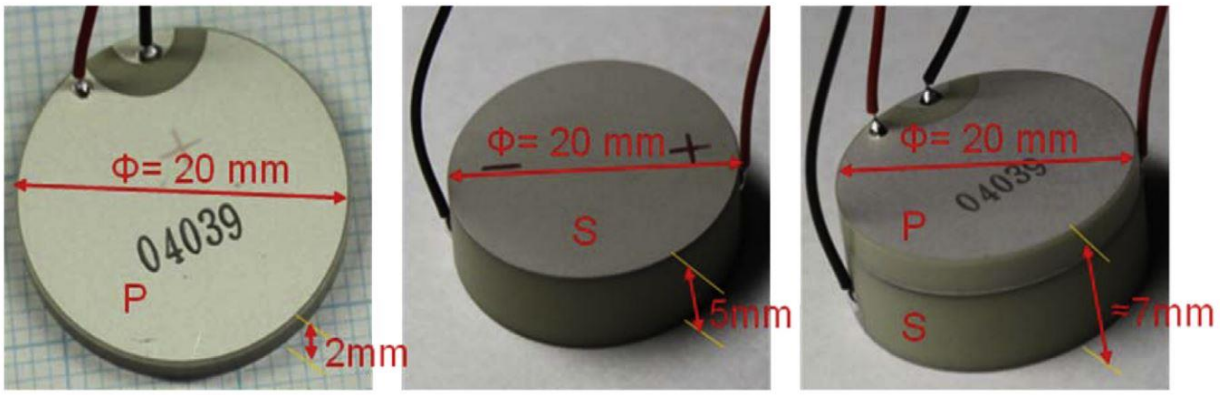

Figure 2-5. a) P-type element, b) S-type element, and c) PS-type element (Suwal and Kuwano, 2013)

Several shortcomings were associated with such type of the transducer. The main problem is the large impedance mismatch between the elements and that of the tested soil specimen. In short, the mechanical motion that is transferred from the element to the soil is small because the element exhibits a small movement with a large force and the soil exhibits a large movement with a small force (Shirley and Hampton, 1978).

Brignoli et al. (1996) determined that the shear-plate transducer yielded shear waveforms comparable to those generated with bender elements. Shear-plate transducers give weak signals at low confining pressures that increase rapidly while increasing confining pressure. The strength of shear-plate transducer signal are larger than those from bender transducers at confining pressures above 50 kPa.

It is also pertinent to mention the shortcomings of shear-plate transducers found in the work of other researchers including Suwal and Kuwano (2013) and Nakgawa et al. (1996).

Suwal and Kuwano (2013) reported that a good contact between the surface of the transducer and the tested specimen is necessary. The disk transducer is suitable for coarse grained material only when the diameter of the disk transducer is more than 10 times of mean diameter of the tested materials. In addition, the noise level was high (i.e. the frequency of the system noise was found

to be in a range of 22–25 kHz), which required using a low pass filter along with signal stacking and averaging to increase the signal-to-noise (SNR) ratio to an acceptable levels and cross-talk (duplicate of the input sine wave on the output/received signal) was also observed as shown in Fig.2-6. The amplitude of cross-talk decreases with the distance between the channels, therefore, the input and the output channels are chosen at the two extremities but the authors reported that they were never able to completely eliminate the cross-talk.

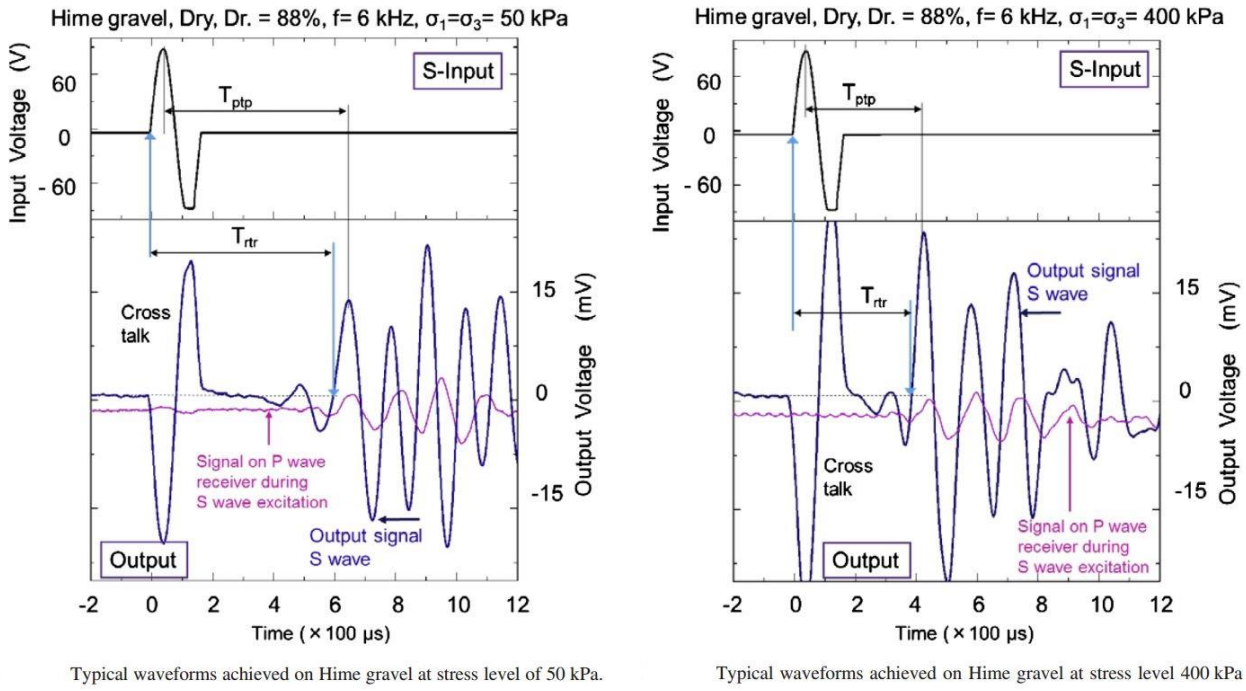

Figure 2-6. Cross-talk on the signals obtained by Suwal and Kuwano (2013)

Suwal and Kuwano (2013) noted that S-waves in a certain frequency range (approximately 10–20 kHz) were not able to be successfully transmitted. They recommend using frequency <8 kHz when measuring the S-wave velocity employing their transducers.

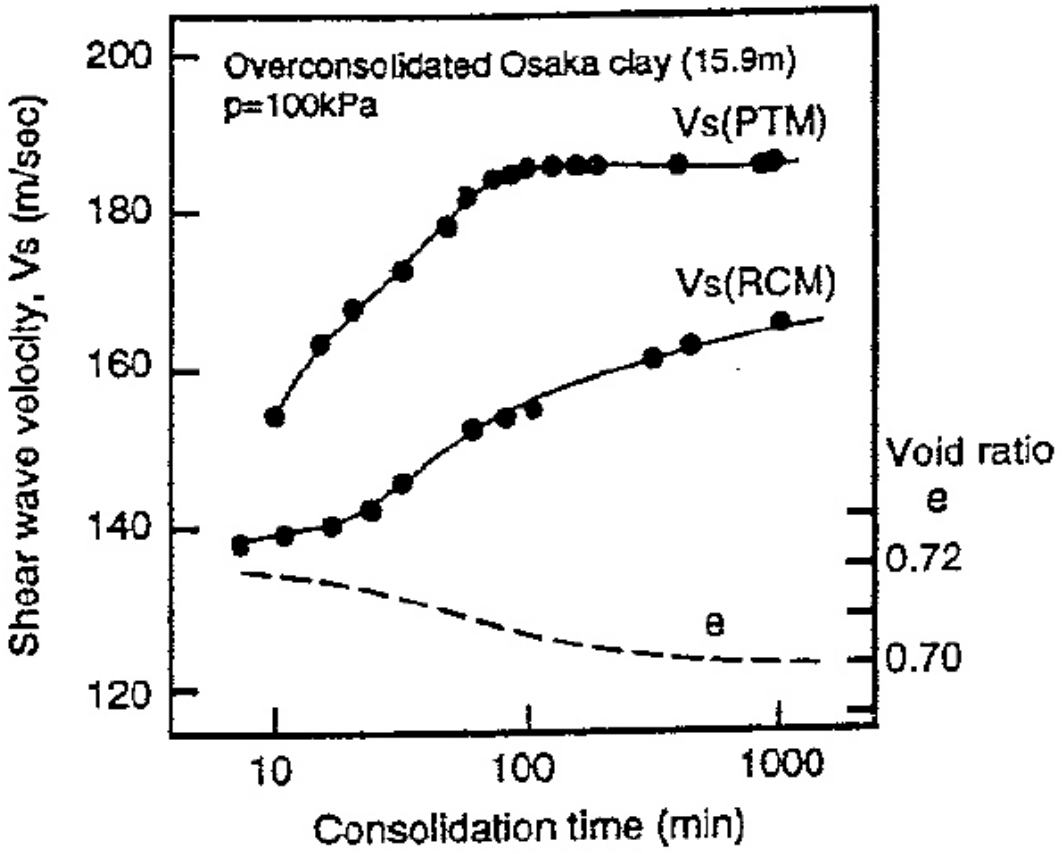

Figure 2-7. Change in V_s during Consolidation of Osaka-Bay Clay by Pulse Transmission and Resonant Column (Nakagawa et al., 1996)

Nakagawa et al. (1996) used shear plates to create torsional excitations for measuring shear wave velocity of triaxial samples. They used high voltage input signal (around 500V) to test saturated kaolinite clay. They had to amplify the output signal by more than 100 times (in two phases), and filtered output signals through high pass or low pass analog filters to increase the signal to noise ratio. Nakagawa et al. (1996) also reported the reflection of unknown waves or reflections of S-wave on their output signals. They demonstrated the difference in performance between the shear plate transducers and resonant column technique by measuring the change in S-wave velocity during consolidation of Osaka-Bay clay using both techniques as shown in Fig.2-7. It is obvious from Fig.2-7 that the shear plate transducers give higher values of V_s than the resonant column

methods. They theorized that the shear-plates measure V_s at the center of the specimen where the disturbance due to sample preparation is little or none, while the resonant column technique evaluates the average rigidity of the entire specimen. Since the disturbed peripheral/bordering part of the test specimen decreases its rigidity, the reported V_s values by resonant column technique were lower as compared to the pulse technique

2.3.1.3 Bender-Extender Element

A common practice is to use separate pairs of S-wave and P-wave piezoceramic elements mounted in the same apparatus to measure S and P wave velocities respectively (e.g. Brignoli et al. 1996, and Nakagawa et al. 1996 etc.). Lings and Greening (2001) introduced a single hybrid element called the "bender-extender element". Leong et al. (2009), and Kumar and Madhusudhan (2010) used the bender-extender element to find the P and S wave velocities. A simple alteration in bender element can easily convert it into an extender element. This is achieved by changing the wiring configuration of bender element from a two-wiring configuration to a three-wire configuration and then matching it with the corresponding type of polarization (Leong et al. 2009). Lings and Greening (2001) reported that using such hybrid element allows both P and S wave velocity measurements to be made on the exact same path in the soil specimen. This benefit helps identifying the arrival of S wave, especially under conditions when it is masked by the near-field effect.

In the bender-extender element test, a pair of piezoceramic elements is used. One piezoceramic element behaves as an S-wave transmitter as well as the P-wave receiver, while the other piezoceramic element is used a P-wave transmitter as well as an S-wave receiver. A schematic diagram form the work of Leong et al. (2009) of their bender-extender element test setup inside the triaxial cell is shown in Fig.2-8. Leong et al. (2009) used the bender-extender elements to study their performance in measuring P and S wave velocities in terms of the recorder resolution, size of the bender-extender elements, and the excitation voltage frequency. While Kumar and Madhusudhan (2010) used the bender-extender elements to study the Poisson's ratio and the effect of relative density and confining pressure on the Poisson's ratio of sandy soils. Leong et al. (2009) concluded that the performance of the bender-extender elements can be improved by considering

the following: (1) the digital oscilloscope used to record the bender-extender element signals should have a high analog to digital (A/D) conversion resolution; (2) the size of the bender-extender plays an important role in the strength and quality of the received signals, especially when dealing with P-waves: (3) using a wave path length to wavelength ratio (L/λ) of 3.33 enables a more reliable determination of V_s and eliminates the near-field effect.

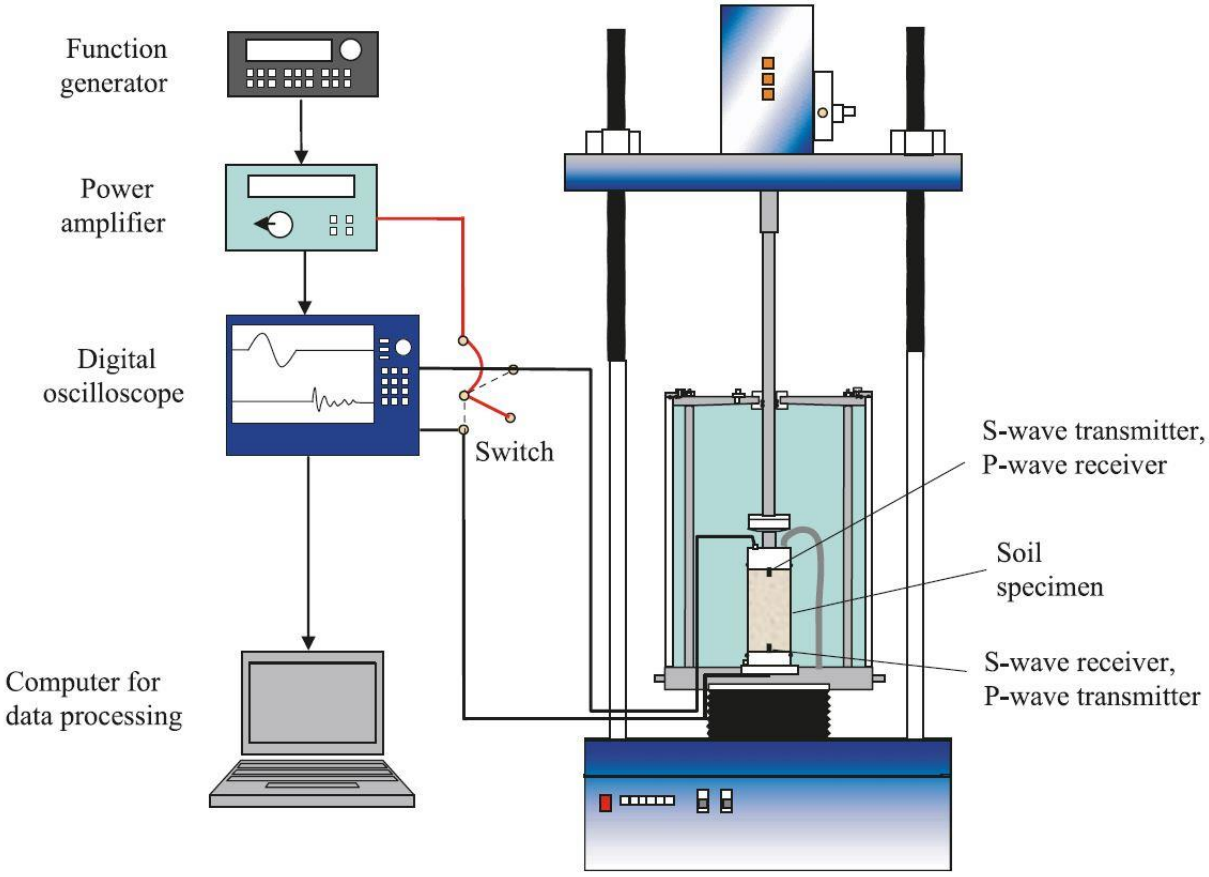

Figure 2-8. Bender-extender element test Setup (Leong et al. 2009)

2.3.1.4 Resonant Column Technique

Resonant column (RC) test is one of the most commonly used laboratory technique for measuring the low-strain properties of soils including the stiffness (V_s and G_{max}) and damping ratio. It subjects the solid or hollow cylindrical specimen to harmonic torsional or axial loading by an electromagnetic loading system (Kramer, 1996). The loading systems usually apply harmonic

loading that can be varied in frequency and amplitude but random noise loading and impulse loading have also been used (Kramer, 1996). There are a number of different types of RC devices, which vary in their boundary conditions and mode of vibration e.g. longitudinal or torsional (Yu, 2013).

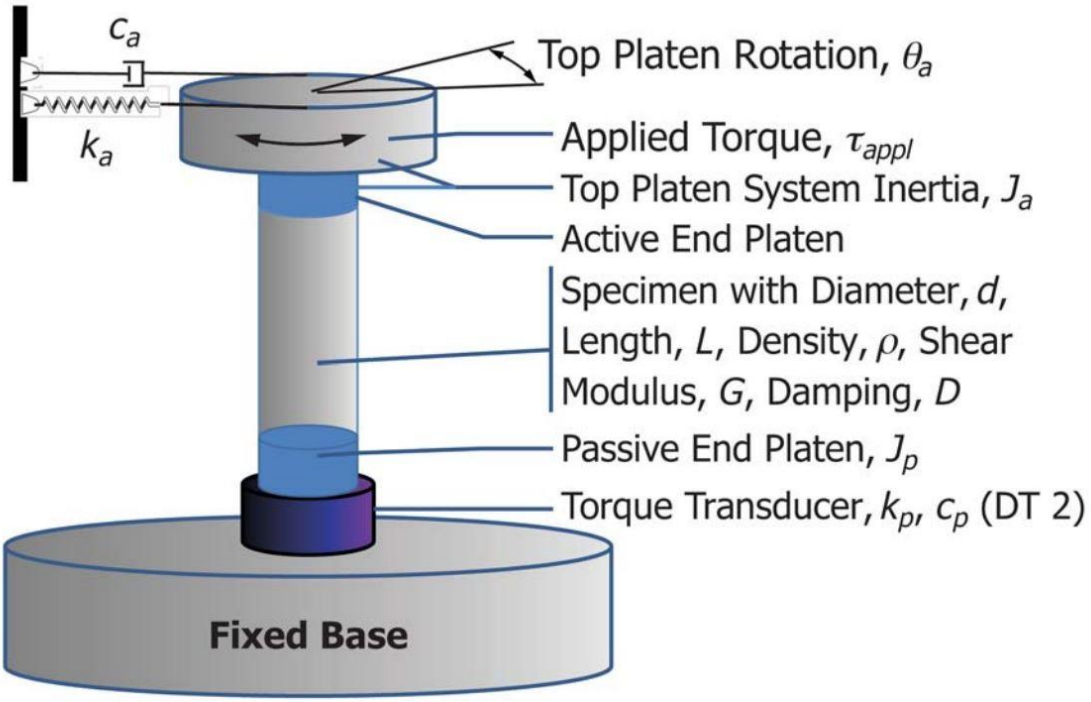

Figure 2-9. A schematic of a typical fixed Base Resonant Column (ASTM, 2015)

A schematic of the typical fixed base resonant column is given in Fig.2-9 while Fig.2-10 shows the typical resonant column test apparatus (EPRI 1993). Many researchers and authors including Kramer (1996) have discussed this testing technique.

After preparing the soil sample, it is subjected to cyclic loading. The loading frequency is initially low and is then gradually increased until the response (strain amplitude) reaches its maximum. The least frequency corresponding to the maximum localized response is the fundamental frequency ($\boldsymbol{f_n}$) of the specimen. Fig.2-11 shows the typical response from a RC test showing the $\boldsymbol{f_n}$ **= 41 Hz** for the tested soil specimen. The fundamental frequency ($\boldsymbol{f_n}$) of the specimen is the function of the soil's G_{max}, its geometry and certain characteristics of the used resonant column apparatus.

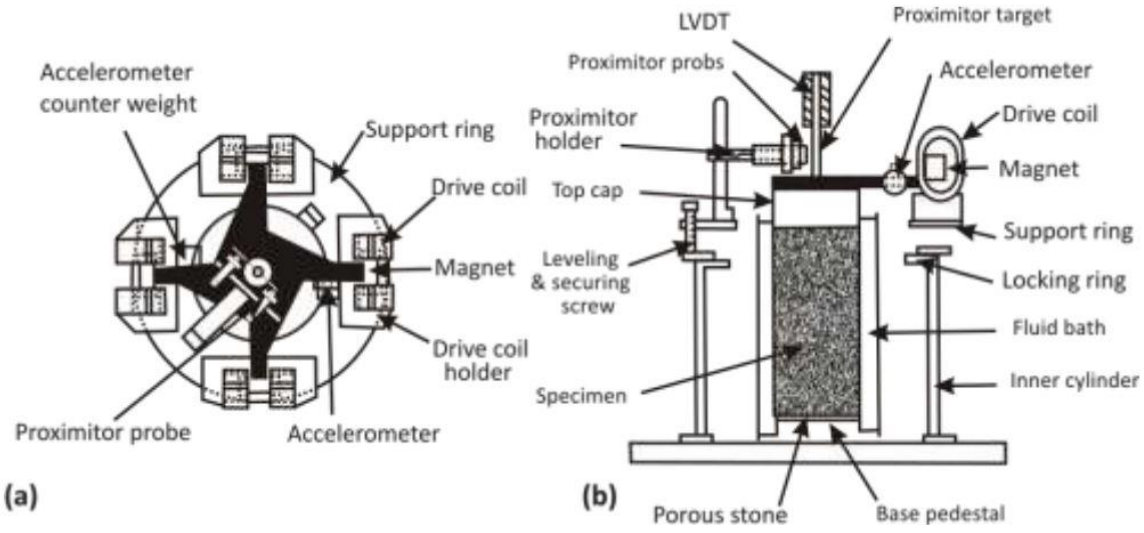

Figure 2-10. Typical resonant column test apparatus: (a) top view of loading system, and (b) profile view of loading system and soil specimen. (After EPRI, 1993)

Knowing the constants/parameters related to the device and the specimen along with the experimentally measured f_n, the V_s and hence G_{max} can be measured. The damping ratio can be determined from the frequency response curve using the half-power bandwidth method or from the logarithmic decrement by placing the specimen in free vibration.

The use of hollow specimens is preferred over solid cylindrical specimens in torsional loaded RC tests. This is because in solid specimens the shear strain varies from zero at the centerline of the specimen to a maximum value at the outer periphery and such non-uniformity can be significant in certain conditions (Drnevich, 1967, 1972) while such non-uniformity of shear strain is either very small or does not exists in the hollow specimens.

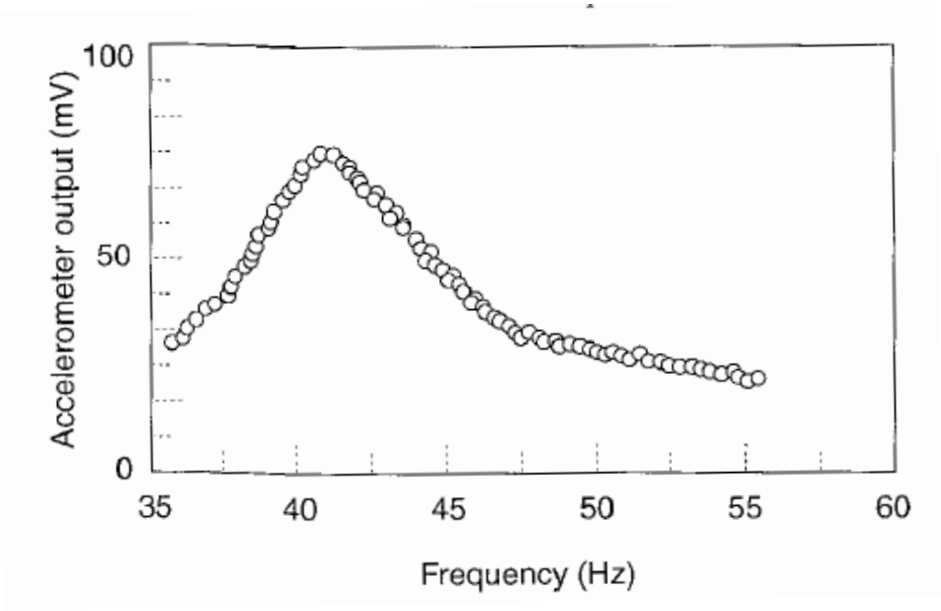

Figure 2-11. Typical output from the RC test (Kramer 1996)

2.3.2 High-Strain Tests

2.3.2.1 Cyclic Triaxial Test

Cyclic triaxial test is the most commonly used test for measuring dynamic response of soils and dynamic soil properties at high strain amplitudes. The difference between the axial stress and the radial stress (confining pressure) is known as the *deviator* stress. In cyclic triaxial test, the deviator stress is applied cyclically, either under stress controlled or strain controlled conditions. Cyclic triaxial tests are usually performed by keeping the effective confining pressure constant and the axial stress is applied cyclically at a loading frequency of typically 1 Hz (Kramer, 1996).

The stresses and strains measured in the cyclic triaxial tests are used to compute the shear modulus reduction curve and damping ratio curve. For a given cyclically applied shear strain amplitude, the shear stress-strain curves take a form of a hysteresis loop given in Fig.2-12. The slope of the line joining the two extremities of this loop gives the secant shear modulus G_{sec}, while the area contributes to the damping ratio ξ. As the strain levels are increased in increments, each applied

shear strain amplitude results in a new value of G_{sec} and ξ. G_{sec} decreases with the increase in strain-amplitude while ξ increases. The G_{sec} at each strain amplitude normalized with the G at the very low strain amplitude (known as G_{max}) and plot with strain amplitudes is known as shear modulus reduction curve, while the plot of damping ratio for each strain amplitude with the applied strain amplitudes is known as damping ratio curve. Both curves are shown if Fig-2.13.

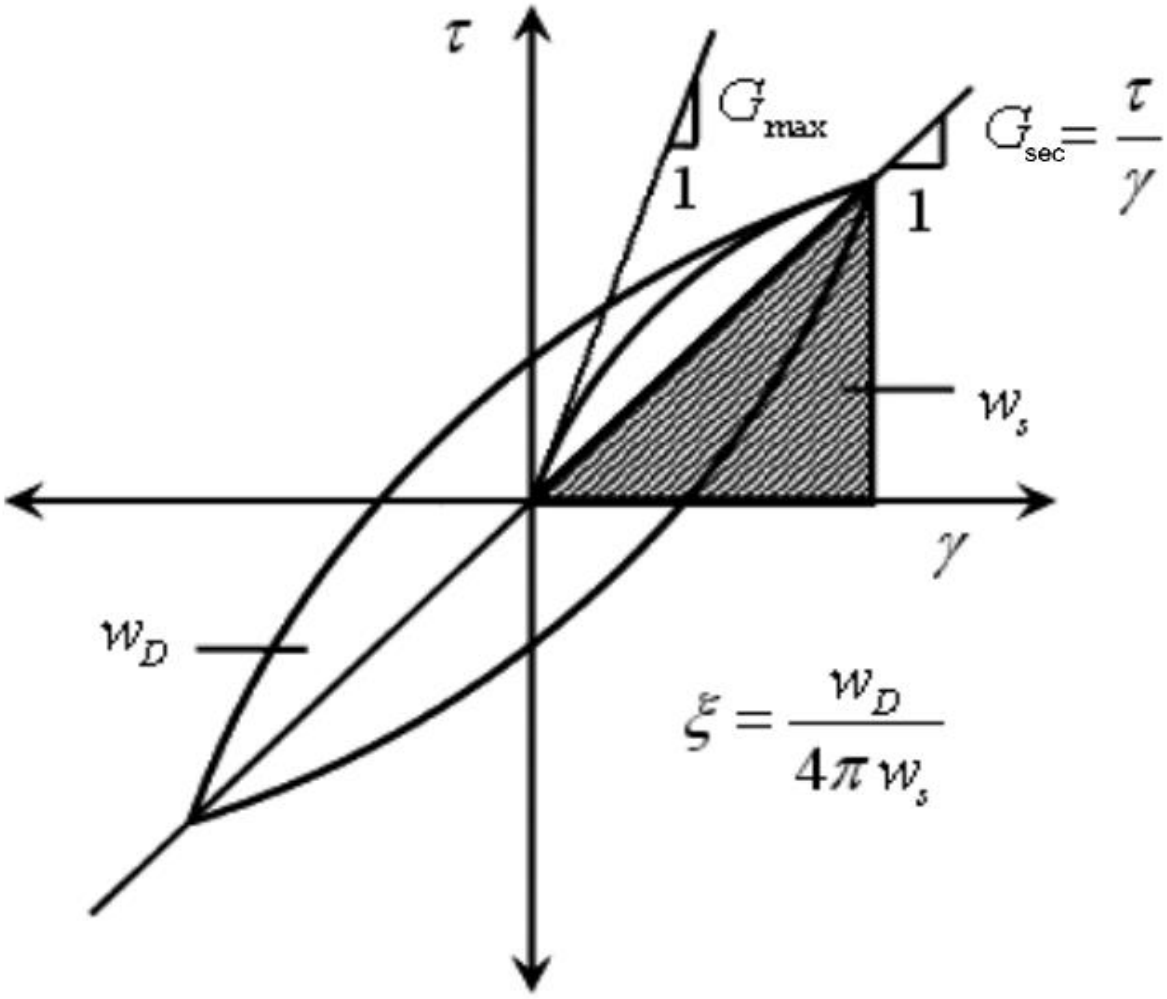

Figure 2-12. Typical Hysteresis Loop obtained from the cyclic triaxial Kramer (1996)

Other high strain-amplitude lab tests which are beyond the scope of this study includes;

- Cyclic Direct Simple Shear Test and
- Cyclic Torsional Shear Test etc.

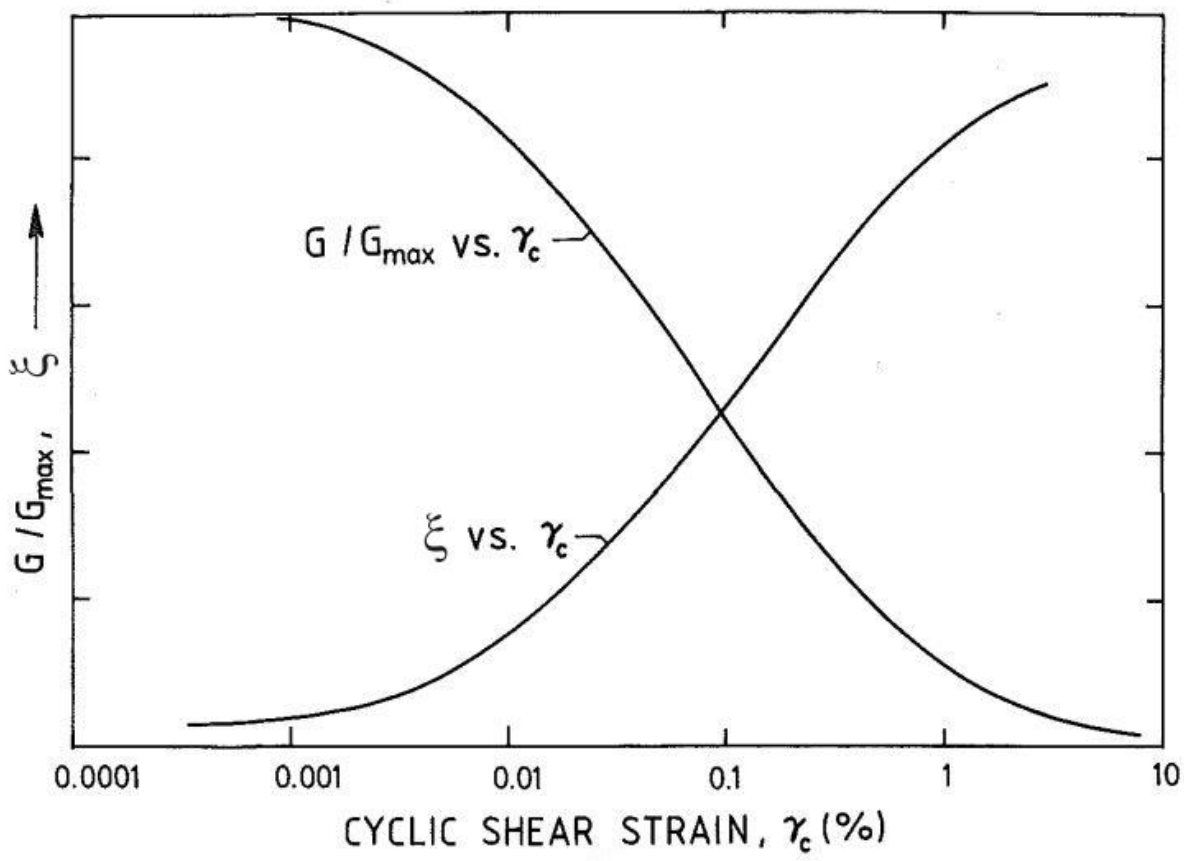

Figure 2-13. Typical Shear modulus reduction curve and damping ratio curve, Vucetic and Dobry (1991)

2.4 Field Techniques for Measuring Dynamic Soil Properties

There are several field methods for in-situ measurement of dynamic soil properties. Field tests do not require sampling and hence the complex effects of existing stress, chemical, thermal and structural conditions are preserved and reflected in the measured parameters. Field tests measure the soil response over large volumes of soil instead of small specimens. The soil deformations

induced by the field tests are similar to those of wave propagation and foundation design problems (Kramer 1996). However, field tests have several shortcomings. They do not allow testing the soil at conditions other than the in-situ conditions, and don't allow controlling pore water drainage. In many field tests, the specific soil property of interest is not measured but must be determined indirectly, by theoretical analysis or using empirical correlations (Kramer, 1996). Finally, field tests could be quite costly and are susceptible to the possibility of unfavorable and harsh weather. The field tests are only mentioned here and more details presented in several published literature e.g. Kramer, (1996).

Field tests can be classified into two broad categories; a) low-strain field tests and b) high-strain field tests. The low-strain field tests include: seismic reflection; seismic refraction; suspension logging; steady-state vibration (Rayleigh Wave); spectral analysis of surface waves; seismic cross-hole; seismic down-hole; and seismic cone penetration.

The high strain filed approach includes the following tests: standard penetration test; cone penetration test; dilatometer test; and pressuremeter test.

2.5 Shortcomings of Laboratory Techniques Used in Measuring Shear Wave Velocity

Bender elements test suffers from several shortcomings and disadvantages reported by several authors. Ismail and Rammah (2006) reported the physical disadvantages of bender elements given below:

i. The bender element necessitates penetration into the soil specimen to transfer its bending deformation to the surrounding soil as a shear deformation. The process is invasive and it causes disturbance to undisturbed and cemented specimens. Excavating holes into specimens involves more work to refill the holes with a coupling material, (typically gypsum or epoxy). More disturbances to the specimens are possible during such handling.

ii. The coated bimorph (cantilever bender that consists of two piezoceramic layers) is in direct contact with the soil, and this makes it susceptible to damage; failure of the epoxy coat will lead to a short circuit and hence loss of signal.

iii. The bender element is affected by the stresses within the sample, most notably in the conical zone adjacent to the rough, conventional platens of the triaxial apparatus.

iv. The bender element is not suitable for harsh environments, where electrolytes may penetrate through the epoxy, as in the case of electrokinetic treatment in laboratory experiments.

v. Because of its relatively small thickness (0.5 - 1.0 mm), the bender element is prone to depolarization at high voltage (maximum working voltage ≈ 100 V per 1 mm thickness). However, this depends on the number of working cycles and shape of the input signal. A higher voltage may be required in situations where signal attenuation is of concern, such as in the case of soft soils or stiff soils with a long travel distance.

vi. Two different types of electrical connection are used for the transmitter and receiver for any pair of bender elements, to amplify both the transmitted and received signals: a parallel connection is required for the transmitter and a series connection for the receiver. This requires special care during manufacturing and testing.

vii. Most bender element apparatus are quite rigid in their application. The applied voltage is quite low which typically cannot be amplified. Shape of the input signal, its amplitude and the frequency cannot be altered.

Major shortcoming of the shear-plate transducers are as follows:

i. Suwal and Kuwano (2013), confirmed that the disk transducer is more beneficial only to coarse grained materials, when the diameter of the disk transducer is more than 10 times of mean diameter of the tested materials.

ii. Suwal and Kuwano (2013) reported very high noise levels (the frequency of the system noise was found to be in a range of 22–25 kHz) which required using a low pass filter along with signal stacking and averaging to increase the signal to noise ratio to an acceptable levels.

iii. Suwal and Kuwano (2013) reported cross-talk was also observed as shown in Fig.2-6. The amplitude of cross-talk decreases with the distance between the channels, therefore, the input and the output channels are chosen at the two extremities but the authors reported that they were never able to completely eliminate the cross-talk.

iv. Another reported shortcoming reported by Suwal and Kuwano (2013) was in regards to the applied frequency range. In S-wave propagation when using their equipment, they noted that the waves in a certain frequency range (approximately 10–20 kHz) were not able to be successfully transmitted. They recommend to use the frequency of less than 8 kHz when measuring the S-wave velocity using their transducers.

v. Ismail and Rammah (2006) reported that their shear-plate needs high voltage to produce enough energy for a readable output signal.

vi. Ismail and Rammah (2006) found that the output signal amplitude of bender elements is 10 times that of shear plates when testing soft clay sample, although the input voltages were 40 V and 200 V, respectively. The authors attributed this fact to the better coupling between the benders and soil.

vii. Typical shear-plate transducers are solid metal disks and they are not very well suited for testing cohesive soils as drainage in and out of sample is not possible with solid disk transducers.

The resonant column test, which is considered as one of the most reliable tests used for the measurement of small-strain stiffness, still has some limitations. It is limited in its ability to investigate other aspects of soil behavior (Airey and Mohsin, 2013). These limitations can be summarized as presented below:

i. Cannot be used to measure dynamic soil properties at high shear strain amplitudes or stiff specimens.

ii. They are relatively expensive, highly sophisticated, and time consuming and also have issues regarding the coupling between the specimens and end platens.

iii. They are also fairly complex to perform as they require several calibration constants depending upon the type of device.

iv. It is difficult to measure the porewater pressure in a RC test (Kramer, 1996).

v. The material properties are usually measured at frequencies above those of most earthquake motions (Kramer, 1996).

vi. RC tests underestimate the actual stiffness of tested specimens as compared to that obtained from the pulse testing (shear-plate transducer and bender element) because it

measures the average stiffness/rigidity of the specimen that includes the outer disturbed portion of the specimen resulting in lower stiffness. (Nakagawa, 1996)

The shortcomings of the cyclic triaxial tests are given below

i. Stress concentrations can exist at the cap and base (Kramer 1996).
ii. It lacks in modeling the stress conditions that takes places in most actual seismic wave propagations problems.
iii. In the absence of local strain measurements, bedding errors and system compliance effects usually restricts measurement to shear strain amplitudes greater than about 0.01%.

2.6 Improvements Introduced in the New Technique

Recent developments at Sherbrooke University focused on utilizing piezoelectric ring actuators (PRA) to overcome some of the shortcomings of pulse testing techniques (e.g. Gamal El-Dean, 2007). The following improvements are claimed in the new PRA technique:

i. The PRA device is non-invasive, hence reduces the overall sample disturbance.
ii. It is deemed suitable for all soil types including very stiff and cemented soils that cannot be readily tested with BE.
iii. It does not require penetration of the test specimen, and hence eliminates the need for coupling material as filler.
iv. Unlike BE, the PRA device shears the entire soil base (soil as a mass), while the BE applies the shear deformation at a relatively small area.
v. The PRA device is quite robust as it allows applying a variety of input signals shapes (sine, square, step or any other custom shape etc.). It is also capable of applying a variety of input voltage amplitudes and frequencies which is usually not possible with conventional BE and shear-plate transducers pulse testing.
vi. The PRA performs well over a wide frequency range and produces clear output signals with high SNR as compared to BE and or Shear-Plate transducers due to its capability of shearing the entire soil base.

vii. The PRA can be installed in the oedometer and cyclic triaxial apparatuses which facilitates performing these conventional testing, but simultaneously measuring V_s of the tested material.

2.7 Interpretation Techniques for Wave Travel Time in Pulse Testing

Several methods of interpretation of the signals from the pulse testing have been reported and discussed in the literature (e.g. Viggiani and Atkinson, 1995; Greening and Nash, 2002; Arulnathan et al., 1998; Yamashita et al., 2009; Blewett et al., 1999; Jovičić et al., 1996; Styler and Howie, 2013; Gamal El-Dean, 2007; Kawaguchi et al., 2001; Leong et al. 2005). Some of the important and regularly used methods for determining the time of flight t_s are given below.

2.7.1 Phase and Group Velocity Techniques (Frequency Domain Analyses).

Group velocity (V_g) is the speed of propagation of a group or band of frequencies, while the phase velocity (V_{ph}) is the propagation speed at a particular (single) frequency (Styler and Howie, 2013). In a nondispersive medium, V_g and V_{ph} are similar and equal and independent of the frequency. In such a medium, and in the absence of reflections, a pulse wave does not distort with the propagation distance. An example of a nondispersive medium is a perfectly linear elastic continuum (Styler and Howie, 2013). Contrary, a dispersive medium is the one in which the V_g and V_{ph} are not equal. An example of dispersive medium would be a fluid saturated porous medium (Biot 1956a, b) such as soil.

The phase and the group velocity are both frequency domain techniques. The frequency-domain analysis comprises of interpreting the “phase-change” between the input (transmitted) and output (received) signals. Frequency domain techniques are less intuitive than interpretations of time domain signals (Styler and Howie, 2013).

According to Viggiani and Atkinson (1995), the input and output signals as shown in Fig.2-14 in the time domain can be presented as X (T) and Y (T). The linear spectrum L_x (f) of a signal X (T) is a function of frequency and can be expressed as:

$$L_x(f) = FFT\ [X\ (T)] \tag{2.3}$$

The linear spectrum as defined in Eq.2.3 is a vector in the complex field whose phase and magnitude are the phase shift and amplitude of each of the harmonic component of the signal respectively. The linear spectrum of the typical input sine (transmitter) and output (receiver) signals are given in Fig.2-15a and Fig.2-15b, respectively. The cross-power spectrum G_{xy} (f) of the two signals can be defined as

$$G_{xy}(f) = L_x(f).L_y{}^*(f) \tag{2.4}$$

where $L_y{}^*$ is the complex conjugate of linear spectrum of Y (T).

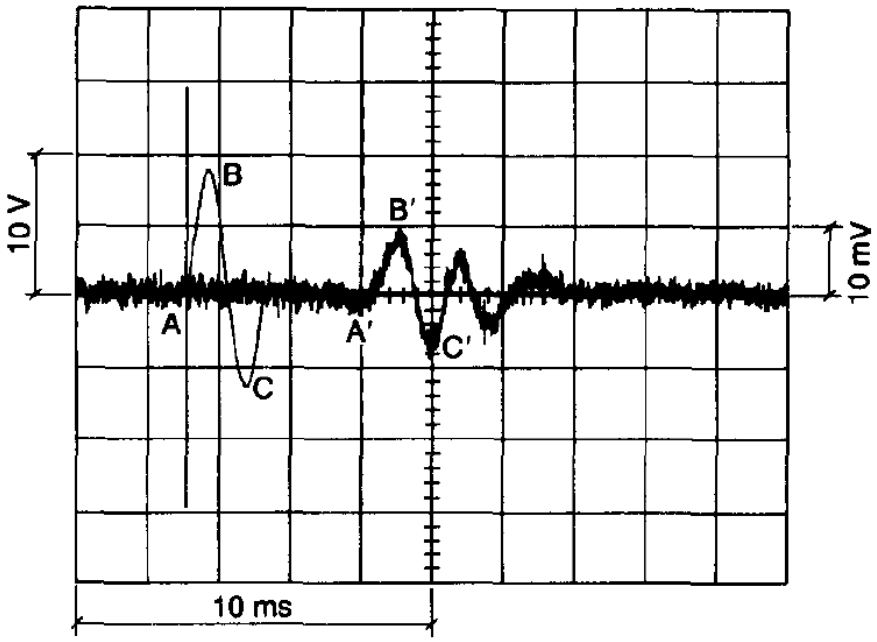

Figure 2-14. Input (sine) and ouput signals (Viggiani and Atkinson, 1995)

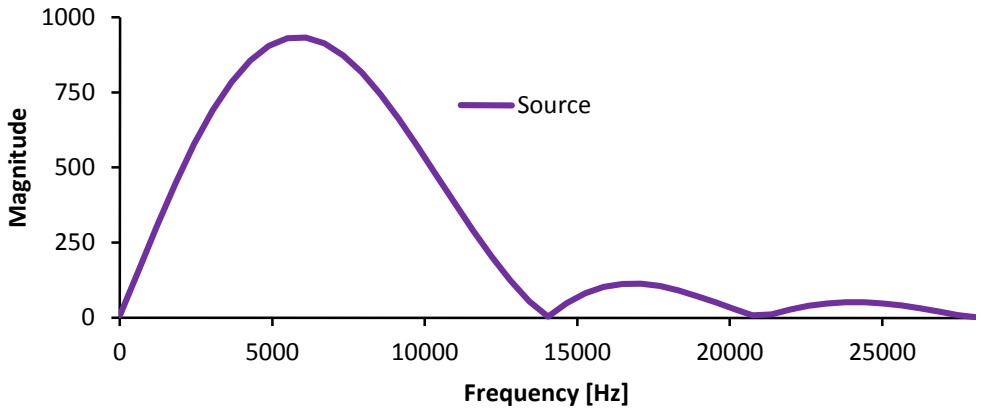

(a) Input sinosoidal signal

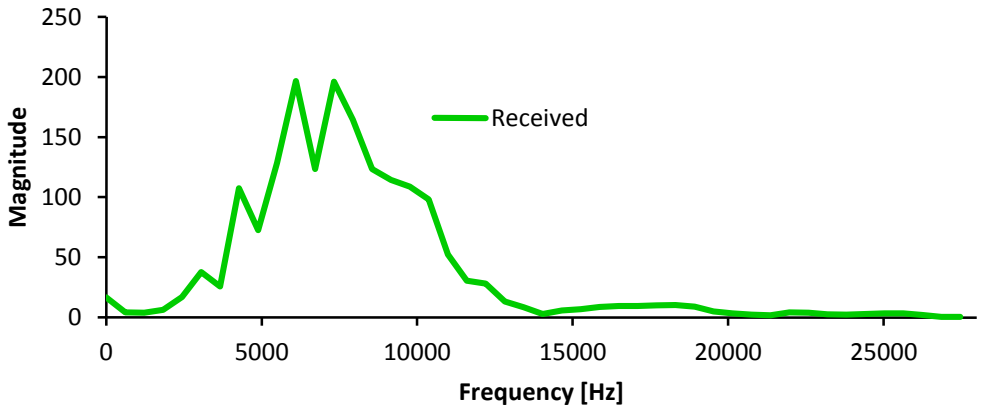

(b) Output signal

Figure 2-15. Linear spectrums

At each frequency, the magnitude of $G_{xy}(f)$ i.e. $|G_{xy}|$ is a product of the amplitudes of both signals at that frequency. While the phase of the cross-power spectrum is the phase differences of the components of the two signals at that frequency. By plotting the $|G_{xy}|$-f, the frequency ranges that are common to both the input and output signals can be seen. (Vilhar and Jovičić, 2009; Viggiani and Atkinson, 1995)

The phase shift between the two signals can be computed as

$$\phi(f) = \phi_y(f) - \phi_x(f) \tag{2.5}$$

where ϕ_x (f) and ϕ_y (f) are stacked (unwrapped) phases of the two signals. The frequency dependent phase velocity, V_{ph} (f) of each frequency component can be calculated from the secant of the $f - \phi$ graph (Fig.2-16) using Eq.2.6 (Vilhar and Jovičić, 2009).

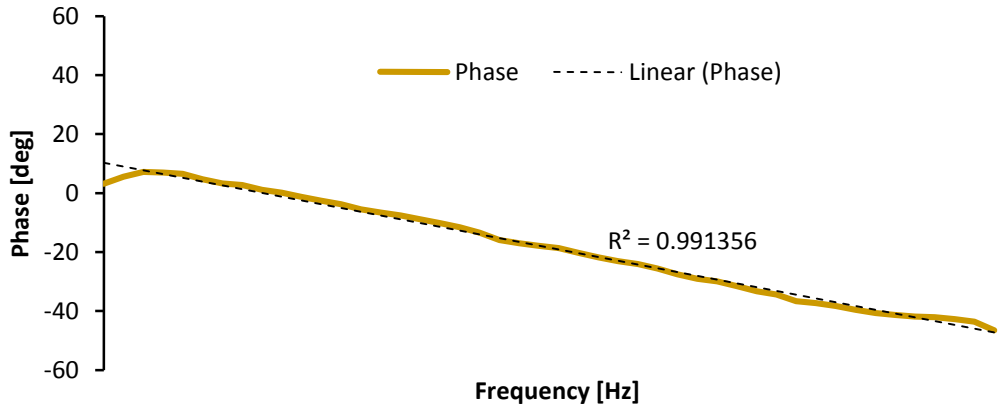

Figure 2-16. Cross-power spectrum phase diagram for input and output signals

$$V_{ph}\,(f) = 2\pi H \frac{f}{\phi(f)} \tag{2.6}$$

where: H is the travelling distance or height of the sample or tip-to-tip distance in case of bender elements.

The group velocity, V_g for a train/packet of wave for a given frequency interval can be determined using the slope of the tangent of d_f/d_ϕ from the chosen frequency range using the Eq.2.7 (Vilhar and Jovičić, 2009).

$$V_g\ = 2\pi H \frac{df}{d\phi} \tag{2.7}$$

The group travel time t_g is actually is the slope (linear interpolation) of $f-\phi$ plot also know absolute cross-power spectrum phase diagram (Fig.2-16) for the selected range of frequencies divided by 2π i.e.

$$t_g = \frac{1}{2\pi}\frac{d\phi}{df} \tag{2.8}$$

Vilhar and Jovičić, (2009) among many others have presented some guidelines in implementing the group velocity method. The authors suggested using the broadest possible frequency interval covering the linear relation of $\varphi - f$ (Fig.2-16). The authors also suggested using a frequency range such that it covers the major amplitudes in $|G_{xy}|$-f graphs.

Vilhar and Jovičić, (2009) also highlighted the scarcity in the group velocity technique. A slight change in the chosen frequency range can lead to a relatively big change in the estimated travel time. To overcome this issue, they suggested to use the widest possible range of frequencies in $\varphi - f$ plot (Fig.2-16) as such that it covers most amplitudes in $|G_{xy}|$-f graph and still remains highly linear. On top of these guidelines, the correlation coefficient (R^2) for the linear fit in $\varphi - f$ plot (Fig.2-16) is another guideline and R^2 should have the highest possible value along with satisfying the other specified guidelines.

2.7.2 Cross-Correlation Method.

Mancuso et al. (1989) originally proposed presented the cross-correlation technique for the analysis of the results from the cross-hole test. Viggiani and Atkinson (1995) later presented this time domain method and used it to analyze the bender element signals. This method along with the phase and the group velocity method is one of the most common methods of analyzing the signals for the arrival time in the pulse testing of soils. This method requires the time domain record to be decomposed into a group of harmonic waves of known frequency and amplitude typically using Fast Fourier Transformation (FFT) (Mitaritonna et al. 2010).

The cross-correlation function CC_{xy} (t) is a measure of the degree of correlation of two signals X (T) [input] and Y (T) [received] and can be presented by an analytical function given in Eq.2.9 i.e.

$$CC_{xy}(t) = \lim_{T_r \to \infty} \frac{1}{T_r} \int_{T_r} X(T)\, Y(T+t)\, dT \tag{2.9}$$

where T_r is the time record/length of sampled signal and t the shift between the two signals which is the arrival time of the signal between the two sensors. The cross-correlation, CC_{xy} (t), is the inverse FFT of the cross-power spectrum, G_{xy} given in Eq.2.4. The typical cross-correlation function of an input sine function and its output can be seen in Fig.2-17.

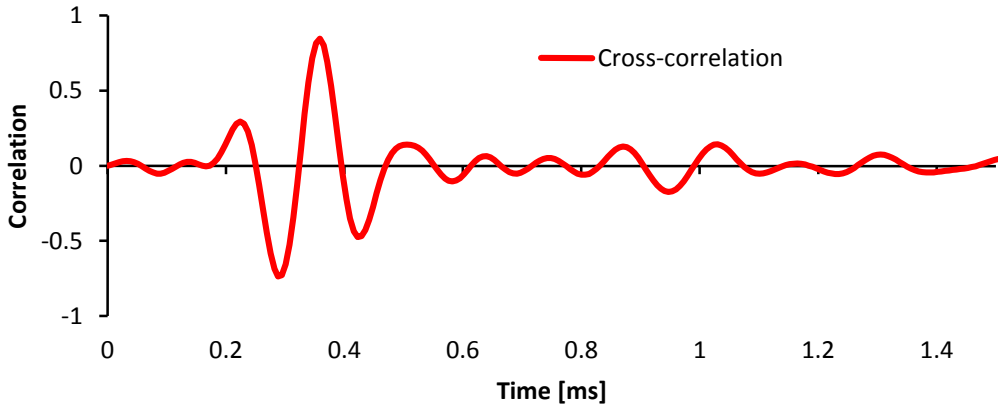

Figure 2-17. Cross-Correlation of typical input and ouput signals

The cross-correlation methods seeks the time shift needed to obtain the closest match between the trigger (input) and response (output) signals (Styler and Howie, 2013). It assumes that the travel time is equal to the time shift corresponding to the maximum of Eq.2.9.

Cross-correlation method assumes that the input and output signals of similar/same nature and have the similar frequency content which may not typically happen in bender element test due to the signal distortion, peripheral devices, interference of waves with the boundary of the soil specimens along with the near-field effects (Arulnathan et al. 1998).

When the input and output signals have different frequencies, the cross-correlation function may yield many maximum absolute values that makes difficult to identify the correct arrival time. Arroyo et al. (2006) concluded that the cross-correlation needs subjective interpretation as the peak cross-correlation may not identify the true arrival. Kim et al. (2015) reported the issue of bender

element sampling frequency and time resolution to effect the final results when using cross-correlation method for analysis.

2.7.3 Combined Time Domain and Frequency Domain Determination of the Phase Velocity

As the soil and the response of the bender element are dispersive in nature, and since the group velocity requires a non-dispersive system, the phase velocities should be measured instead of the group velocity. Styler and Howie (2013) proposed a new technique by combining the time and frequency domain methods. The technique was initially applied on the synthetic signals and later on the real bender element test signals of saturated Fraser River sand. The authors advocated on measuring the phase velocity instead of the group velocities since the group velocities are sensitive to dispersion, not reproducible and depends upon the chosen frequency window/range. The method proposed by Styler and Howie (2013) is a combination of earlier discussed cross-power spectrum technique with a phase-sensitive detection approach proposed by Blewett et al. (1999).

For a time function $g(t)$, a positive shift along the time axis results in a function, $g(t - \Delta t)$. An input sine wave can be presented by a function $g(t) = \sin(2\pi ft + \theta)$. This frequency of this input signal is f, whereas, θ is the phase angle. The time shift of this input/trigger signal can be presented by a function $g(t - \Delta t) = \sin(2\pi f(t - \Delta t) + \theta)$. This shifted signal has the same frequency, f, but a shifted phase angle of $-2\pi f \Delta t + \theta$. The phase shift between the two signals can be presented as $\Delta\theta$, where $\Delta\theta = -2\pi f \Delta t$. Since the phase angles can only be measured between the ranges $-\pi$ to π (i.e. a full range of 2π) the measured phase shift can be written as $\Delta\theta - 2\pi n = -2\pi f \Delta t$, where n is an integer that presents the phase degeneracy.

The cross-power spectrum technique calculates the group velocity. It uses the unwrapped or stacked algorithm to remove discontinuities in the measured phase which happens when it jumps between the boundaries $+\pi$ to $-\pi$. This technique measures the time of flight or group travel time t_g (and hence the group velocity) by utilizing the slope of $f - \theta$ plot using a linear regression, for a given frequency range, without caring for the integer n. On the contrary, the phase velocity technique uses the absolute phase difference between the input and the output signals to determine the propagation time and this requires to determine the constant n.

The coherence function of the two waves (input and output) indicates how well correlated the waves are. It ranges between 0 and 1 depending upon the linearity between the input and output signal. The chosen frequency range required for the cross-power spectrum technique to measure the group velocity can be optimized and can be selected based on the coherence function. It is only reasonable to compute the travel time for frequencies of highest coherence, near unity Ferreira et al. (2007).

Styler and Howie (2013) presented Eq.2.10 to measure the phase velocity at a given frequency.

$$V_s(f) = \frac{-2\pi f H}{\Delta\theta_r - 2\pi n} \tag{2.10}$$

where, H is the sample height or tip-to-tip distance for bender element tests, $\Delta\theta_r$ is the unwrapped phase shift, f is the frequency and n is the required phase degeneracy constant to determine the required phase velocity. The authors demonstrated their proposed technique on the simplified synthetic signals presented in Fig.2-18. The steps and the procedure to find the phase velocity at a given frequency is as follows.

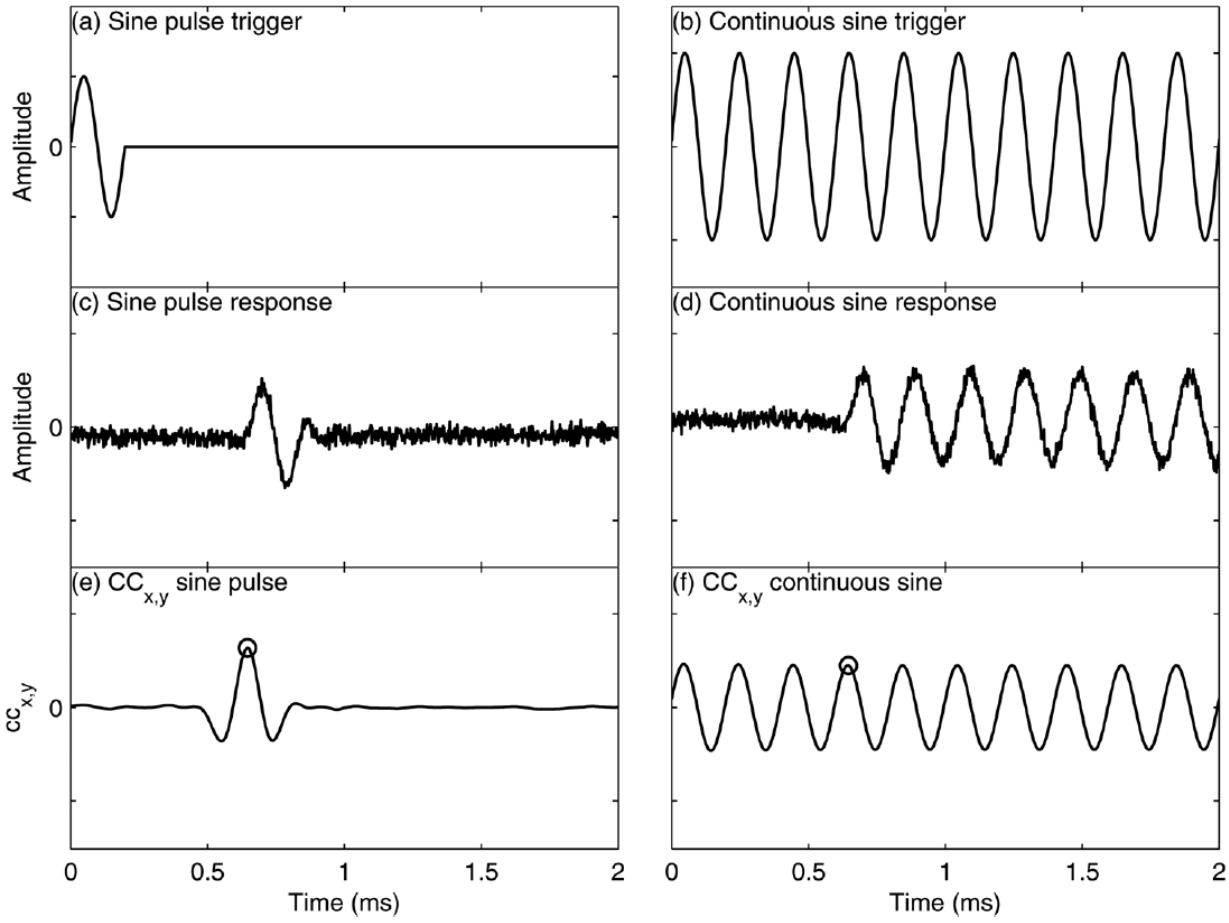

Figure 2-18. Synthetic bender-element trigger and response signals: (a) 5-kHz sine pulse trigger, (b) 5-kHz continuous sine-pulse trigger, (c) sine-pulse response, (d) continuous sine response, (e) cross correlation of sine-pulse trigger and response, and (f) cross correlation of continuous sine with circle point marking the peak cross correlation of the sine pulse. (Styler and Howie, 2013)

As shown in Fig.2-18a and b, the authors used two input/trigger signals to determine the absolute phase shift, θ_a ($\Delta\theta_a = \Delta\theta_r - 2\pi n$) at a single frequency. These two input signals are continuous sine wave over 20 ms and a sine pulse as shown in Fig.2-18 (a and b). Both these signals have the same frequency e.g. 5 kHz as shown in Fig.2-18. As shown in Fig.2-18e, the peak cross correlation of the sine pulse (single sine wave) takes place at 0.646 ms. The cross-correlation of the continuous sine signal yields a set of peaks [0.044, 0.244, 0.444, 0.644, 0.844 ms, ...] given in Fig.2-18f. The peak corresponding to the arrival of the shear wave is chosen based on the results of a sine-pulse

test. E.g. in Fig.2-18e, among the several peaks shown the one with time axis value of 0.644 min correlates to the sine-pulse results. This propagation time for the continuous sine wave and the frequency of the continuous wave is used to solve for the absolute phase shift $\Delta\theta_a$ at 5 kHz i.e. $\Delta\theta_a$ = -2πf Δt = -2π *5 kHz*0.644 ms = -20.30 radians.

The sweeping sine trigger frequency changes from 0 to 10 kHz over 20 ms as shown in Fig.2-19a. The output/response signal to this input is shown in Fig.2-19b. As seen in Fig.2-19b and comparing it with Fig-2.18 (c and d) it can be seen that the visual interpretation of the response of the sweeping sine input cannot take place in the time domain. Fig.2-19c shows that the sweeping sine-wave input has a wide band of uniform magnitude in the frequency domain. The same figure also shows that the magnitude of the output/response shows a peak at the resonant frequency of the bender element, 9 kHz.

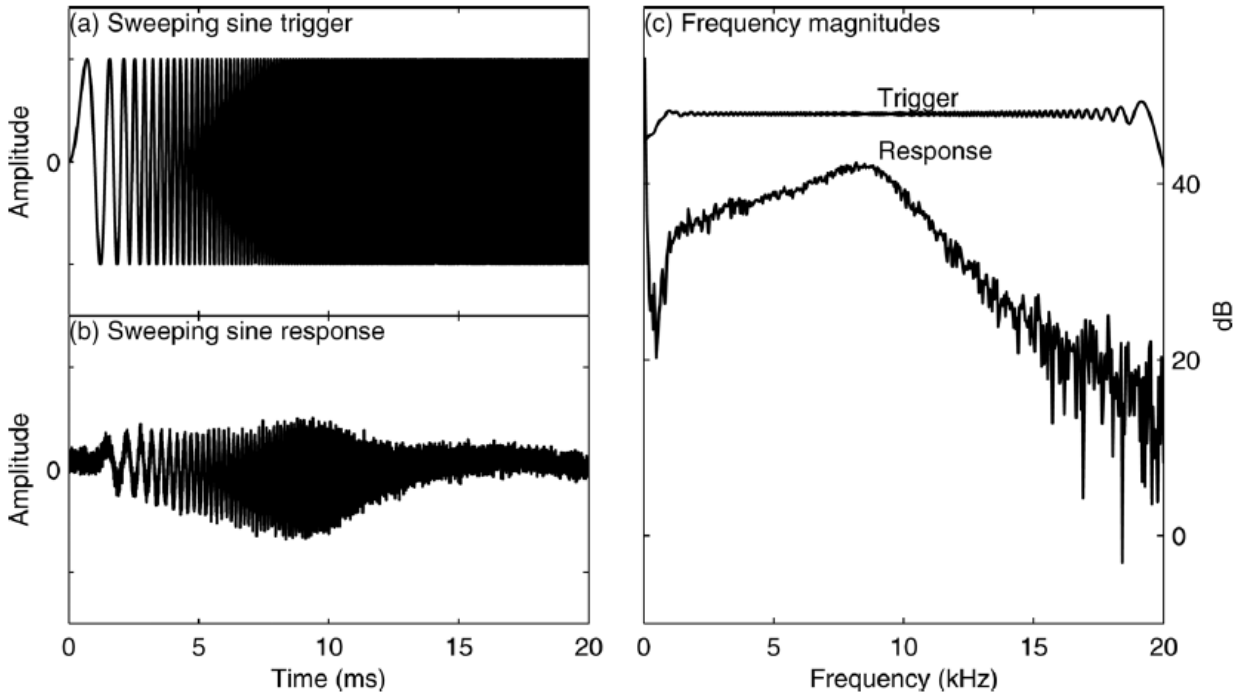

Figure 2-19. Synthetic bender-element results: (a) linear sweeping sine wave trigger, (b) response, and (c) magnitude of the trigger and response signals in the frequency domain. (Styler and Howie, 2013)

Fig.2-20a shows the calculated coherence function. The authors calculated the coherence function for the sweeping sine output by generating ten simulated bender-element signal. The coherence function gradually decreases for the frequencies higher than 12 kHz and it also drops off at low frequencies.

Fig.2-20c shows the calculated unwrapped phase shift, $\Delta\theta_r$ as a dashed line. At 5 kHz, $\Delta\theta_r$ is -13.92 radians. The $\Delta\theta_a$ determined at this frequency (5 kHz) in Fig.2-20 was -20.30 radians. The difference between these two values is the phase offset/phase degeneracy, ($2\pi n$). Since $\Delta\theta_a = \Delta\theta_r - 2\pi n$, $-20.30 = -13.92 - 2\pi n \Rightarrow -2\pi n = -6.38$ radians $\approx -2\pi$. The phase shift in Fig.2-20c is corrected by -6.38 radians and is shown by the solid line in Fig.2-20c. Knowing the corrected cross-power spectrum diagram, the phase velocity at any given frequency can be calculated using Eq.2.6. The procedure was repeated for many other input frequencies and new phase velocity at each new frequency was calculated using the discussed procedure. Fig.2-20d shows the variation of the measured V_{ph} with the input frequency. The group velocity was calculated from the slope of the phase shift in a moving 4-kHz frequency window such that the average of the frequency range corresponds to the value at which the V_{ph} is calculated.

The calculated $\Delta\theta_a$ is compared to the relative phase shift $\Delta\theta_r$ from the linear sweeping sine, to find the phase degeneracy, $-2\pi n$. The $\Delta\theta_a$ and $\Delta\theta_r$ are compared at multiple frequencies to confirm that they agree on the same phase degeneracy, i.e., that n is constant for each unwrapped relative phase shift. Once the relative phase shift and phase degeneracy are determined, Eq.2.10 can be solved for the phase velocity.

Although the authors reported a fair amount of merits of their proposed technique it can be seen in Fig.2-20d that the both the group and phase velocities are smaller than the actual shear wave velocity, with the V_{ph} being within 5 to 10 % of the specified velocity. Styler and Howie (2013) attributed this to the choice of resonance model that they used to represent the receiver element. As the travel distance reduces as in case of oedometer test specimens, the time of flight is highly influenced by the bender element transfer function (Wang et al., 2007; Lee and Santamarina, 2005).

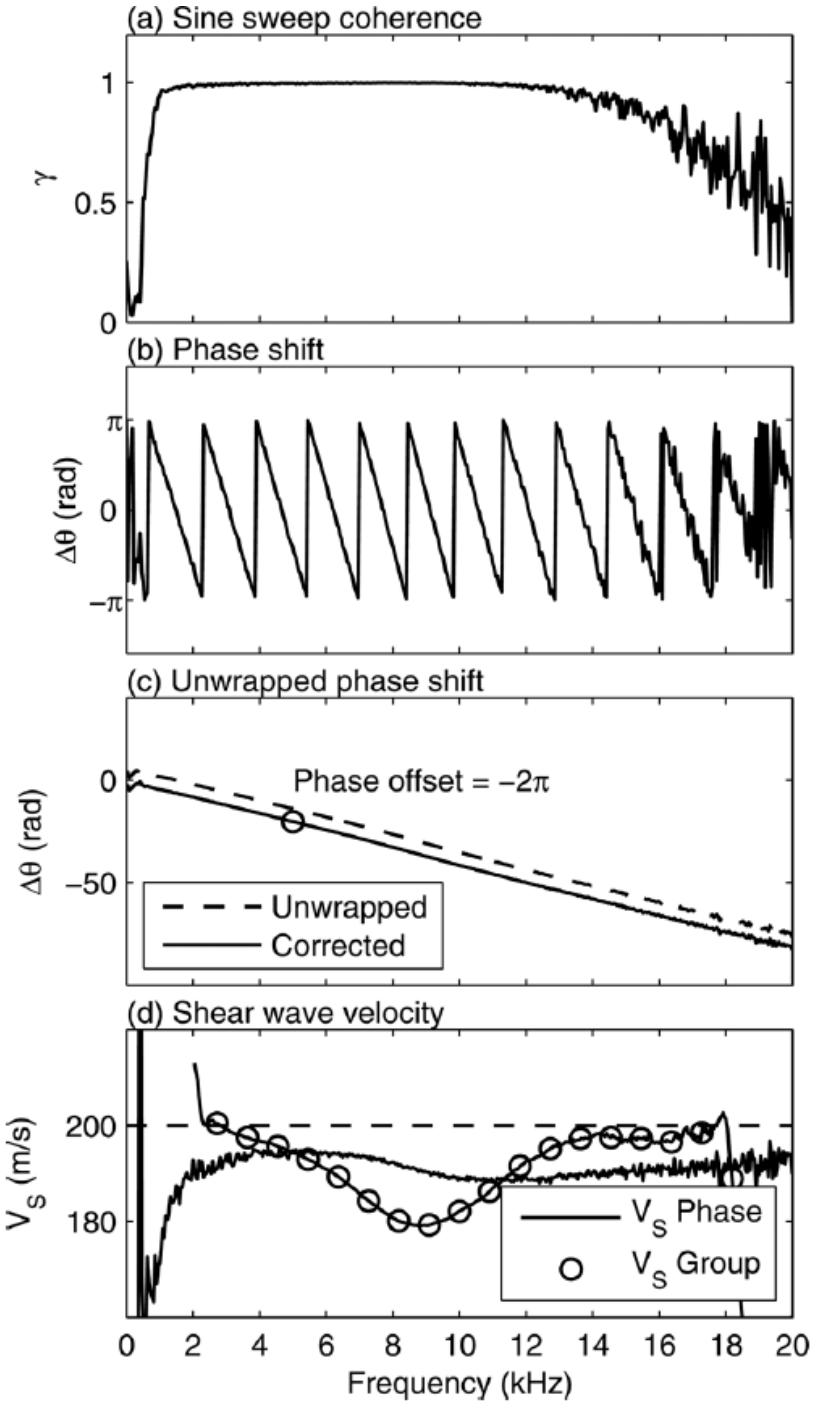

Figure 2-20. Interpreted synthetic frequency domain results: (a) coherence function, (b) calculated phase shift, (c) unwrapped and corrected phase shift, and (d) phase and group velocities. (Styler and Howie, 2013)

In a nutshell, their proposed phase velocity method uses only measured input values. Their method finds the relative phase shift ($\Delta\theta_r$) in the frequency domain, while the absolute phase shift ($\Delta\theta_a$) is determined in the time domain. $\Delta\theta_r$ and $\Delta\theta_a$ are used to correct the unwrapped relative phase shift (offset) and calculate the V_{ph} at a given frequency. They demonstrated that the input sine pulse signal frequency is arbitrary. All the used frequencies (7, 9, 11, and 13 kHz) resulted in the same phase offset.

2.7.4 Travel Time to First Direct Arrival in Output Signal

Travel time of an impulse wave between two points in space may be taken as the time between the first direct arrivals of the wave at each point. (Arulnathan et al. 1998). The underlying assumption for this method of interpretation is that there is no reflected or refracted waves and the wave fronts are plane. In other words, the time difference between the wave generated at source/emitter and the wave captured at receive at the receiver is time-of-flight using this technique.

For bender element tests using this method of analysis, the travel time has been estimated as the time between the start of the voltage pulse input to the transmitting bender and the first deflection in the output signal from the receiving bender. (Arulnathan et al. 1998). Different points have been suggested by several authors as the point of arrival of shear wave e.g. Points A, B and C and D in Fig.2-21.

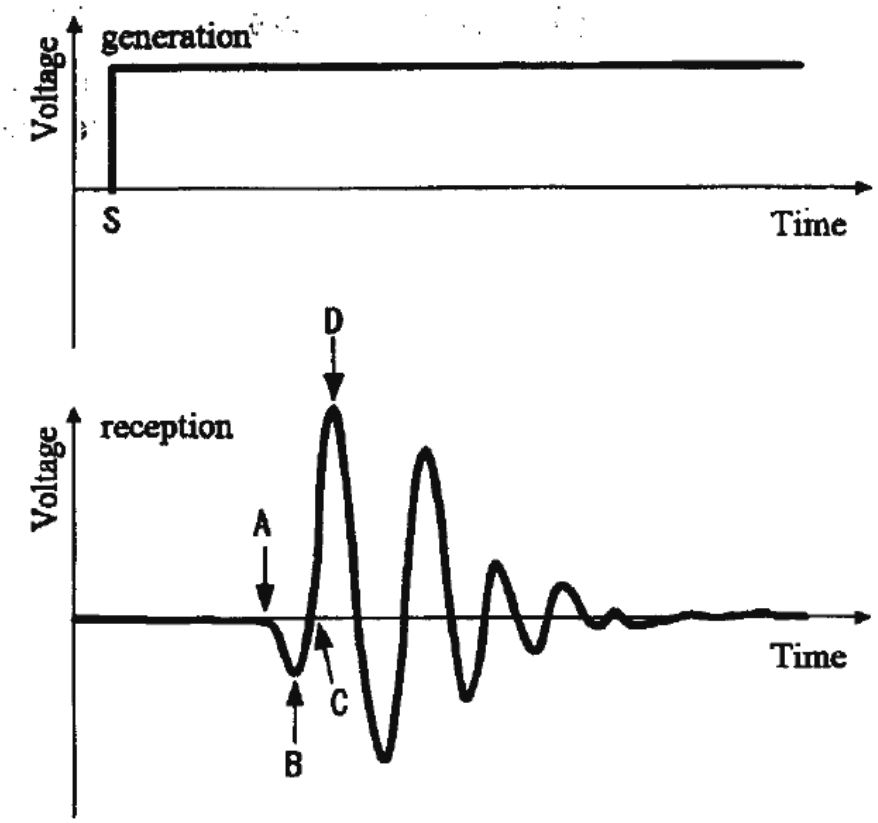

Figure. 2-21. Typical input (square) and output signals with points representing the possible arrival of shear wave. (Arulnathan et al. 1998)

Viggiani and Atkinson (1995), Arulnathan et al. (1998), Blewett et al. (1999) among many others reported the issues with the travel time measurement using this method. According to Blewett et al. (1999) this methods suffers from a major problem. The group velocity dispersion (GVD) in the sample leads to different frequency components within the voltage-edge wave form arriving at different times, thus severely distorting the transmitted signal. According to Arulnathan et al. (1998), interpretations based on the first direct arrival in the output signal are often masked by near-field effects and may be difficult to define reliably. Nevertheless, this method is one of the most commonly used the method of analysis due to its simplicity and has been widely used in the analyses of bender element signals and other similar pulse tests. The near field effects are typically controlled and overcome by using a high L/λ among many other factors.

E.g. Leong et al. (2005) preferred using the sinusoidal input voltage and travel time based on first deflection. Leong et al. (2005) suggested that the in order to improve the quality of the receiver signal: the signal-to-noise ratio (SNR) of the receiver signal should be kept at least 4 dB, and the wave path length to wavelength ratio (L_{tt}/λ) is at least 3.33. The SNR can be improved by increasing the applied voltage to the transmitter bender element using a power amplifier ensuring that the highest voltage should be lower than the one that causes depolarization. Leong et al. (2005) also suggested using filtering and stacking to the receiver signal and/or using signal amplifier for the receiver signal to further enhance the SNR of the received signal. Therefore, Leong et al. (2005) strongly advocated for using a power amplifier in a bender element test setup, whereas the signal amplifier is optional. The L_{tt}/λ can be enhanced by increasing the frequency of the applied voltage to the transmitter bender element.

2.7.5 Travel Time between Characteristic Peaks of Input and Output Signals

The travel time of an impulse signal between the two points in space can be taken as the time between the characteristics points in the signals recorded at these two points. The aforementioned statement hold true only for plane wave fronts and in the absence of any reflected or refracted waves (Arulnathan et al. 1998).

The travel time for a wave can be determined using these characteristics peaks as shown in Fig.2-22. The travel time might be taken as the time between Points A and A' (peak of input to the peak of output) or Points B and B′ (trough of input to the trough of output). It can also be taken as time between A′ to A″ (first peak of output (first arrival) to the first peak of output (second arrival)), B′ to B″ (first trough of output (first arrival) to the first trough of output (second arrival)), or C′ to C″ (second peak of output (first arrival) to the second peak of output (second arrival)).

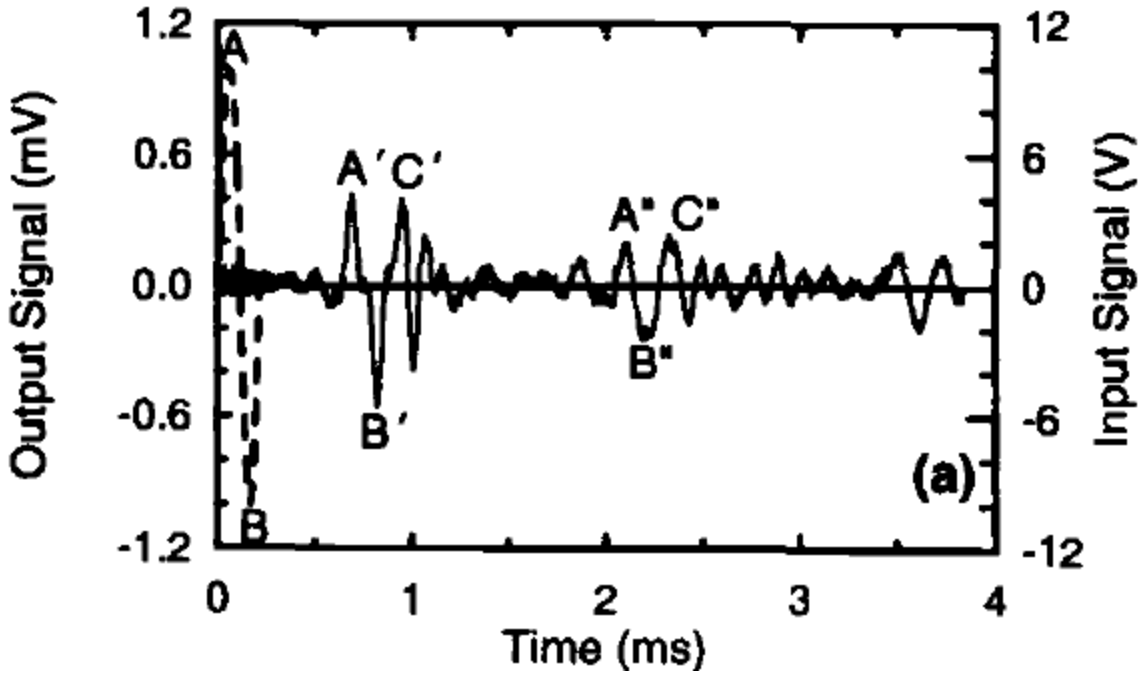

Figure. 2-22. Input and output signals from Bender test result on Sacramento River Sand, *f* = 4.5 kHz, (Arulnathan et al. 1998)

Arulnathan et al. (1998) performed 1D wave propagation and 2D finite element analysis and concluded that the travel time using characteristics peaks or cross-correlation between the input and output signals in BE tests are theoretically incorrect in most cases. The chief reasons being; (1) the output signal from the receiving bender is measuring a complex interaction of incident and reflected waves; (2) the transfer functions relating the physical wave forms to the measured electrical signals introduce significant phase or time lags that are different at the transmitting and receiving benders; and (3) non-1D wave travel and near field effects are not accounted for. Moreover, the coupling between the waves (compression and shear) obscure the first direct arrival of the shear waves and also affect the travel times calculated using characteristics peaks, cross-correlation, or phase velocity methods at locations near the source.

For an input sine signal, Viggiani and Atkinson, (1995) reported the travel time using different technique including cross-correlation, cross-power spectrum and by observing characteristics peaks and the travel time reported by all these method in general agreed well with each other.

Kawaguchi et al. (2001) validated the conclusions of Arulnathan et al. (1998) by reporting that peak-to-peak travel time between the input and output signals as suggested by Viggiani and Atkinson (1995) could essentially be incorrect. Such definition may only be practically acceptable when the frequency of shear wave is high enough.

2.7.6 Travel Time Using the Second Arrival in the Output Signal

The output response signal obtained from the work Arulnathan et al. (1998) i.e. Fig.2-22 clearly shows a second arrival of the input wave. This second arrival is in fact the input wave after the reflection from the receiver cap. The wave after reflection travels back to the transmitter cap and is reflected again back to the receiver cap for a second time. The time elapsed between the first and the second arrival in the output signal is equal to twice the travel time of the wave from cap to cap (Riemer et al. 1998). This is only true in case of plane wave propagation.

Arulnathan et al. (1998) found that the travel time and hence V_s values obtained using the second arrival method were essentially the same for interpretations based on finite element analysis either using the tip displacements or bending moments. Such an outcome is expected for the second arrival method because the effects of transfer functions and wave interference should be equally present in the first and second arrivals and thus should cancel out in the calculation of travel time.

Arulnathan et al. (1998) observed that the shear wave velocity found using the second arrival methods, tends to increase with increasing L_{tt}/λ, where L_{tt} is tip-to-tip distance between the bender element and λ is the wavelength. Their analysis also concluded that the V_s determined using the second arrival method provides a lower bound on the true V_s with the error being relatively small at L_{tt}/λ values greater than about 2.

Arulnathan et al. (1998) concluded that the travel time determination using this technique are hypothetically least affected the interference of waves at the specimen boundaries or the transfer functions that relate electrical signals to physical waves, but are still subjected to errors from nearfield and non 1D wave travel effects.

2.8 Empirical Correlations between V_s, G_{max} and Basic Soil Properties

There are several empirical correlations available in the literature based on the lab testing for both cohesive and cohesionless soils and their blends relating V_s and G_{max} to basic soil properties. Most of these lab tests based correlations for estimating V_s and G_{max} for cohesionless soils relate them with the void ratio and applied effective stress while the ones for cohesive soils usually includes a factor that depends upon the soil's plasticity and its stress history i.e. overconsolidation ratio (OCR). There are also many correlations based on the field testing relating the measured V_s and G_{max} with the measured field parameters most notably SPT and CPT values. Kallioglou et al., (2008) and Sawangsuriya (2012) complied and summarized the proposed relationships in literature for the estimation of G_{max} for cohesive and cohesive and cohesionless soils respectively, based on laboratory cyclic and dynamic tests (Fig.2-23 & Fig.2-24). It can be seen that all the correlations summarized in Fig.2-23 and Fig.2-24 for G_{max} have the following general form.

$$G_{max} = A\, f(e)\sigma_o'^{n} P_a^{\,1-n} g(OCR, PI) \tag{2.11}$$

where A is a constant, $f(e)$ is the void ratio function, σ_o' is the applied mean effective stress (confining stress), n is the stress exponent, P_a is the atmospheric pressure ($P_a \approx 100$ kPa), and g (OCR, PI) is the function of overconsolidation ratio (OCR) and plasticity index (PI) of the tested soils. G_{max} and σ_o' are in kPa.

Some of these lab and field correlations that are deemed important and relevant to the current study are presented in the following groups:

General form of equation†	Constants & functions: A	f(e)	n	g(PI, OCR)	Soil type	Testing method††	Reference
$G_{max} = A\, f(e)\, (\sigma'_o)^n$	3231	$(2.97\text{-}e)^2/(1+e)$	0.5		Kaolinite & Boston blue clay	R.C.	Hardin and Black [1968]
	445	$(4.4\text{-}e)^2/(1+e)$		0.5	Betonite PI = 60%	R.C.	Marcuson and Wahls [1972]
	4500	$(2.97\text{-}e)^2/(1+e)$	0.5		Kaolinite PI = 25%		
	141	$(7.32\text{-}e)^2/(1+e)$	0.6		Thirty natural soils (e = 1.5–4.0 & PI = 40–100 %)	C.T.	Kokusho *et al.* [1982]
	9600	$1/(1+1.2e^2)$	0.5		Clays (PI = 9–27 % & e = 0.583–1.068)	R.C.	Vrettos and Savidis [1999]
$G_{max} = A\, f(e)\, (\sigma'_v)^n$	5000	$1/e^{1.5}$	0.5		Seven clays	Lab & field tests	Shibuya and Tanaka [1996]
$G_{max} = A\, f(e)\, (\sigma'_o)^n\, (p_a)^{(1-n)}$	370	$1/(0.3+0.7e)^2$	0.54		Silty clays	R.C.	Stokoe *et al.* [1995]
	600	$1/e^{1.3}$	0.5		Quaternary Italian clays	Lab tests	Jamiolkowski *et al.* [1995]
	358	$1/e^{1.21}$	0.57		Sandy silts – silty sands	R.C.	D'Elia and Lanzo [1996]
	506	$1/e^{1.1}$	0.42		Clayey silts		
$G_{max} = A\, f(e)\, (\sigma'_o)^{ng\,(OCR,\,PI)}$	3231	$(2.97\text{-}e)^2/(1+e)$	0.5	OCR^K, K = g(PI)‡	PI = 0–85 %	R.C.	Hardin and Black [1969]
	1576	$(2.97\text{-}e)^2/(1+e)$	0.5		e = 0.48–1.36 & PI = 12–30 %	R.C.	Kim and Novak [1981]
$G_{max} = A\, f(e)\, (\sigma'_o)^n \times (p_a)^{(1-n)g\,(OCR,\,PI)}$	625	$1/(0.3+0.7e)^2$	0.5	OCR^K, K = g(PI)‡	Normally consolidated clays (e = 0.4–1.2)	R.C.	Hardin [1978]
	677	$1/(0.3+0.7e)^2$	0.487	OCR^K, K = 0.419	Kaolinite	R.C.	Athanasopoulos [1981]
$G_{max} = A\, p_r^{(1-n)}\, (\sigma'_o)^n \times g(OCR, PI)$	100 + 2900 × (1-PI/50)		0.6 + 0.25 × (PI/50) < 0.85	OCR^K, K = 0.18 + 0.1 × (PI /50) < 0.28	Clays p_r = 1kPa	B.E.	Viggiani and Atkinson [1995]
$G_{max} = A\, g\, (OCR)$	47750			OCR^K, K = 0.42	Kaolinite clay	R.C.	Athanasopoulos [1994]
$G_{max} = (\sigma'_o)^{ng\,(PI)}$			1	285−(2 × PI)	PI > 30%	R.C.	Zen *et al.* [1987]
$G_{max} = A\, (\sigma'_o)^{ng\,(PI)}$	280		0.82	$(1/(PI\text{-}Ir))^{(PI\text{-}Ir)}$ in decimal!	Mexico clay PI = 92–234% e = 4.00–9.37	R.C.	Romo [1995]
$G_{max} = f(e)\, (\sigma'_o)^{ng\,(PI)}$		$1/(0.4+0.7e)$	1	358–(3.8 × PI)	PI = 30–50%	R.C.	Kagawa [1992]

†G_{max} & σ'_o in kPa and p_a: atmospheric pressure (= 100 kPa).
††R.C.: Resonant-column test, C.T.: Cyclic triaxial test, B.E.: Bender element test.
‡K = 0, 0.18, 0.30, 0.41, 0.48, 0.50 for PI = 0, 20%, 40%, 60%, 80%, ≥ 100%, respectively.
!Ir = (LL-w)/PI.

Figure 2-23. Shear Modulus correlations of Cohesive Soils (Kallioglou et al. 2008)

Type of geomaterials	A	f(e)	n	References
Round-grained Ottawa sand	6,900	$(2.17-e)^2/(1+e)$	0.5	Hardin and Black (1968)
Angular-grained crushed quartz	3,270	$(2.97-e)^2/(1+e)$	0.5	
Clean sand	41,600	$0.67-e/(1+e)$	0.5	Shibata and Soelarno (1975)
Clean sand ($C_u < 1.8$)	14,100	$(2.17-e)^2/(1+e)$	0.4	Iwasaki and Tatsuoka (1977)
Clean sand	9,000	$(2.17-e)^2/(1+e)$	0.4	Iwasaki et al. (1978)
Toyoura sand	8,400	$(2.17-e)^2/(1+e)$	0.5	Kokusho (1980)
Clean sand	7,000	$(2.17-e)^2/(1+e)$	0.5	Yu and Richart (1984)
Ticino sand	7,100	$(2.27-e)^2/(1+e)$	0.4	Lo Presti et al. (1993)
Clean sand	9,300	$1/e^{1.3}$	0.45	Lo Presti et al. (1997)
Reconstituted NC Kaolinite (PI = 20) and undisturbed NC clays	3,270	$(2.97-e)^2/(1+e)$	0.5	Hardin and Black (1968)
Reconstituted NC Kaolinite (PI = 35)	4,500	$(2.97-e)^2/(1+e)$	0.5	Marcuson and Wahls (1972)
Reconstituted NC Bentonite (PI = 60)	445	$(4.4-e)^2/(1+e)$	0.5	
Remolded clay (PI = 0~50)	2,000~4,000	$(2.97-e)^2/(1+e)$	0.5	Zen et al. (1978)
Undisturbed NC clay (PI = 40~85)	90	$(7.32-e)^2/(1+e)$	0.6	Kokusho et al. (1982)
Clay deposits (PI = 20~150)	5,000	$1/e^{1.5}$	0.5	Shibuya and Tanaka (1996)†
Remolded clay (PI = 20~60)	24,000	$1/(1+e)^{2.4}$	0.5	Shibuya et al. (1997)†
Sand and clay	6,250	$1/(0.3+0.7e^2)$	0.5	Hardin (1978)
Several soils	5,700	$1/e$	0.5	Biarez and Hicher (1994)

Note: G_o and σ_o' are in kPa, † using effective vertical stress (σ_v') instead of σ_o' , Cu = Coefficient of Uniformity

Figure 2-24. Shear Modulus correlations of Cohesive and Cohesionless Soils (Sawangsuriya 2012)

2.8.1 Correlations presented by Hardin (1961), Hardin and Richart (1963) and Hardin and Black (1968).

Hardin (1961) and Hardin and Richart (1963) performed a series of Resonant Column tests on clean cohesionless soil specimens. They concluded that at very low shear strain amplitudes

(typically less than 10^{-3} %), the shear wave velocity, V_s, depends essentially upon the void ratio, e, and the effective confining pressure, σ_o'. The results were presented as the empirical correlations presented below.

$$V_s = (110.8 - 50.95e)\ \sigma_o'^{0.25} \tag{2.12}$$

For round-grained soils with $e < 0.8$

$$V_s = (103.6 - 34.93e)\ \sigma_o'^{0.25} \tag{2.13}$$

For angular-grained soils.

$$V_s = (103.6 - 34.93e)\ OCR^K\ \sigma_o'^{0.25} \tag{2.14}$$

For the above equations (2.12-2.14), V_s in m/s and σ_o' in kPa. Hardin and Black (1968) found that the Eq.2.13 also gave reasonable results for normally consolidated clays of low surface activity at the end of one day of pressure application. Thus Eq.2.13 can be used as a first estimate of the V_s for a cohesive soil. A slightly modified version of Eq.2.13 is Eq.2.14 by introducing a factor accounting for the Plasticity (K = f (PI)) and stress history (OCR).

2.8.2 Correlations presented by Kim and Novak (1981)

Kim and Novak (1981) tested seven undisturbed cohesive soils from Ontario using resonant column test and presented their work in terms of empirical correlations for V_s and G_{max} with other clay properties. For example, V_s to void ratio and OCR, i.e.

$$V_s = (73.03 - 33.86e)\ OCR^{\frac{K}{2}}\ \sigma_o'^{0.25} \tag{2.15}$$

where V_s is shear wave velocity (m/s), e is void ratio, OCR is overconsolidation ratio, K is a function of plasticity index, σ_o' is the mean effective pressure or confining pressure in (kPa). Kim and Novak (1981) compared their results with Hardin and Black (1968) and found that the empirical correlation suggested by Hardin and Black (1968) significantly overestimates the V_s for the examined cohesive soils. They also evaluated G_{max} independent of V_s measurements and compared the measured G_{max} with the findings of Hardin and Black (1968) and found that the upper

bound for G_{max} defined by Hardin and Black (1968) significantly overestimates G_{max} and most of their measured values were clustered around the lower bound. They attributed these discrepancies to greater sensitivity of silty materials to confining pressure, the effects of fissures and weathering in clays and the non-linear relationship between e and V_s for $e < 0.6$.

Kim and Novak (1981) revised the Hardin and Black (1968) equation to better describe the observed behavior of the tested soils, i.e.

$$G_{max} = \frac{C_o\,(2.973 - e^2)}{1 + e}\,OCR^K\,\sigma_o'^{0.5} \tag{2.16}$$

where C_o is a constant and n is the slope of the G_{max}-σ_o' function. . For normally consolidated soil, n varied between 0.46-0.61 with an average of 0.55, C_o varied between 893-1726 with an average of 1395. For overconsolidated clay, n ranged between 0.51-0.73 with an average of 0.65 while C_o varied between 443-1450 with an average of 767. Kim and Novak (1981) concluded that for clay with $e < 0.8$, the effect of confining pressure on G_{max} is more important than OCR.

2.8.3 Correlation presented by Shibuya et al. (1997)

Shibuya et al. (1997) evaluated the results of field seismic surveys and laboratory bender element tests on reconstituted clay specimens and suggested an empirical expression for G_{max} of normally consolidated soft clays, i.e.

$$G_{max} = A\,(1 + e)^{-2.4}\,\sigma_v'^{0.5} \tag{2.17}$$

where σ_v' is the vertical effective stress and A is a soil-dependent constant. The void's ratio function $F(e)$ = (1+e) avoided sharp reduction in G_{max} as $e \rightarrow 2.973$ as in the case of Hardin and Black (1968) void ratio function. Shibuya et al. (1997) reported that using an appropriate $F(e)$, such as theirs, the OCR has negligible influence on G_{max}. Shibuya et al. (1997) reported the A values between 18000 and 30000 with an average value of 24000

2.8.4 Correlation presented by Vardanega and Bolton (2013)

Vardanega and Bolton (2013) compiled the data available in the literature including the work of Kim and Novak (1981) along with the $F(e)$ proposed by Shibuya et al. (1997). Unlike Shibuya et

al. (1997), Vardanega and Bolton (2013) presented a semi-empirical expression in terms of mean effective stress (σ_m' or p') Eq.2.18, i.e.

$$\frac{G_{max}}{P_r'} = \frac{B}{(1+e)^{2.4}}\left(\frac{P'}{P_r'}\right)^{0.5} \tag{2.18}$$

In Eq.2.18, p_r' is the reference pressure taken as 1 kPa (to give equation a dimensionless form). For stiff, overconsolidated aged clays, a very high ***B*** value ≈ 50,000 was found. ***B*** values of <15,000 was reported for highly fissured London clay. But for most soft soils, the authors reported that parameter ***B*** generally varies between 15,000 and 25,000 with an average of 20,000.

2.8.5 Correlations presented by Robertson et al. (1995)

Robertson et al. (1995) tested Ottawa sand (C-109) with *e* varying between 0.89 (very loose) to 0.57 (dense) in a triaxial apparatus using bender elements. Specimens were isotropically consolidated and the consolidation completed within a minute of the application of each consolidation stress increment, but the specimen was allowed 5 min before taking V_s readings. They proposed a relationship between V_s, *e* and σ'_m, i.e.

$$V_s = (381 - 259e)\left(\frac{\sigma_m'}{P_a}\right)^{0.26} {}^{m}/_{sec} \tag{2.19}$$

Where *e* is the void ratio, σ'_m (kPa) is the mean effective stress and P_a is the atmospheric pressure (≈ 100 kPa) and the material constants 381 and 259 are in velocity units. The stress exponent of 0.26 is close to the 0.25 proposed by Hardin and Richart (1963). To evaluate the relationship among the three independent measurements (V_s, *e*, σ'_m), they normalized the V_s values using σ'_m. The normalized shear wave velocity, V_{s1} is given below

$$V_{s1} = V_s\left(\frac{P_a}{\sigma_m'}\right)^{0.26} \tag{2.20}$$

They found that V_{s1} for Ottawa sand is linearly related to *e*, i.e.

$$V_{s1} = (381 - 259e)\ {}^{m}/_{sec} \tag{2.21}$$

2.9 Penetration-Based V_S Correlations

Several researchers have studied and presented the relations between the V_s and penetration test results that include SPT, CPT and the Becker Penetration test (BPT). G_{max} and V_s are small strain properties while the penetration tests are conducted at large strains associated with the failure of the soil surrounding the sampler or cone (Wair et al. 2012).

Although being at the two extremes in terms of the applied strain, both the small-strain soil properties and the penetration-based tests have some similarity. Both of them are primarily depending upon on the void ratio, applied confining stress, and the stress history (Wair et al. 2012). Despite being at the opposite ends of the strain spectrum, this common association can be used to develop correlations between the two parameters (Mayne and Rix 1993).

Wair et al. (2012) reported from Sykora (1987) that in addition to penetration resistance itself, estimation of low-strain properties (V_s and G_{max}) is improved when supplementary parameters such as confining stress (depth), geology (depositional environment, aging, etc.), and soil type are considered.

Author(s)	I.D.	All soils	Sand	Silt	Clay
Shibata (1970)	A	-	$V_s = 31.7\ N^{0.54}$	-	-
Ohba and Toriuma (1970)	B	$V_s = 84\ N^{0.31}$	-	-	-
Imai and Yoshimura (1975)	C	$V_s = 76\ N^{0.33}$	-	-	-
Ohta et al (1972)	D	-	$V_s = 87.2\ N^{0.36}$	-	-
Fujiwara (1972)	E	$V_s = 92.1\ N^{0.337}$	-	-	-
Ohsaki and Iwasaki (1973)	F	$V_s = 81.4\ N^{0.39}$	-	-	-
Imai et al (1975)	G	$V_s = 89.9\ N^{0.341}$	-	-	-
Imai(1977)	H	$V_s = 91\ N^{0.337}$	$V_s = 80.6\ N^{0.331}$	-	$V_s = 80.2\ N^{0.292}$
Ohta and Goto (1978)	I	$V_s = 85.35\ N^{0.348}$	-	-	-
Seed and Idriss (1981)	J	$V_s = 61.4\ N^{0.5}$	-	-	-
Imai and Tonouchi (1982)	K	$V_s = 96.9\ N^{0.314}$	-	-	-
Sykora and Stokoe (1983)	L	-	$V_s = 100.5\ N^{0.29}$	-	-
Jinan (1987)	M	$V_s = 116.1\ (N+0.3185)^{0.202}$	-	-	-
Okamoto et al (1989)	N	-	$V_s = 125\ N^{0.3}$	-	-
Lee (1990)	O	-	$V_s = 57.4\ N^{0.49}$	$V_s = 105.64\ N^{0.32}$	$V_s = 114.43\ N^{0.31}$
Athanasopoulos (1995)	P	$V_s = 107.6\ N^{0.36}$	-	-	$V_s = 76.55\ N^{0.445}$
Sisman (1995)	Q	$V_s = 32.8\ N^{0.51}$	-	-	-
Iyisan (1996)	R	$V_s = 51.5\ N^{0.516}$	-	-	-
Kanai (1966)	S	$V_s = 19\ N^{0.6}$	-	-	-
Jafari et al (1997)	T	$V_s = 22\ N^{0.85}$	-	-	-
Kiku et al (2001)	U	$V_s = 68.3\ N^{0.292}$	-	-	-
Jafari et al (2002)	V	-	-	$V_s = 22\ N^{0.77}$	$V_s = 27\ N^{0.73}$
Hasancebi and Ulusay (2006)	W	$V_s = 90\ N^{0.309}$	$V_s = 90.82\ N^{0.319}$	-	$V_s = 97.89\ N^{0.269}$
Ulugergerli and Uyanık (2007)	X	$^{a}V_{SU} = 23.291\ Ln(N)+405.61$	-	-	-
Ulugergerli and Uyanık (2007)	Y	$^{b}V_{SL} = 52.9\ e^{-0.011N}$	-	-	-
Dikmen (2009)	Z	$V_s = 58\ N^{0.39}$	$V_s = 73\ N^{0.33}$	$V_s = 60\ N^{0.36}$	$V_s = 44\ N^{0.48}$
Pitilakis et al. (1999)	AA	-	$V_s = 145(N_{60})^{0.178}$	-	$Vs = 132(N_{60})^{0.271}$
Hasancebi and Ulusay (2006)	AB	$V_s = 104.79(N_{60})^{0.26}$	$V_s = 131(N_{60})^{0.205}$		$V_s = 107.63(N_{60})^{0.237}$

Figure 2-25. V_s-SPT-N correlations (Bellana (2009))

where N = SPT N, N_{60} = SPT N corrected for 60% hammer efficiency

SPT is been the most popular and most widely performed field/in-situ geotechnical test around the globe. It is also the most well studied and most correlated test with the V_s. The common practice of normalizing SPT N-values by the reference effective overburden pressure is not appropriate to be exercised for the purpose of site classification, estimation of V_s from the penetration data, and or/ calculation of V_{s30}.

Soil Type	Study	Geologic Age	Number of Data Pairs	r^2	V_S (m/s)
All Soils	Hegazy & Mayne (1995)	Quaternary	323	0.70	$(10.1 \log(q_c) - 11.4)^{1.67} (100\ f_s/q_c)^{0.3}$
	Mayne (2006)	Quaternary	161	0.82	$118.8 \log(f_s) + 18.5$
	Piratheepan (2002)	Holocene	60	0.73	$32.3\ q_c^{0.089}\ f_s^{0.121}\ D^{0.215}$
	Andrus et al. (2007)	Holocene & Pleistocene	185	(H) 0.71 (P) 0.43	$2.62\ q_t^{0.395}\ I_C^{0.912}\ D^{0.124}\ SF^a$
	Robertson (2009)	Quaternary	1,035	----	$[(10^{(0.55Ic+1.68)})\ (q_t - \sigma_v) / p_a\ ]^{0.5}$
Sand	Sykora & Stokoe (1983)	----	256	0.61	$134.1 + 0.0052\ q_c$
	Baldi et al. (1989)	Holocene	----	----	$17.48\ q_c^{0.13}\ \sigma'^{0.27}_v$
	Hegazy & Mayne (1995)	Quaternary	133	0.68	$13.18\ q_c^{0.192}\ \sigma'^{0.179}_v$
	Hegazy & Mayne (1995)	Quaternary	92	0.57	$12.02\ q_c^{0.319}\ f_s^{-0.0466}$
	Piratheepan (2002)	Holocene	25	0.74	$25.3\ q_c^{0.163}\ f_s^{0.029}\ D^{0.155}$
Clay	Hegazy & Mayne (1995)	Quaternary	406	0.89	$14.13\ q_c^{0.359}\ e_0^{-0.473}$
	Hegazy & Mayne (1995)	Quaternary	229	0.78	$3.18\ q_c^{0.549}\ f_s^{0.025}$
	Mayne & Rix (1995)	Quaternary	339	0.83	$9.44\ q_c^{0.435} e_0^{-0.532}$
	Mayne & Rix (1995)	Quaternary	481	0.74	$1.75\ q_c^{0.627}$
	Piratheepan (2002)	Holocene	20	0.91	$11.9\ q_c^{0.269}\ f_s^{0.108}\ D^{0.127}$

Units: q_c, q_t, f_s, σ_v, and σ'_v are measured in kilopascals (kPa), and depth (D) is measured in meters (m). $p_a = 100$ kPa.
[a]SF = 0.92 for Holocene and 1.12 for Pleistocene

Figure 2-26. *V_s*-CPT-*q* correlations (Wair et al. 2012)

where q_c = measured cone penetration resistance, q_t = total cone tip resistance, f_s = sleeve friction, σ_v = overburden pressure, σ'_v = effective overburden pressure, e_o = insitu void ratio

Wair et al. (2012) have compiled a large data base of the correlation between the SPT-N and V_s for a wide range of soils. Other researcher including Bellana (2009) have done the same. Out of the huge data base of such correlations a few of them are summarized in Fig.2-25 taken from the work of Bellana (2009).

Just like SPT, CPT is also an extremely popular field test and very well documented in the literature. There is vast amount of correlations available in the literature correlating V_s with the CPT results. Out of such enormous data, Wair et al. 2012 have compiled a few popular correlations summarized and presented in Fig.2-26. In these correlations, D is the depth in meters, while f_s, q_c and σ'_v are sleeve friction resistance, measured tip resistance and effective overburden pressure respectively in kPa. Wair et al. 2012 have modified the original equations to have unit consistency (SI units).

Typically, CPT measurements are taken every 5 cm, whereas V_s measurements are taken every 1 to 1.5 m (Robertson, 2009). The scatter in data (low r^2) for CPT-based correlations is due to this reason. The correlations given in Fig.2-26 are presented in their original form. If pore pressure measurements are available, correlations presented herein should use the corrected cone resistance q_t especially for cohesive (soft fine-grained) soils. The correction is relatively insignificant for sands (less than 10% error) (Wair et al. 2012). The detailed list of reference for all the researches mentioned in Figs.2-25 and 2-26 can be found in the respective articles they are taken from.

References

Airey D., Mohsin A.K.M., (2013). "Evaluation of shear wave velocity from bender elements using cross-correlation." *Geotechnical Testing Journal* 36(4): 506-514.

AnhDan, L.Q., Koseki, J., and Sato, T., (2002)."Comparison of Young's Moduli of Dense Sand and Gravel Measured by Dynamic and Static Methods." Geotechnical Testing Journal, 25(4), 349-368.

APC International. <https://www.americanpiezo.com/> [Accessed 24 Nov. 2015].

Arroyo, M., Muir Wood, D., Greening, P. D., Medina, L., and Rio, J. (2006). "Effects of sample size on bender-based axial G_o measurements." *Geotechnique,* 56(1), 39–52.

Arulnathan, R., Boulanger, R.W. and Riemer, M.F., (1998). "Analysis of bender element tests." *ASTM Geotechnical Testing Journal*, 21(2), 120-131.

ASTM D4015 – 15. (2015) "Standard Test Methods for Modulus and Damping of Soils by Fixed-Base Resonant Column Devices." *ASTM International, West Conshohocken, PA*, 2015, DOI: 10.1520/D4015-15, www.astm.org.

Bellana, N., (2009). Shear wave velocity as function of SPT penetration resistance and vertical effective stress at California bridge sites, Master dissertation, University of California, Los Angeles.

Biot, M. A., (1956a). "Theory of Propagation of Elastic Waves in a Fluid-Saturated Porous Solid. I. Low Frequency Range," J. Acoust. Soc. Am., 28(2), 168–178.

Biot, M. A., (1956b). "Theory of Propagation of Elastic Waves in a Fluid-Saturated Porous Solid. II. Higher Frequency Range," J. Acoust. Soc. Am., 28(2), 179–191.

Blewett, J., Blewett, I. J., Woodward, P.K. (1999), "Measurement of Shear-Wave Velocity Using Phase-Sensitive Detection Techniques." *Canadian Geotechnical Journal*, 36 (5), 934-939.

Brignoli, E. M., Goti, and Stokoe, II (1996). "Measurement of Shear Waves in Laboratory Specimens by Means of Piezoelectric Transducers." *ASTM Geotechnical Testing Journal*, 19(4), 384-397.

Camacho-Tauta, F.J., Alvarez, J.D.J and Reyes-Ortiz, J.O, (2012). "A procedure to calibrate and perform the bender element test." Dyna, 79(176), 10-18.

Drnevich, V. P., (1967). "Effects of strain history on the dynamic properties of sand," Ph.D. Thesis, University of Michigan, 151 pp.

Drnevich, V.P., (1972). "Undrained cyclic shear of saturated sand." *ASCE Journal of Soil Mechanics & Foundations Division*, 98(8), 807-825.

Dyvik, R. Madshus, C. (1985). "Lab Measurements of Gmax Using Bender Elements." *Proc. ASCE Annual Convention, Advances in the Art of Testing Soils under Cyclic Conditions*, Detroit, Michigan, 186-196.

Electrical Power Research Institute (EPRI) "Guidelines for Determining Design Basis Ground Motions," Final Report, EPRI TR-102293, Palo Alto, CA, November 1993.

Ferreira, C., da Fonseca, A. and Santos, J.A., 2007. "Comparison of simultaneous bender elements and resonant column tests on Porto residual soil." *In Soil Stress-Strain Behavior: Measurement, Modeling and Analysis, Vol 146 of Solid Mechanics and Its Applications*, 523-535 Springer Netherlands.

Gamal El-Dean, D., (2007). Development of a new piezo-electric pulse testing device and soil characterization using shear waves (Doctoral dissertation, These de doctorat en genie civil, Université de Sherbrooke).

Greening, P. D. and Nash, D. F. T. (2002). "Frequency Domain Determination of G0 Using Bender Elements." *ASTM Geotechnical Testing Journal*, 27(3), 1-7

Gu, X., Yang, J. and Huang, M., (2013). "Laboratory measurements of small strain properties of dry sands by bender element." *Soils and Foundations*, 53(5), 735-745.

Hardin, B.O., (1961). “Study of elastic wave propagation and damping in granular materials.” University of Florida at Gainesville, Florida.

Hardin, B.O., Black, W.L., (1968). “Vibration modulus of normally consolidated clay,” *Journal of the Soil Mechanics and Foundation Division, ASCE,* 94 (2): 353–369.

Hardin, B.O., Richart, E.F Jr., (1963). “Elastic wave velocities in granular soils,” *Journal of the Soil Mechanics and Foundation Division, ASCE,* 89 (1): 33–65.

Ismail, M. A. & Rammah, K. I. (2006). “A New Setup for Measuring Go during Laboratory Compaction.” *ASTM Geotechnical Testing Journal*, 29(4), 1-9.

Jovicic, V., Coop. M. R. and Simic, M. (1996). “Objective Criteria for Determining G_{max} from Bender Element Tests”. Technical Note, *Geotechnique,* 46(2), 357-362

Kallioglou, P., Tika, Th. and Pitilakis, K. (2008). “Shear Modulus and Damping Ratio of Cohesive Soils.” *Journal of Earthquake Engineering*. 12(6), 879 – 913.

Kawaguchi, T., Mitachi, T. and Shibuya, S. (2001), “Evaluation of Shear Wave Travel Time in Laboratory Bender Element Test.” the XVth International Conference on Soil Mechanics and Geotechnical Engineering, Istanbul, August 27-31, 155-158.

Kim, T., Zapata-Medina, D.G. and Vega-Posada, C.A., 2015. “Analysis of Bender Element signals during triaxial testing.” *Revista Facultad de Ingeniería Universidad de Antioquia*, (76), 107-113.

Kim, T.C. and Novak, M., (1981). “Dynamic properties of some cohesive soils of Ontario.” *Canadian Geotechnical Journal*, 18(3), 371-389.

Kramer, S.L., (1996). “Geotechnical Earthquake Engineering” (Vol. 80). Upper Saddle River, NJ: Prentice Hall.

Kumar, J. and Madhusudhan, B.N., (2010). “Effect of relative density and confining pressure on Poisson ratio from bender and extender elements tests.” *Géotechnique,* 60(7), 561-567.

Lee, J.-S., and Santamarina, J. C., 2005, "Bender Elements: Performance and Signal Interpretation," *ASCE Journal of Geotechnical and Geoenvironmental Engineering*, 131(9), 1063–1070.

Leong, E.C., Cahyadi, J. and Rahardjo, H., (2009). "Measuring shear and compression wave velocities of soil using bender-extender elements." *Canadian Geotechnical Journal*, 46(7), 792-812.

Leong, E.C., Yeo, S.H. and Rahardjo, H., (2005). "Measuring shear wave velocity using bender elements." *Geotechnical Testing Journal*, 28(5), 488-498.

Lings, M. L., Greening, P. D. (2001). "A Novel Bender/Extender Element for Soil Testing, Technical Note." *Geotechnique*, 51, (8), 713-717.

Mancuso, C., Simonelli, A. L., Vinale, F. (1989). "Numerical Analysis of in Situ S-Wave Measurements", *In Proc., 12th Int. Conf. on Soil Mechanics and Foundation Engineering, Rio de Janeiro*, 277-280.

Mayne, P.W., and Rix, G.J. (1993). "G_{max}-q_c relationships for clays." *ASTM Geotechnical Testing Journal,* 16 (1), 54-60.

Mitaritonna, G., Amorosi, A. and Cotecchia, F., (2010). "Multidirectional bender element measurements in the triaxial cell: equipment set-up and signal interpretation." *RIG Rivista Italiana di Geotecnica*, 44(1), 50-69.

Nakagawa, K., Soga, K. and Mitchell, J. K. (1996). "Pulse Transmission System for Measuring Wave Propagation in Soils." *Journal of Geotechnical Engineering*, 122(4), 302-308.

Riemer, M. F., Gookin, W. B., Bray, J. D., and Wartman, J., (1998), "Using Reflected Shear Waves to Measure Small Strain Dynamic Properties," Research Report No. UCB/GT-98-01, Department of Civil Engineering, University of California, Berkeley, CA.

Robertson, P.K., (2009). "Interpretation of cone penetration tests-a unified approach." *Canadian Geotechnical Journal*, 46(11), 1337-1355.

Robertson, P.K., Sasitharan, S., Cunning, J.C. and Sego, D.C., (1995). “Shear-wave velocity to evaluate in-situ state of Ottawa sand.” *Journal of Geotechnical Engineering*, 121(3), 262-273.

Sanchez-Salinero, I., Roesset, J. M. & Stokoe, K. H. (1986). “Analytical studies of body wave propagation and attenuation.” Geotechnical Report GR 86-15, Civil Engineering department, University of Texas, Austin.

Sawangsuriya, A., (2012). “Wave Propagation Methods for Determining Stiffness of Geomaterials.” INTECH Open Access Publisher.

Shibuya, S., Hwang, S.C., Mitachi, T., (1997). “Elastic shear modulus of soft clays from shear wave velocity measurement.” Géotechnique 47 (3), 593–601.

Shirley, D. J. (1978). “An improved shear wave transducer.” J. Acoust. Soc. Am., 63(5), 1643–1645.

Shirley D. J. and Hampton L. D. (1978). “Shear-wave measurements in laboratory sediments.” *Journal of the Acoustical Society of America*, 63(2), 607-613.

Styler, M.A. and Howie, J.A., 2013. “Combined Time and Frequency Domain Approach to the Interpretation of Bender-Element Tests on Sand.” *ASTM Geotechnical Testing Journal*, 36(5), 649-659.

Suwal, L.P. and Kuwano, R., (2013). “Disk shaped piezo-ceramic transducer for P and S wave measurement in a laboratory soil specimen.” *Soils and foundations*, 53(4), 510-524.

Sykora, DW (1987). “Examination of existing shear wave velocity and shear modulus correlations in soils.” *Department of the Army, Waterways Experiment Station, Corps of Engineers*, Miscellaneous Paper GL-87-22.Vardanega, P. J. and Bolton, M. D. (2013). "Stiffness of clays and silts: normalizing shear modulus and shear strain." *Journal of Geotechnical and Geoenvironmental Engineering* 139 (9): 1575 – 1589.

Viggiani, G. and Atkinson, J. H. (1995), “Interpretation of Bender Element Tests.” Technical Note, *Geotechnique*, 45, (1), 149-154.

Vilhar, G. and Jovičić, V., (2009). “Measurement and interpretation of the small strain stiffness of boštanj silty sand.” *Acta Geotechnica Slovenica*, 6(2), 57-75.

Vucetic, M. and Dobry, R. (1991). "Effect of Soil Plasticity on Cyclic Response." *Journal of Geotechnical Engineering*, 1(89), 89-107.

Wair, B.R., DeJong, J.T. and Shantz, T., (2012). “Guidelines for estimation of shear wave velocity profiles.” *Pacific Earthquake Engineering Research Center, PEER Report*, 8.

Wang, Y. H., Lo, K. F., Yan, W. M., and Dong, X. B., 2007, “Measurement Biases in the Bender Element Test.” *ASCE Journal of Geotechnical and Geoenvironmental Engineering*, 133(5), 564–574.

Yamashita, S., Kawaguchi, T., Nakata, Y., Mikami, T., Fujiwara, T. and Shibuya, S., (2009). “Interpretation of international parallel test on the measurement of G_{max} using bender elements.” *Soils and Foundations*, 49(4), 631-650.

Yu, B., (2013). “Advancements in resonant column testing of soils using random vibration techniques” (Doctoral dissertation, Iowa State University).

Chapter 3

3 Measurements of Shear Wave Velocity of Sand Using a Novel Piezoelectric Device

3.1 Abstract

A new piezoelectric device for measuring shear wave velocity of soils was developed. A new piezoelectric device for measuring shear wave velocity of soils was fabricated based on the original development at University of Sherbrooke (e.g. Gamal El Dean, 2007). The oedometer PRA setup was fabricated at University of Western Ontario from scratch with modifications to improve the performance of the PRA setup and hence the quality of the output signals.Ring actuators were used to generate planar shear waves to eliminate several issues associated with bender elements tests. The fabrication and testing of the developed device and its use for measuring the shear wave velocity (V_s) of a sand is presented. The testing setup incorporates piezoelectric ring-shape transducers into an oedometer cell in order to generate shear waves at one end and record the arrival of the waves at the other end of a soil specimen. The fabricated device was rigorously examined by measuring the V_s of a well characterized material (Ottawa sand). The device performance was further verified by comparing its measurements with those obtained using bender elements under the same testing conditions. Furthermore, the effects of different factors on the V_s of Ottawa sand were examined using the fabricated device. The studied factors include initial state/void ratio (e_o), vertical/mean effective stress (σ_v'/σ_m'), mean particle size (D_{50}), and fines content (FC). The results showed that the measured V_s values using the developed device were in good agreement with the results published in literature. For a given e, V_s and hence low strain shear modulus, $G_{max,}$ increase by increasing σ'_m, while *f*or a given e, and σ_m', V_s was found to be independent of mean particle size (D_{50}). The FC was found to significantly reduce G_{max}. An empirical correlation for the low strain shear modulus of clean Ottawa sand is also presented. Furthermore, as a preliminary investigation the obtained signals from the fabricated device were used to evaluate the dynamic Poisson's ratio (v) of clean Ottawa sand.

Keywords: Piezoelectric ring actuators, shear wave velocity, dynamic shear modulus, Ottawa sand, fines content, Poisson's ratio.

3.2 Introduction

The shear modulus, G_{max}, is a key parameter in dynamic analyses such as soil-structure interaction during earthquakes, blasting, or machine or traffic vibrations (Thomann and Hryciw, 1990). There are different field and laboratory techniques that can be used to measure the shear modulus, $G_{max.}$ Field tests include seismic reflection and refraction, suspension logging, steady-state vibration, spectral analysis of surface waves, seismic cross-hole and seismic down-hole (Kramer, 1996). Laboratory tests to measure G_{max} include: resonant column (RC) test (Khan et al., 2008), ultrasonic pulse test (Khan et al., 2011) and the piezoelectric bender element (BE) test (Dyvik and Madshus, 1985). RC and BE are the common and popular tests used to measure, V_s, while there are some concerns associated with them. The RC test is relatively expensive and involves dedicated and typically expensive device that requires time consuming specimen preparation and may require extensive calibration depending upon the type of device. On the other hand, BE test has its own shortcomings. Gamal El-Dean (2007) showed that BE tests can lead to highly unreliable and erroneous results. Ismail and Rammah (2005) listed the limitations of using bender elements in measuring V_s. These include: bender elements penetrate through soil samples causing disturbance for undisturbed and cemented soils; they require filling the holes made in soil with coupling material like epoxy or gypsum; they may experience short circuiting and loss of signal due to failure of epoxy coating on the elements; they induce high stresses in the conical zone adjacent to conventional platens of the triaxial apparatus; they cannot be used in harsh environments (e.g. electrokinetic treatment); and depolarization at high voltages due to their small thickness.

The main objective of this chapter is to fabricate, model and test the proposed device for measuring the V_s of the tested soil as a new lab technique to overcome the shortcoming of other pulse lab tests. The fabricated device considers the soil anisotropy (soil as a mass) instead of single-plane measurements made by other devices. It causes the soil specimen to deform over its entire circular cross-sectional area unlike bender elements, which have a localized effect. Moreover, the proposed device was used to study the parameters controlling the V_s or G_{max} of silica sand including the effects of initial state/void ratio, confining pressure and fines content. The obtained results were compared with the results available in literature to evaluate the effectiveness of the proposed lab

technique for measuring V_s. Finally, the obtained results were compared with the results obtained using the bender element tests.

3.3 Literature Review

Robertson et al. (1995) reported that V_s of sand is influenced primarily by the mean effective confining stresses (σ'_m) and void ratio (e), the intrinsic characteristics of the soil (grain size distribution, grain shape, angularity, surface roughness, and mineralogical composition), and the structure (fabric, interparticle forces, and bonds). They found that the intrinsic characteristics are not affected with changes in e and σ'_m, unless significant crushing of particles occurs. They suggested that e and σ'_m define the initial state of soil.

3.3.1 Effects of mean effective confining pressure and void ratio on soil stiffness

Robertson et al. (1995) tested Ottawa sand (C-109) with e varying between 0.89 (very loose) to 0.57 (dense) in a triaxial apparatus using bender elements. Specimens were isotropically consolidated and the consolidation completed within a minute of the application of each consolidation stress increment, but the specimen was allowed 5 min before taking V_s readings. They proposed a relationship between V_s, e and σ'_m, i.e.

$$V_s = (381 - 259e)\left(\frac{\sigma'_m}{P_a}\right)^{0.26} {}^{m}/_{sec} \tag{3.1}$$

where e is the void ratio, σ'_m (kPa) is the mean effective stress and P_a is the atmospheric pressure (≈ 100 kPa) and the material constants 381 and 259 are in velocity units. The stress exponent of 0.26 is close to the 0.25 proposed by Hardin and Richart (1963). To evaluate the relationship among the three independent measurements (V_s, e, σ'_m), they normalized the V_s values using σ'_m. The normalized shear wave velocity, V_{s1} is given below

$$V_{s1} = V_s\left(\frac{P_a}{\sigma'_m}\right)^{0.26} {}^{m}/_{sec} \tag{3.2}$$

They found that V_{s1} for Ottawa sand is linearly related to e, i.e.

$$V_{s1} = (381 - 259e)\ {}^{m}/_{sec} \tag{3.3}$$

Cho et al. (2006) investigated the stiffness and strength of natural and crushed sands. They measured V_s using bender elements installed in 100mm diameter oedometer cell both during loading and unloading. They tested six natural and ten crushed dense sand specimens (relative density, D_r = 80-90%), including Ottawa sands. Based on their measurements, they correlated V_s to mean effective stresses, i.e.

$$V_s = \alpha \left(\frac{\sigma'_{mean}}{1kPa}\right)^{\beta} = \alpha \left(\frac{\sigma'_{\parallel} + \sigma'_{\perp}}{2kPa}\right)^{\beta} \tag{3.4}$$

where α factor (m/s) is V_s at 1 kPa and the exponent β shows sensitivity of V_s to σ'_{mean} in the polarization plane. $\sigma'_{\perp}$ and $\sigma'_{\parallel}$ are the effective stresses in the direction of particle motion (along the sample's diameter) and in the direction of wave propagation (along the height of the sample), respectively. They concluded that as sphericity, roundness and regularity decrease, α decreases and β increases. The evaluated values of α and β satisfied the inverse relationship presented by Santamarina et al. (2001), i.e.

$$\beta = 0.36 - \frac{\alpha}{700} \tag{3.5}$$

Lee et al. (2005) reported ranges of β for different soil types: β = 0.16~0.20 for rounded smooth particles and dense sands; $\beta \approx 0.25$ for loose sands or angular sands; β = 0.3 for soft clays, and $\beta \leq$ 0.15 for over consolidated clays and cemented soils. Cho et al. (2006) proposed the following relationship for Ottawa sand:

$$V_s = 73 \left(\frac{\sigma'_{mean}}{P_a}\right)^{0.223} \tag{3.6}$$

It should be noted that Cho et al. (2006) correlated V_s to the average value of the stress in direction of wave propagation and perpendicular direction, whereas Robertson et al. (1995) defined σ'_m as the mean of the stresses in three directions, i.e. axial and two lateral.

Salgado et al. (2000) studied G_{max} of clean Ottawa sand and also investigated the effects of non-plastic fines on V_s of Ottawa sand employing BE tests on triaxial samples. Samples were prepared at different relative densities (D_r) and were subjected to various levels of mean effective consolidation pressure. Ottawa sand was mixed with 5, 10, 15 and 20% non-plastic silt. They found that at a given D_r and confining pressure, G_{max}, decrease drastically with the addition of even small percentage of non-plastic fines (silt).

Hardin and Richart (1963) related G_{max} to e and σ'_m, i.e.

$$G_{max} = C_g P_a^{1-n_g} \frac{(e_g - e^2)}{1+e} \sigma_m'^{\,n_g} \tag{3.7}$$

where C_g, e_g, and n_g are regression constants and are a function of intrinsic soil variables, which are independent of soil state and are only function of its particle shape, mineral composition and particle size distribution. These variables include critical state friction angle (ϕ_{cv}'), specific gravity (G_s), e_{max} and e_{min} (Lee et al., 2004). These intrinsic parameters change by changing the amount of fines in the soil. Jamiolkowski et al. (1991) proposed a revised equation, i.e.

$$G_{max} = C_g P_a^{1-n_g} e^{a_g} \sigma_m'^{\,n_g} \tag{3.8}$$

where the exponent of void ratio a_g is another regression constant. Salgado et al. (2000) conducted extensive BE testing, and evaluated the regression constants defined in Eq. 3.7 and Eq.3.8 for clean Ottawa sand and Ottawa sand mixed with 5, 10, 15 and 20 % silt (presented in Table.3-1). In the present study the comparison of the obtained results will be made only by using the Eq. 3.7 of Hardin and Richart (1963) by using the regression parameters provided in Table.3-1 by Salgado et al. (2000). These regression constants will be used later along with Eqs. 3.7 to compare the measured G_{max} with the predicted G_{max} for both clean sand and sand-silt mixtures.

Table 3-1. Regression Parameters for both Eq's 3.7 & 3.8 taken from Salgado et al. (2000)

Silt (%)	Hardin and Richart (1963), Eq.3.7				Jamiolkowski et al. (1991), Eq.3.8			
	C_g	e_g	n_g	r^2	C_g	a_g	n_g	r^2
0	612	2.17	0.439	0.96	547	-1.051	0.443	0.97
5	454	2.17	0.459	0.94	410	-1.044	0.458	0.95
10	357	2.17	0.592	0.91	135	-2.376	0.557	0.96
15	238	2.17	0.745	0.85	101	-2.069	0.715	0.94
20 (D_R > 59 %)	270	2.17	0.686	1	---	---	---	---
20 (D_R < 59 %)	207	2.17	0.809	0.98	---	---	---	---

3.3.2 Effects of mean particle size and soil gradation on soil stiffness

Wichtmann and Triantafyllidis (2009) conducted a comprehensive study of the influence of grain size distribution of quartz sand with sub-angular shape on its G_{max}. They performed a total of 163 resonant column tests on specimens with 25 different grain size distribution curves to evaluate the effects of D_{50} and coefficient of uniformity, C_u on G_{max}. The mean grain size was in the range $0.1 \leq D_{50} \leq 6$ mm and C_u was varied in the range of $1.5 \leq C_u \leq 8$. The specimens were 10 cm in diameter and 20 cm high and were tested under air-dry condition. The specimens were tested under isotropic conditions in seven stress increments of 50, 75, 100, 150, 200, 300 and 400 kPa. They concluded that for a constant e, G_{max} does not depend upon D_{50}, but significantly decreases as C_u increases.

Yang and Gu (2013) tested three uniformly graded types of glass beads with different mean particle sizes (0.195, 0.920 and 1.750 mm) and showed that G_{max} does not vary appreciably with particle size, and could practically be assumed independent of particle size. Similarly, Iwasaki and Tatsuoka (1977), based on RC tests, found that for clean sand with no fines, G_{max} is independent

of the grain size in the range of D_{50} from 0.16 mm to 3.2 mm, and that it is slightly affected by the grain shape. They also concluded that for sand with fines, G_{max} decreases with an increase in C_u and with an increase in fines content.

Chang and Ko (1982) studied the effects of grain size distribution on the dynamic properties of Denver sand with D_r = 30%. The specimens had D_{50} ranging between 0.149 to 1.68 mm and C_u between 2 and 16. They showed that G_{max} is strongly affected by C_u but D_{50} has little or no effect. On the other hand, Menq (2003) performed RC tests to evaluate the effects of D_{50} and C_u on stiffness of sands and gravels using large size specimens (d =15 cm). They tested medium dense to very dense sand and gravelly specimens under dried condition with constant $C_u \approx 1.2$ and D_{50} between 0.33-17.4 mm. In contrast to other researchers, they found a slight increase in G_{max} with an increase in D_{50} for constant e and σ'_m. They also observed that as C_u increases, G_{max} increases but the effect of C_u is minor. However, Menq (2003) used a wide range of D_{50}. For the present study, the range of D_{50} is narrow and hence for all practical reasons G_{max} is assumed to be independent of D_{50}.

3.4 Fabrication of the Setup

The piezoelectric material used in the fabricated device is lead zirconate/lead titanate- 850E from APC Int'l, Ltd. The ring shaped piezoelectric element (ring actuator), shown in Fig.3-1, was chosen over the disc shape. Both of them can vibrate radially to emit planar waves over large area. However, piezoelectric discs are impervious and may adversely impact soil drainage during consolidation process. Hence, the ring configuration was chosen so that porous stones could be installed inside the piezoelectric rings ensuring soil drainage, which is a key requirement to test natural cohesive soils under consolidation. The inner and outer diameters of the used piezoelectric rings are 38 mm and 44 mm respectively and it is 3.5 mm in height. The rings were silver coated on the inside and outside walls, which acted as wall electrodes. When voltage is applied between inner and outer diameters (i.e. radially), the piezoelectric element deforms and vibrates in the radial direction according to the shape and polarity of the input signal. This radial deformation causes the shearing of the soil base thus producing shear waves.

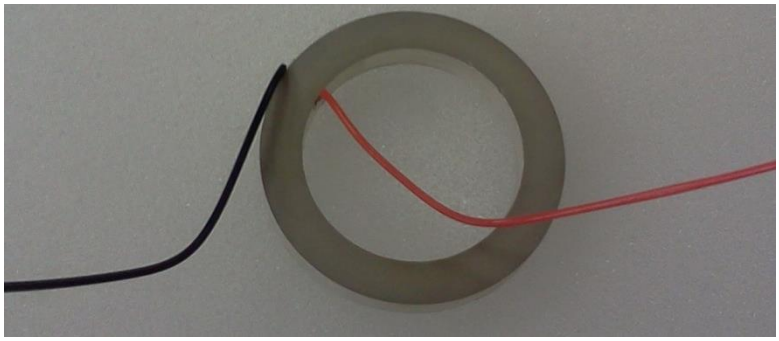

Figure 3-1. Ring shape piezoelectric elements

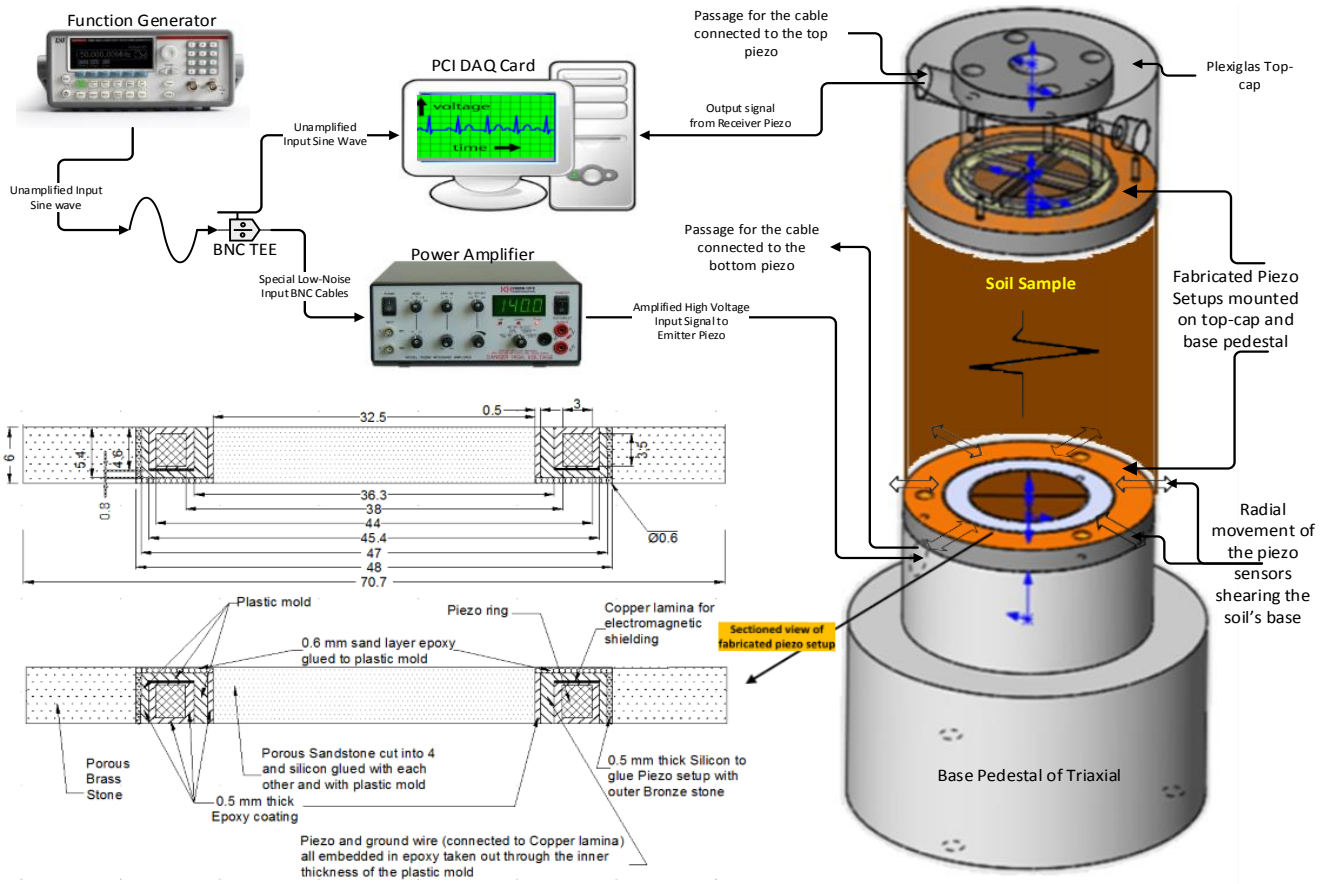

a)

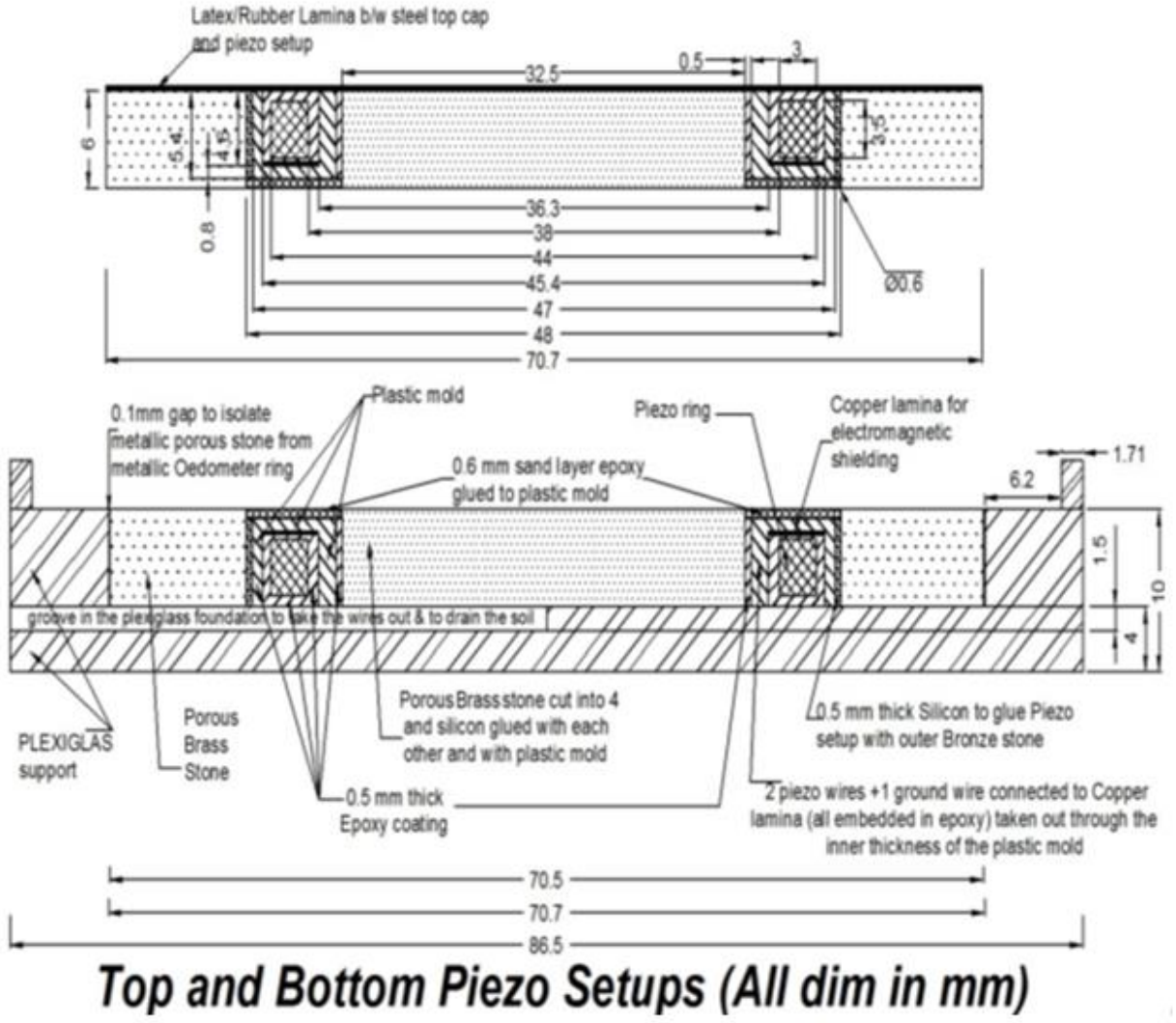

b)

Figure 3-2. a) Schematic diagram of PRA setup, b) Detailed drawing of the finalized piezoelectric element setup

As piezoelectric elements do not penetrate into the soil, roughness of the contact surface both at porous stones and piezo rings is important in transmitting a stronger signal to the soil specimen. Excitation at soil's end is generated through friction and/or adhesion between the inner metallic porous stone and soil. Therefore, rough/coarse metallic porous stones (bronze or brass) were used

to enhance interaction with soil specimen, which ensured a stronger output signal from the emitter piezoelectric element. Fig.3-2 shows the detailed schematic drawing of the fabricated PRA setup.

It is important to protect the piezoelectric elements from the harsh environment, especially water (moisture and humidity). Therefore, several layers of protections were applied to the piezoelectric elements. This includes coating the elements first with the conformal spray and then were coated with high performance epoxy to make them waterproof. After the epoxy was dried, another layer of conformal spray was sprayed and a thin layer of silicone coating was applied to seal the epoxy coating.

Figure 3-3. Plastic mold to house the piezoelectric elements for uniform epoxy coating and centering

In order to achieve a smooth and uniform coating of epoxy on the piezoelectric rings, a Delrin mold (shown in Fig.3-3) was used to house the piezo rings. Using this mold also ensured the vertical and horizontal alignment of the piezo transducers inside the porous stones. The plastic mold also acts as an additional insulation giving more protection to the piezo rings. The mold is 5.4 mm high, which is 0.6 mm less than the height of the inner and outer metallic porous stones as noted on Fig.3-2. The height difference between the mold and porous stones allowed gluing a 0.6 mm uniform layer of sand, which ensured a rough contact surface between the specimen and the setup for a stronger shear wave.

“Crosstalk” is a phenomena that takes place due to electromagnetic coupling between the source (emitter) and receiver piezoelectric elements (Lee and Santamarina, 2005; Leong et al., 2009). It can appear on the output signal as a duplicate of the input sine-wave. Crosstalk can be very significant in conductive soils such as wet clays. Leong et al. (2009) observed crosstalk during their studies and attributed this to the improper grounding. Crosstalk can interfere with the output signal and can mask the arrival of the shear wave, especially when testing short specimens at low frequencies and/or at high pressures. In such cases, the shear wave arrival time, t_s, is either very close or less than the period of the input wave.

To eliminate the crosstalk in the developed device, proper shielding and grounding was provided to the piezoelectric elements. When grounding is cut-off on purpose, it can be seen in Fig.3-4a that the output signal has a duplicate (cross-talk) of the input sine wave. Fig.3-4b shows that the output signal devoid of cross-talk when the ground wires are connected to the appropriate ground resulting in a clean signal making the fabricated device very reliable for measuring V_s for different soil types under different loading conditions and different specimen sizes. The grounding was accomplished by using copper lamina, cut into circular shape and placed inside the plastic mold and connected to a ground wire as shown in Fig.3-5. Insulation was applied to the small metal surfaces exposed at the connection of ground wire and copper lamina and at the connection of the wires to the inner and outer electrodes of the piezoelectric elements as presented in Fig.3-5.

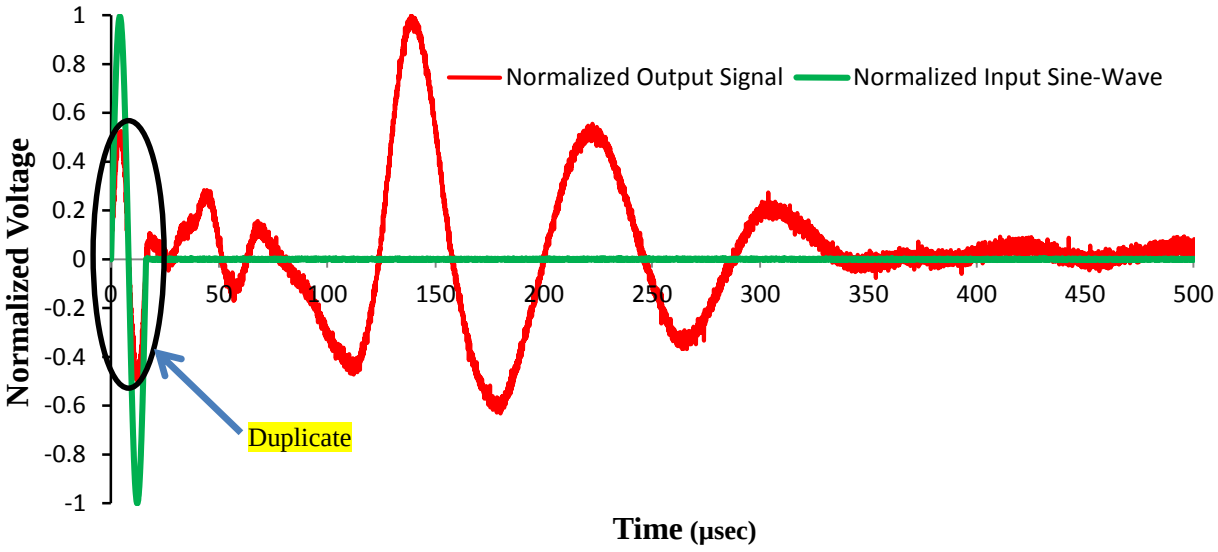

a) Normalized input & output signals showing duplicate of the input sine-wave **"crosstalk"**

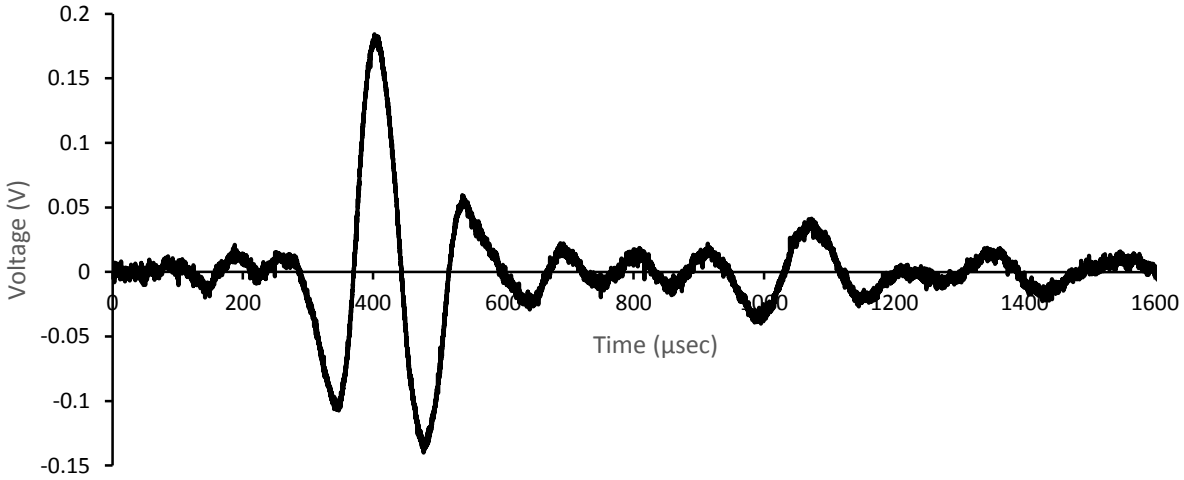

b) **No "crosstalk"** observed when the fabricated device is properly grounded

Figure 3-4. Typical Output signals

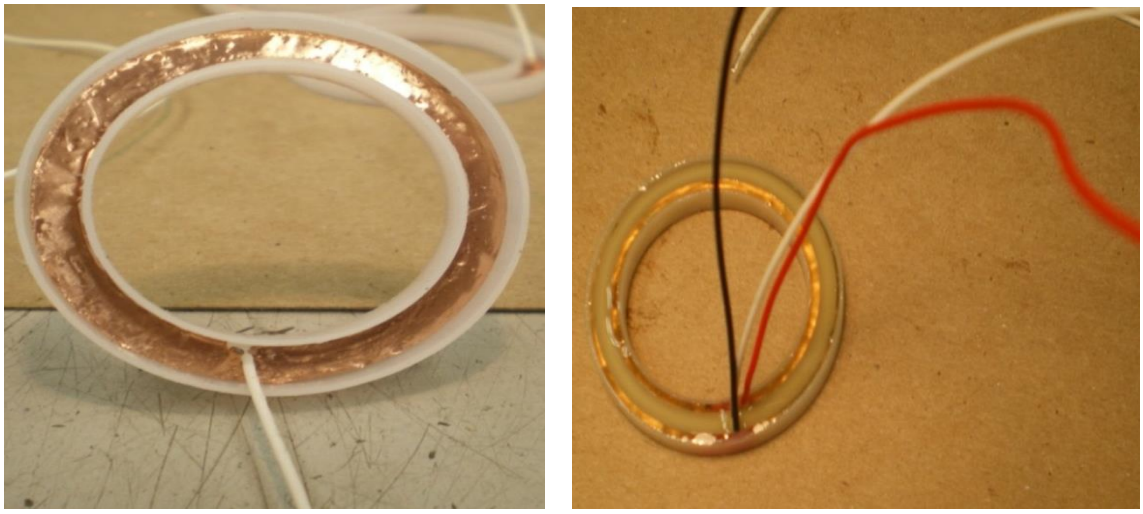

(a) (b)

Figure 3-5. a) Copper lamina and ground wire for shielding and grounding to prevent crosstalk; b) Piezoelectric element and copper lamina housed in plastic mold embedded in epoxy

After completing the insulation and shielding, the inner metallic porous stone was epoxied to the plastic mold. Epoxy was preferred over soft bonding agents like silicone so that the assembly strictly behaves as one unit and the deformations of the piezo rings are transmitted to the inner porous stone causing it to vibrate the same way as the piezoelectric elements. The inner stone before epoxied was cut into four pieces, and these pieces were then glued together using soft material (silicone) in order to facilitate uniform distribution of shear deformations to the specimen surface. The entire inner setup (piezo element in Delrin mold and the inner metallic stone glued to it) was then glued to the outer metallic porous stone using silicone. Here, silicone was preferred over epoxy to ensure that the entire inner setup can vibrate easily due to the flexibility of the silicone, and hence can create a strong signal. Some of the steps of fabrication and assembly of the piezoelectric setups are shown in Fig.3-6.

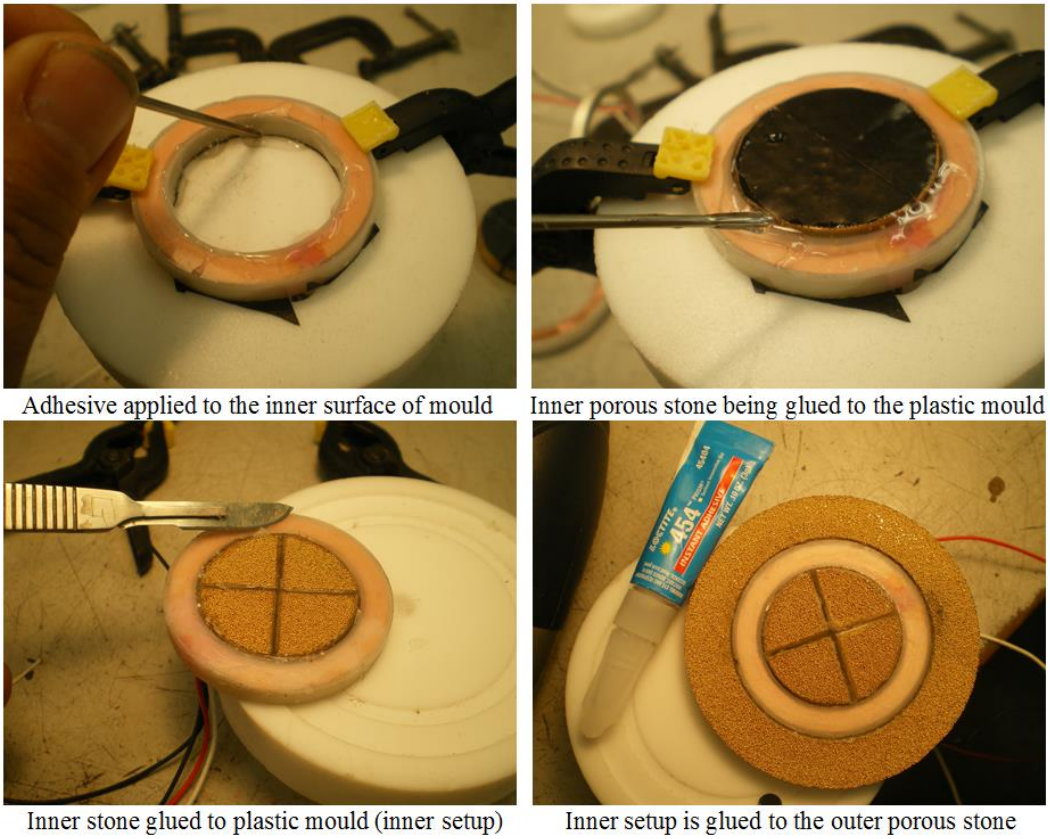

Figure 3-6. Different setups of setup preparation and assembly

3.5 Peripheral Equipment

The function/waveform generator used was Keithley 3390 arbitrary function & waveform generator. It is an easy-to-use programmable signal generator with advanced function, pulse, and arbitrary waveform capabilities. It has superior signal integrity, faster rise and fall times, lower noise, and greater waveform memory combine to provide high quality output signals. Its technical features includes a 50MHz sine wave frequency, 25 MHz pulse frequency, arbitrary waveform generator with 256k-point, 14-bit resolution, frequency sweep and burst capability, built in function generator capability includes: sine, square, noise etc.

The power amplifier used was Krohn-Hite 7602M. It is a wideband power amplifier that offers extended output power and voltage capabilities, low distortion (<0.01%), and versatility with a voltage gain of up to 42dB. It is able to deliver a differential output of 34 watts of continuous power and 282V rms ($800V_{p\text{-}p}$). It can also provide plus and minus dc voltages simultaneously. It

measures the largest peak voltage independent of polarity with a 1 second time constant. It has an accuracy of ±0.5V (at 1 kHz).

The DAQ card used was GaGe CompuScope 8349. It is a 14 bit vertical resolution, single-slot PCI card with 4 channels with a sampling rate of 125 MS/s per channel. It has an on-board acquisition memory of 128MS with a Bandwidth of more than 100 MHz

All the peripheral equipment was connect to each other and with the piezo setups using the special low-noise cables. The data acquisition system recorded the unamplified input signal as well as the output signals/waves travelling through the soil specimen. A computer program was developed in the LabVIEW® environment to control the wave generation, observation and data acquisition.

3.6 Soil Specimens.

The soil tested in this study was Ottawa sand. It is pure silica sand with round to subround particles. Two different gradations of Ottawa sand were tested to investigate the effect of particle size distribution on V_s. The grain size distribution curves of the two soils as per ASTM C136-06 are shown in Fig.3-7a. The two tested soils have commercial names as Barco 32 and Barco 71 and has a specific gravity, $\boldsymbol{G_s}$ = 2.65. For Barco 32, Average Size: $\boldsymbol{D_{50}}$ = 0.479 mm, Effective Size: $\boldsymbol{D_{10}}$ = 0.300 mm and $\boldsymbol{C_u}$ = 1.29; and for Barco 71, Average Size: $\boldsymbol{D_{50}}$ = 0.192 mm, Effective Size: $\boldsymbol{D_{10}}$ = 0.112 mm and $\boldsymbol{C_u}$ = 1.89. The C_u values indicate that the sands can be classified as very poorly graded or uniformly graded (classified as SP on the Unified Soil Classification System). The maximum and minimum void ratios, $\boldsymbol{e_{max}}$ and $\boldsymbol{e_{min}}$ were 0.75 and 0.47, for Barco 32 and 0.79 and 0.46 for Barco 71 using ASTM D4254 and ASTM D4253, respectively. The samples were prepared using air-pluviation technique.

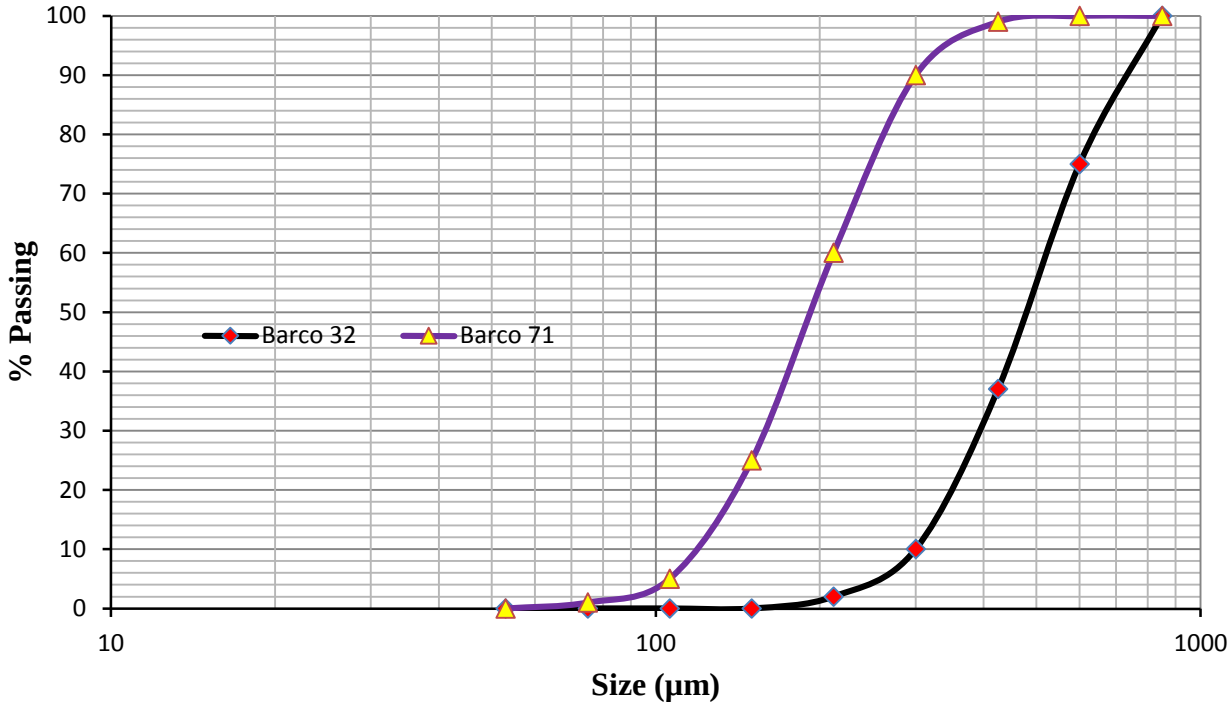

a) Tested Ottawa sands

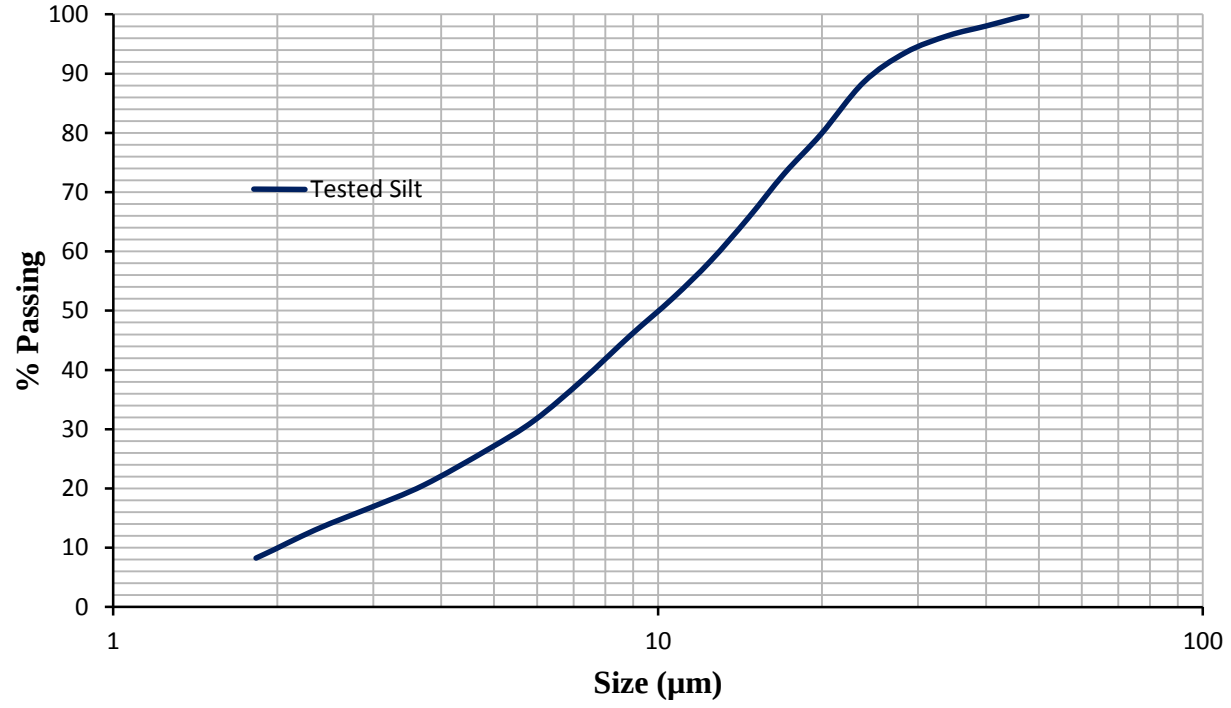

b) Tested non-plastic silica silt

Figure 3-7. Grain size distribution curves

To investigate the effect of fines on V_s of Ottawa sand, non-plastic silica silt (MIN-U-SIL® 40) was used. It is an inert, fine ground, white crystalline silica with $\boldsymbol{D_{50}}$ = 10.5 µm, with top-size of 40 µm and $\boldsymbol{G_s}$ = 2.65. The grain size distribution curves of the used non-plastic silt as per ASTM C136-06 is shown in Fig.3-7b.

The vertical pressures were applied to the soil specimen in an Oedometer ring in increments, i.e. 25, 50, 100, 200, 300, 400, 500, 600, 700 and 800 kPa. V_s was measured immediately after the application of each pressure increment. The mean pressure σ'_m was evaluated for each value of applied vertical pressure, σ'_v, applied in the oedometer using coefficient of lateral earth pressure at rest, K_o. The friction angle of the clean Ottawa sand was determined using direct shear apparatus, and consequently K_o was calculated, and were found consistent with the values reported in the literature. (e.g. Thomann and Hryciw, 1990).

3.7 Methodology, Testing Details and Interpretation Techniques

3.7.1 Selection of input signal parameters

A sinusoidal signal was used in the current study as an input wave to avoid the issues associated with square signal (Leong et al., 2005; Jovičić et al., 1996; and Viggiani and Atkinson, 1995). The power amplifier was used to amplify the signal because the maximum output voltage of the function generator is a $10V_{p\text{-}p}$ (at 50 Ω impedance), which is not sufficient to create a powerful input signal at the emitter. The amplifier facilitated the generation of a strong shear wave and hence a strong output at the receiver. The original and amplified signals were checked carefully and it was ensured that they do not have time lag between them, which could affect the interpretation and results.

The magnitude of the applied voltage signal affects the signal-to-noise-ratio (SNR) (Leong et al., 2005). The input voltage of the waveform generator and the gain on the power amplifier were set to achieve an amplified output signal with very high SNR. As discussed in Chapter 2, the ring piezoelectric elements used in the current study are thick and can sustain a very high input voltage without being depolarized, which is not possible with BE due to their small thickness. For most tests, input sinusoidal signals of magnitude between 50-100 $V_{p\text{-}p}$ were used; the signal amplitude

can even be further increased without depolarization, while typical voltage for BE tests is around 14V.

Brignoli et al. (1996) advocated monitoring the received signals for gradually increasing excitation frequencies of transmitter for each velocity measurement. In the present study, the frequency of the input signal was gradually increased and the shape of the output signal was analyzed. Depending on e and σ'_m of the tested specimen, the starting frequency was generally around 10-15 kHz, and gradually increased with increments of 3 kHz up to around 40 kHz and the output waves/signals were captured at each new frequency. The height of the specimen is also a key factor in choosing the testing frequency range. Samples with bigger heights can be tested at lower input frequency.

It was found that an increase in frequency of the input signal reduces the arrival time and hence increases V_s because the piezoelectric rings response to each input/excitation frequency (i.e. transfer function) is frequency dependent. The difference between V_s measured at the highest and the lowest tested frequency was less than about 5-8%, which is acceptable for all practical purposes. Increasing the excitation frequency also caused small reduction in the amplitude of the output signal, but that did not cause any major concern given the large amplitude of the output signal. Little or no effect of frequency was observed on the shape of the output signals in the present study. This may be attributed to the small height of the tested samples. The V_s was generally measured for $L/\lambda \geq 2$ (where L is the sample height and λ is wavelength of the signal), which usually corresponds to the middle values of the tested frequency range. For each value of applied pressure and input frequency, the recorded output signal was converted from the time domain into the frequency domain to find the shear wave velocity using the frequency domain analysis.

3.7.2 Interpretation of Output Signal and Evaluation of First Wave Arrival

Different methods are available for the interpretation of the output waveforms and the determination of the first arrival of the shear wave required for evaluating the travel time, t_s, and V_s as reported in Chapter 2. Arulnathan et al. (1998) summarized the different methods of interpretation, namely: using first direct arrival in output signal; using characteristic peaks of input

and output signals; using cross-correlations of input to output signals; using phase velocity; and using the second arrival in the output signal.

Both the characteristic peaks and cross-correlation were considered in this study but yielded erroneous results, consistent with the findings of Arulnathan et al. (1988) and Leong et al. (2005). In addition, the cross-correlation of the input-output signal in the present study was found to overestimate the travel time, and hence underestimate V_s. This could be attributed to using relatively high input frequencies and high L/λ and short specimen height in the present study. Same observations were made by Gamal El-Dean (2007) and Arulnathan et al. (1998) who concluded that travel time errors are difficult to quantify and are expected to become increasingly significant as the specimen length decreases as in the case of oedometer application.

Accordingly, three methods are considered in the present study for determining the wave travel time: first direct arrival (first zero crossing before a major event or peak); using the second arrival (only when second arrival is obvious in the output signal); and the group velocity method. All three methods yielded consistent results.

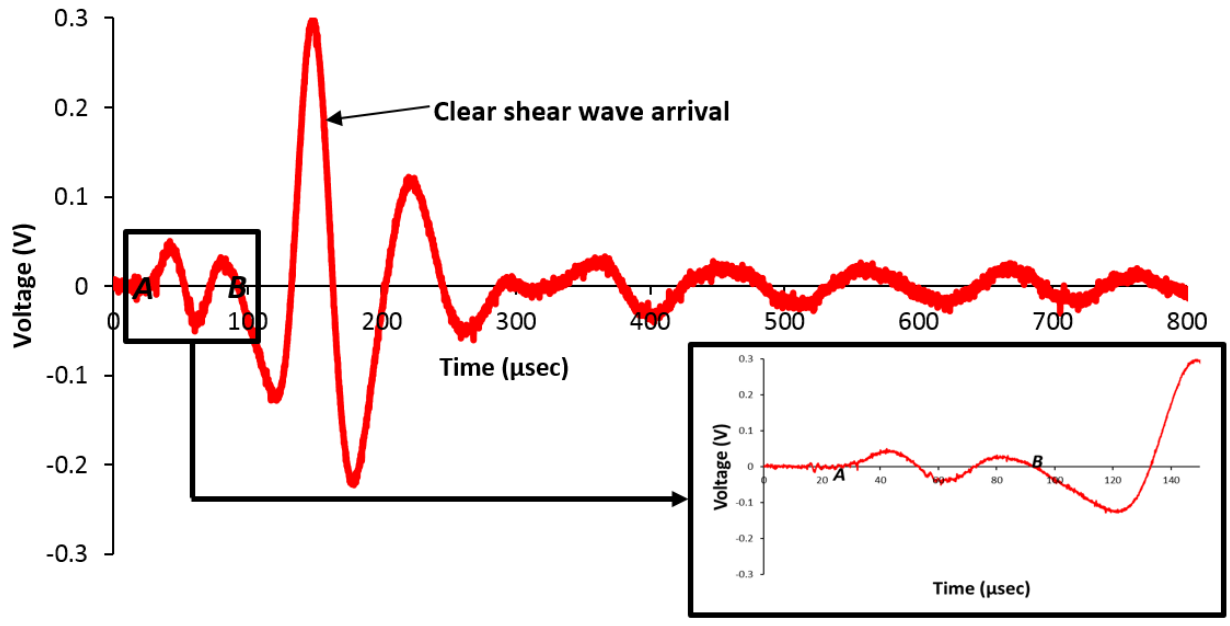

Figure 3-8. Typical output signal with a clear V_s

(Pt **A** is possible arrival of P-wave & Pt **B** is the arrival of S-wave)

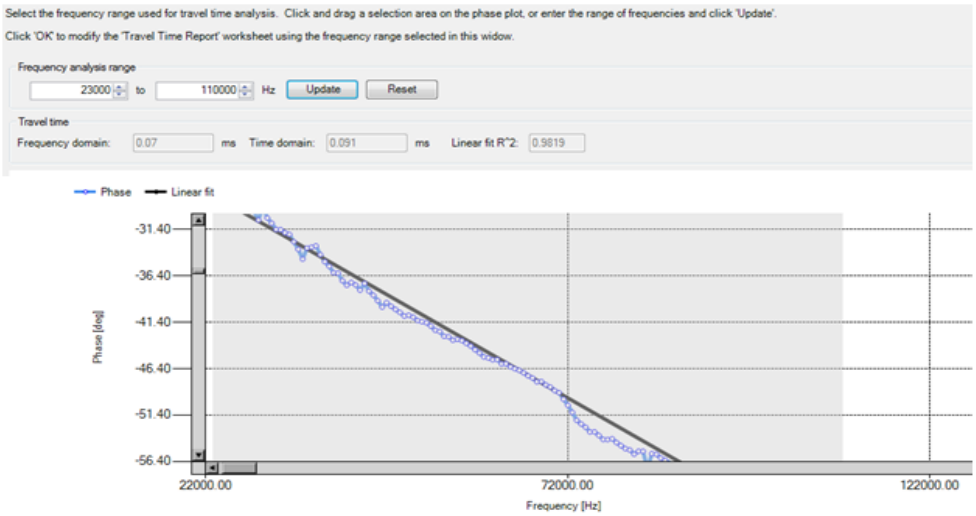

a) Phase diagram of cross power spectrum of source and received signals

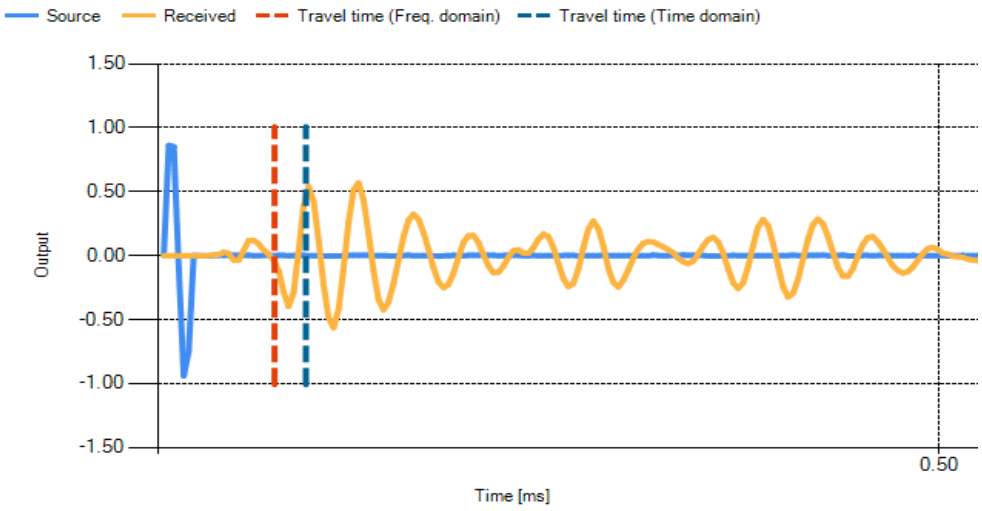

b) Time (cross-correlation) and frequency domain (group velocity method) arrival times

Figure 3-9. Evaluation of travel time using GDS BEAT for Barco 71 specimen with σ_v' = 800 kPa, e_o = 0.52, f_{input} = 50 kHz

Considering the fact that almost all the output signals obtained during the present study had only one and a very clear major peak (shear-wave), the direct arrival method could be safely used to determine V_s. The first clear major event/peak is the shear wave and the first zero crossing before the start of this major event (Pt. **B** on Fig.3-8) is considered as the arrival point, which is also

consistent with Brignoli et al. (1996). The direct arrival method was used consistently on all measurements and produced very reliable V_s values.

In the present study, it was found that the second arrival method presented by Arulnathan et al. (1998) can also be used to determine the travel time but only when the second arrival was clearly noted on the output signal. This method (using second arrival) validated and confirmed the results from the other two methods (direct arrival and phase/group velocity method) used.

The group velocity technique presented by Viggiani and Atkinson (1995) was also used herein to calculate shear wave travel time and an example of the obtained results is shown in Fig.3-9. The travel time using the slope of the phase diagram shown in Fig.3-9a leads toward the same point (Fig.3-9b) fixed using the direct arrival technique (i.e. the first zero before the major peak) validating the fact that both these methods synchronize with each other. The method resulted in travel time that was identical to that determined using the direct arrival method as shown in Fig.3-9b. The signal analysis following group velocity technique was performed using the Microsoft Excel-based GDS Bender Element Analysis Tool, GDS BEAT.

3.8 Verification of Methods Used for the Evaluation of Travel Time

It is necessary to validate the ability of the developed piezoelectric actuator setup to accurately measure V_s of soils. For this purpose, a series of BE tests were conducted to measure V_s of Ottawa sand specimens mounted on SRS-150 Residual Ring Shear Testing equipment from GCTS Testing Systems. The BE tests were performed under 1-D loading condition, which is similar to the test conditions for the fabricated piezo setup mounted on an oedometer.

The signals obtained during the BE tests in ring shear equipment were extremely noisy, so they were filtered using low pass filter of sixth-order. Filtering the BE signals using different filters were also found to significantly affect the shape of the signal. Fig.3-10 shows the filtered signal from BE testing. The unfiltered signal had a significant noise that completely masked the arrival of the shear wave.

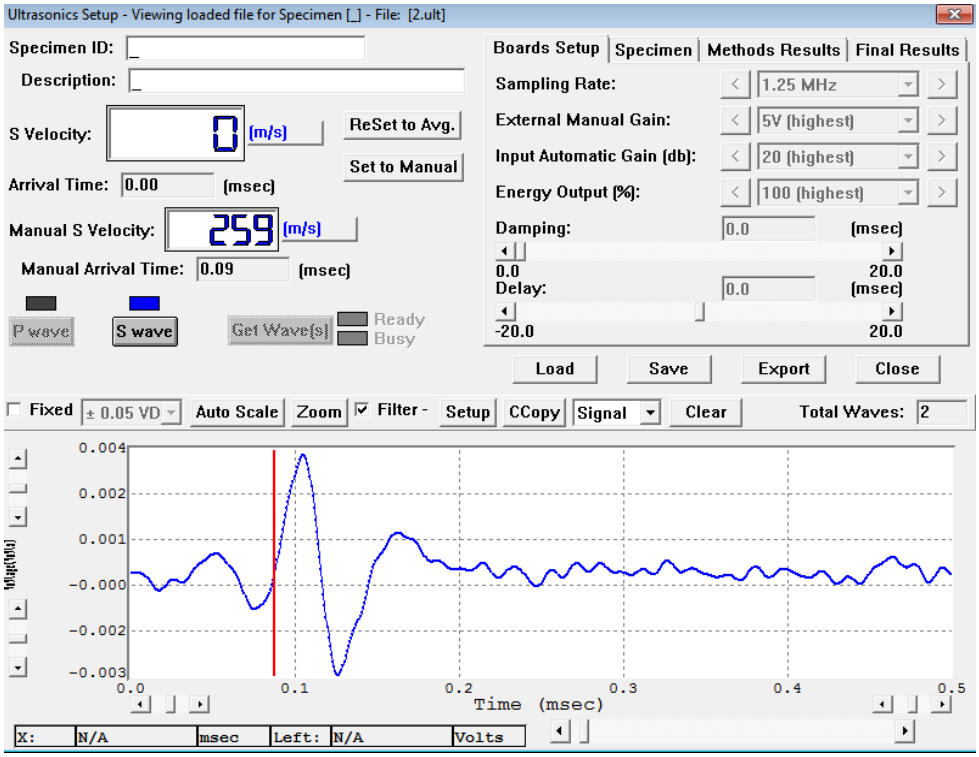

Figure 3-10. V_s determination using BE in ring shear equipment, e_0 = 0.61, σ'_v = 300 kPa

In contrast to the noisy signals obtained during BE tests, the signals obtained from the piezoelectric actuators during this study were clear and with sufficiently high amplitudes, and hence did not require any filtering. The signal-to noise (SNR) of the signals obtained employing the piezoelectric actuators in the present study were much higher than those obtained in BE tests, which further highlighted the superiority of the fabricated device. The weakness of the output signal from BE can also be noted from the magnitude of output voltages as shown in Fig.3-10 compared to that obtained from the developed device (e.g. Fig.3-8).

The repeatability and reliability of the PRA setup are attributed to several features. For example, it allows a variety of input signal shapes with a wide range of frequencies and voltage amplitudes. This may not be the case in most conventional BE testing. In addition, the developed ring actuator does not penetrate the soil specimen and hence does not disturb it. On the other hand, the BE device is likely to cause disturbance of the tested soil specimen. Furthermore, BE testing may cause local non-linearity and hence may not give the true low-strain V_s.

3.9 Results and Discussion

3.9.1 Performance Assessment of the Fabricated Device

The measured V_s using the developed device and BE tests for the clean Ottawa sand specimens at three different e_o = 0.52, 0.58 and 0.61 over a wide range of applied pressures are presented in Fig.3-11. It can be observed from Fig.3-11 that the values of V_s measured using the developed device are in good to excellent agreement with the values measured using the BE test at medium densities (e_o = 0.58 and 0.61). This comparison validates the performance of the fabricated ring actuator device. A minor disagreement is observed between the measured values for the sand in dense state at low pressures as presented in Fig.3-11a. This can primarily be attributed to the filtering to eliminate the noise from the extremely noisy BE signals, which was found to change the shape of the received signals and hence arrival time. The measured velocity at dense state was found to be more sensitive to the measured time as compared to the loose state. The comparison overall confirms that the use of the fabricated device yields better results for all test conditions.

In order to evaluate the consistency of the signals obtained at a wide range of applied pressure, a sand Barco #32 specimen with an initial void ratio e_o = 0.58 was subjected to different pressures and the output wave form was monitored. Fig.3-12 displays some of the output waveforms recorded at early stages of device fabrication under different applied pressures for the Barco #32 specimen, which demonstrate the decrease in the arrival time hence increase in V_s with an increase in σ_v due to increase in the particles interlocking, and subsequent densification.

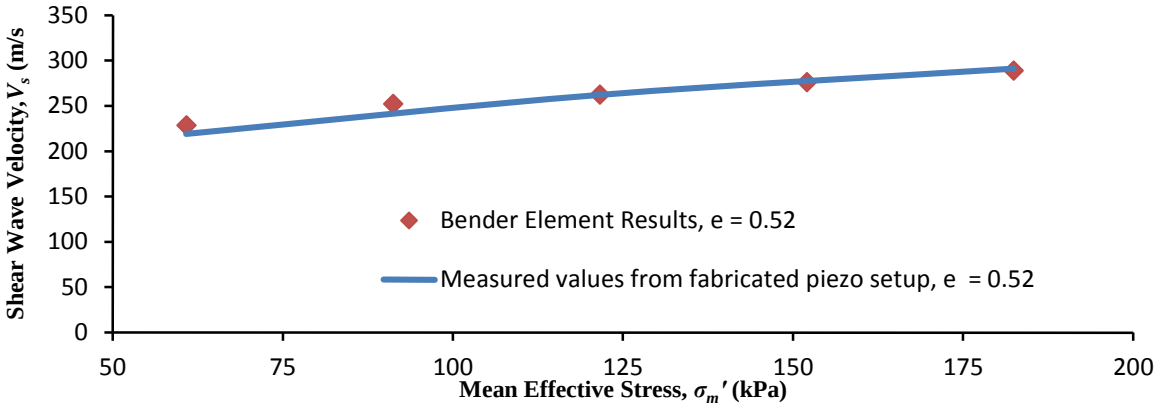

(a) e_o = 0.52

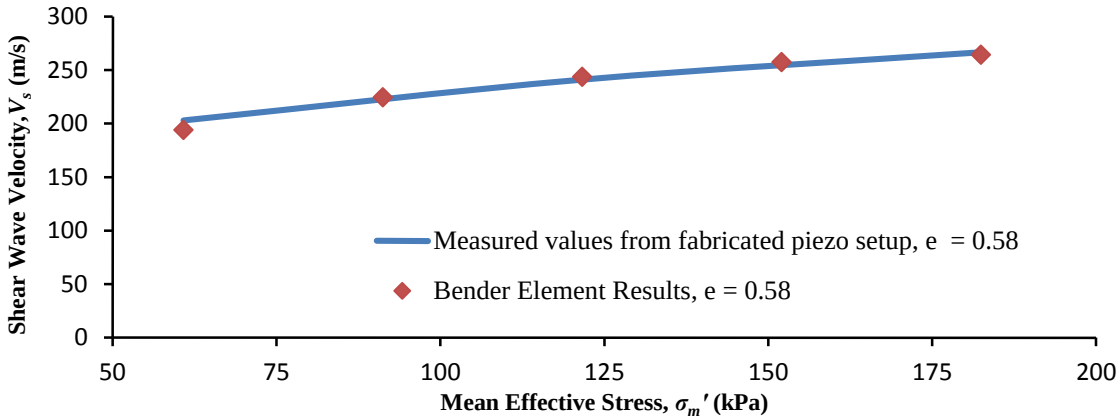

(b) e_o = 0.58

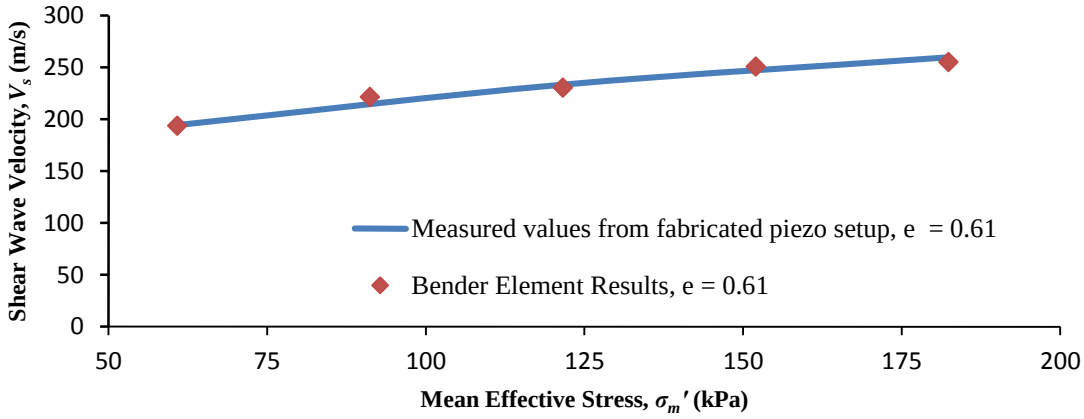

(c) e_o = 0.61

Figure 3-11. Comparison of V_s measured using the developed device and BE

3.9.2 Analysis of Results using the Fabricated Device

3.9.2.1 V_s of clean Ottawa sand

The void ratio of the test specimen is expected to change with the application of each load increment. Therefore, a new void ratio was calculated from the settlement data, which will be shown later, and the measured V_s values were compared with those reported in the literature considering the actual specimen heights and void ratios at each load increment.

The V_s measurements using the ring piezoelectric actuators for both Barco 71 and Barco 32 specimens are presented in Fig.3-13. The results are obtained for three different e_o values of each sand type and the specimens were tested for a range of applied vertical pressures varying from 25 kPa to 800 kPa. The values of V_s measured by Robertson et al. (1995) are also plotted in Fig.3-13 for the purpose of comparison. These results clearly demonstrate that, as expected, for a given e, V_s increased with an increase in σ_m'. Fig.3-13 shows that the measured V_s values using the fabricated device are very close to those reported by Robertson et al. (1995), and consistently fall between the average and lower bounds of their results. It can be noted that their average curve slightly overestimates V_s at high pressures, but otherwise the measured values in the current study fall well between the bounds defined by Robertson et al. (1995). The good agreement between the two sets of V_s values further confirms the ability of the developed device to accurately measure the V_s of soils, considering a wide range of applied pressures.

Fig.3-14 summarizes the results of Fig.3-13 as an average of all tests and demonstrates the effect of initial state/void ratio and the mean effective stress on V_s for clean Ottawa sand. Fig.3-14 indicates that the V_s increases with the increase in the mean stress and decrease in e.

$$V_s = \alpha \, {\sigma_m'}^{\beta} \tag{3.9}$$

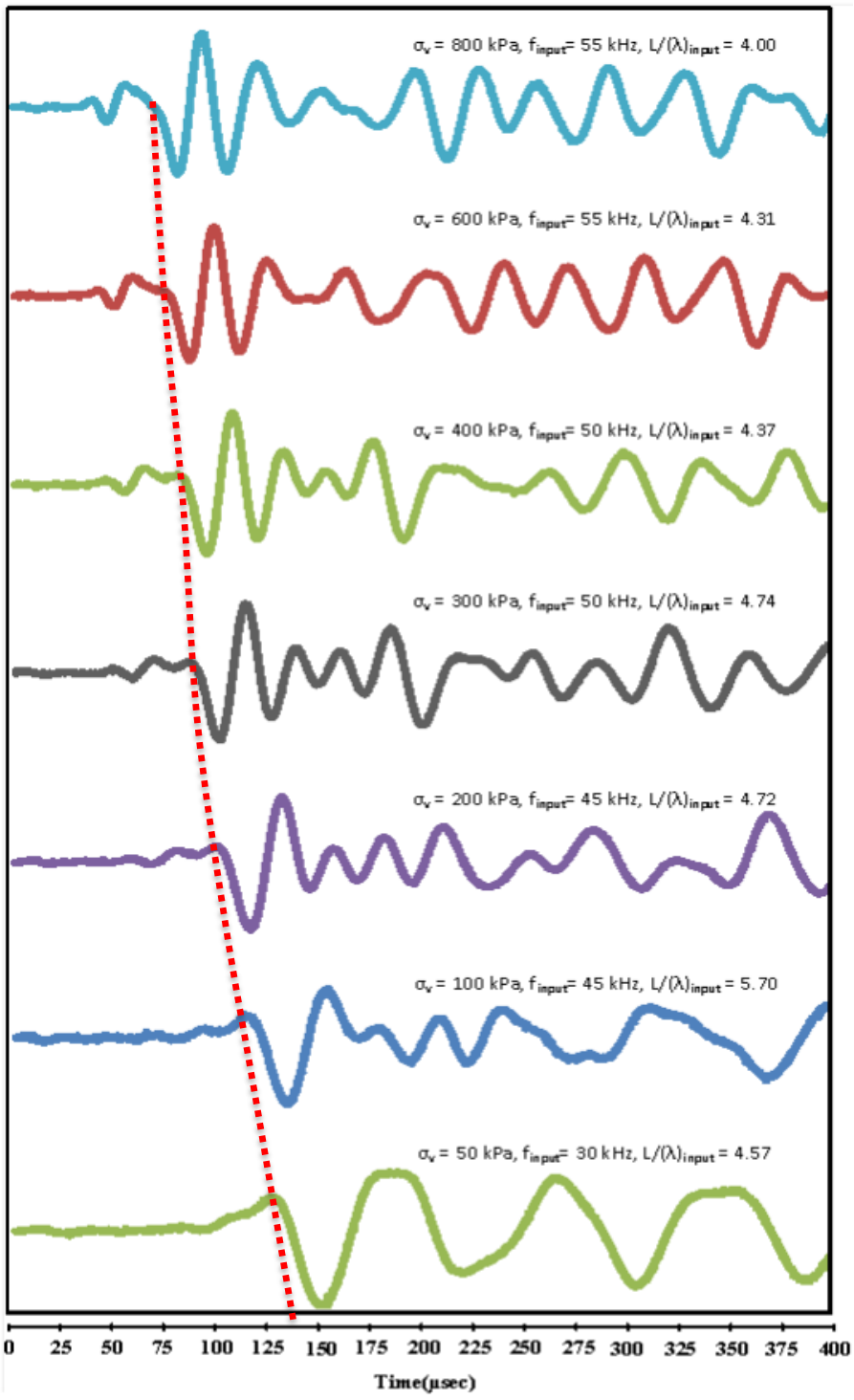

Figure 3-12. Output waveforms captured for Barco 32 specimen with e_o = 0.58 in the odometer cell

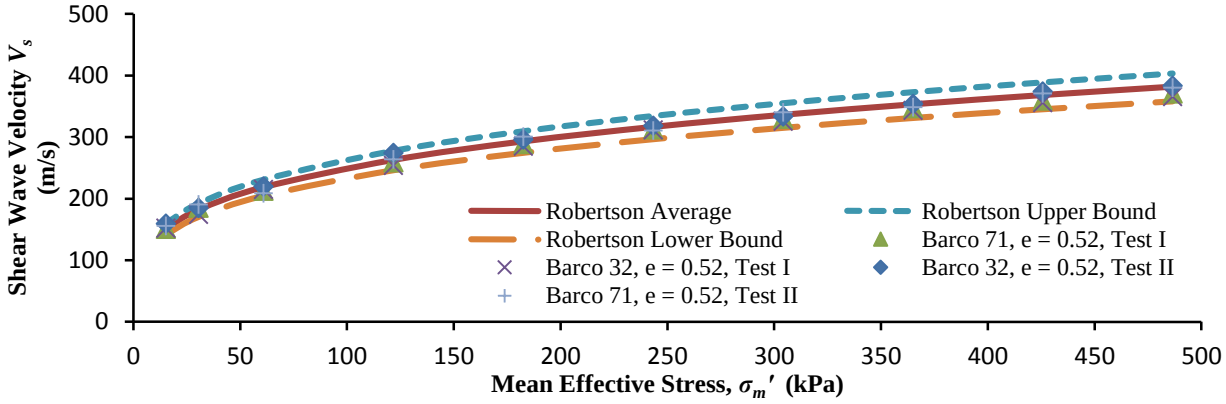

a) e_o = 0.52

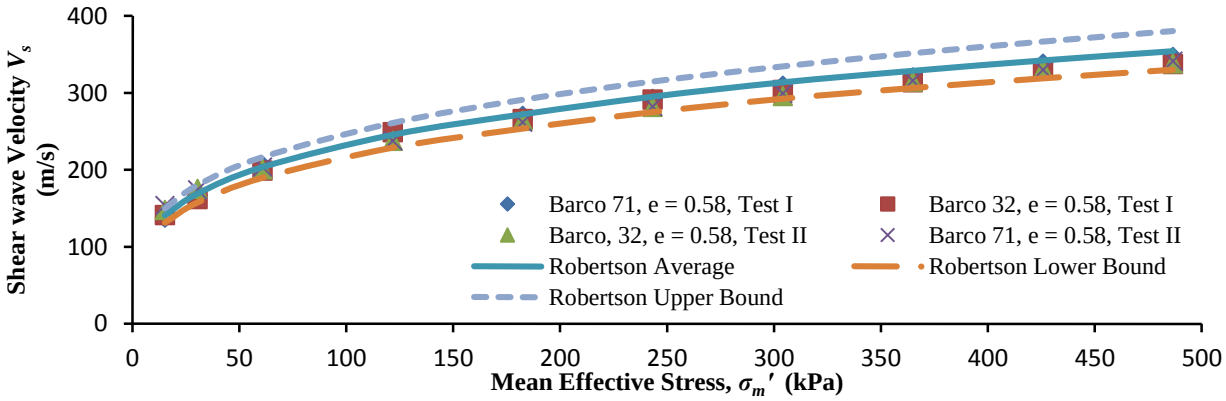

b) e_o = 0.58

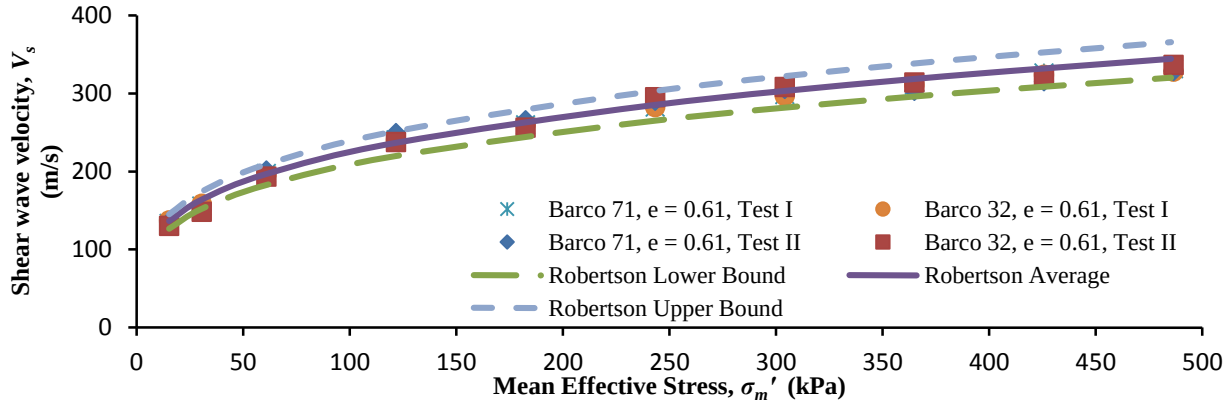

c) e_o = 0.61

Figure 3-13. Comparison of measured V_s values of Ottawa sand, with Robertson et al (1995), on both Barco 32 and Barco 71 at different initial void ratios

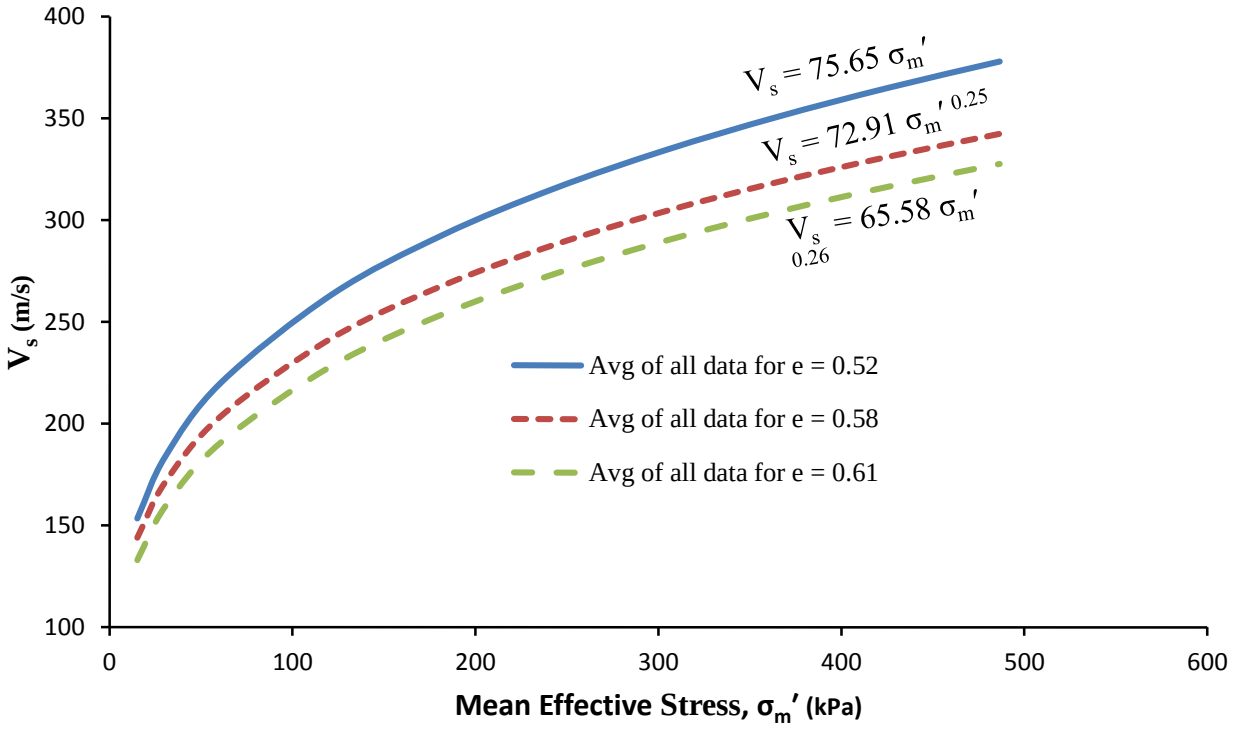

Figure 3-14. Effect of mean stress for specimens with different e_o on V_s of clean Ottawa sand

For each value of e_0, a curve was fitted to the measured V_s values presented in Fig. 14 following the form of Eq.3.1 and a stress exponent (β) was evaluated. The obtained exponent (β) was found to be around 0.25 and 0.26, which is consistent with the findings of Robertson et al. (1995). The coefficient α varied depending upon the initial void ratio, i.e. α = 75.65, 72.91 and 65.58 for e_o = 0.52, 0.58 and 0.61, respectively. Santamarina et al., (2001) and Cha et al. (2014) provided the inverse relationships between the fittings parameters α and β, applicable to a variety of soils. The measured fitting parameters are in good agreement with the calculated ones using these correlations.

3.9.2.2 Shear modulus of clean Ottawa sand

The very small strain shear modulus, G_{max} is related to the soil shear wave velocity, i.e.

$$G_{max} = \rho V_s^2 \tag{3.10}$$

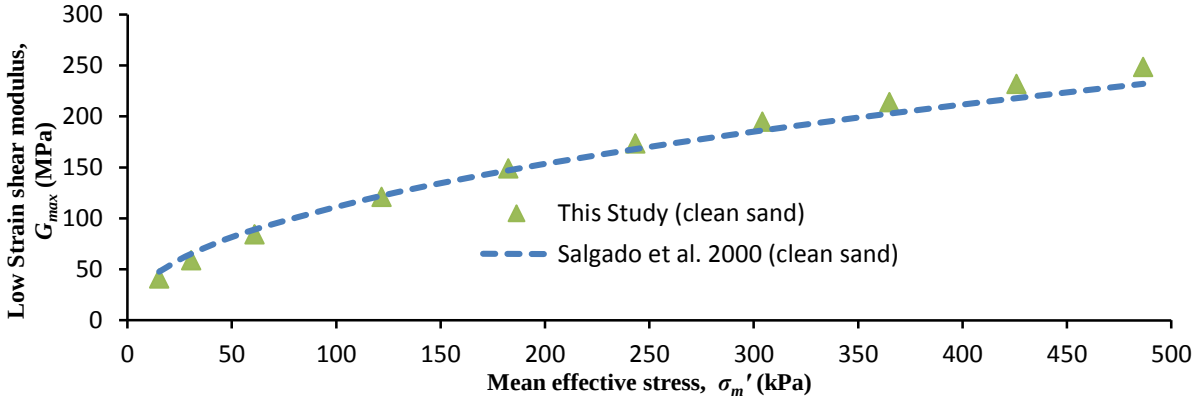

a) e_o = 0.52

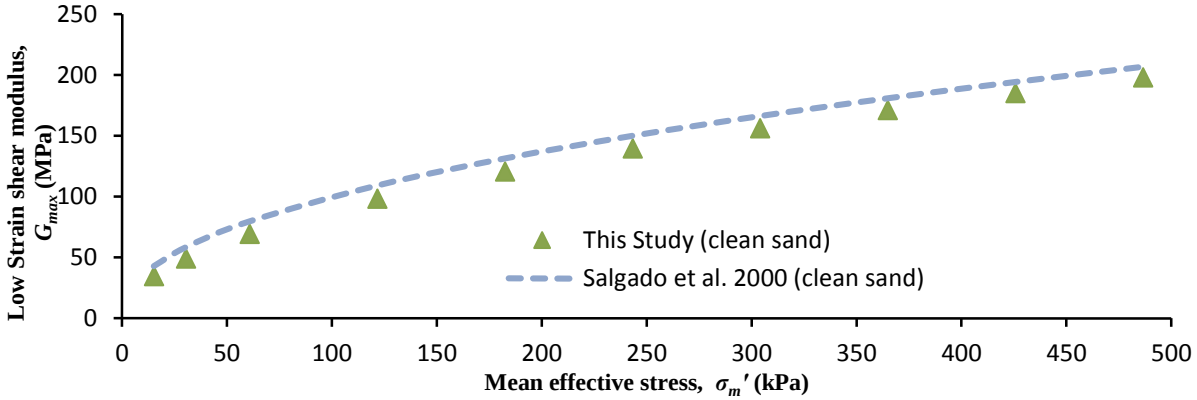

b) e_o = 0.58

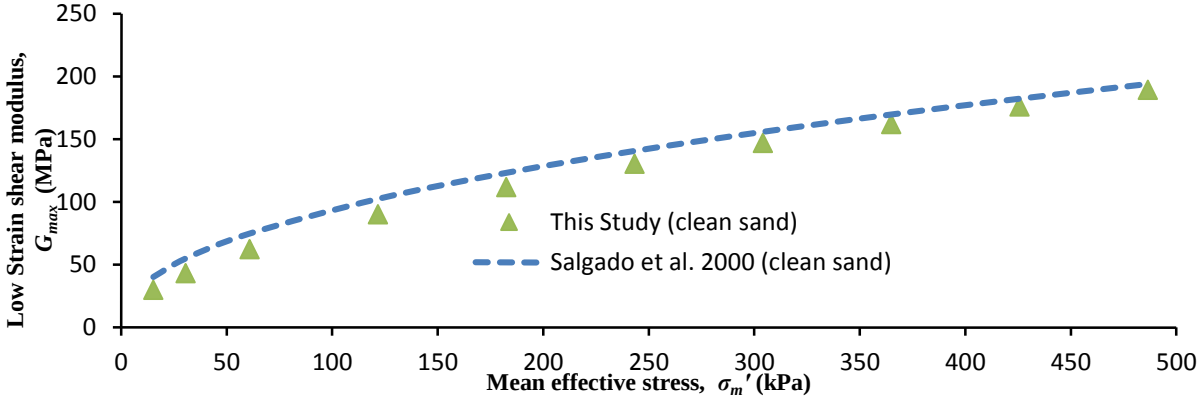

c) e_o = 0.61

Figure 3-15. Measured and predicted G_{max} using Salgado et al. (2000) regression constants at different initial void ratios

where ρ is the soil's bulk density. Fig.3-15 compares the calculated G_{max} values based on the V_s obtained from the fabricated device with those reported by Salgado et al. (2000) for clean Ottawa sand. Salgado et al. (2000) evaluated the regression constants to be used for clean Ottawa sand and sand mixed with different percentages of fines. It is clear from the Fig.3-15 that the measured G_{max} values are in good agreement with the predicated G_{max} values. However, at higher void ratio (Fig.3-15b and Fig.3-15c), the measured values are slightly lower than the predicted values, while at low void ratio (e_o= 0.52, Fig.3-15a) and high confining pressures, the measured values are found slightly greater than the predicted values. These small discrepancies could be attributed to several factors. The potential factors include the difference in sample preparation techniques, the different test devices (BE vs. Ring piezoelectric actuators), different methods of analysis for the measurement of arrival time, the use of an appropriate k_o to convert the vertical stresses into mean stress, and different specimen sizes etc.

3.9.2.3 Effect of fines content on shear modulus of Ottawa sand

In order to suitably evaluate the effect of fines content (FC) on G_{max} of Ottawa sand, the variation of G_{max} with pressure was investigated using the vertical stress (σ_v') rather than the mean stress (σ_m'). This was considered to eliminate the effect of K_o on σ_m' as K_o is lower for clean sand than it is for silty sands (Salgado et al., 2000), i.e., at the same σ_v', clean sand and silty sand will be under different σ_m' and hence the results cannot be compared. Furthermore, the effect of the applied pressure on e of the test specimen should be evaluated as it affects V_s and G_{max} of soil. Fig.3-16 shows the variation of e with σ_v' for clean Ottawa sand at different e_o, and the effect of FC effect on e at different σ_v' values for initial void ratio, e_o = 0.58. It is clear from Fig.3-16 that for clean sand, e decreased slightly as σ_v' increased, while the effect of σ_v' on e was more pronounced as FC increased.

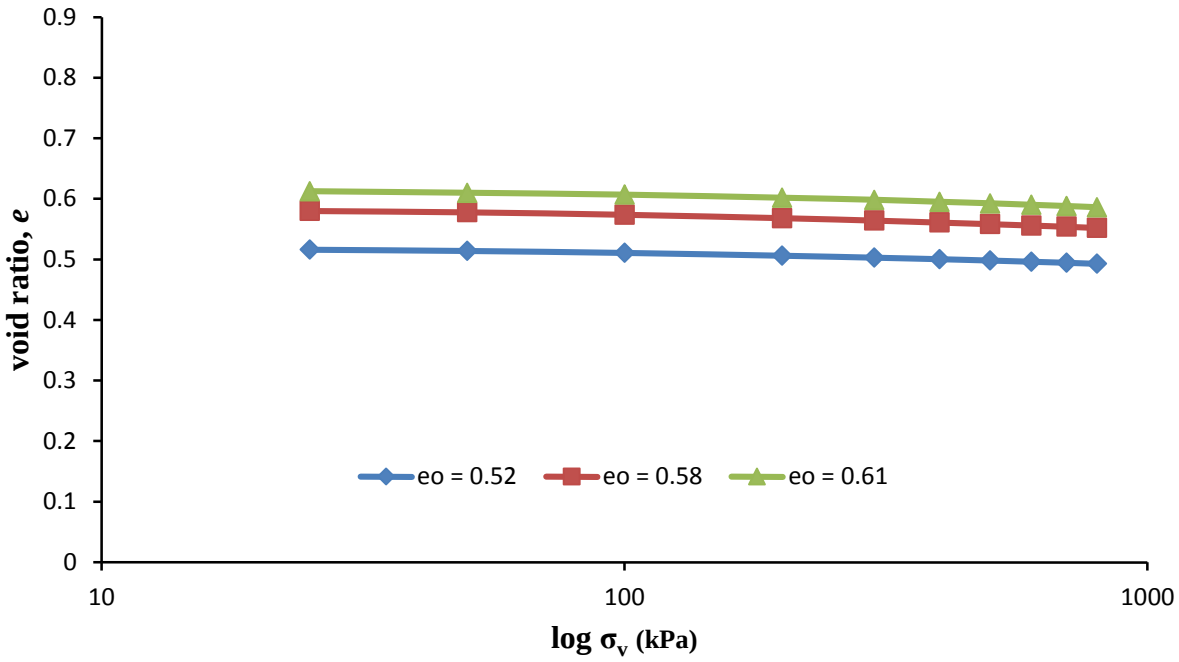

a) Clean Ottawa sand at different e_o

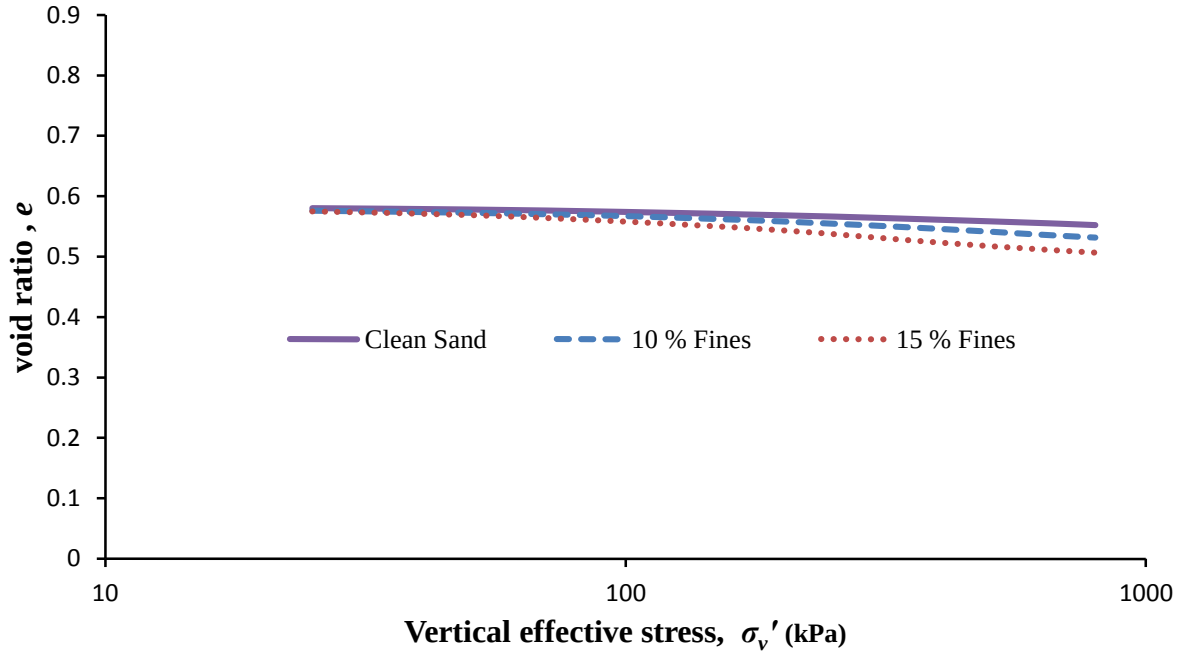

b) Effect of fines on e-log σ_v' of Ottawa sand with fines at e_o = 0.58

Figure 3-16. e-log σ_v

The effect of FC on G_{max} for Ottawa sand was investigated only for the case e_o = 0.58 at two different percentages of fines content, FC = 10 % and 15 % and the results are presented in Fig.3-17. To study the effect of fines on V_s of Ottawa sand, for a given fines content, three tests were conducted and the results are presented as an average values. As observed in Fig.3-17a, a small percentage of fines (FC = 10%) resulted in a significant decrease in $G_{max,}$ i.e. $(G_{max})_{FC = 10\%} \approx 0.7$-0.75 $(G_{max})_{\text{clean-sand}}$, which is similar to the observations made by Salgado et al. (2000). The percentage decrease in G_{max} was higher at lower pressures. In the case of specimens with FC = 15 %, G_{max} decreased further, i.e. $(G_{max})_{FC = 15\%} \approx 0.6\ (G_{max})_{\text{clean-sand}}$ as shown in Fig.3-17b. The significant reduction in the stiffness due to the addition of fines can be possibly attributed to the orientation/pattern of fine particles in soil matrix. Adding fines to the clean sand can lead to the poor interaction between the fine and coarse particles and when load is applied, sideways slippage of fine particles can occur resulting in the reduction of the soil stiffness.

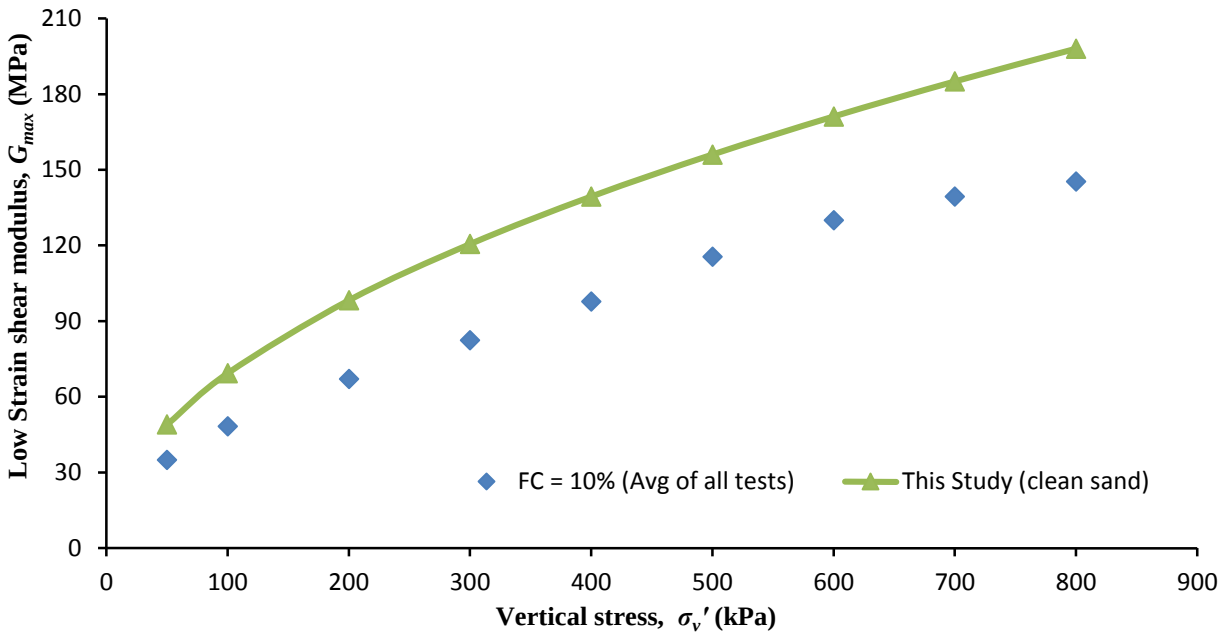

a) FC = 10%;

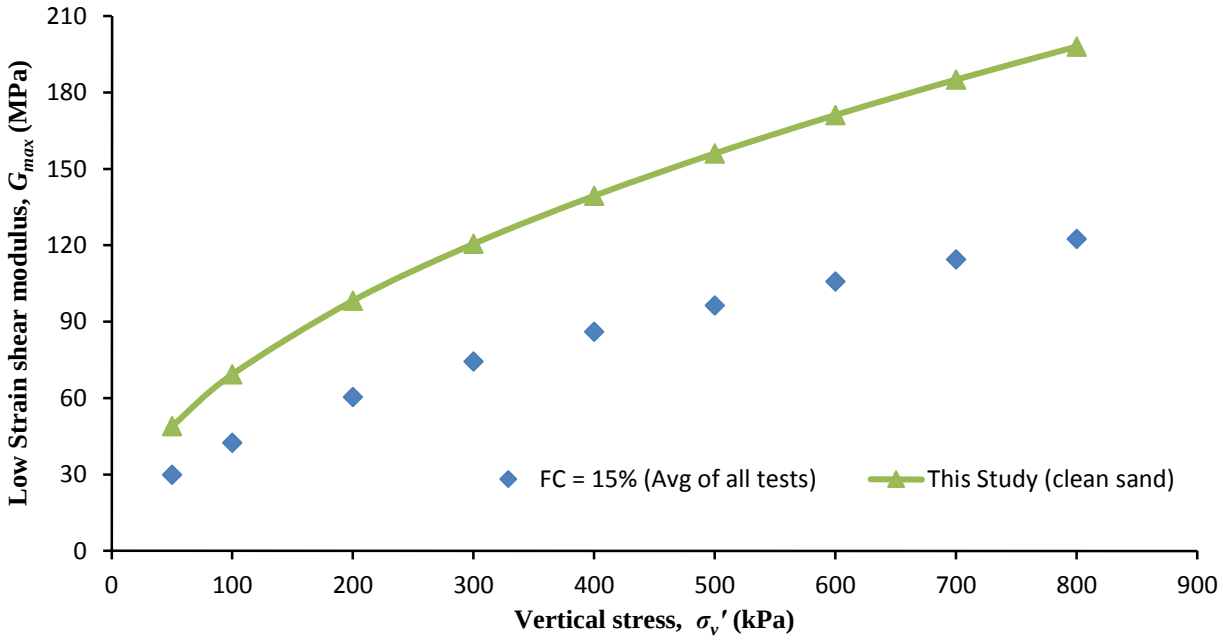

b) FC = 15%

Figure 3-17. Effect of fines content on G_{max} of Ottawa sand

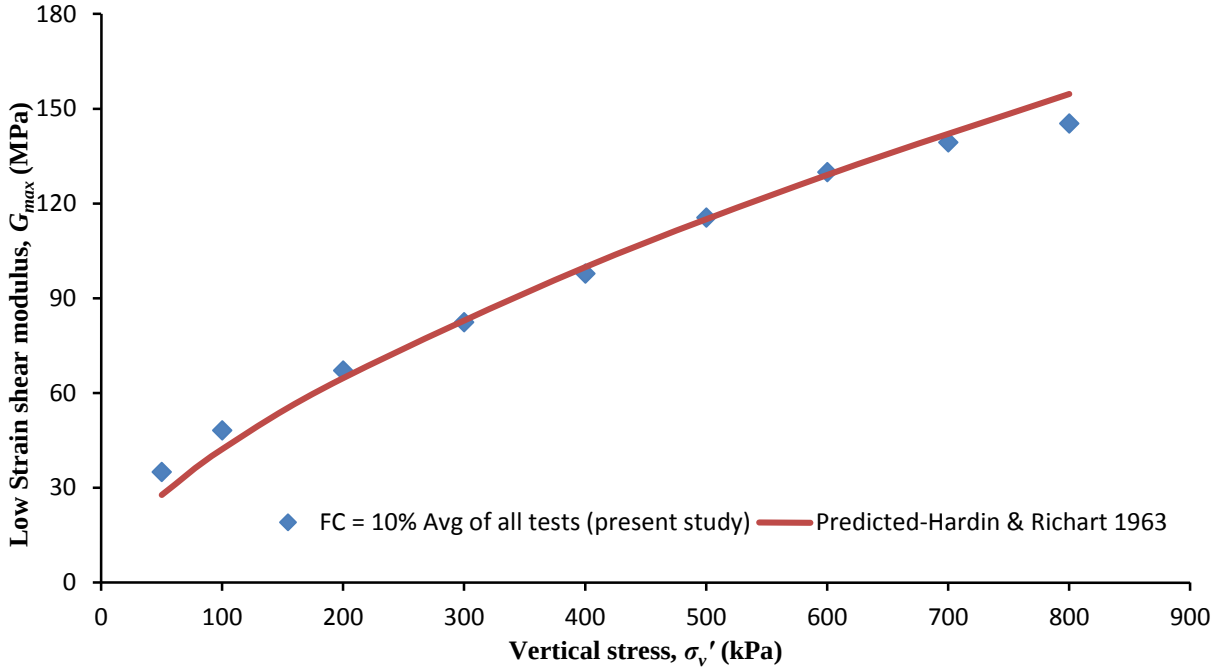

a) FC = 10%;

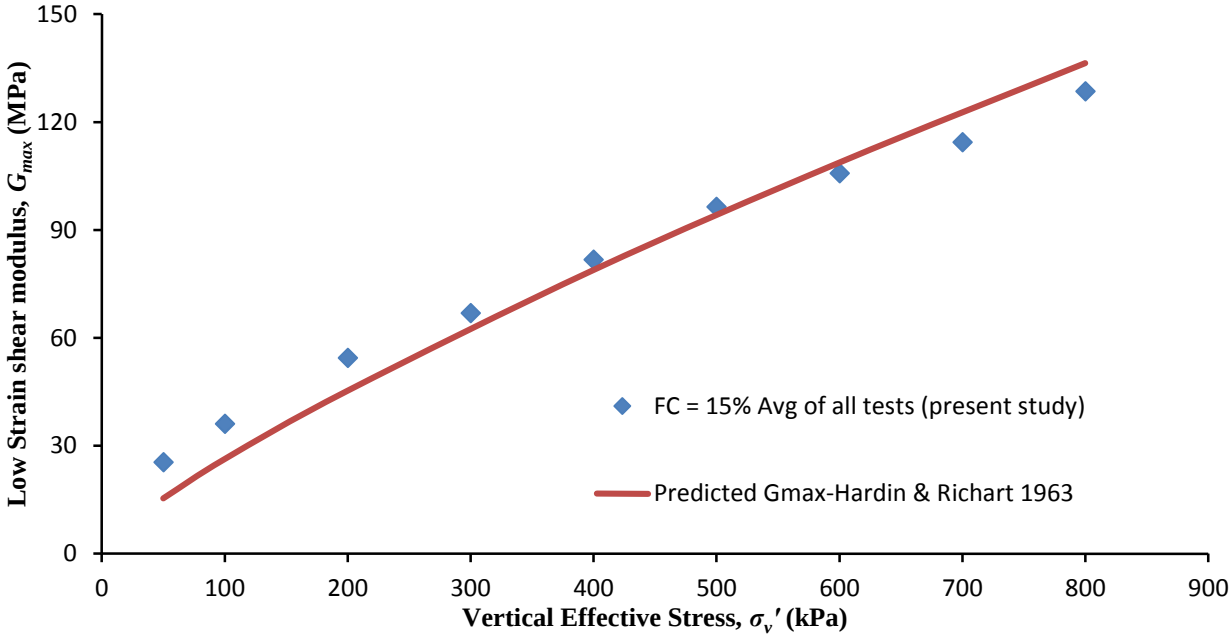

b) FC = 15%

Figure 3-18. Measured and predicted G_{max} values, e_o = 0.58

The measured and predicted G_{max} of silty-sand with different FC is presented in Fig.3-18. As mentioned earlier the results from the present study are only compared with the results of Salgado et al. (2002) by using their regression constants given in Table.3-1 along with the Eq.3.7 by Hardin and Richart (1963). It can be seen from Fig.3-18 that the measured and predicted values are in agreement with the published data, which further confirms the reliability of the measurements obtained using the ring piezoelectric actuators. However, as presented in Fig.3-18b for the case of FC = 15%, there was a small difference between the measured and predicted values of G_{max} at low pressure. The slight difference between the measured values and those predicated from equations presented by Salgado et al. (2000) can be attributed to several factors. These factors include: specimen size, type of fines used, and mixing method etc. Furthermore, the excitation parameters, including: the input waveform (square wave vs. sine wave); input voltages and frequencies of signals; and interpretation methods used to determine travel time etc. can all impact the final results and can be the source of difference between measured and predicted G_{max}. Moreover, Salgado et al. (2000) highlighted the fact that the variations of their G_{max} measurements could be about 15% due to uncertainties involved in bender element testing. However, the agreement between the two sets is better for higher pressure values.

3.9.2.4 Effect of Particle Size on V_s and G_{max} of Clean Ottawa sand

The results presented in Fig.3-13 demonstrated that V_s is independent of D_{50}, which is consistent with the findings of several researchers (e.g. Wichtmann and Triantafyllidis, 2009; Yang and Gu, 2013; Iwasaki and Tatsuoka, 1977; and Chang and Ko, 1982). Thus, for the limited range of D_{50} tested in the present study, G_{max} was considered to be independent of D_{50}.On the other hand, Menq (2003) evaluated the effects of D_{50} and C_u on the stiffness of sands and gravels and reported a slight increase in G_{max} with an increase in D_{50} for constant e and σ'_m. However, it is important to mention that Menq (2003) tested a wide range of D_{50} as compared to the present study.

3.9.2.5 Correlation of shear modulus with void ratio and mean pressure

In practice, approximate evaluation of G_{max} is required to enable preliminary design of important projects, or even final design for smaller projects, subjected to dynamic loading. This approximate

evaluation can be undertaken through empirical correlations of G_{max} to some basic soil conditions such as the void ratio and confining pressure. The results obtained in the current study were used to curve fit an exponential function in the form:

$$G_{max} = C\, f(e) P_a^{1-n} (\sigma_m')^n \tag{3.11}$$

where C and n are regression constants and $f(e)$ is a void ratio function that can be evaluated through the curve fitting.

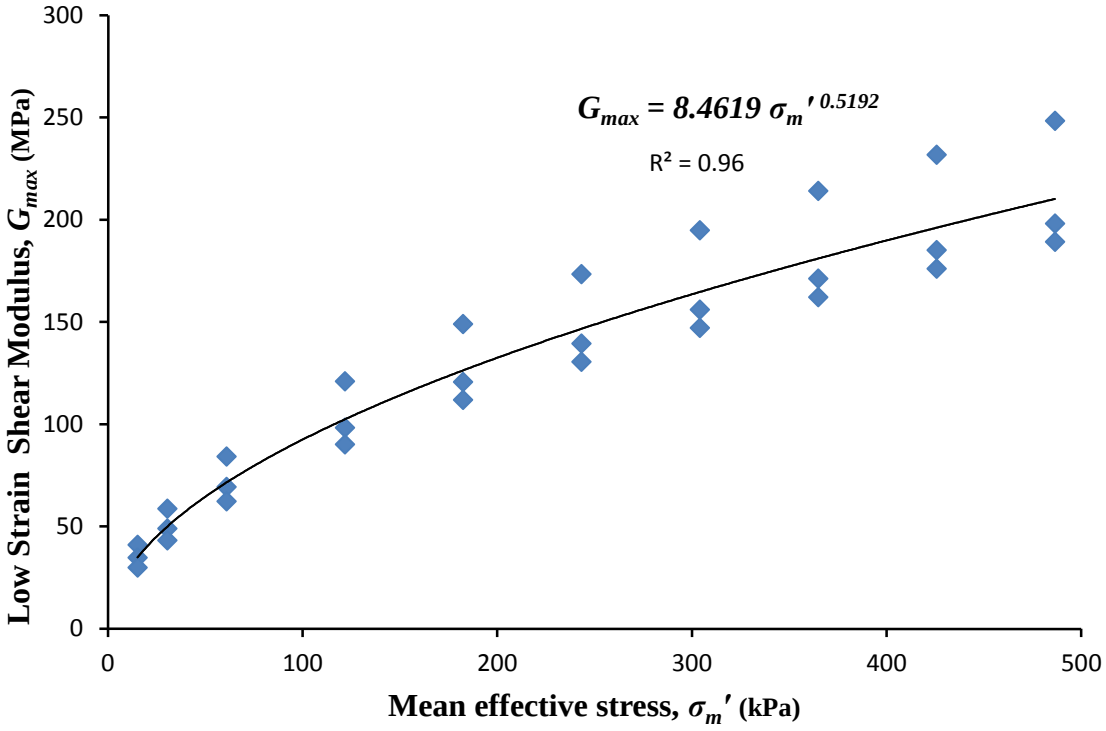

Figure 3-19. Power curve fitting between all the measured G_{max} values (for all e) to find an average value of stress exponent, $n \approx 0.52$

The best curve using least square fit of the laboratory test data for the range of e values considered in this study suggests that G_{max} can be expressed as a function of σ_m' with stress exponent, n that varies between 0.5 and 0.53 depending upon the initial state/void ratio of the sand, with an average $n = 0.519 \approx 0.52$ as shown in Fig.3-19. Rewriting Eq.3.11 as Eq.3.12 and substituting $n = 0.52$ into Eq.3.12, the value of $C\, f(e)$ for each e value can be evaluated.

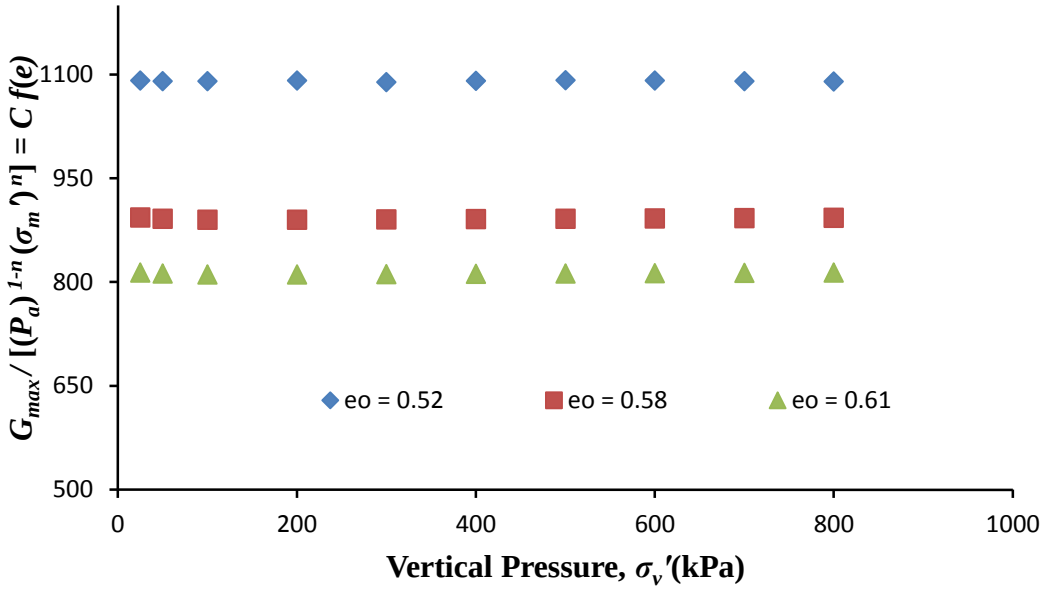

a) ***C f (e)*** vs. σ_v' for different e_o values

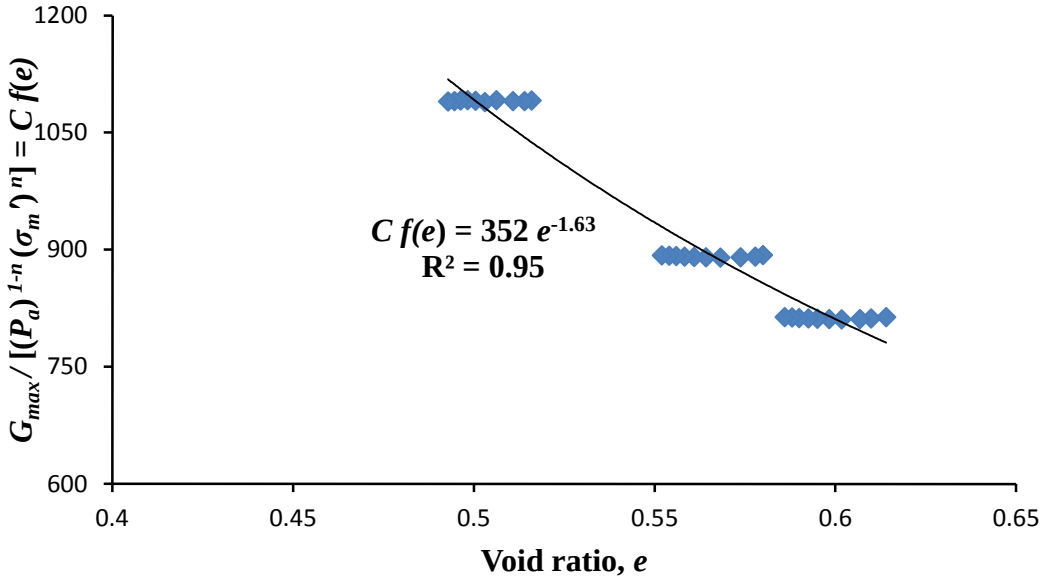

b) ***C f (e)*** vs. ***e***

Figure 3-20. *C f (e)* vs. σ_v' and *e*

$$G_{max}/[P_a^{1-n}(\sigma'_m)^n] = C\ f(e) \tag{3.12}$$

$$G_{max}/[P_a^{1-0.52}(\sigma'_m)^{0.52}] = C\ f(e) \tag{3.13}$$

Table.3-2 presents the G_{max} values along with the corresponding values of $C\,f\,(e)$. Table.3- 2 along with the Fig.3-20a and Fig.3-20b shows that $C\,f\,(e)$ changes as e_o changes but for a given e_o, $C\,f\,(e)$ remains almost constant with an increase in vertical pressure or the decrease in the void ratios. Curve fitting the plot of $C\,f\,(e)$ versus void ratio (e), as shown in Fig.3-20b, yielded C = 352 and $f\,(e) = e_o^{-1.63}$. Substituting these values into Eq.3.13 gives:

$$G_{max} = 352(e)^{-1.63}P_a^{1-0.52}(\sigma'_m)^{0.52} \tag{3.14}$$

For SI units, $P_a \approx 100$ kPa, the low strain shear modulus G_{max} of dry Ottawa sand for e_o = 0.49 - 0.61 and for vertical pressures up to 800 kPa ($\sigma_m' \approx 500$ kPa), can then be evaluated by:

$$\boldsymbol{G_{max} = 3210\ (e)^{-1.63}(\sigma'_m)^{0.52}\ \ (kPa)} \tag{3.15}$$

The G_{max} values obtained using Eq.3.15 are compared with those obtained from actual measurements using actual void ratios as shown in Fig.3-21a, b and c. The results show an excellent agreement between the measured and predicted values for the tests with e_o = 0.52 and 0.61. For tests with e_o = 0.58, and at moderate to high pressures, the predicted values are slightly off (higher) from the measured values. The reason for this offset can be attributed to the stress exponent n. Eq.3.15 has a stress exponent of 0.52 which is the exact one for e_o = 0.52 and very close to the actual for e_o = 0.61 but slighter higher for e_o = 0.58 resulting in predicted values slightly higher than the measured ones. The actual stress exponents are given in Table.3-2.

Table 3-2. G_{max} values for three e values along with n & average value of $C\,f\,(e)$ for each e

G_{max}(MPa) e = 0.52	$G_{max} / [(P_a)^{1-n} (\sigma_m')^n] = C\,f\,(e)$ $e = 0.52$ $n = 0.5206$	G_{max}(MPa) e = 0.58	$G_{max} / [(P_a)^{1-n} (\sigma_m')^n] = C\,f\,(e)$ $e = 0.58$ $n = 0.5035$	G_{max}(MPa) e = 0.61	$G_{max} / [(P_a)^{1-n} (\sigma_m')^n] = C\,f\,(e)$ $e = 0.61$ $n = 0.5334$
40.92	1091.11	34.59	893.12	29.79	813.65
58.67	1090.33	48.93	891.09	43.04	812.17
84.15	1090.23	69.29	890.08	62.20	811.03
120.85	1091.38	98.22	889.98	90.02	810.91
148.93	1089.04	120.51	890.34	111.77	811.05
173.29	1090.90	139.38	890.86	130.40	811.61
194.79	1091.77	156.03	891.29	146.96	812.04
214.04	1091.04	171.11	891.75	162.08	812.58
231.77	1090.30	185.01	892.17	176.06	813.02
248.35	1089.84	197.99	892.69	189.17	813.51
Average	***1090.59***	***Average***	***891.34***	***Average***	***812.16***

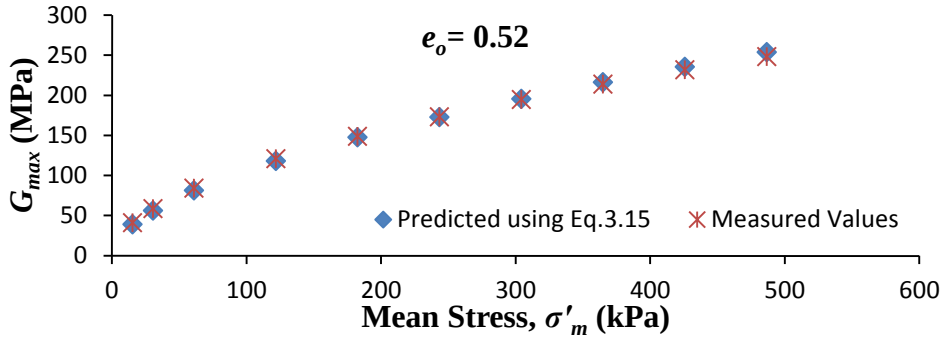

a) e_o = 0.52

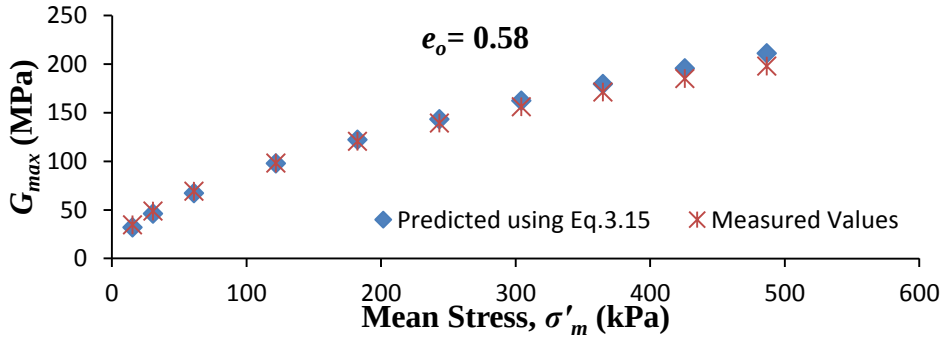

b) e_o = 0.58

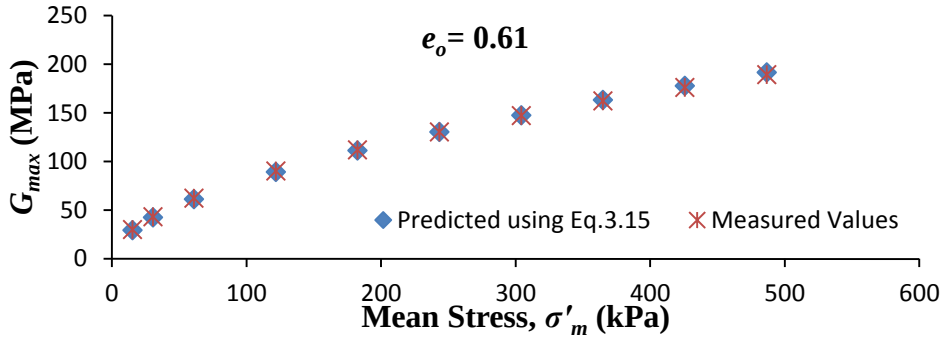

c) e_o = 0.61

Figure 3-21. Comparison of measured and predicted G_{max} at various e_o

3.9.2.6 Evaluation of Dynamic Poisson's ratio of Ottawa sand

Knowing both V_p and V_s, dynamic Poisson's ratio, ν, can be calculated, i.e.

$$\nu = \frac{(V_p^2 - 2\,V_s^2)}{2\,(V_p^2 - V_s^2)} \tag{3.16}$$

However, Hardin and Richart (1963), among others, reported issues with regards to finding ν from measured wave velocities. Hardin and Richart (1963) showed that a small error in V_p/V_s would lead to a large error in ν, and they suggested that ν values obtained with confining pressures below 145 kPa (3000 psf) could be questionable.

Assuming that the very first deflection/movement on the output signal (i.e. Pt. ***A*** in Fig.3-8) represents the P-wave arrival, V_p could be measured and used along with V_s, to calculate ν. Thus, V_p, was obtained for the clean Ottawa sand specimens tested in this study. The range of ν calculated using Eq.3.16 was found to be between 0.27-0.30 with an average of around **0.29**. This value is within the range (0.25-0.33) given in the literature for silica sand (Werner, 1957; Pucci, 2010). On the other hand, several researchers suggested that Poisson's ratio is a function of confining pressure and decreases with an increase in pressure (e.g. Pucci, 2010; Kumar and Madhusudhan, 2010; Menq, 2003; Saxena and Reddy, 1989). However, no clear trend was observed in the current preliminary investigations.

3.10 Conclusions

A new device was fabricated using ring shaped piezoelectric transducers and was incorporated in an Oedometer to be employed for laboratory measurements of soils shear wave velocity. The performance of the fabricated devised was verified by comparing its measurements of V_s of Ottawa sand with the published literature and good agreement was observed. Its performance was further validated through comparisons with measurements made using bender elements on soil specimens under the same conditions and good agreement was also observed. The ring piezoelectric device was then used to investigate the effect of different factors on the dynamic properties of silica sand.

The following conclusions were drawn:

1. The fabricated device, unlike bender elements, is non-invasive and provides consistent and repeatable measurements of V_s. The obtained wave-forms have a clear shear wave with high signal to noise ratio and hence does not require any signal filtering.
2. The shear wave arrival is clear in the received signal as a single major peak, which demonstrates the excellent performance of the fabricated device.
3. The PRA setup allows applying a range of input voltages and frequencies and variety of shapes of the input signals, which facilitates accurate measurements of V_s of soil specimens with different stiffness, density and height.
4. The interpretation methods that gave most accurate arrival times include: group travel time (frequency domain), direct arrival (using first zero before the major event/peak: and using the second arrival (only if second arrival is evident).
5. For clean Ottawa sand, at constant e, V_s increased by increasing σ_m' with a stress exponent, β, of 0.25-0.26.
6. For a given e, and σ_m', V_s was found to be independent of mean particle size (D_{50}).
7. For the tested sand, G_{max} decreased significantly (by almost 25-40%) due to adding a small percentage (10-15%) of non-plastic fines.
8. A new empirical correlation has been suggested for G_{max} of clean-dry Ottawa sand.
9. The dynamic Poisson's ratio for clean Ottawa sand was evaluated and an average value of 0.29 was found.

References

Arulnathan, R., Boulanger R.W., and Riemer M.F. (1998). “Analysis of Bender Element Tests.” *ASTM Geotechnical Testing Journal* 21 (2): 120–131.

ASTM C136-06 (2006), “Standard Test Method for Sieve Analysis of Fine and Coarse Aggregates”, *Annual Book of ASTM Standards*, ASTM International, West Conshohocken, PA.

ASTM D4253-00 (2006), “Standard Test Methods for Maximum Index Density and Unit Weight of Soils Using a Vibratory Table”, *Annual Book of ASTM Standards*, ASTM International, West Conshohocken, PA.

ASTM D4254-00 (2006), `”Standard Test Methods for Minimum Index Density and Unit Weight of Soils and Calculation of Relative Density`”, *Annual Book of ASTM Standards*, ASTM International, West Conshohocken, PA.

Brignoli, E.G.M., Gotti, M., and Stokoe, K.H. (1996). “Measurement of Shear Waves in Laboratory Specimens by Means of Piezoelectric Transducers.” *ASTM Geotechnical Testing Journal* 19 (4): 384–397.

Cha, M., Santamarina, J., Kim, H., and Cho, G. (2014). Technical Note. ”Small-Strain Stiffness, Shear-Wave Velocity, and Soil Compressibility.” *Journal of Geotechnical and Geoenvironmental Engineering.*, 140(10), 06014011.

Chang, N.Y., and Ko, H.Y. (1982). "Effect of Grain Size Distribution on Dynamic Properties and Liquefaction Potential of Granular Soils." *Research Report R82-103, University of Colorado at Denver*. 145 p.

Dyvik, R., and Madshus, C. (1985). "Lab Measurements of G_{max} Using Bender Elements." In *Proc. ASCE Convention on Advances in the Art of Testing Soils Under Cyclic Conditions*: 186–196.

Gamal El-Dean, D.G. (2007). "Development of a new piezoelectric pulse testing device and Soil characterization using shear waves". PhD thesis, Université De Sherbrooke.

Hardin, B.O., and Richart Jr, F.E. (1963). "Elastic Wave Velocities in Granular Soils." *Journal of the Soil Mechanics & Foundations Division* 89 (SM1): 33–65.

http://www.gdsinstruments.com/gds-bender-elements-analysis-tool [Accessed June 01, 2013].

Ismail, M.A., and Rammah K.I. (2006). "Shear-plate Transducers as a Possible Alternative to Bender Elements for Measuring G_{max}." *Géotechnique* 55 (5): 403–407.

Iwasaki, T., and Tatsuoka, F. (1977). "Effects of Grain Size and Grading on Dynamic Shear Moduli of Sands." *Japanese Society of Soil Mechanics and Foundation Engineering* 17 (3): 19–35.

Jovičić, V., Coop, M.R., and Simić, M. (1996). "Objective Criteria for Determining Gmax from Bender Element Tests." *Géotechnique* 46 (2): 357–362.

Khan, Z.H, Cascante, G., El Naggar, M.H. and Lai, C.G. (2008). "Measurement of frequency dependent dynamic properties of soils using the resonant column device". *Journal of Geotechnical and Geoenvironmental Engineering* 134 (9):1319-1326.

Khan, Z.H, Cascante, G. and El Naggar, M.H. (2011). "Measurement of dynamic properties of cemented sand using ultrasonic waves." *Canadian Geotechnical Journal*, 48 (1): 1-15.

Kramer, S.L., (1996), *Geotechnical Earthquake Engineering*, Prentice Hall, Inc., Upper Saddle River, New Jersey, p.653.

Kumar, J. and Madhusudhan, B. N. (2010). "Effect of Relative Density and Confining Pressure on Poisson Ratio from Bender and Extender Elements Tests." *Géotechnique* 60 (7): 561–567.

Lee, J-S., and Santamarina, J.C. (2005). "Bender Elements: Performance and Signal Interpretation." *Journal of Geotechnical and Geoenvironmental Engineering* 131 (9): 1063–1070.

Leong, E.C., Yeo, S.H., and Rahardjo, H. (2005). "Measuring Shear Wave Velocity Using Bender Elements." *Geotechnical Testing Journal* 28 (5): 1–11.

Leong, E. C., Cahyadi, J., and Rahardjo, H. (2009). "Measuring Shear and Compression Wave Velocities of Soil Using Bender–extender Elements." *Canadian Geotechnical Journal* 46 (7): 792–812.

Menq, F.-Y. (2003). "Dynamic Properties of Sandy and Gravelly Soils." PhD thesis, The University of Texas at Austin.

Pucci, M.J. (2010). "Development of a Multi-Measurement Confined Free-Free Resonant Column Device and Initial Studies." M.Sc. thesis, The University of Texas at Austin.

Robertson, P. K., Sasitharan, S., Cunning, J. C., and Sego, D. C. (1995). "Shear-Wave Velocity to Evaluate In-Situ State of Ottawa Sand." *Journal of Geotechnical Engineering* 121 (3): 262–273.

Salgado, R., Bandini, P., and Karim, A. (2000). "Shear Strength and Stiffness of Silty Sand." *Journal of Geotechnical and Geoenvironmental Engineering* 126 (5): 451–462.

Santamarina, J. C., Klein, K. A., and Fam, M. A. (2001). *Soils and Waves: Particulate Materials Behavior, Characterization and Process Monitoring*. *Particulate Materials Behavior, Characterization and Process Monitoring,* Wiley, New York, p.508.

Saxena, S.K., and Reddy, K.R. (1989). "Dynamic Moduli and Damping Ratios for Monterey No. 0 Sand by Resonant Column Tests." *Japanese Society of Soil Mechanics and Foundation Engineering* 29 (2): 37–51.

Thomann, T.G., and Hryciw, R.D. (1990). "Laboratory Measurement of Small Strain Shear Modulus under K_o Conditions." *Geotechnical Testing Journal* 13 (2): 97–105.

Viggiani, G, and Atkinson, J.H. (1995). "Interpretation of Bender Element Tests (Technical Note)." *Géotechnique* 45 (1): 149–154.

Werner, R.R. (1957). "A Study of Poisson's Ratio and the Elastic and Plastic Properties of Ottawa Sand." Agricultural and Mechanical College of Texas.

Wichtmann, T., and Triantafyllidis, T. (2009). "Influence of the Grain-Size Distribution Curve of Quartz Sand on the Small Strain Shear Modulus G_{max}." *Journal of Geotechnical and Geoenvironmental Engineering* 135 (10): 1404–1418

Yang, J., and Gu, X.Q. (2013). “Shear Stiffness of Granular Material at Small Strains: Does It Depend on Grain Size?” *Géotechnique* 63 (2): 165–179.

Chapter 4

4 Dynamic Properties of Cohesive Soils Using Innovative Ring Piezoelectric Actuator

4.1 Abstract

An innovative piezoelectric ring actuator-oedometer setup (PRA) was developed and was used for measuring shear wave velocity (V_s) for a variety of cohesive soils. The variations of V_s and G_{max} of the soil specimens with the effective vertical and mean stresses are evaluated. The soil specimens were also subjected to isotropically consolidated undrained (CIU) triaxial tests to evaluate their undrained shear strength (S_u) at different confining pressures. The V_s and G_{max} measurements were correlated to the results of oedometer and CIU tests. The obtained results showed clear signals from the fabricated device with a single major peak that supports the efficiency of the new technique. Practical empirical correlations are proposed to predict the V_s using the readily measured soil parameter, C_c, without direct measurement for V_s by utilizing the concept of both mean and vertical effective stress. Good agreement was observed between the proposed empirical correlations and the available data in literature. Moreover, the correlations between the measured V_s or G_{max} and S_u for the tested soils are proposed to be used as a guideline for similar soils. The G_{max} value for the tested soils was found to vary from 400 to 1400 times the soil undrained strength, S_u while the stiffness ratio ($G_{dynamic}/G_{static}$) for the tested soil specimens varied between 5 and 13 and decreased with the increase in G_{static}. The stiffness ratios E_{dyn}/E_{oed}, $E_{dynamic}/E_{static}$, E_{stat}/E_{oed} for the tested soils were determined and found to be around 40, 8 and 5, respectively. Finally, the average dynamic Poisson's ratio for the tested soils was found to be around 0.42.

Keywords: Piezoelectric transducers, shear wave velocity, shear modulus, undrained shear strength, oedometer, and cohesive soils.

4.2 Introduction

Very low-strain shear modulus or dynamic shear modulus (G_o or G_{max}) is a fundamental soil property, which depicts the deformation behavior of soils under small-strain conditions. It is an

essential soil property for dynamic soil-structure interaction analyses that involve earthquakes, explosions, machine or traffic vibrations as well as small-strain cyclic loading situations such as those caused by wind or wave loading (Dyvik and Madshus, 1985). At very low strains (typically less than 0.001%), G_{max} can be related to V_s, i.e.

$$G_{max} = \rho V_s^2 \tag{4.1}$$

where: ρ is soil's bulk density and V_s is the shear wave velocity.

Kim and Novak (1981) tested seven undisturbed cohesive soils from Ontario using resonant column test and presented their work as an empirical correlation for V_s given by:

$$V_s = (73.03 - 33.86e)\, OCR^{\frac{K}{2}}\, \sigma_o'^{0.25} \tag{4.2}$$

where V_s is in (m/s), e is void ratio, OCR is overconsolidation ratio, K is a function of plasticity index, and σ_o' is the confining pressure (kPa). The obtained results from their study were compared with the results presented by Hardin and Black (1969). The comparison demonstrated that the correlation suggested by Hardin and Black (1969) significantly overestimates V_s for the examined cohesive soils.

Kim and Novak (1981) also compared G_{max} from their study with the predictions of the Hardin and Black (1969) correlation and most of their measured values clustered around the lower bound of the Hardin and Black (1969) predictions, while the upper bound for G_{max} defined by Hardin and Black (1969) significantly overestimated G_{max}. To better describe the observed behavior of the tested soils, they revised Hardin and Black (1969) correlation, i.e.

$$G_{max} = \frac{C_o\,(2.973 - e^2)}{1 + e}\, OCR^K\, \sigma_o'^{0.5} \tag{4.3}$$

where C_o is the slope of the G_{max} - σ_o' function, which they evaluated for both normally and overconsolidated soils.

Shibuya et al. (1997) evaluated the results of field seismic surveys and laboratory bender element tests on reconstituted clay specimens and suggested an empirical expression for G_{max} of normally consolidated soft clays, i.e.

$$G_{max} = A(1+e)^{-2.4}\,\sigma_v'^{0.5} \tag{4.4}$$

where σ_v' is the vertical effective stress and A is a soil-dependent constant. The void ratio function $F(e) = (1+e)$ suggested by the authors avoids the sharp reduction in G_{max} when $e \rightarrow 2.973$ as in the case of Hardin and Black's (1969) void ratio function. They reported that by using an appropriate $F(e)$, OCR has negligible influence on G_{max} and hence can be ignored (i.e. Eq.4.4). Shibuya et al. (1997) reported parameter A values between 18,000 and 30,000 with an average value of 24000.

Vardanega and Bolton (2013) compiled data available in the literature along with the $F(e)$ proposed by Shibuya et al. (1997) and presented a semi-empirical expression in terms of mean effective stress (σ_m' or p'), i.e.

$$\frac{G_{max}}{p_r'} = \frac{\boldsymbol{B}}{(1+e)^{2.4}}\left(\frac{p'}{p_r'}\right)^{0.5} \tag{4.5}$$

In Eq.4.5, p_r' is the reference pressure taken as 1 kPa. For most soft soils, the authors reported that parameter B generally varies between 15,000 and 25,000 with an average of 20,000. For stiff, overconsolidated aged clays, they reported $B \approx 50{,}000$, and for highly fissured London clay, they reported B <15,000.

In the absence of capillary effects, the effective stresses govern the shear stiffness of un-cemented soils (Lee et al., 2005). Hence, V_s depends upon the effective stresses in the direction of wave propagation in the polarization plane (Hardin and Drnevich, 1972; Roesler, 1979; Knox et al., 1982; Yu and Richart, 1984; Petrakis and Dobry, 1987), i.e.

$$V_s = \alpha\left(\frac{\sigma'_{mean}}{1kPa}\right)^{\beta} = \alpha\left(\frac{\sigma'_{\parallel} + \sigma'_{\perp}}{2kPa}\right)^{\beta} \tag{4.6}$$

where α (m/s) is V_s at 1 kPa; $\sigma'_{\perp}$ and $\sigma'_{\parallel}$ are the effective stresses in the direction of particle motion (along the sample's diameter) and in the direction of wave propagation (along the height of the sample), respectively. The exponent β reflects the sensitivity of V_s to σ'_{mean} in the polarization plane and depends on the nature of interparticle contacts and fabric changes during loading (Cha et al. 2014). The factor α inherently incorporates the effect of the void ratio function that generally exists in the conventional V_s correlations. Together, these fitting parameters reflect contact behavior and changes in fabric associated with effective stress, i.e., the velocity-stress power relationship captures both contact stiffness and soil fabric (Cha et al., 2014). The exponent β increases as the soil compressibility increases, while the factor α decreases with the increase in compressibility.

Cha et al. (2014) compiled the experimental results from the literature, obtained primarily from oedometer cells instrumented with bender elements, for a wide range of soils, and range of σ_m' from 10 to 1200 kPa. Based on this data set, they proposed a correlations between α and β factors, i.e.

$$\beta = 0.73 - 0.27\, log\left(\frac{\alpha}{\frac{m}{s}}\right), \qquad 1m/s \leq \alpha \leq\sim 500\, m/s \tag{4.7}$$

Several studies (e.g. Brocanelli and Rinaldi 1998; Lee et al., 2005; Yun and Santamarina 2005; and Cho et al., 2006) reported values of α and β for sands while limited studies reported their values for natural undisturbed cohesive soils (e.g. Viggiani and Atkinson, 1995) and apparently no such relationship exists in terms of vertical effective stress up to authors' knowledge .

The main objectives of the present study are: (1) to check and validate the performance of the PRA setup for the measurement of V_s for a variety of cohesive soils; (2) provide useful practical correlations between the fitting parameters for V_s and the commonly measured compression index C_c, using both the mean and vertical effective stress concept. The proposed correlations can be used to predict the approximate V_s profile without actually making *Vs* measurements; (3) to empirically correlate the small strain properties (V_s and G_{max}) with the large strain ones (S_u, E_{static} and $E_{oedometric}$), which can provide useful information for dynamic analyses such as for the design of machine foundation for similar soils. To achieve these objectives, a new test setup made of

piezoelectric ring actuators (PRA) incorporated in the oedometer device was used to measure the dynamic soil properties (V_s and hence G_{max}) for a variety of cohesive soils. The variation of V_s and G_{max} with the effective applied pressure was evaluated for the tested soils and the results are presented as $V_s - \sigma'$ and $G_{max} - \sigma'$ models. The results were used to evaluate values of fitting parameters for the cohesive soils tested. These parameters are discussed in details in the later sections. In addition, the undrained shear strength (S_u) of the test specimens was measured at different confining pressures using CIU triaxial tests.

4.3 Materials and Methods

Five different cohesive soils were tested in this study including four natural undisturbed soils and an artificial clay manufactured by mixing kaolin (K) and silt (S). This artificial clay, referred to as K-S soil, is widely used in laboratory and centrifuge studies (e.g. Alnuaim et al., 2015). In the current study, it was prepared by mixing kaolin and silt at equal proportions by weight, and was preconsolidated to a 300 kPa pressure. The four natural soils were Sombra, Ottawa, Brantford and Denfield clay. Sombra and Ottawa clay are soft cohesive soils, Brantford is a clayey silt, while Denfield is stiff, heavily overconsolidated silt. The index properties of the tested soils are given in Table.4-1. The grain-size distribution analysis for the tested soils was conducted using ASTM D422 (ASTM, 2007) and the results are presented in Fig.4-1.

Atterberg Limits were measured following ASTM D4318 (ASTM, 2010). Among the tested soils, Sombra clay has the highest plasticity, while Brantford clayey-silt has the least. The average water content of the Sombra clay was found to be close to its liquid limit thus giving it a soft consistency; similarly, the Ottawa soil had water content slightly higher than its liquid limit giving it a soft consistency and a liquidity index of slightly more than unity indicating that soil may have some degree of sensitivity. The Denfield soil was very stiff, heavily overconsolidated with a low void ratio and it had natural moisture content less than its plastic limit, which is a common property of heavily overconsolidated soils. Specific gravity (G_s) for all soils was measured using ASTM D854 (ASTM, 2014).

Table 4-1. Index Properties of the tested soils

Soil	Avg. Initial Void Ratio, e_0	Specific Gravity, G_s	Avg. Natural Water Content, W_N (%)	Unit Weight, γ_t (kN/m^3)	Liquid Limit, W_L *(%)*	Plasticity Index, I_P *(%)*	*Effective Friction Angle, ϕ' (deg)
Sombra	1.07	2.70	45	18.49	51	27	28
Ottawa	0.96	2.74	34.5	18.45	32	17	29
Denfield	0.48	2.70	16	21.09	35.5	17	31.5
K-S	0.85	2.63	30	18.25	38	15.7	25
Brantford	0.51	2.70	18.2	20.97	24.7	8.7	34

* From CIU triaxial test

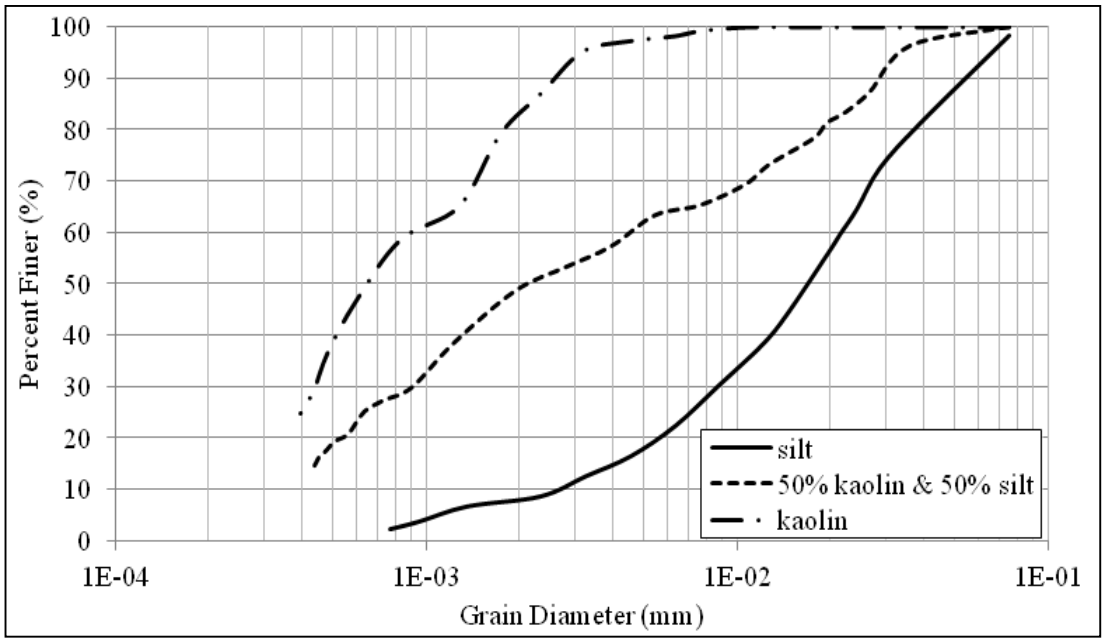

a) K-S soil and its constituents

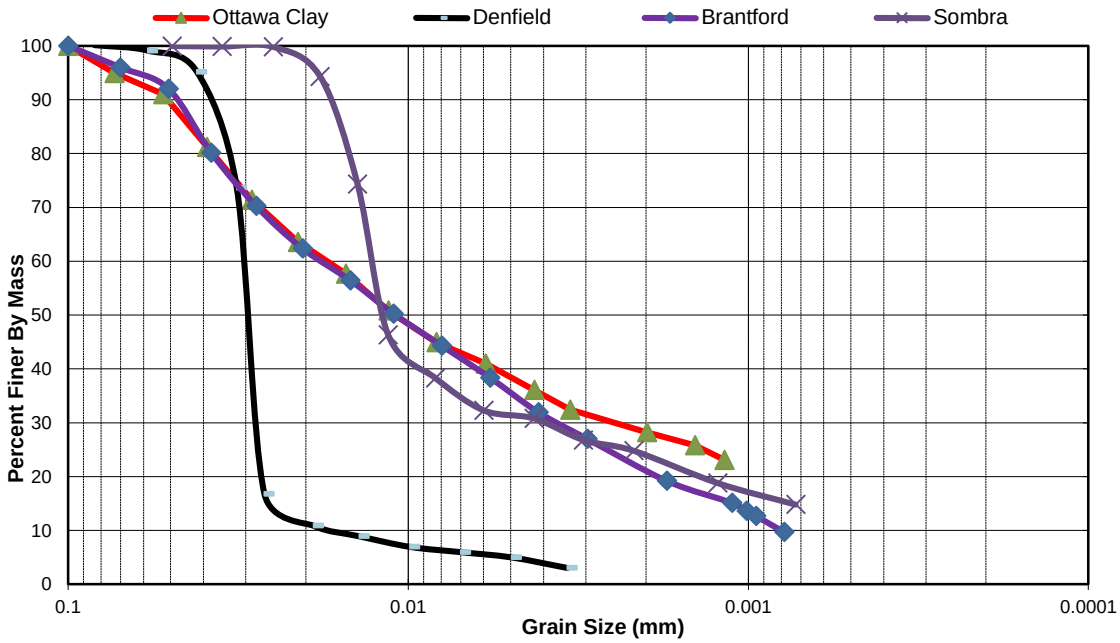

b) Natural soils

Figure 4-1. Particle-size distribution curves of tested soils

A new device developed in the current study utilizing piezoelectric ring actuators (PRAs) was incorporated in an oedometer to measure V_s. The device utilizes ring shape piezoelectric elements with inner and outer diameters i.e. $\varnothing_{inner}$ = 38 mm, $\varnothing_{outer}$ = 44 mm respectively and height, H = 3.5 mm. The detailed setup for the new PRAs device incorporated in an oedometer device is presented in Fig.4-2. It is possible to conduct 1D consolidation test using this set-up and to simultaneously measure the V_s of the soil specimen at various applied pressures.

This technique allows more accurate measurement of V_s by overcoming the limitations associated with the traditional bender elements. For example, Ismail and Rammah (2005) listed several limitations of using bender elements in measuring V_s, including: they penetrate the soil samples which cause disturbance and/or local nonlinearity for undisturbed and cemented soils; they require filling the holes made in soil with coupling material like epoxy or gypsum; they induce high stresses in the conical zone adjacent to conventional platens of the triaxial apparatus; and they may suffer depolarization at high voltages due to their small thickness. On the other hand, the device used in the current study does not penetrate the test specimen, ensuring no disturbance of specimen

or local nonlinearity. This also allows testing very stiff and heavy overconsolidated soils which can damage bender element during penetration through such soils and can test the soils at a wide range of pressures from very low to very high.

Moreover, the size of piezoelectric ring actuators employed allows using a fairly high voltage input signal without causing any depolarization. This allows testing soft soils or soils under low pressures, which may require a high voltage input signal in order to achieve an output signal with high signal to noise ratio (SNR), hence ensuring accuracy of measurements. More details about the fabrication of the new device can be found in Chapter 3.

When voltage is applied between the inner and outer diameters (i.e. radially), the piezoelectric element deforms and vibrates in the radial direction according to the shape of the input signal. This radial deformation causes shearing of the soil base thus producing shear waves that propagate through the soil specimen. High voltage input sinusoidal signals ($\approx$ 50 -100V_{p-p}) were used to measure V_s. The input voltage can be further increased if required to 300V_{p-p} or even more without depolarizing the PRAs which is not usually the case with bender elements.

Sinusoidal input signals of different frequencies typically between 10-40 kHz were used and both the input and output signals were captured using a program written in the LabVIEW environment. Different frequencies were used to evaluate the effect of L/λ (L = height of soil sample and λ = wavelength of input wave). The results from the testing program reported herein demonstrated that reliable measurements of V_s could be accomplished for cohesive soils when $L/\lambda \geq$ 2-3. Similar conclusions were drawn by other researchers employing bender elements (e.g. Leong et al., 2005; Leong et al., 2009; and Mancuso and Vinale, 1988).

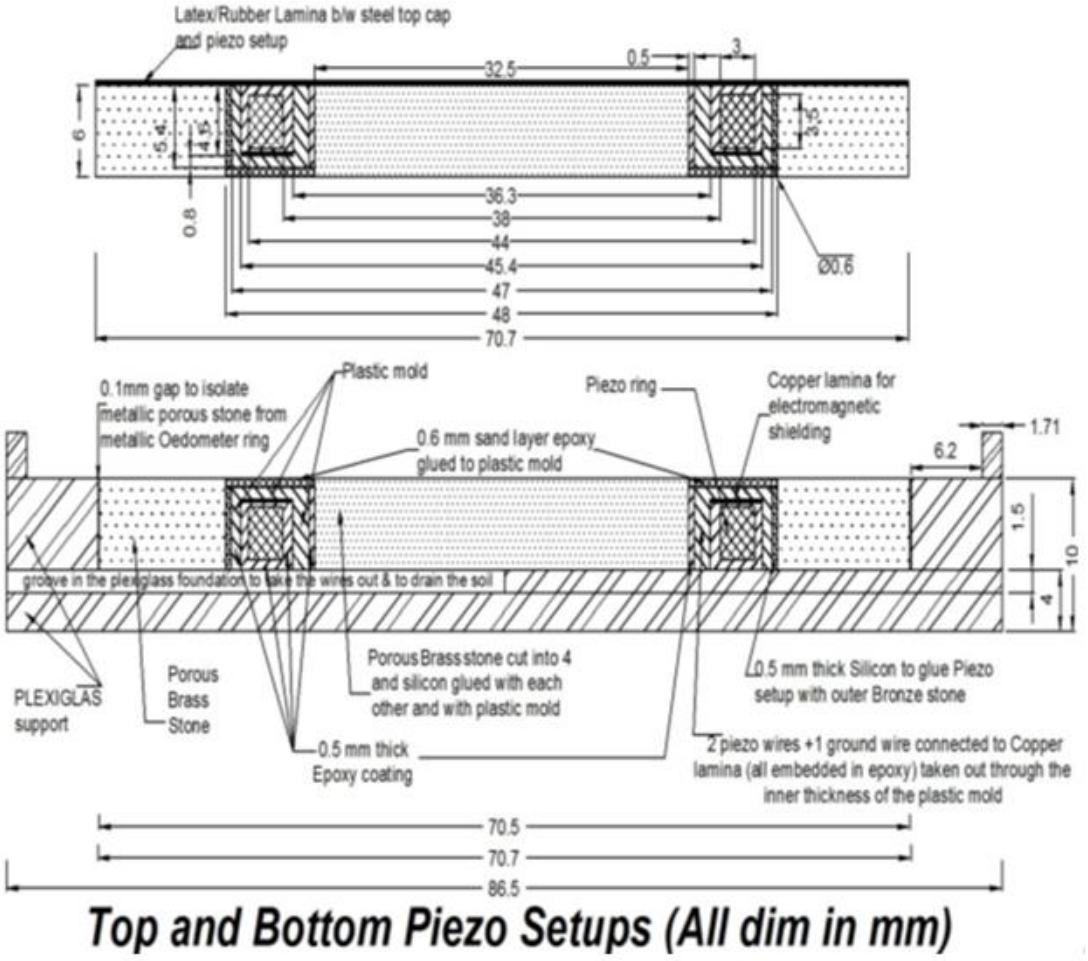

Figure 4-2. Piezoelectric Ring actuator piezoelectric setup incorporated in oedometer

Fig.4-3 shows the typical signals captured for the Brantford soil with the PARs device. The signals are captured at different σ_v' starting from low value of 25 kPa to a high value of 500 kPa. It is evident from Fig.4-3 that the output signals at all pressures are very clear as they all have only one major peak (shear wave) and have very high SNR.

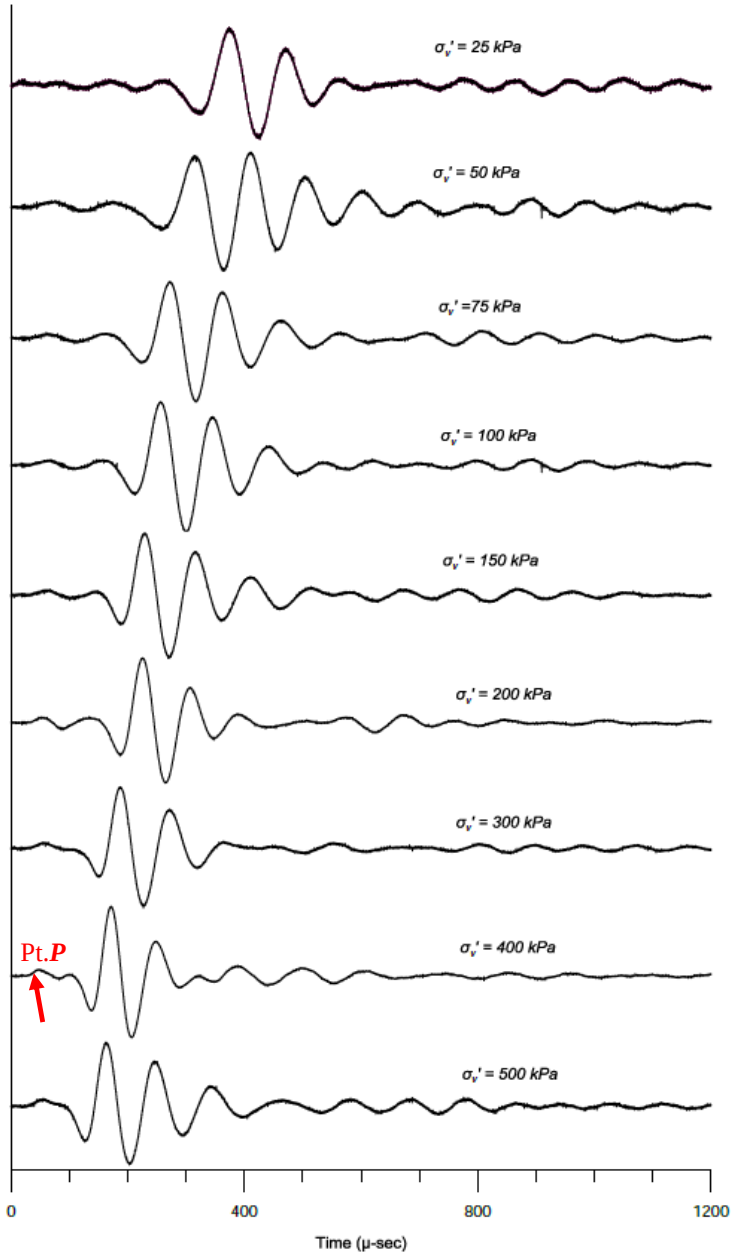

Figure 4-3. Output signals with clear shear waves for Brantford soil at different σ_v'

Fig.4-3 also demonstrates that all signals are devoid of Crosstalk, thanks to appropriate grounding and shielding used in the PRAs device employed in this study. Crosstalk is a phenomena that occurs due to electromagnetic coupling between the source (emitter) and receiver piezoelectric elements (Lee and Santamarina, 2005; Leong et al., 2009). It appears on the output signal as a duplicate of the input sine-wave. Crosstalk can be very significant in conductive soils such as wet clays. Leong

et al. (2009) observed the crosstalk during their studies and attributed this to the improper grounding. Crosstalk can interfere with the output signal and can mask the arrival of the shear wave, especially when testing short specimens at low frequencies and/or at high pressures. In such cases, the shear wave arrival time, t_s, is either very close or less than the period of the input wave. It is also evident from Fig.4-3 that increasing the pressure, decreases the arrival time and hence increase the V_s.

There are several methods to identify the first arrival of shear wave and to calculate shear wave travel time (t_s). The group velocity technique (frequency domain analysis) presented by Viggiani and Atkinson (1995) was used herein to calculate t_s and an example of the obtained results is shown in Fig.4-4. The method gives arrival point of first shear wave as pt. ***A***. The arrival time for all captured signals was found to be at or very close to the first zero crossing before the major event/peak. The direct arrival technique (i.e. the first zero before the major peak) and group velocity method provided results in very close agreement with each other.

Point ***A*** was established by substantial testing on a well-documented material (i.e. Ottawa sand presented in) and was further authenticated by testing Ottawa sand in a ring shear apparatus incorporating bender elements (Chapter 3). A detailed analysis of output signals was performed in both time and frequency domain using GDS **B**ender **E**lement **A**nalysis **T**ool (BEAT). As seen in Fig.4-4, a cross-correlation technique using time domain analysis significantly overestimated t_s and hence underestimated V_s and, therefore, was not pursued further.

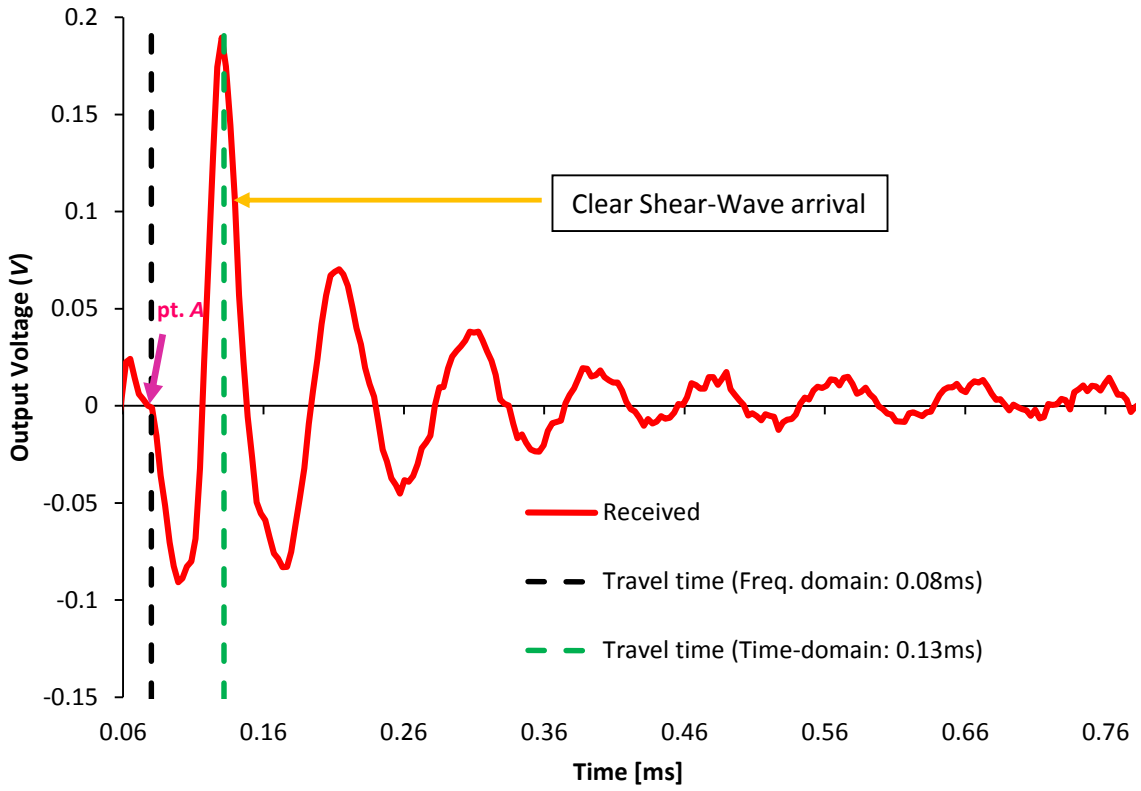

Figure 4-4. Time (cross-correlation) & frequency domain (group velocity method) arrival times

The tested oedometer soil specimens were trimmed from undisturbed Shelby tube samples. The oedometer specimens were 70 mm in diameter and 25.4 mm in height. The specimens were tested under different σ_v' ranging from 25 kPa up to 500 kPa, usually in 9 increments. Four specimens of each soil type were tested in oedometer for 1D-consoldiation and for V_s measurements. The V_s measurements were made at every load increment at the end of the consolidation using several input sine wave frequencies as discussed earlier.

The undisturbed triaxial samples were 50 mm in diameter and 100 mm in height. The samples of each soil type were tested under different confining pressures. Depending upon the availability of the samples, 3-4 CIU triaxial tests were conducted on specimens of each soil type. The strain rate during undrained shearing stage was usually kept around 0.0081mm/min.

In order to facilitate correlations between the measured V_s and G_{max} values with undrained shear strengths (S_u) obtained from CIU triaxial tests, it was necessary to convert data from K_o conditions (oedometer test) into isotropic conditions (triaxial tests), i.e. transforming σ_v' values into corresponding σ_m', which required an accurate measurement of K_o (at rest coefficient). For virgin compression loading, K_o was calculated using the equation proposed by Jaky (1944) i.e. $(K_o)_{NC} = 1\text{-}sin\phi'$ and was then modified for the OCR effect along the recompression curve [$(K_o)_{oc} = (1\text{-}sin\phi')OCR^{sin\phi'}$]. Therefore, the effective friction angle (ϕ') was determined for each soil type from the results of the CIU triaxial tests and the results are summarized in Table. 1.

4.4 Results and Discussion

4.4.1 Oedometer Test Results

Fig.4-5 shows the $e - log\ \sigma_v'$ of the tested soils. The K-S soil was preconsolidated to an effective vertical pressure of 300 kPa. This is manifested in Fig.4-5, as the soil displayed overconsolidated behavior. Likewise, the Denfield soil specimens were recovered from a relatively shallow depth of 1.44m – 1.83m from an area characterized by very stiff to hard crust. Relatively high field SPT values of 15 to 20 were recorded at the site along the top 2.0 m. Employing the correlations between SPT values and soil effective preconsolidation pressure (σ_p') due to Mayne and Kemper (1988), σ_p' was found to be 634-720 kPa. Given that the in-situ effective overburden pressure was about 33.5 kPa, the OCR was computed employing the empirical equations provided by Mayne and Kemper (1988) and was found to be between 19 and 21.5. Abdelaziz and El Naggar (2014) reported similar results for heavily overconsolidated soil (OCR varied between 25 and 35 for the top 2.0 m) retrieved from nearby site. The high overconsolidation behavior of the Denfield soil is clearly demonstrated in Fig.4-5, for the range of applied σ_v' (i.e. it displayed overconsolidated behavior for σ_v' up to 500kPa).

The V_s - σ_m' and G_{max} - σ_m' models require accurate determination of K_o for transforming σ_v' values into σ_m' values. Therefore, it is necessary to accurately evaluate the preconsolidation pressure (σ_p') in order to determine K_o reasonably accurate. In the absence of the actual measurement of σ_p' and given the uncertainty related to OCR, the V_s - σ' and G_{max} - σ' models for Denfield soil will be presented only in terms of σ_v' as compared to both σ_v' and σ_m' as it is the case for all other soils.

The results of V_s and G_{max} measurements for Denfield soil will be correlated with the CIU triaxial results considering the same value of σ_v' instead of σ_m'. Since Denfield soil did not exhibit normally consolidated behavior, the comparisons and correlations that require the compression index C_c cannot be considered for Denfield soil. For the other soils, σ_v' values were transformed into σ_m' values using appropriate k_o values.

4.4.2 V_s - σ' and G_{max} - σ' Models

The results from the current study are presented as V_s - σ' and G_{max} - σ' relationships. It is more conventional to present the variation of V_s and G_{max} with σ_m', where σ_m' is defined by the average of the three stresses i.e.

$$\sigma_m' = \frac{(1 + 2k_o)}{3}\sigma_v' \tag{4.8}$$

On the other hand, the variation of V_s and G_{max} with σ_v' is more convenient given the usually conducted tests and practically eliminates the need to evaluate the in-situ k_o values. Therefore, it was decided to present variations of V_s and G_{max} with both σ_m' and σ_v' in order to allow comparisons with the published literature, and to allow using readily available σ_v' in conducted tests and field applications. The V_s - σ' power relationship in its general form is given by:

$$V_s = \alpha\sigma'^{\beta} \tag{4.9}$$

The power curve fitting parameters (i.e. a constant and an exponent in Eq.4.9) for the V_s - σ' models with $\sigma' = \sigma_v'$ are denoted α_v and β_v. These parameters for the models with $\sigma' = \sigma_m'$, where σ_m' is defined by the average of the three stresses (Eq.4.8) are denoted as α_{m3} and β_{m3} whereas, the parameters for the models with $\sigma' = \sigma_m'$, are denoted as α_{m2} and β_{m2} or simply α β. The summary of the fitting parameters for the first two models for each soil (Fig.4-6 and Fig.4-7) are presented in Table.4-2 for the full pressure range while these parameters during the virgin compression and also for the comparison with work of Cha et al. (2014) are given in Table.4-3.

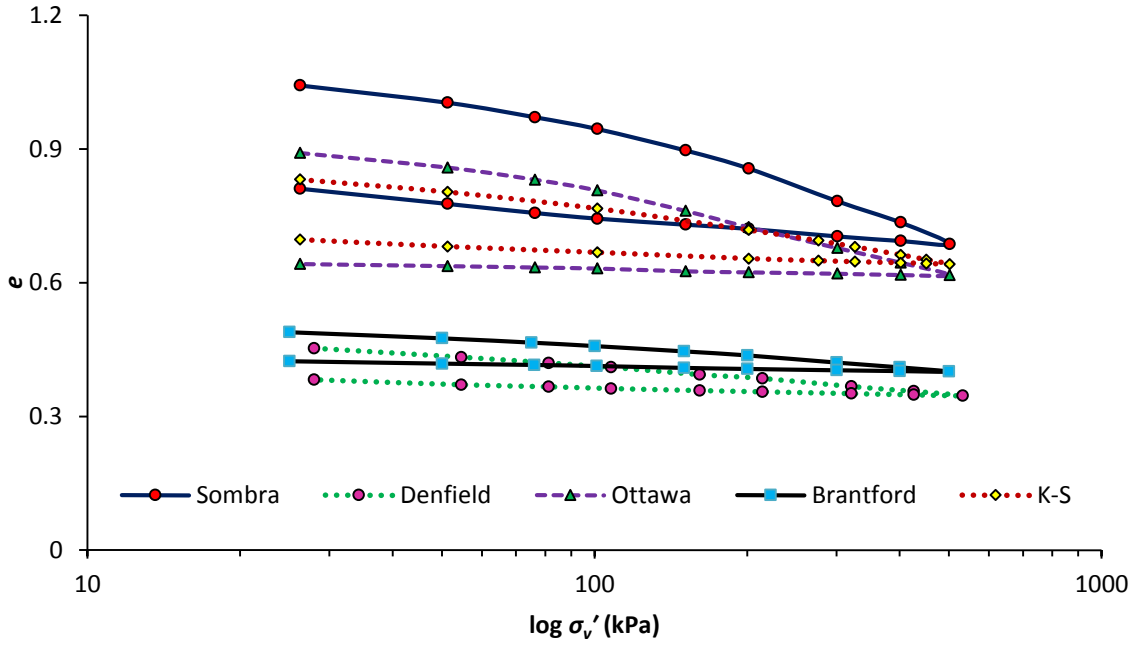

Figure 4-5. 1D consolidation results of the tested soils

Fig. 4-6 presents the V_s - σ_v' models for all tested soils covering the full applied pressure range (i.e. both overconsolidated and normally consolidated phases).

Figure 4-6 shows that Sombra clay exhibited the highest stress exponent, β_v (0.3) and lowest constant, α_v (30.6) among the tested soils. This may be attributed to its soft consistency, high natural water content, high e_o and high plasticity. Sombra was also the most compressible (highest C_c) among the tested soils as presented in Table.4-3.

The Brantford soil exhibited the highest α_v (65) and a lowest β_v (0.23) among all the natural and normally consolidated or lightly overconsolidated soils, which represents the typical behavior of stiff silty soil with low plasticity (Cha et al. 2014). The Ottawa clay displayed V_s and G_{max} variations in between that of the Sombra and Brantford clays, the values of its PI and C_c were similarly in between those measured for Sombra and Brantford clays. On the other hand, the Denfield soil being very stiff and heavy overconsolidated soil, it exhibited the highest α_v and lowest β_v value as seen in Fig.4-6.

The K-S soil displayed overconsolidated behavior during most of the applied pressure (i.e. up to 300 kPa), and displayed normally consolidated soil behavior afterwards. Thus, it showed a relatively high α_v and low β_v values as compared to other tested soils (excluding Denfield), which is attributed to the effect of its overconsolidation and medium plasticity.

Table 4-2. Fitting parameters for the V_s - σ' models for full pressure range

	$V_s = \alpha_v (\sigma_v')^{\beta v}$		$V_s = \alpha_{m3} (\sigma_m')^{\beta m3}$	
Soil	**Fig.4-6**		**Fig.4-7**	
	α_v	β_v	α_{m3}	β_{m3}
Sombra	30.59	0.3	27.68	0.34
Brantford	65.07	0.23	54.51	0.295
Ottawa	40.85	0.27	38.23	0.30
K-S	78.99	0.19	60.23	0.254
Denfield	111.74	0.18	--------	--------

The V_s - σ_m' models are presented in Fig.4-7. It should be noted that the V_s results plotted in Fig.4-6 and Fig.4-7 for each soil represent the average of four tested samples. Also, the values of σ_m' plotted in this graph (Fig.4-7) were calculated from σ_v' values.

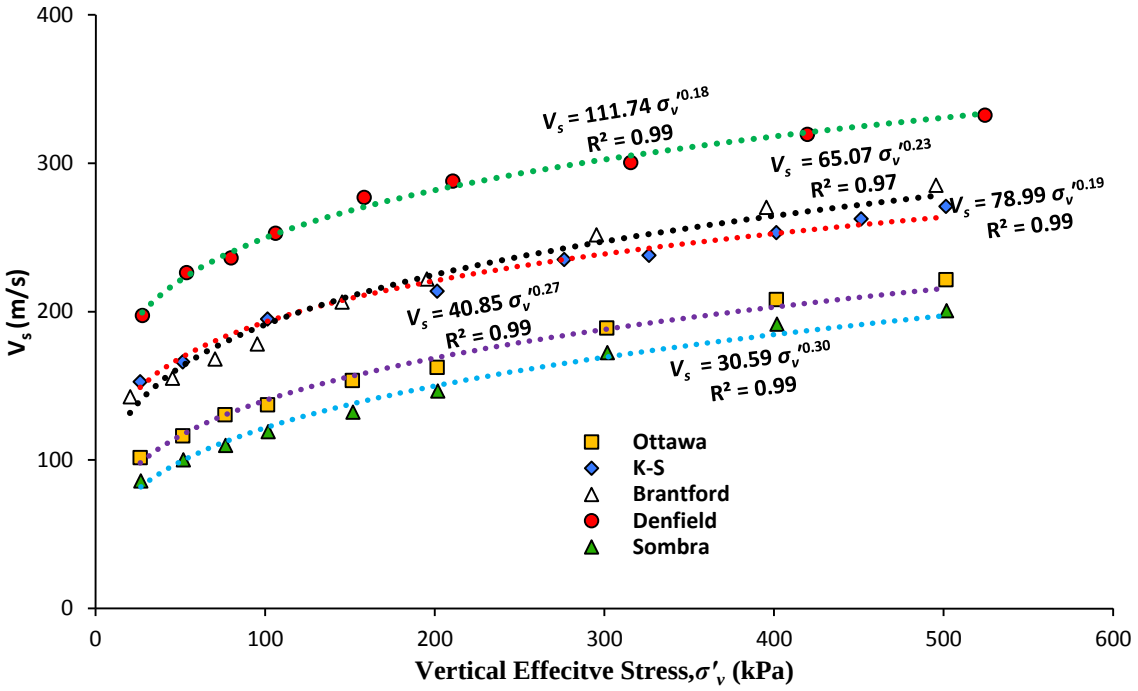

Figure 4-6. V_s - σ_v' models for the tested clays

As can be noted from Fig.4-7, the stress-exponent β_{m3} is higher than β_v (i.e. stress-exponent of σ_m' is higher than that of σ_v'), while the opposite trend is observed for the constant α_{m3}. The V_s values predicted using Eq.4.2 (Kim and Novak, 1981) considering the actual void ratios (e) and σ_m' are also presented in Fig.4-7 for comparison purposes. The comparison of the measured and predicted V_s values reveals very good agreement for soft normally consolidated/lightly overconsolidated soils with medium to high void ratios (Ottawa and Sombra clays). For stiff clayey-silt (Brantford soil) with low initial void ratio, the measured and predicted values are in good agreement within the low pressure range. As the pressure increased, e reduced further and at very low e, the predicted values were consistently lower than the measured values. This discrepancy indicates the limitation of Eq.4.2 with regards to representing the soils with very low to low void ratios. The same behavior was observed for the reconstituted and overconsolidated K-S soil, i.e., the predicted values are smaller than the measured values at medium to high pressures. The difference between the measured and the predicted V_s increased as the pressure increased and void ratio decreased. Thus, Eq.4.2 can be considered suitable for predicting V_s for soils with medium to high void ratios ($e \geq$

0.6), while, it may not be suitable for the prediction of V_s for cohesive soils having very low to low void ratios.

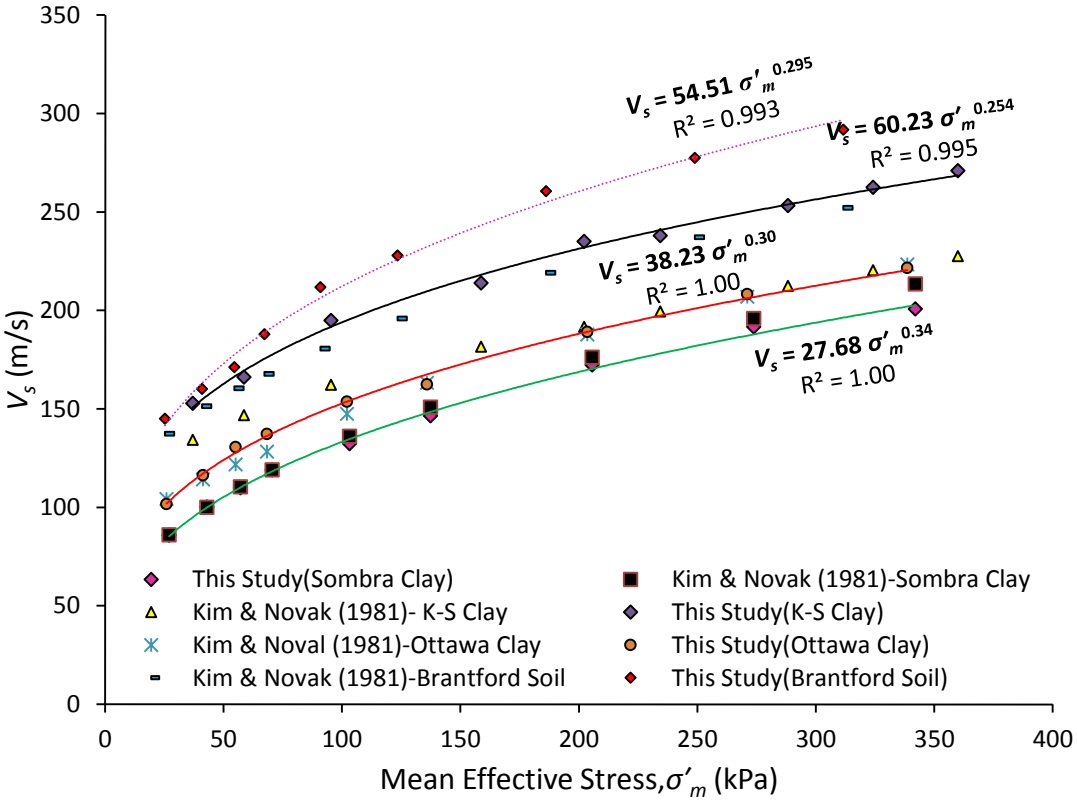

Figure 4-7. $V_s - \sigma_m'$ models for the tested clays and comparison with Kim and Novak (1981)

The density of tested soil samples at each load increment was found during the 1D consolidation testing. The measured densities along with the measured V_s values were used to calculate G_{max} employing Eq.4.1. The obtained G_{max} - σ_v' and G_{max} - σ_m' are presented in Figs.4-8 and 4-9, respectively. Both G_{max} - σ' models cover the entire range of applied pressure (i.e. recompression and virgin compression segments).

As expected, both G_{max} - σ_v' and G_{max} - σ_m' show that the stress exponent is approximately twice the exponent of the corresponding V_s - σ' models. In addition, the same general observations hold, i.e. β reduces and α increases as the stiffness and overconsolidation increase; β increases and α decreases with increases in the plasticity, compression index, and initial void ratio and water content.

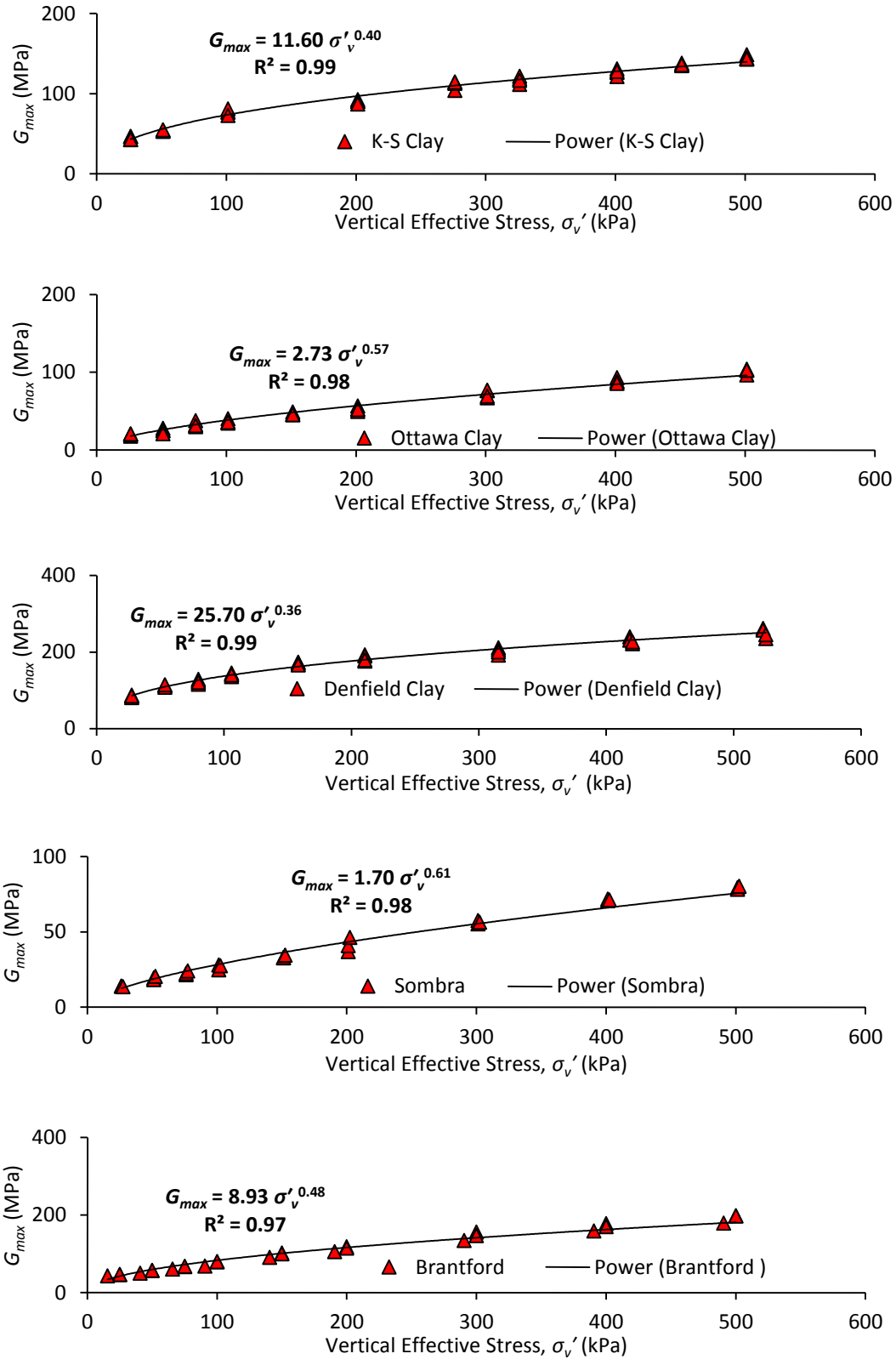

Figure 4-8. G_{max} - σ_v' models for the tested clays

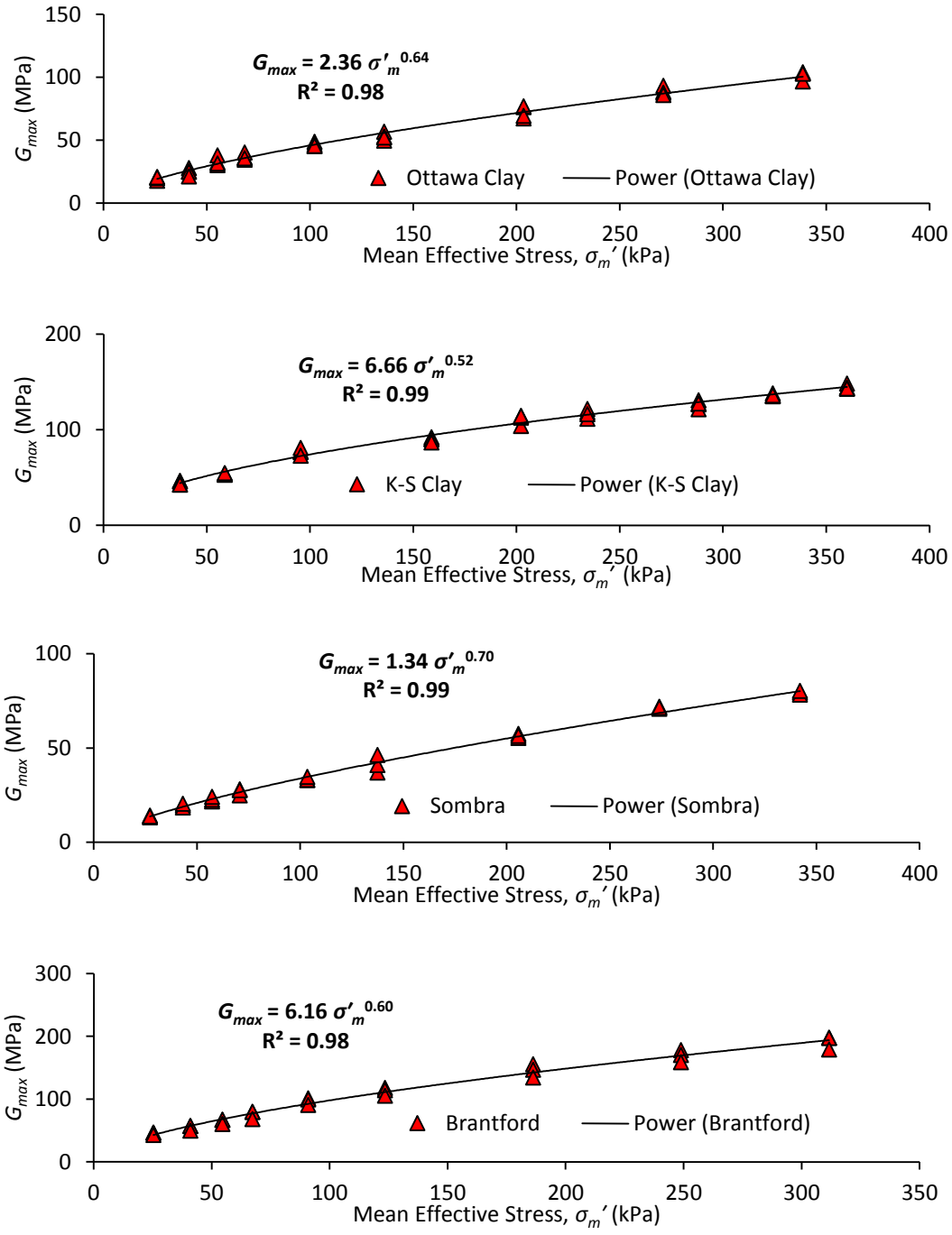

Figure 4-9. $G_{max} - \sigma_m'$ models for the tested clays

4.4.3 Curve fitting parameters α & β correlations and comparison with the published literature.

Cha et al. (2014) correlated the power curve fitting parameters α and β of different soils with their compression indices (C_C) i.e.

$$\alpha = 13.5\left(\frac{m}{s}\right)C_c^{-0.63} \tag{4.10}$$

$$\beta = 0.17\ logC_c + 0.43 \tag{4.11}$$

In order to compare the results from the present study with the predictions of Eq. 4.10 and Eq.4.11, the curve fitting parameters of the tested soils for the normally consolidated pressure range only were considered and σ_m' was defined using Eq.4.6 (i.e. the average of two stresses). It should be noted that the curve fitting parameters, α_{2m}, β_{2m}, α_v, and β_v, were obtained considering the measured V_s values versus σ_v' and σ_m' only for the pressure increments along the virgin compression. The obtained curve fitting parameters are presented in Table.4-3 along with the corresponding measured C_c values. These curve fitting parameters are plotted versus the average C_c in Fig.4-10 and with each other in Fig.4-11 to obtain some empirical correlations between these parameters themselves and the parameters with the average compression index.

It can be noted that for all tested soils, β_v for loading representing normally consolidated soil behavior (Table.4-3) is higher than β_v for considering the full pressure range (Table.4-2 and Fig.4-6). Overconsolidation tends to decrease β and increase α as reported by several researchers (e.g. Cha et al., 2014; and Lee et al., 2005).

The curve fitting parameters presented in Table.4-3 are plotted in Figs.4-10 and 4-11 versus the corresponding C_c values and with each other. Fig. 4-10 shows that the stress exponent β_v for the correlation of V_s - σ_v' and β_{m2} for the correlation of V_s – σ_m' for the virgin compression are same (i.e. $\beta_v = \beta_{m2}$) but have different constant α. All data points that represent the natural clays are placed quite well on the fitted trend-lines, while the data point representing reconstituted K-S soil, is slightly off; the overall curve fitting, however, and has a very high correlation $R^2 \approx 1$.

Curve fitting the data presented in Fig.4-10, the following equations are obtained:

$$\alpha_v = 12.1\, C_c^{-0.65} \tag{4.12a}$$

$$\alpha_{2m} = \alpha = 13.2\, C_c^{-0.65} \tag{4.12b}$$

$$\beta_v = \beta_{2m} = \beta = 0.152 \log(C_c) + 0.424 \tag{4.13}$$

These equations are compared with Eq. 4.10 and Eq. 4.11 (Cha et al., 2014) in Fig.4-10. It is clear from Fig.4-10 that there is good agreement between α established in the present study and that proposed by Eq.4.10. However, there is some discrepancy between exponent β established in the present study and that predicted by Eq.4.11. The estimated values are slightly lower than the ones obtained in the present study, especially for stiff soils with low C_c. For soils with high C_c, Eq.4.11 and Eq.4.13 yield quite similar values.

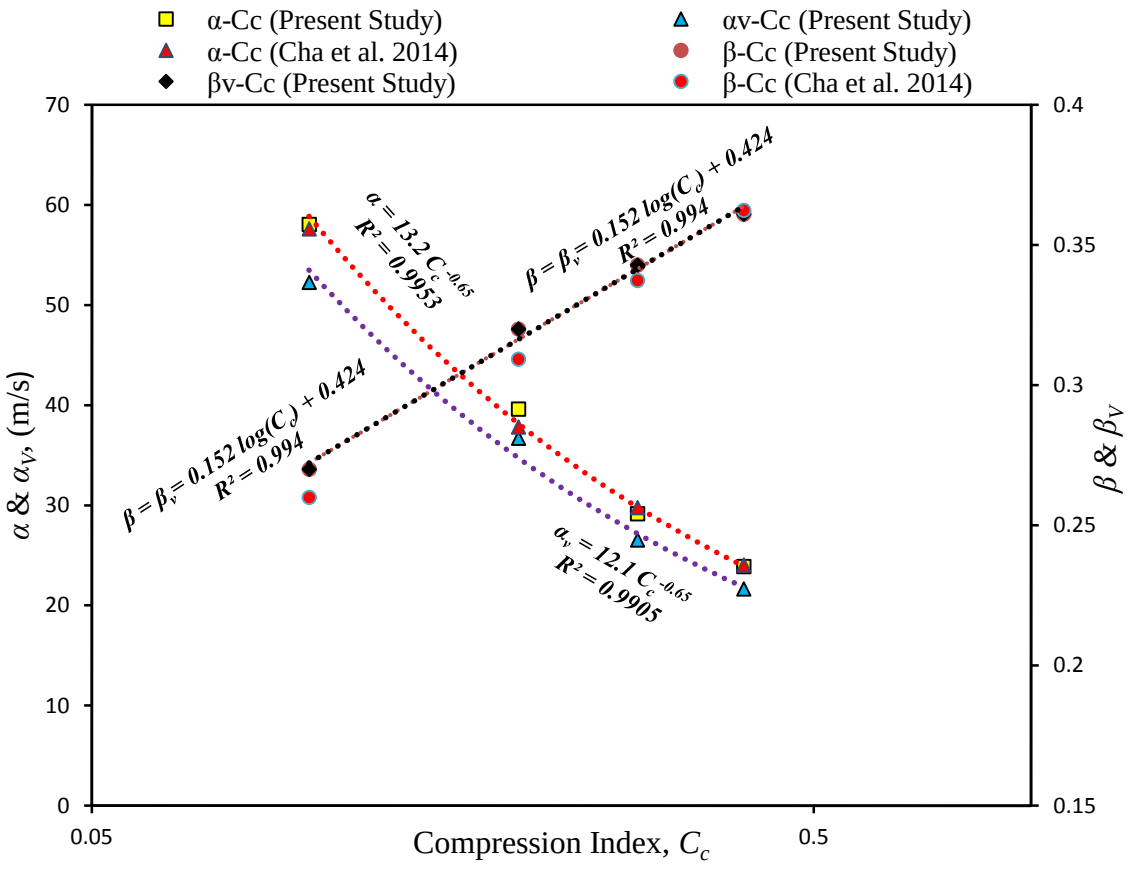

Figure 4-10. Curve fitting parameters plotted against compression index

Fig.4-11 presents the correlations between the measured α and β parameters for σ_v' and σ_m' (σ_m' is defined as per Eq.4.6). Fig.4-11 presents this correlation along the virgin compression. Along the virgin compression (Fig.4-11), both the lines showed the same slope i.e. changing from σ_v' to σ_m' during virgin compression did not change the stress exponent β but it did increase the α factor slightly. The reason is k_o which for both the lines is a constant value during virgin compression. The results of Fig.4-11 are summarized in Eq.4.14 and Eq.4.15.

Table 4-3. Measured C_c, and fitting parameters: α, β and α_v, β_v during virgin compression

Soil	C_C	This Study (for normal consolidation only)			
		$\alpha_{m2} = \alpha$	$\beta_{m2} = \beta$	α_v	β_v
Sombra	0.40	23.90	0.361	21.63	0.361
Brantford	0.11	58.06	0.27	52.28	0.27
Ottawa	0.285	29.15	0.343	26.52	0.343
K-S	0.205	39.61	0.32	36.71	0.32

The parameters α and β established in the present study were found to be sensitive to soil initial void ratio, friction angle, k_o, and preconsolidation pressure (and hence OCR). Therefore, special attention should be given to the measurement of these parameters.

$$\beta = 0.684 - 0.233 \log(\alpha) \tag{4.14}$$

$$\beta_v = 0.672 - 0.233 \log(\alpha_v) \tag{4.15}$$

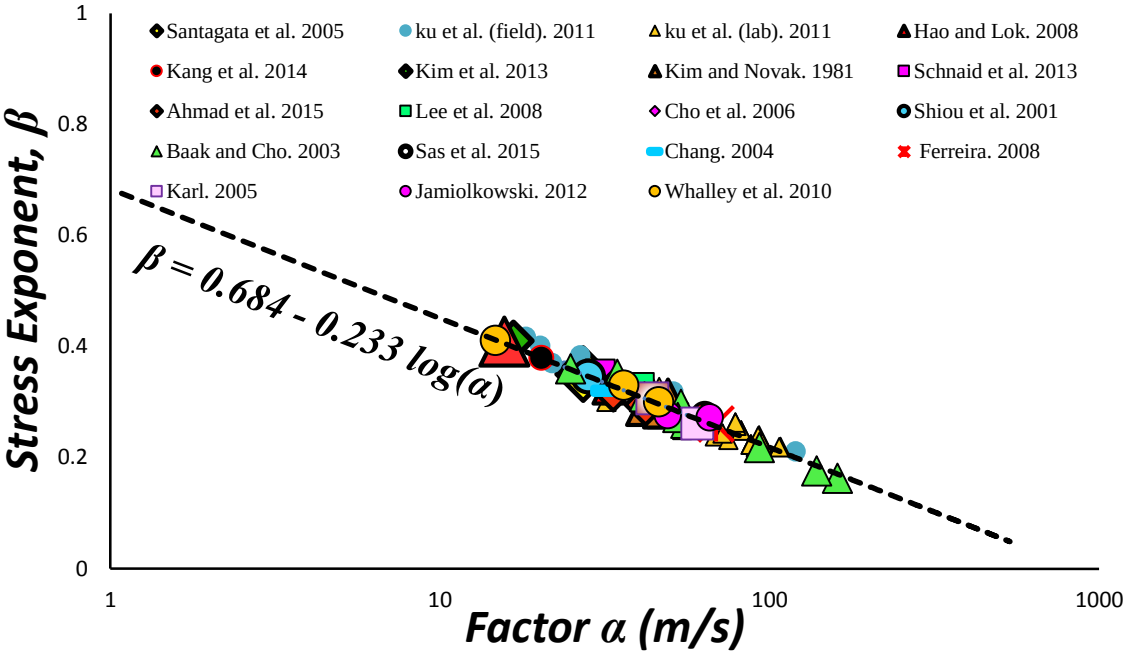

(a) For mean effective stress

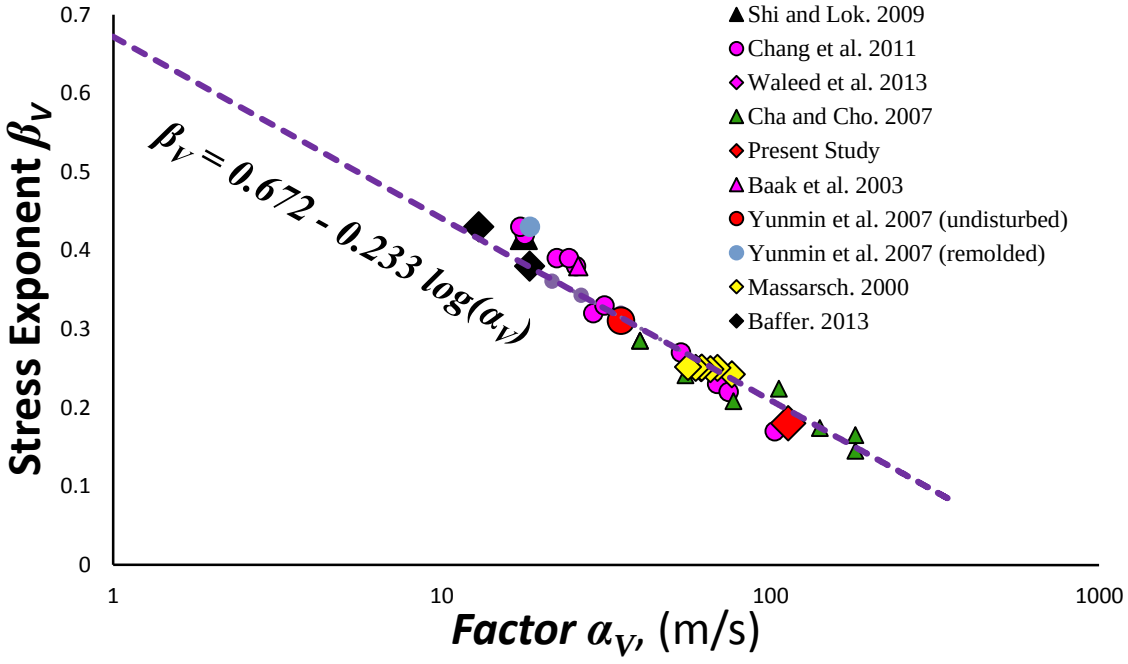

(b) For vertical effective stress

Figure 4-11. $\alpha - \beta$ relationships during Virgin-Compression

Table 4-4. Regression Statistics for Fig.4-11a

Regression Statistics (*Mean Effective Stress*)	
Multiple R	0.976
R Square	0.953
Adjusted R Square	0.952
Standard Error	0.013
Observations	83

Table 4-5. Regression Statistics for Fig. 4-11b

Regression Statistics (*Vertical Effective Stress*)	
Multiple R	0.976
R Square	0.953
Adjusted R Square	0.951
Standard Error	0.020
Observations	33

The results from the current study presented in Fig.4-11 (summarized as Eq.4.14 and Eq.4.15) are compared with the published literature in the same figure. As can be noted from Fig.4-11, a very

good correlation exists between the two sets. The statistical analysis is presented in Table.4-4 and Table.4-5 reveals a high correlation ($R^2 > 0.95$) for both cases, which confirms the appropriateness of the proposed correlations

It is important to note that the soils tested in this study only present a relatively narrow range of α and β. Comparing these parameters with the literature for relatively wide range still showed a very good comparison proving the sturdiness of these results and their usefulness. Consequently, the proposed equations (4.12 to 4.15) can be used to predict the fitting parameters β and α for different types of cohesive soils and hence the complete V_s profile at low strains.

As discussed earlier, Vardanega and Bolton (2013) provided a broad range for parameter ***B*** (Eq.45). Therefore, an attempt is made here to evaluate the appropriate values of the parameter ***B*** for the soils tested in the current study. Thus, the measured G_{max} are plotted versus confining pressure in the form of Eq.4.5, i.e. $\frac{G_{max}}{p_r'}$ versus $\frac{1}{(1+e)^{2.4}}\left(\frac{\sigma_m'}{p_r'}\right)^{0.5}$, as shown in Fig.4-12. It can be noted from Fig.4-12 that the current results are within the range reported by Vardanega and Bolton (2013). However, the soft soils (i.e. Sombra and Ottawa clays) exhibited ***B*** values lower than the average value (20,000) reported by Vardanega and Bolton (2013), while for the stiff soils (i.e. K-S and Brantford) exhibited higher ***B*** values greater than the average. Fig.4-12 also shows that the fit for the points that represent normal consolidation behavior is better than the points that represent the overconsolidation/recompression behavior.

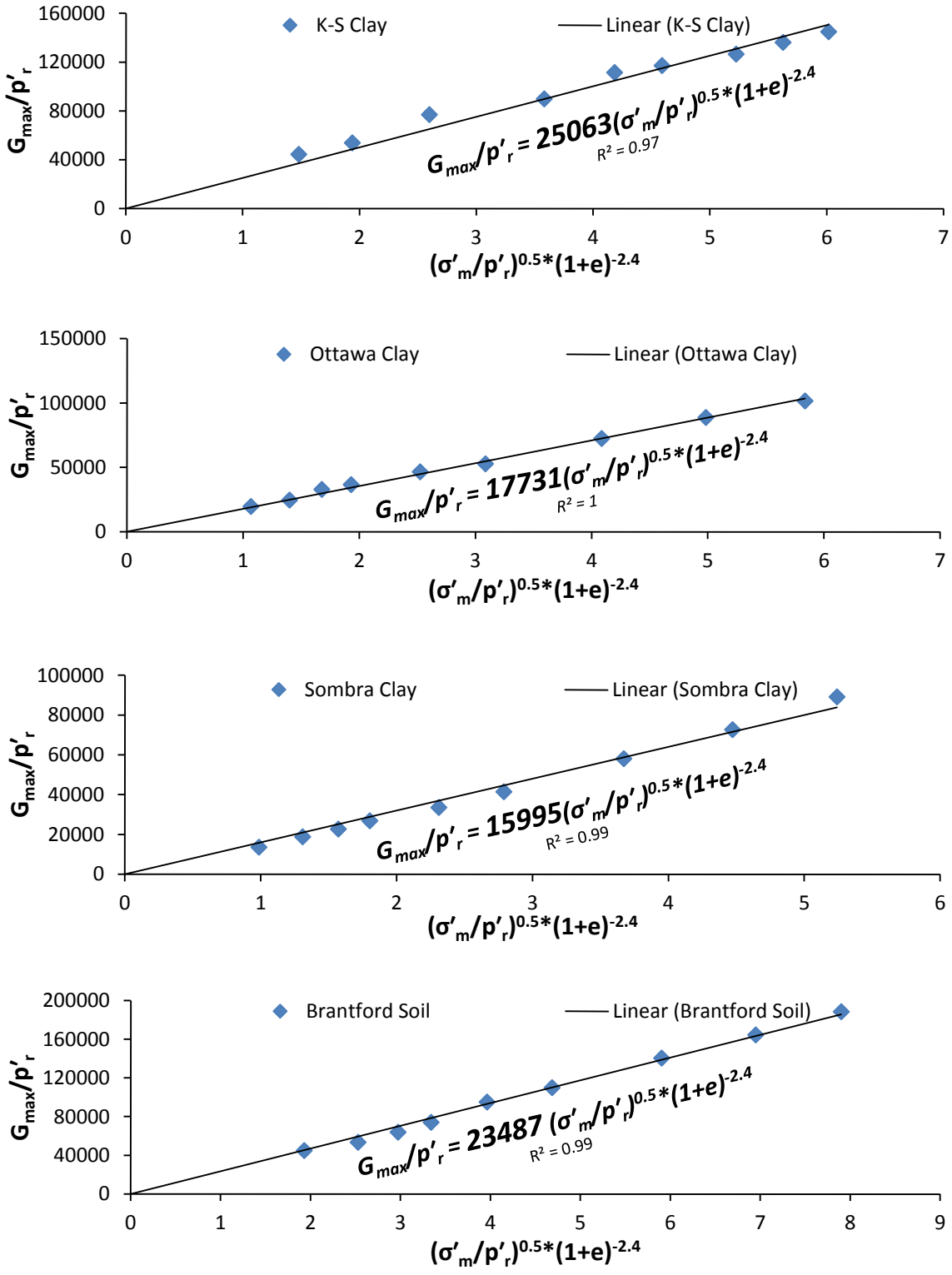

Figure 4-12. Parameter *B* exact values for all the tested soils

4.4.4 S_u – V_s – G_{max} relationships

Correlations between the soil undrained shear strength (S_u) and its stiffness (V_s & G_{max}) parameters are useful for approximate evaluation of the soil shear modulus in case it is not measured. To establish such correlations for the tested soils, it is necessary to establish an appropriate criterion to characterize the soil undrained shear strength.

Brandon et al. (2006) reported that engineering behavior of low-plasticity silts is more difficult to characterize than clay or sand due to their tendency to dilate during shear. They reported difficulties establishing a consistent and practically useful failure criterion for both undisturbed and remolded low-plasticity silts. They discussed six different failure criteria and reported that the failure criterion based on Skempton (1954) pore pressure parameter Ā provides consistent values of the undrained strength ratio, S_u/p (ratio of undrained shear strength and confining pressure) if Ā is properly selected (they suggested using Ā= 0). In addition, it results in tolerably small values of strains at failure.

Brandon et al. (2006) presented variation of S_u/p (undrained shear strength normalized with the effective confining pressure) with Ā for different effective friction angles (ϕ'), i.e.

$$\frac{S_u}{p} = \frac{Sin\phi'}{1-(1-2\bar{A})Sin\phi'} \qquad (4.16)$$

Fig.4-13 shows the deviator stress (q) versus axial strain (ε) relationship for the soil samples subjected to CIU triaxial tests in the current study. The conventional failure criterion of maximum deviator stress, q_{max} was used for the interpretation of soil undrained shear strength for the Sombra, K-S and Ottawa clays. For, the low plasticity Brantford silt which exhibited significant dilation during undrained shearing as shown in Fig.4-14, the failure criterion of Ā = 0 was used in the interpretation of its results. For Denfield soil, which had an intermediate PI, Ā = 0 criterion was utilized where applicable, otherwise, the conventional failure criterion of maximum deviator stress, q_{max} was used. It should be noted, however, that the difference in S_u values obtained from both criteria was small.

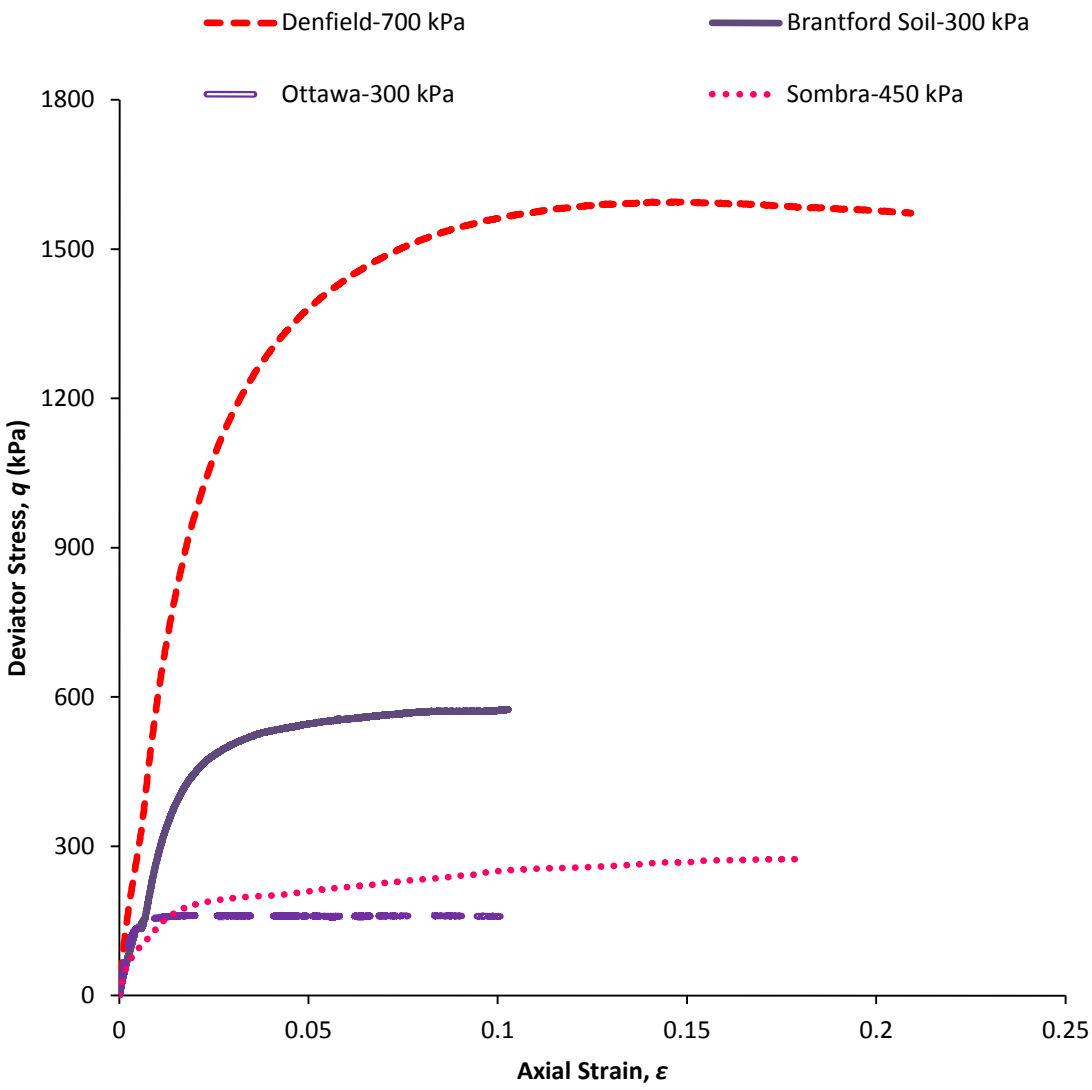

Figure 4-13. Stress-Strain Curves of the natural clays at different isotropic confining pressures

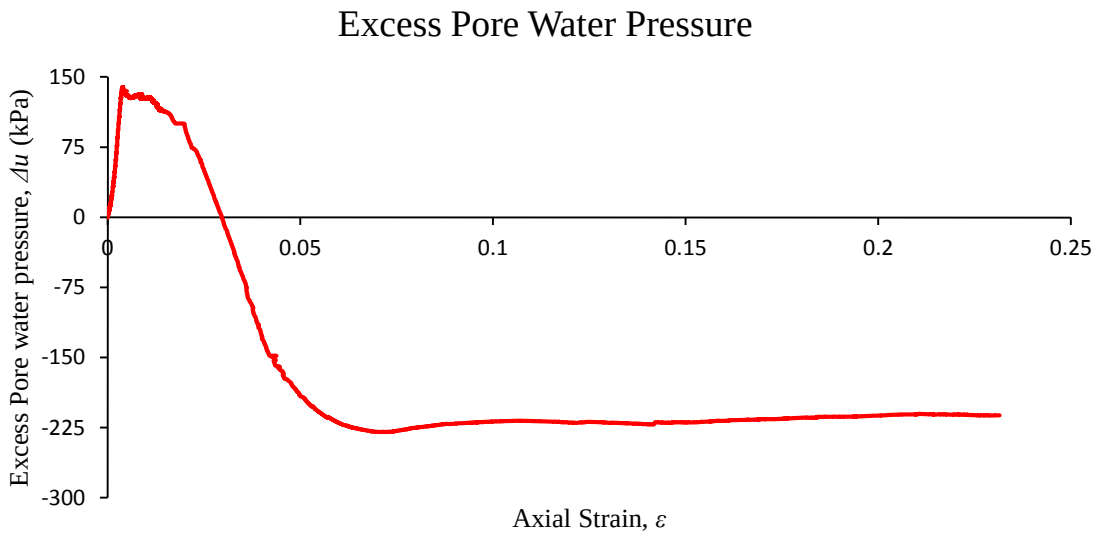

a) Δu vs. ε

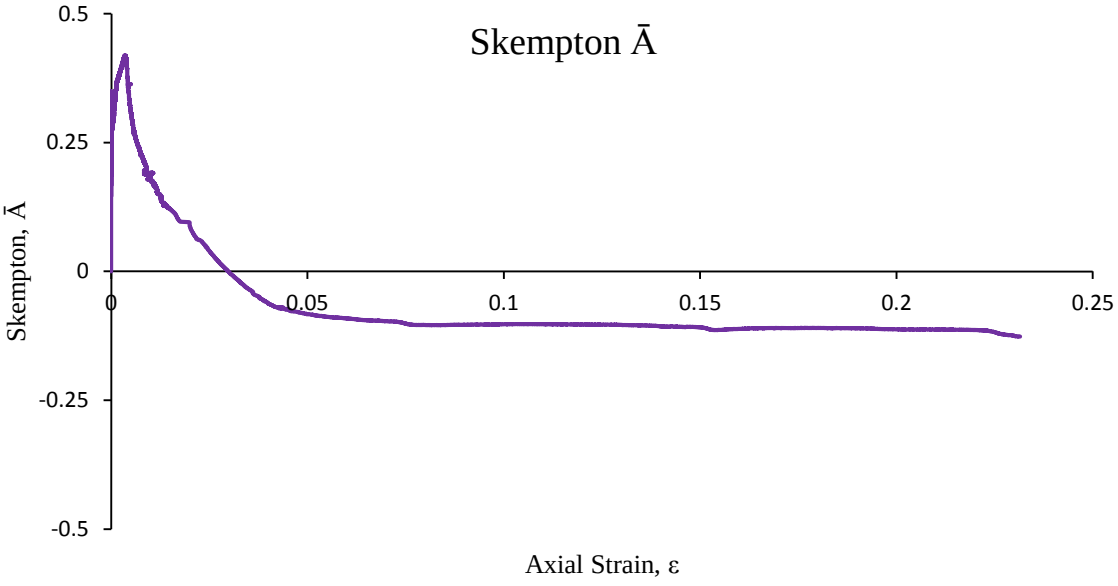

b) Skempton Ā vs. ε

Figure 4-14. Static triaxial results of low plasticity Brantford clayey-silt

Fig.4-15 shows the variation of S_u with the effective confining pressure after consolidation (i.e. before shearing). Forcing the intercept zero results in a lower correlation R^2 specially for K-S soil but yields interesting results as it gives Undrained strength ratios, S_u/p = constant. These ratios were greater than unity for low plasticity silts and overconsolidated soils, while it was around 0.3 for the normally consolidated soft cohesive soils including Ottawa and Sombra clays. For K-S soil, it is slightly higher i.e. around 0.36 with a least correlation R^2. The reason for slightly high undrained strength ratio and low correlation lies in the fact that soil remained overconsolidated during most of the CIU tests as most of the selected confining pressures were smaller than the preconsolidation pressure of the soil. The effect of the OCR is to increase undrained strength ratios, and the S_u versus σ'_c relationship for overconsolidated soils follows a nonlinear power relationship (Ladd et al. 1977). The undrained strength ratios (S_u/p) for the tested soils are summarized in Table 4-6

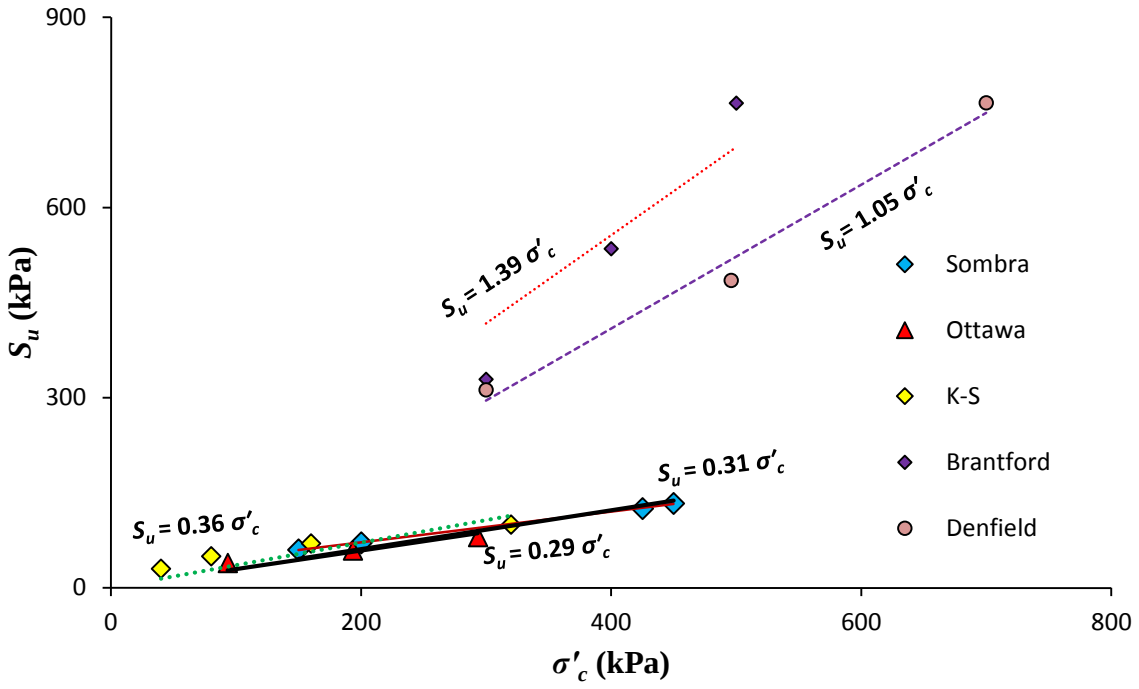

Figure 4-15. Undrained shear strength (S_u) vs. effective consolidation pressure (σ_c')

For Brantford and Denfield soils, the measured S_u/p or (S_u/σ'_c) was around 1.3 and 1.04, respectively. Utilizing Eq.4.16 and substituting the ϕ' values obtained from CIU tests and

summarized in Table.4-1, along with Ā = 0, the calculated S_u/p using Eq.4.12 matched exactly with the measured values validating the results.

The values of G_{max} were evaluated using Table.4-2 or Fig.4-7 considering the mean effective/confining pressures at which S_u values were measured. For Denfield soil, the values of G_{max} were evaluated using the same effective vertical pressures at which S_u was determined using Fig.4-6 or Table.4- 2. These G_{max} values are plotted against the corresponding S_u values in Fig.4-15. The results in Fig.4-15 are fitted with linear function i.e.

$$G_{max} = \boldsymbol{c}S_u \tag{4.17}$$

where ***c***, for tested soils varies between 400 and 1400 and summarized in Table 4-6. The soft soils with intermediate plasticity (K-S and Ottawa) has the highest G_{max}/S_u. The soft soil with highest plasticity (Sombra) has intermediate values of G_{max}/S_u, while the stiff and low plasticity silts/clayey-silts have the lowest G_{max}/S_u ratio.

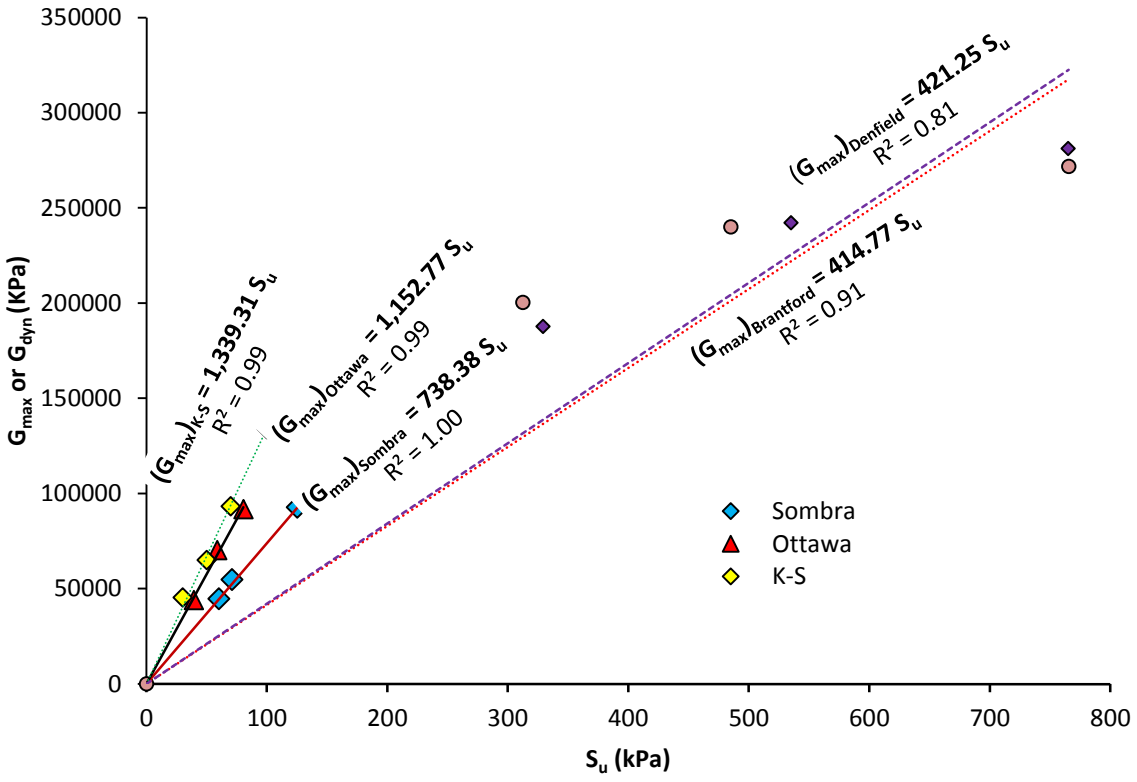

Figure 4-16. $G_{max} - S_u$ Models

Table 4-6. Exact value of parameter "*c*" defined in Eq. 4.17 for each soil

Soil Type	S_u/p	Parameter "*c*"
Sombra	0.31	738.38
Ottawa	0.29	1152.77
K-S	0.36	1339.31
Brantford	1.39	414.77
Denfield	1.05	421.25

4.5 Relationship between static and dynamic moduli

The slope of the initial linear part of deviator stress (q) vs. axial strain (ε) curve obtained from CIU tests (displayed in Fig.4-13) defined here as undrained static elastic modulus E_u or E_{static}. Since the test was conducted under undrained conditions, Poisson's ratio (ν) = 0.5 was used to calculate the corresponding static shear modulus, G_{static}, i.e.

$$G_{static} = \frac{E_u}{2(1+\nu)} \tag{4.19}$$

The static shear modulus described by Eq.4.19, in many situations is confused with the very low strain shear modulus, G_{max}. To avoid this confusion, especially in applications involving design of machine foundations, sometimes G_{max} is referred to as $G_{dynamic}$, while the shear modulus obtained from the q-ε graph of the conventional triaxial tests (Eq.4.19) is referred to as G_{static}. It is therefore, beneficial to evaluate the ratio $G_{dynmaic}/G_{static}$ to appreciate the difference between them, and to evaluate $G_{dynamic}$ in case only measurements of G_{static} are made.

In this comparison, G_{max} was predicted for each applied mean effective confining pressure at which G_{static} measurements were made. G_{max} for all soils, except Denfield clay, were predicted using Fig.4-7 (or Table.4-2), while for Denfield soil it was estimated using Fig.4-6 (or Table.4-2). Fig.4-17 displays the variation of $G_{dynmaic}/G_{static}$ with confining pressure (σ'_c). It is noted from Fig.4-17

that $G_{dynmaic}/G_{static}$ ranges from 5 to 13 for natural clay soils and it decreases as confining pressure increases. For example, $G_{dynmaic}/G_{static}$ for Ottawa clay varied between 5 and 8 as G_{static} varied between 5 MPa and 18 MPa (while the confining pressure varied from 93 kPa to 293 kPa). For K-S clay, $G_{dynmaic}/G_{static}$ varied between 8 and 17 for the range of confining pressure considered. It can also be noted from the figure that $G_{dynmaic}/G_{static}$ varied between 7 and 14 for stiff silty soils (Denfield and Brantford) while it varied between 5 and 13 for soft Sombra clay.

The soil's constrained modulus (M or E_o') is usually determined from oedometer test measurements. The oedometric tangent constrained modulus for the normally consolidated loading (along the virgin compression line) was calculated from the oedometer tests using the following relationship (Karlsrud and Hernandez-Martinez, 2013; Janbu (1963, 1967))

$$M = \frac{2.3(1+e)}{C_c}\sigma'_v = m\sigma'_v \qquad (4.20)$$

where m is the modulus number, e is void ratio, C_c is compression index and σ'_v is the applied vertical effective stress. The modulus number, m = 2.3/$C.R$, where $C.R$ is the compression ratio and $C.R = C_c/(1+e)$

Fig.4-18 shows the variation of the tangent constrained modulus along the virgin compression line with the applied σ'_v. It should be noted that Fig.4-18 shows the average for test specimens of each soil type. The slope of different curves in Fig.4-18 represents the Janbu's (1963, 1967) modulus number m. The reported modulus numbers are consistent with the findings of other researchers (e.g. Karlsrud and Hernandez-Martinez, 2013; Den Haan, 1992).

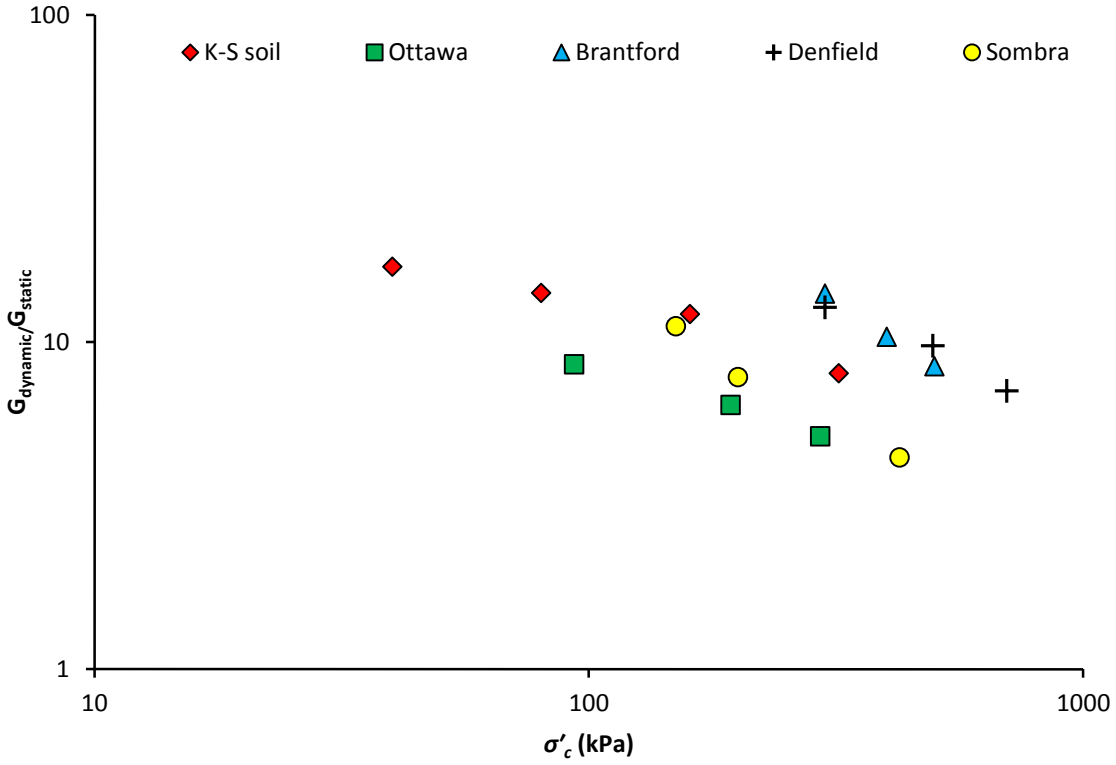

Figure 4-17. Variation of ratio of dynamic and static shear moduli with confining pressure

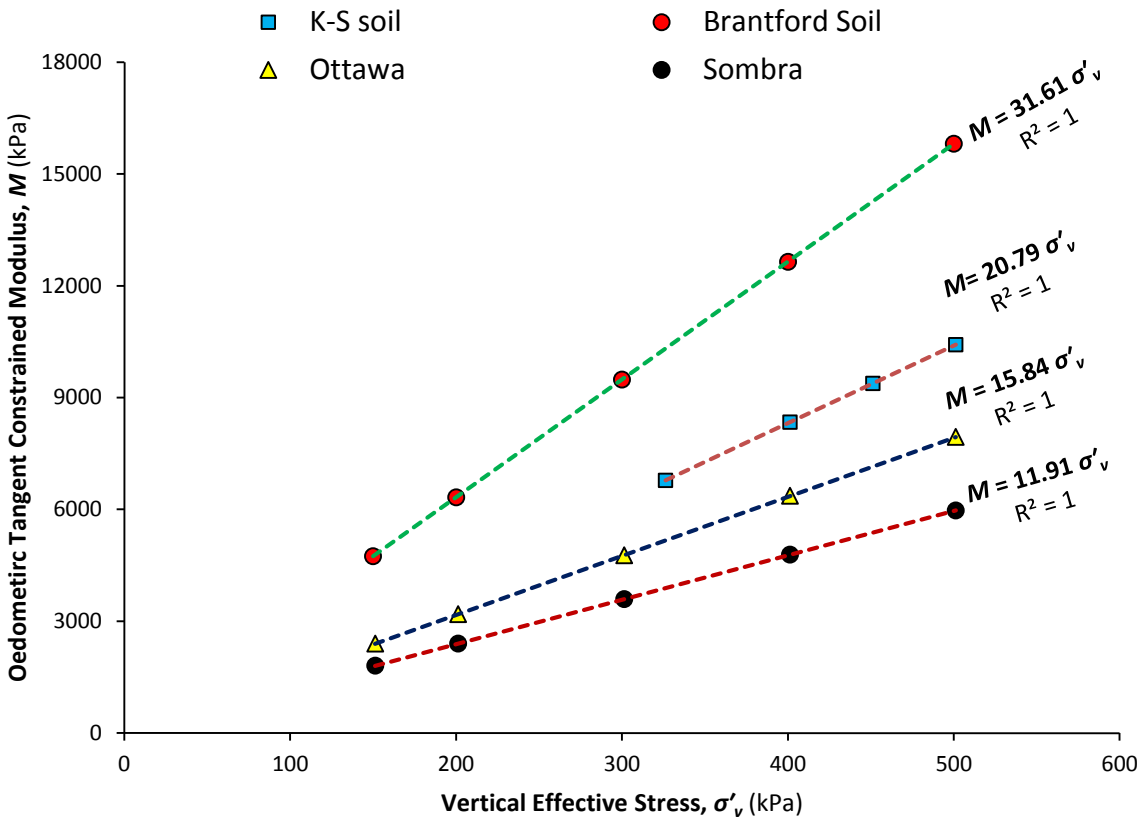

Figure 4-18. Modulus number, *m*

The drained oedometric tangent constrained modulus and G_{max} values were determined for each pressure increment along the normal consolidation loading range. The dynamic constrained modulus ($E_{dynamic}$ or E_{max}) can be calculated using G_{max} and dynamic Poisson's ratio (ν).

Dynamic Poisson's ratio can be calculated from the measurements of shear and compressional wave velocities (V_s and V_p), i.e.

$$\nu = \frac{1}{2}\frac{\left(V_p/V_s\right)^2 - 2}{\left(V_p/V_s\right)^2 - 1} \tag{4.21}$$

Inspecting the output signal obtained from the PRA device, the very first movement in the arrived signal (Pt. P in Fig.4-3) may define the arrival of the P-wave, which can be used to calculate the P wave arrival time. The calculated ν values employing Eq.4.21 and using the measured wave velocities varied between 0.39 and 0.43 with an average of 0.42, which is close to the typical values

of v reported in literature for cohesive soils. The measured v values were found to decrease with an increase in the applied pressure. Similar observation was made by several researchers (Pucci, 2010; Menq, 2003; Werner, 1957; Saxena and Reddy, 1989; and Kumar and Madhusudhan, 2010).

Fig.4-19 compares different measured moduli, i.e. oedomertic tangent stiffness, (E_{oed} or M), $E_{dynamic}$ and E_{static}. A general observation can be made from this comparison. For the cohesive soils tested within the normally consolidation loading, $E_{dyn}/E_{oed} \approx 40$, $E_{stat}/E_{oed} \approx 5$ and $E_{dyn}/E_{stat} \approx 8$.

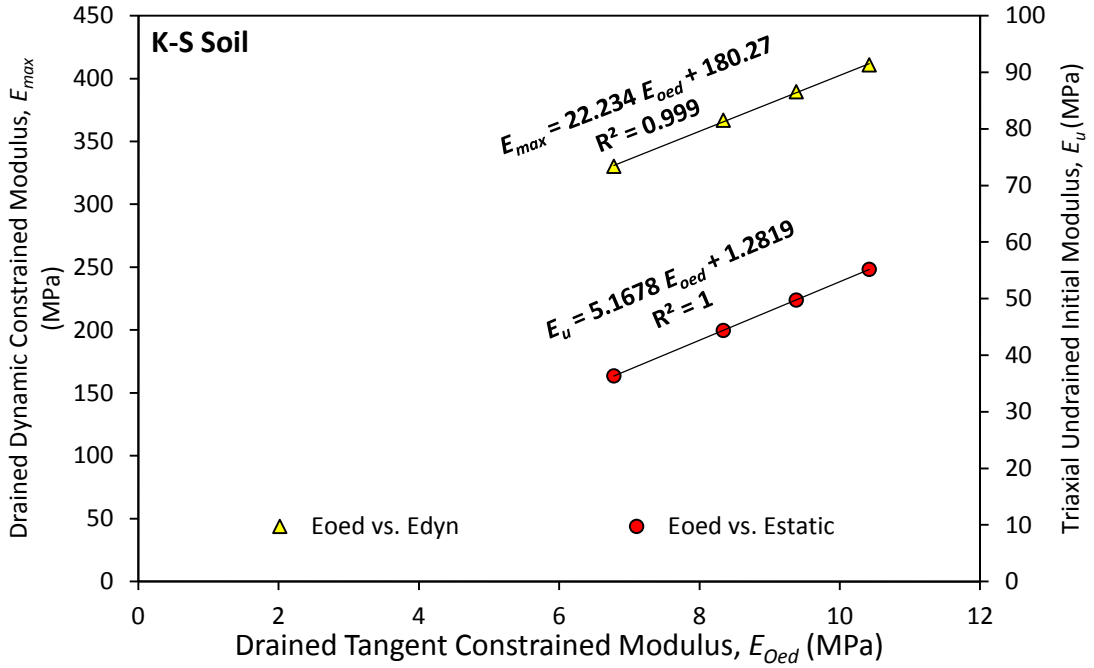
K-S Soil
E_{max} = 22.234 E_{oed} + 180.27
R^2 = 0.999
E_u = 5.1678 E_{oed} + 1.2819
R^2 = 1
Eoed vs. Edyn
Eoed vs. Estatic
Drained Dynamic Constrained Modulus, E_{max} (MPa)
Triaxial Undrained Initial Modulus, E_u (MPa)
Drained Tangent Constrained Modulus, E_{Oed} (MPa)
0
50
100
150
200
250
300
350
400
450
0
10
20
30
40
50
60
70
80
90
100
0
2
4
6
8
10
12

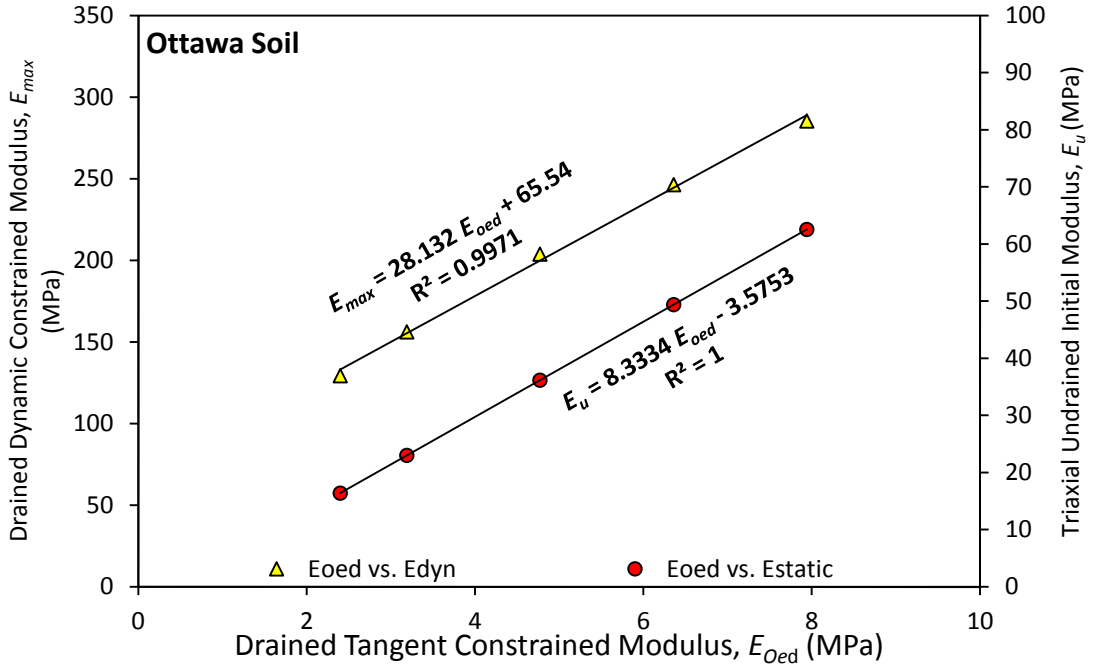
Ottawa Soil
E_{max} = 28.132 E_{oed} + 65.54
R^2 = 0.9971
E_u = 8.3334 E_{oed} - 3.5753
R^2 = 1
Eoed vs. Edyn
Eoed vs. Estatic
Drained Dynamic Constrained Modulus, E_{max} (MPa)
Triaxial Undrained Initial Modulus, E_u (MPa)
Drained Tangent Constrained Modulus, E_{Oed} (MPa)
0
50
100
150
200
250
300
350
0
10
20
30
40
50
60
70
80
90
100
0
2
4
6
8
10

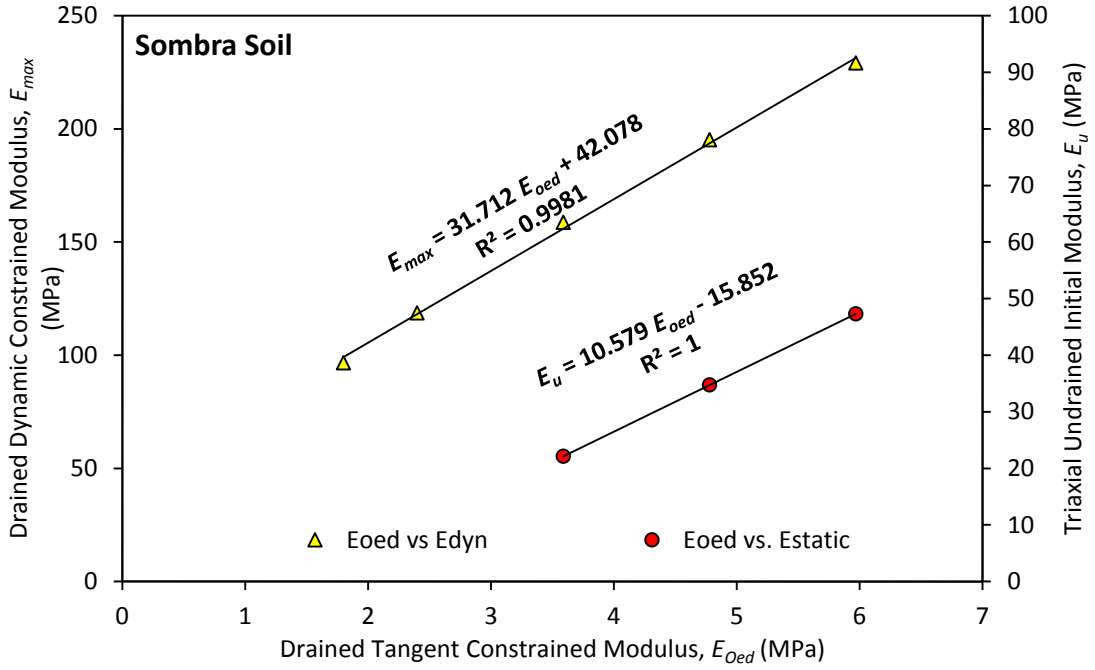

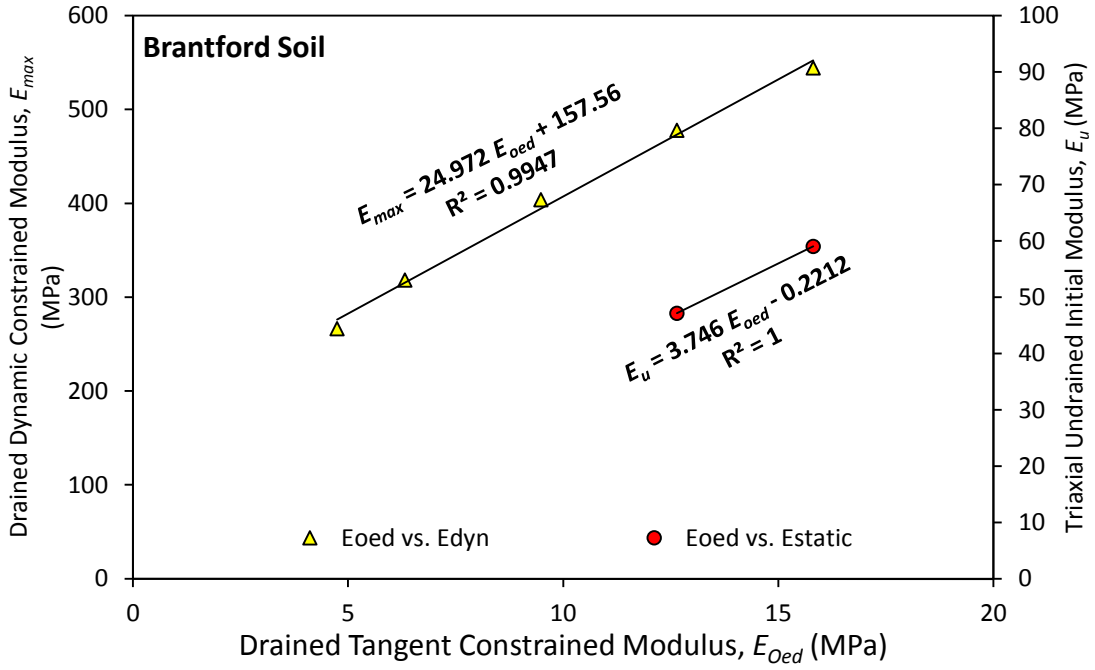

Figure 4-19. Comparison of different moduli

4.6 Conclusions

A variety of cohesive soils were tested to measure their very small strain stiffness properties (V_s and G_{max}), using an innovative piezoelectric ring actuator device incorporated in an oedometer. The undrained shear strength and elastic modulus of the test soils were measured from CIU triaxial tests. Based on the obtained results, the following key conclusions can be drawn:

1. A new device was fabricated to measure the V_s by overcoming the major issues of bender elements. A variety of cohesive soils tested using the fabricated device has yielded very clear signals with only one major peak and hence a reliable technique for measuring V_s instead of using conventional bender elements.
2. The proposed correlations (Eq's 4.12 – 4.15), can be used to predict the V_s using the readily measured soil parameter, C_c without direct measurement for *Vs.* The obtained correlations were examined with the available data in literature and strong matching is observed.
3. Soil specific empirical correlations are proposed to be used for the estimation of G_{max} from measured S_u for cohesive soils. In general, the low strain shear modulus, G_{max} was found to vary from 400 to 1400 times the soil undrained strength, S_u
4. The ratio ($G_{dynamic}/G_{static}$) varied between 5 and 13 for the tested soil specimens and was found to decrease as the confining pressure increases.
5. As a preliminary estimate, the average dynamic Poisson's ratio for the tested cohesive soils was found to be around 0.42.
6. Based on the conducted small and large strain measurements, the stiffness ratios E_{dyn}/E_{oed}, $E_{dynamic}/E_{static}$, E_{stat}/E_{oed} were found to be around 40, 8 and 5 respectively.

References

Abd Elaziz, A.Y. and El Naggar, M.H. (2014). “Evaluation of geotechnical capacity of hollow bar micropiles in cohesive soils.” *Canadian Geotechnical Journal*, Vol. 51, No. 10, pp. 1123-1138.

Alnuaim, A., El Naggar, M.H. and El Naggar, H. (2015). “Performance of micropiled raft in clay subjected to vertical concentrated load: centrifuge modeling.” *Canadian Geotechnical Journal*, 52(12): 2017-2029.

ASTM Standard D422, (2007), “Standard Test Method for Particle-Size Analysis of Soils," ASTM International, West Conshohocken, PA, www.astm.org.

ASTM Standard D4318, (2010), “Standard Test Methods for Liquid Limit, Plastic Limit, and Plasticity Index of Soils," ASTM International, West Conshohocken, PA, www.astm.org.

ASTM Standard D854, (2014), “Standard Test Methods for Specific Gravity of Soil Solids by Water Pycnometer," ASTM International, West Conshohocken, PA, www.astm.org.

Baak, S. H., Kwon, T. H., & Cho, G. C. (2003). “Evaluation of particulate materials using wave-based techniques”. *KSCE Journal of Civil Engineering*, *7*(6), 763-772.

Baffer, B. A. (2013). “Relationship between small strain shear modulus and undrained shear strength in direct simple shear". Master thesis, University of Rhode Island.

Brandon, T., Rose, A., and Duncan, J. (2006). ”Drained and Undrained Strength Interpretation for Low-Plasticity Silts.” *Journal of Geotechnical and Geoenvironmental Engineering*, 132 (2), 250–257

Brocanelli, D., and Rinaldi, V. (1998). Measurement of low-strain material damping and wave velocity with bender elements in the frequency domain. *Canadian Geotechnical Journal*, 35(6), 1032-1040.

Cha, M., & Cho, G. (2007). “Shear strength estimation of sandy soils using shear wave velocity”. *Geotechnical Testing Journal*, *30*(6), 484-495.

Cha, M., Santamarina, J., Kim, H., and Cho, G. (2014). Technical Note. ”Small-Strain Stiffness, Shear-Wave Velocity, and Soil Compressibility.” *Journal of Geotechnical and Geoenvironmental Engineering*., 140 (10), 06014011.

Chang, H. P. N. (2005). “The relationship between void ratio and shear wave velocity of gold tailings.” Master of Engineering dissertation, University of Pretoria.

Chang, I., Kwon, T. H., & Cho, G. C. (2011). “An experimental procedure for evaluating the consolidation state of marine clay deposits using shear wave velocity”. *Smart Structures and Systems*, *7*(4), 289-302.

Chen, Y., Chen, Y., & Huang, B. (2007). “Experimental investigation of the influence on static and cyclic deformation of structural soft clay of stress level”. *Frontiers of Architecture and Civil Engineering in China*, *1*(4), 422-429.

Cho, G., Dodds, J., and Santamarina, J. (2006). ”Particle Shape Effects on Packing Density, Stiffness, and Strength: Natural and Crushed Sands.” *Journal of Geotechnical and Geoenvironmental Engineering*, 132 (5), 591–602.

Den Haan, E. J. (1992). The formulation of virgin compression of soils. *Géotechnique*, *42* (3), 465-483.

Dyvik, R., and Madshus, C. (1985). “Lab Measurements of G_{max} Using Bender Elements.” In *Proc. ASCE Convention on Advances in the Art of Testing Soils Under Cyclic Conditions*, 186–196.

El-Sekelly, W., Mercado, V., Abdoun, T., Zeghal, M., & El-Ganainy, H. (2013). “Bender elements and system identification for estimation of Vs”. *International Journal of Physical Modelling in Geotechnics*, 13(4), 111-121.

Ferreira, C.M.F. (2008). “The use of seismic wave velocities in the measurement of stiffness of a residual soil.” PhD Thesis. University of Porto.

Gang, H. A. O., & Lok, T. M. H. (2008). "Study of shear wave velocity of Macao marine clay under anisotropic stress condition." *The 14th World Conference on Earthquake Engineering* October 12-17, 2008, Beijing, China.

Hardin, B.O., and Black, W.L. (1968). "Vibration modulus of normally consolidated clay". *Journal of the Soil Mechanics and Foundations Division*. 94 (2), 353-369.

Hardin, B.O., and Black, W.L. (1969). "Vibration modulus of normally consolidated clay (closure)". *Journal of the Soil Mechanics and Foundations Division*. 95 (6), 1531-1537

Hardin, B. O., and Drnevich, V. P. (1972). "Shear modulus and damping in soils: Measurement and parameter effects." *Journal of Soil Mechanics and Foundation Division*, 98 (6), 603–624.

http://www.gdsinstruments.com/gds-bender-elements-analysis-tool [Accessed April 10, 2014].

Ismail, M.A., and Rammah K.I. (2005). "Shear-plate Transducers as a Possible Alternative to Bender Elements for Measuring G_{max}." *Géotechnique* 55 (5), 403–407.

Jaky, J. (1944), "The Coefficient of Earth Pressure at Rest", *Journal for Society of Hungarian Architects and Engineers*, 355-358.

Jamiolkowski, M. (2012). "Role of geophysical testing in geotechnical site characterization." *Soils and Rocks International Journal of Geotechnical and Geoenvironmental Engineering*, *35*(2), 1-21

Janbu, N. (1963). "Soil compressibility as determined by oedometer and triaxial tests". *In Proceedings of the 3rd European Conference Soil Mechanics*, Wiesbaden. Vol. 1, 19–25.

Janbu, N. (1967). "Settlement calculations based on the tangent modulus concept". Technical University of Norway.

Kang, X., Kang, G. C., & Bate, B. (2014). "Measurement of Stiffness Anisotropy in Kaolinite Using Bender Element Tests in a Floating Wall Consolidometer." *Geotechnical Testing Journal*, 37(5).

Karl, L. (2005). “Dynamic soil properties out of SCPT and bender element tests with emphasis on material damping*”*. Doctoral dissertation, Ghent University.

Karlsrud, K., & Hernandez-Martinez, F. G. (2013). “Strength and deformation properties of Norwegian clays from laboratory tests on high-quality block samples”. *Canadian Geotechnical Journal*, *50* (12), 1273-1293.

Kim, H. S., Cho, G. C., Lee, J. Y., and Kim, S. J. (2013). “Geotechnical and geophysical properties of deep marine fine-grained sediments recovered during the second Ulleung Basin Gas Hydrate expedition, East Sea, Korea.” *Marine and Petroleum Geology, 47*, 56-65.

Kim, T. C., and Novak, M. (1981). “Dynamic properties of some cohesive soils of Ontario”. *Canadian Geotechnical Journal*, 18(3), 371-389.

Knox, D. P., Stokoe, K. H., and Kopperman, S. E. (1982). “Effect of state of stress on velocity of low-amplitude shear waves propagating long principal stress directions in dry sand.” *Technical Report. GR 82-23*, Geotechnical Engineering Center, Univ. of Texas–Austin, Austin, TX.

Ku, T., Mayne, P. W., and Gutierrez, B. J. (2011). “Hierarchy of Vs modes and stress-dependency in geomaterials”. In *Proceedings of the Fifth International Symposium on Deformation Characteristics of Geomaterials, Seoul, Korea*, 533-540.

Kumar, J. and Madhusudhan, B. N. (2010). “Effect of Relative Density and Confining Pressure on Poisson Ratio from Bender and Extender Elements Tests.” *Géotechnique* 60 (7), 561–567.

Ladd, C., Foot, R., Ishihara, K., Schlosser, F., and Poulos, H. (1977). “Stress-deformation and strength characteristics”. *In Proceedings of the 9th International Conference on Soil Mechanics and Foundation Engineering, Tokyo. Japanese Society of Soil Mechanics and Foundation Engineering*, (2), 421–494.

Lee, C., Lee, J. S., Lee, W., & Cho, T. H. (2008). “Experiment setup for shear wave and electrical resistance measurements in an oedometer.” *Geotechnical Testing Journal, 31*(2), 149-156.

Lee, J-S., and Santamarina, J.C. (2005). "Bender Elements: Performance and Signal Interpretation." *Journal of Geotechnical and Geoenvironmental Engineering* 131 (9), 1063–1070.

Leong, E.C., Yeo, S.H., and Rahardjo, H. (2005). "Measuring Shear Wave Velocity Using Bender Elements." *Geotechnical Testing Journal* 28 (5), 1–11.

Leong, E. C., Cahyadi, J., and Rahardjo, H. (2009). "Measuring Shear and Compression Wave Velocities of Soil Using Bender–extender Elements." *Canadian Geotechnical Journal* 46 (7), 792–812.

Mancuso, C. and Vinale, F. 1988. Propagazione delle onde sismiche: teoria e misura insito. Atti del Convegno del Gruppo Nazionale di Coordinamento per gli Studi di Ingegneria Geotecnica, Monselice, Rome: Consiglio Nazionale delle Ricerche. 115-138.

Massarsch, K. R., (2000). "Settlements and damage caused by construction-induced vibrations". Proceedings, Intern. Workshop Wave 2000, Bochum, Germany 13 – 15 December 2000, 299 – 315.

Mayne, P.W. and Kemper, J.B., Jr. (1988). "Profiling OCR in Stiff Clays by CPT and SPT". *ASTM, Geotechnical Testing Journal*, 11 (2), 139-147.

Menq, F.-Y. (2003). "Dynamic Properties of Sandy and Gravelly Soils". PhD thesis, The University of Texas at Austin.

Petrakis, E., and Dobry, R. (1987). "Micromechanical modeling of granular soil at small strain by arrays of elastic spheres." Rep. No. CE-87-02, Department of Civil Engineering, Rensselaer Polytechnic Institute, Troy, NY

Pucci, M.J. (2010). "Development of a Multi-Measurement Confined Free-Free Resonant Column Device and Initial Studies". M.Sc. thesis, The University of Texas at Austin.

Roesler, S. K. (1979). "Anisotropic shear modulus due to stress anisotropy." *Journal of the Geotechnical Engineering Division*, 105 (7), 871-880.

Santagata, M., Germaine, J., and Ladd, C. (2005). ”Factors Affecting the Initial Stiffness of Cohesive Soils.” J. Geotech. Geoenviron. Eng., 131(4), 430–441.

Santamarina, J. C., Klein, K. A., and Fam, M. A. (2001). *Soils and Waves: Particulate Materials Behavior, Characterization and Process Monitoring*. *Particulate Materials Behavior, Characterization and Process Monitoring,* Wiley, New York, p.508.

Schnaid, F., Bedin, J., da Fonseca, A. V., & de Moura Costa Filho, L. (2013). “Stiffness and Strength Governing the Static Liquefaction of Tailings.” *Journal of Geotechnical and Geoenvironmental Engineering*, 139(12), 2136-2144.

Sas, W., Gabryś, K., & Szymański, A. (2014). “Comparison of resonant column and bender elements tests on selected cohesive soil from Warsaw.” *Electronic Journal of Polish Agricultural Universities. Series Civil Engineering*, 17(3), #07.

Saxena, S.K., and Reddy, K.R. (1989). “Dynamic Moduli and Damping Ratios for Monterey No. 0 Sand by Resonant Column Tests.” *Japanese Society of Soil Mechanics and Foundation Engineering* 29 (2), 37–51.

Shi, X. T., & Lok, M. H. (2009). “Experimental study of variation of shear wave velocity of Macao marine clay during one dimensional consolidation”. *Proceedings of the 17th International Conference on Soil Mechanics and Geotechnical Engineering: The Academia and Practice of Geotechnical Engineering*

Shibuya, S., Hwang, S. C., and Mitachi, T. (1997). “Elastic shear modulus of soft clays from shear wave velocity measurement.” *Géotechnique*, 47(3), 593–601.

Skempton, A. W. (1954). “The pore pressure coefficients A and B.” *Geotechnique*, 4, 143–147.

Tzyy-Shiou, C., RamaKumar, V. V., and Kuo-Ping, C (2001). “Improvement of Static and Dynamic Properties of Soft Clay Using High Pressure Jet Grout”. Proceedings: Fourth International *Conference on Recent Advances in Geotechnical Earthquake Engineering and Soil Dynamics.* San Diego, California. Paper 23.

Vardanega, P. J., & Bolton, M. D. (2013). "Stiffness of clays and silts: Normalizing shear modulus and shear strain". *Journal of Geotechnical and Geoenvironmental Engineering*. 139 (9), 1575-1589.

Viggiani, G, and Atkinson, J.H. (1995). "Interpretation of Bender Element Tests (Technical Note)." *Géotechnique* 45 (1), 149–154.

Werner, R.R. (1957). "A Study of Poisson's Ratio and the Elastic and Plastic Properties of Ottawa Sand". Agricultural and Mechanical College of Texas.

Whalley, W. R., Jenkins, M., & Attenborough, K. (2011). "The velocity of shear waves in saturated soil. *Soil Science Society of America Journal*." *75*(5), 1652-1657.

Yang, J., and Gu, X.Q. (2013). "Shear Stiffness of Granular Material at Small Strains: Does It Depend on Grain Size?" *Géotechnique* 63 (2), 165–179.

Yu, P., and Richart Jr, F. E. (1984). "Stress ratio effects on shear modulus of dry sands". *Journal of Geotechnical Engineering*, 110 (3), 331-345.

Yun, T. and Santamarina, J. (2005). "Decementation, Softening, and Collapse: Changes in Small-Strain Shear Stiffness in k0 Loading." *Journal of Geotechnical and Geoenvironmental Engineering*, 131 (3), 350–358.

Chapter 5

5 Evaluation of Variation of Shear Wave Velocity with Shear Strain Using Piezoelectric Ring Actuators in a Triaxial Device

5.1 Abstract

This chapter presents the fabrication of PRA device for the application in cyclic triaxial apparatus, hence facilitating measurement of shear wave velocity at different levels of shear strains. The developed device was used to measure the shear wave velocity (V_s) of various natural cohesive soils and a reconstituted Kaolin-Silt soil pre and post cyclic shear. The tested specimens were consolidated at different confining pressures and V_s was measured employing the PRA device. The shear wave velocity measurements were taken at several isotropic confining pressures up to 350 kPa using the fabricated PRA setup mounted on cyclic triaxial apparatus prior to the application of the cyclic loading. These measurements of V_s are compared with V_s measurements obtained using another PRA setup mounted on oedometer device and excellent agreement was observed, which verified the performance of both PRA (oedometer and the triaxial) setups. The soil specimens were then subjected to varying cyclic shear strains and the soil secant shear modulus, G, and damping ratio, ξ, were evaluated from the cyclic shear test data. In addition, the shear wave velocity of test specimens was obtained at each strain level using the PRA device. Based on measured V_s and G values at different levels of strain, dimensionless empirical correlations are proposed to correlate shear wave velocity at different shear strain level, V_s, normalized by Vs_{max} at very low strain to the shear modulus reduction curve, G/G_{max}. The measured V_s at different strain levels, along with the proposed correlations, can then be used to evaluate the shear modulus reduction curve of the soil without the need to perform cyclic triaxial testing. This approach has the potential to provide reasonable estimate of the shear modulus reduction curve using the conventional triaxial cell when the more expensive cyclic triaxial cell is not available and can eliminate the challenges associated with evaluating the secant shear modulus from hysteretic loops. In addition, empirical correlations are provided to evaluate V_s or G_{max} using a simple mechanical property of soil (i.e. compression index, C_c).

Keywords: Piezoelectric ring actuators, shear-wave velocity, low-strain shear modulus, damping ratio, cyclic triaxial, cohesive soils, oedometer

5.2 Introduction

The shear wave velocity V_s and the small-strain shear modulus (G_{max} or G_o) are fundamental soil properties that are utilized in the analysis of a variety of geotechnical problems. They are required for site classification, and soil–structure interaction, site response and seismic hazard analyses. At very low strains (typically less than 0.001%), using the elastic theory, G_{max} can be related to V_s (Eq.5.1), i.e.

$$G_{max} = \rho V_s^2 \tag{5.1}$$

where: ρ is soil's bulk density and V_s is the shear wave velocity

Several laboratory and field methods are used to measure the small-strain stiffness. For analyses involving different levels of strain and/or confining pressure, laboratory tests are preferred. Resonant column test is considered as one of the most reliable tests used for the measurement of small-strain stiffness. It allows the measurement of shear and primary wave velocities of soils at very low levels of shear strains representative of some geotechnical problems such as analysis of dynamic response of machine foundations. In addition, different soil consistency and levels of confining pressure can be conveniently considered. However, it has some limitations with regards to measuring high strain properties and testing stiff soil specimens. Moreover, the resonant column tests are relatively expensive, time consuming and have issues regarding the coupling between the specimens and end platens (Airey and Mohsin, 2013).

The alternate to the resonant column technique is the bender/extender element test. It involves a pair of piezoelectric elements (i.e. bender elements) placed at opposite ends of the specimen. When excited with an input voltage signal, one element vibrates and emits an elastic wave (shear or compressive) that travels through the soil. When this elastic wave arrives at the other element, it is excited producing an output voltage signal, which is recorded by the system. The travel time of the elastic wave between the two elements and sample height are used to calculate the elastic wave velocity. The bender elements can be incorporated in an oedometer, triaxial cell or a ring shear

device. Thus, it can be used to measure the shear wave velocity for a variety of soil types under a variety of test conditions. However, bender element testing has several shortcomings. Ismail and Rammah (2005) reported the shortcomings in BE which are given in details in Chapter 2. To overcome some of these issues and limitations of resonant column tests, Karray and Lafavbre and their co-workers (e.g. Gamal El-Dean, 2007; Romdhan et al., 2015; Karray et al., 2015) developed a piezoelectric ring actuators device incorporated in an oedometer to measure shear wave velocity. The concept of PRA is similar to the bender element, however, the ring actuators move radially exciting the soil in a more uniform way hence eliminating some of the bender elements major shortcomings.

In the course of this thesis, two PRA devices have been fabricated and were incorporated into two conventional soil testing equipment, i.e. oedometer and cyclic triaxial cell. In the first phase of this study (reported in Chapter 3 and Chapter 4), the PRA incorporated in an oedometer was employed for measuring V_s of cohesive and cohesionless soils. The results from this extensive testing were compared with those reported in the literature and excellent agreement was obtained.

In this chapter, the PRA device is fabricated to allow incorporating it into a triaxial cell, hence facilitating the measurement of soil shear wave velocity at different levels of strain. The details of the development of the device and its use for measurement of shear wave velocity of different cohesive soils are described.

5.3 Objectives and Scope of Work

The main objectives of this study are twofold: first, is to extend the PRA technique by incorporating the device in the cyclic triaxial machine in order to facilitate accurate evaluation of the effect of shear strain (γ) level on soil stiffness; second, is to correlate values of V_s for cohesive soils measured at different shear strain levels using the PRA device with shear modulus reduction curves in order to enable development of shear modulus reduction curves using V_s measurements during conventional triaxial tests (i.e. without conducting cyclic loading).

The development and salient features of the PRA setup are described. The device was then used for investigating the dynamic properties of natural and re-constituted cohesive soils subjected to different levels of shear strain. The secant shear modulus, G, values were determined from the

hysteresis loops during cyclic shearing. In addition, the shear wave velocity was measured at the same shear strain amplitude. The results are utilized to correlate the measured shear wave velocity at very low strains Vs_{max} as well high strains Vs to the secant soil shear modulus, G, at different strain levels as well as very low strain shear modulus G_{max} .

This work is an exploratory study for the application of this technique for measuring V_s and G without resorting to cyclic loading on the tested soil samples.

5.4 Literature Review

5.4.1 Modulus reduction curves

The soil shear modulus reduction curves are used in seismic ground response and soil-structure analyses to simulate the nonlinear behaviour of soils when subjected to high shear strain amplitudes. The shear modulus reduction curve of cohesive soils is primarily a function of the index soil properties (usually PI) and applied strain rate. Shear modulus reduction curves of natural cohesive soils have been reported by several researchers including Kim and Novak (1981), Anderson and Richart (1976), Georgiannou et al. (1991), Rampello and Silvestri (1993), Shibuya and Mitachi (1994), Doroudian and Vucetic (1999) and Teachavorasinskun et al. (2002) among many others. For example, Vucetic and Dobry (1991) presented soil shear modulus reduction curves as a function of plasticity index (PI or I_p), which can be used to simulate the nonlinear behaviour of cohesive soils in seismic design. Vardanega and Bolton (2011, 2013) compiled database from the literature covering a variety of cohesive soils (clays and silts) and utilized it to predict the strain-dependent behaviour of fine-grained soils, based on simple index soil parameters. This database included normally consolidated to heavy overconsolidated cohesive soils, including cohesive soils from Ontario (Kim and Novak, 1981) similar to those investigated in the current study. Vardanega and Bolton (2011, 2013) developed a simple hyperbola model for the normalized secant shear modulus (G/G_o) as a function of normalised shear strain (γ/γ_{ref}) i.e.

$$\frac{G}{G_o} = \frac{1}{\left(1+\frac{\gamma}{\gamma_{ref}}\right)^{\zeta}} = \frac{1}{\left(1+\frac{\gamma}{\gamma_{ref}}\right)^{0.74}} \tag{5.2}$$

where, γ_{ref} is a reference strain defined as; $\gamma_{ref} = \tau_{max}/G_o$; the exponent ζ is curvature parameter introduced to better fit the data of small strains. The secant shear modulus reduces to half of its initial maximum value when $\gamma = \gamma_{ref}$ or γ_{ref} is the γ at $0.5G_o$. The stress-strain curves defined by Eq.5.2 are asymptotic to G_o at zero strain and to τ_{max} at infinite strain. Vardanega and Bolton (2011, 2013) reported the value of the curvature parameter, $\zeta = 0.74$, and the equation fit the data with a high correlation of 0.96 and a low standard error for a large number of data points. The model represented by Eq.5.2 is similar to the model suggested by Darendeli (2001) and Zhang et al. (2005). However, Vardanega and Bolton (2011, 2013) fitted the hyperbola model to the complied literature after modifying it for rate effects. They reported that high values of ζ, result in increased normalised stiffness (G/G_o) at small normalised strains (γ/γ_{ref}) but reduced stiffness at high strains. Vardanega and Bolton (2011, 2013) performed linear regression to find simple correlations between γ_{ref} and common soil properties including plasticity index (I_p), liquid limit (w_L), plastic limit (w_P) and initial void ratio (e_o). In the present study comparisons were made only using the plasticity index (I_p) and the initial void ratio (e_o) i.e.

$$\gamma_{ref} = 2.17\frac{I_p}{1000} \tag{5.3}$$

$R^2 = 0.75$, n = 61, S.E. = 0.00031

where: n = number of data points, S.E. = standard error, γ_{ref} = reference strain, I_p = plasticity index

$$\gamma_{ref} = 0.56\frac{e_o}{1000} \tag{5.4}$$

$R^2 = 0.75$, n = 61, S.E. = 0.00030

Vardanega and Bolton (2011, 2013) also acknowledged the fact that their database includes tests performed using different apparatuses and test frequencies. For strains higher than the linear elastic limit, fine grained soils typically show stiffness and strength increase at all strain rates (Vucetic & Tabata, 2003). Vardanega and Bolton (2011, 2013) corrected the compiled data to two standard strain rates to reduce the discrepancy between data obtained from static and cyclic testing. In order to account for strain rate effects in different test conditions, Vardanega and Bolton (2011, 2013) normalized the entire stiffness data by a standard test rate of $\dot{\gamma} \approx 10^{-6}\ s^{-1}$ (for a static triaxial test),

by assuming a strain-rate effect of 5% increase in the stiffness per $\log_{10}$ cycle of increase in the plastic strain amplitude consistent with the findings of Lo Presti et al (1997) and d'Onofrio et al (1999). Applying such rate-effect correction/adjustment can merge the data from tests such as resonant column and static test data into a single database. However, by doing so, Vardanega and Bolton (2011, 2013) acknowledged that the stiffness of very low plasticity clays at low cyclic strain amplitudes in resonant column tests is likely to be underestimated, while the stiffness for high plasticity clays at large strain amplitudes in resonant column tests may remain overestimated. Nonetheless, the disparity in stiffness between dynamic and static test results should have been reduced. They assumed that the onset of grain slippage (and the first instance of $G < G_{max}$) occurs at a shear strain amplitude of 10^{-5}, and that only shear strains amplitude greater than 10^{-5} will lead to rate effects.

The average shear-strain-rate, $\dot{\gamma}$ for strain controlled cyclic loading test can be determined from:

$$\dot{\gamma}(1/sec) = 4\,\gamma\,f \tag{5.5}$$

where γ is single amplitude shear strain, and f is the loading frequency (used as 1 Hz during the present study), which is typically used for representing earthquake loading. As can be seen from Eq.5.5, for a constant frequency, the strain-rate increases as the strain-amplitude increases.

As discussed earlier, it is important to report that the strain rate effects are only noticeable for strain amplitudes > 10^{-5}, as can be noted from Eq.5.6:

$$\dot{\gamma} = 4\,(\gamma - 10^{-5}) \tag{5.6}$$

To adjust the modulus reduction curve obtained by Eq.5.2 for strain-rate effects, a strain-rate factor, Z, can be determined for each strain amplitude using the following relationship (Vardanega and Bolton, 2011 & 2013)

$$Z = 1 + 0.05\,log_{10}\left(\frac{\dot{\gamma}}{10^{-6}}\right) \tag{5.7}$$

Substituting Eq.5.6 into Eq.5.7 yields,

$$Z = 1 + 0.05\ log_{10}\left(\frac{4\ (\gamma - 10^{-5})}{10^{-6}}\right) \tag{5.8}$$

Vardanega and Bolton (2013) compared their curves with the work of Vucetic and Dobry (1991) and found that Vucetic and Dobry's curves presented stiffer response at all strain amplitudes and attributed it to fast-cyclic resonant column testing with no rate-effect corrections.

The concept of strain rate effects presented above is employed in the current research for two objectives. First, it facilitates the comparison of results obtained during the present study with the work of Vardanega and Bolton (2011, 2013), in order to evaluate the performance of the developed device. Since the empirical correlation provided by the Vardanega and Bolton (2011, 2013) is for a strain rate equivalent to that of the static triaxial test, the estimated values from the empirical correlations provided by Vardanega and Bolton (2011, 2013) are corrected for strain rate effects to match the strain rate of the cyclic triaxial test used in the present study. This is done by using the equations and the procedure given above by Vardanega and Bolton (2011, 2013).

The second objective of examining strain rate effects is to highlight its importance. The resonant column and the cyclic triaxial tests evaluate dynamic properties of soil under two different ranges of strain amplitudes. The resonant column test covers the very low to medium cyclic shear strain amplitudes, while the cyclic triaxial covers the medium to high strains. They have a common, but small, range of strain amplitudes, i.e. medium strain amplitudes. In addition, the loading frequency is very different in both devices, that is resonant column operates at much higher frequencies than the cyclic triaxial test. The results of the two tests for the common medium strain amplitudes cannot be compared unless the rate effects are taken into account.

5.4.2 Limitations of the conventional triaxial test

In the conventional triaxial test, the global deformation of the test specimen is measured using transducers located external to the triaxial cell (Rees, 2015 a, b, c). In such case, the axial displacement transducer is usually affixed to the loading ram, and the radial strains are estimated from back volume change and/or axial displacement readings. Such strain measurements may be of sufficient accuracy for routine triaxial tests, but they do not allow truly accurate measurements of specimen deformation at the small strain level. This is in part due to system compliance, where external transducers read extraneous system movements and component deformations distinct

from specimen straining. Bedding error, or the apparent axial strain recorded as the top-cap is pushed into full contact with the upper specimen surface, also contributes to the difficulty in obtaining accurate measurements at very small strains.

Fig.5-1 presents the generalized shear modulus degradation curve displaying approximate obtainable strain ranges for various laboratory and field tests and also for different geotechnical applications. As indicated by Fig.5-1, the cyclic triaxial test only covers the intermediate to high strain levels, typically > 0.05% shear strain.

The GDS triaxial system used in the current study has global axial strain transducers. The manufacturer reported that, in the absence of local strain measurement transducers, such conventional triaxial apparatuses generally accurately apply and measure the shear strain in excess of 0.1%. In the present study, the soils were tested under the applied shear-strain in several increments that varied between 0.08% to around 3-5 %.

5.4.3 V_s - σ' relationships and fittings parameters correlations

The shear wave velocity is affected by the applied mean effective stress on the soil, and the relationship V_s - σ' can be given in a general form as:

$$V_s = \alpha \, \sigma'^{\beta} \tag{5.9}$$

where α and β are power-curve fitting parameters. Parameter α (m/s) is V_s at 1 kPa. The exponent β reflects the sensitivity of V_s to σ'_{mean} in the polarization plane and depends on the nature of interparticle contacts and fabric changes during loading. The factor α inherently incorporates the effect of the void ratio function that is generally accounted for in conventional V_s correlations. Together, these fitting parameters reflect contact behavior and changes in soil fabric associated with effective stress, i.e., the velocity-stress relationship captures both contact stiffness and soil fabric (Cha et al., 2014). The exponent β increases as the soil compressibility (i.e. compression index, C_c) increases, while the factor α decreases with the increase in compression index, C_c.

In Chapter 4, a variety of cohesive soils were tested employing PRA device incorporated in an oedometer. The measured V_s and G_{max} results were employed to establish empirical expressions, which correlate the curve fitting parameters α and β of the tested soils with their measured

compression index (C_c). In addition, the measured α and β were correlated with each other and presented an inverse relationship. These correlations are given below:

$$\alpha = 13.2\, C_c^{-0.65} \tag{5.10}$$

$$\beta = 0.152 \log(C_c) + 0.424 \tag{5.11}$$

The curve fitting parameters (α and β) can also be related to each other by an inverse relationship, i.e.

$$\beta = 0.684 - 0.233 \log(\alpha) \tag{5.12}$$

As reported in Chapter 4, a variety of cohesive soils were tested using a piezoelectric ring actuator (PRA) device fabricated and incorporated in the Oedometer setup. The values of V_s measured at different levels of applied effective stress were curve fitted to Eq.5.9, and the values of the curve parameters, α and β, were established.

Equations 5.10-5.12 will be used in the current study to compare the results from the oedometer tests with those from the triaxial test. In addition, they will be utilized in order to define the variation of shear wave velocity over a range from very low to high shear strain.

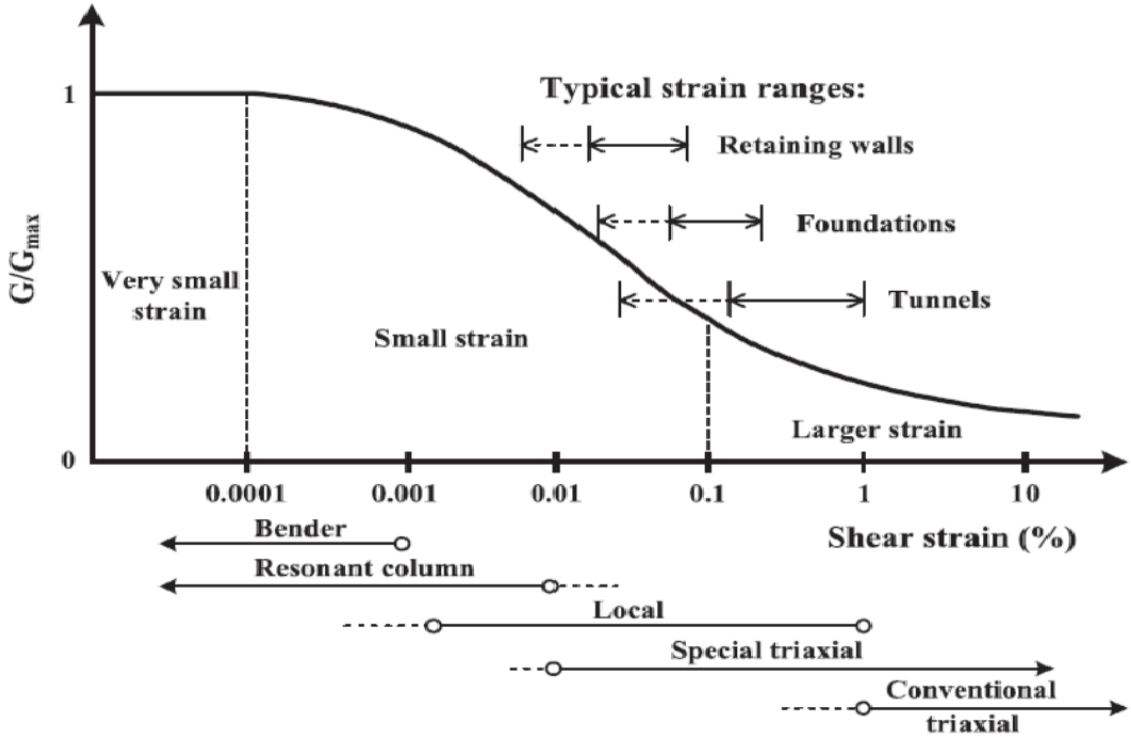

Phenomena		Wave propagation, vibration	Crack, differential settlement	Slide, compaction, liquefaction
Soil behavior		Elastic	Elastic-plastic	Failure
Soil properties		Shear modulus, Poisson's ratio, damping		Angle of internal friction, cohesion
Effect of load repetition		◄———	———	———►
Effect of loading frequency		◄———	———	———►
In situ measure-ment	Seismic wave method	◄———	———	———
	In situ vibration test	———	———	———
	Repeated loading test	———	———	———►
Laboratory measure-ment	Wave propagation test	◄———	———	———
	Resonant column test	———	———	———
	Repeated loading test	———	———	———►

Figure 5-1. Generalized shear modulus reduction curve displaying approximate obtainable strain ranges for various laboratory and field tests and for different geoengineering applications (After Sawangsuriya 2012, Atkinson and Sallfors, 1991 and Mair, 1993)

5.5 Device Fabrication

Ring shaped piezoelectric elements (ring actuators), which can vibrate radially to emit planar waves over large contact area with the test soil specimen, were used in the manufacturing of the device. The ring shape was chosen over the disc shape because piezoelectric discs are impervious and may adversely impact soil drainage during the consolidation process. With the ring shape actuators, porous stones can be installed inside the piezoelectric rings ensuring soil drainage, which is a key requirement to test cohesive soils under saturation and consolidation. The inner and outer diameters of the used piezoelectric rings were 38 and 44 mm, respectively, and it was 3.5 mm high. When electric voltage is applied between inner and outer diameters (i.e. radially), the piezoelectric element deforms and vibrates in the radial direction according to the shape of the input signal. This radial deformation causes the shearing of the soil base thus producing shear waves.

As piezoelectric elements do not penetrate into the soil, roughness of the contact surface both at porous stones and piezo rings is important in transmitting a stronger signal to the soil specimen. Excitation at soil's end is generated through friction and/or adhesion between the inner metallic porous stone and soil. Therefore, rough/coarse bronze porous stones were used to enhance interaction with soil specimen, which ensured a stronger output signal from the emitter piezoelectric element. Fig.5-2 shows the detailed schematic drawing of the fabricated PRA setup.

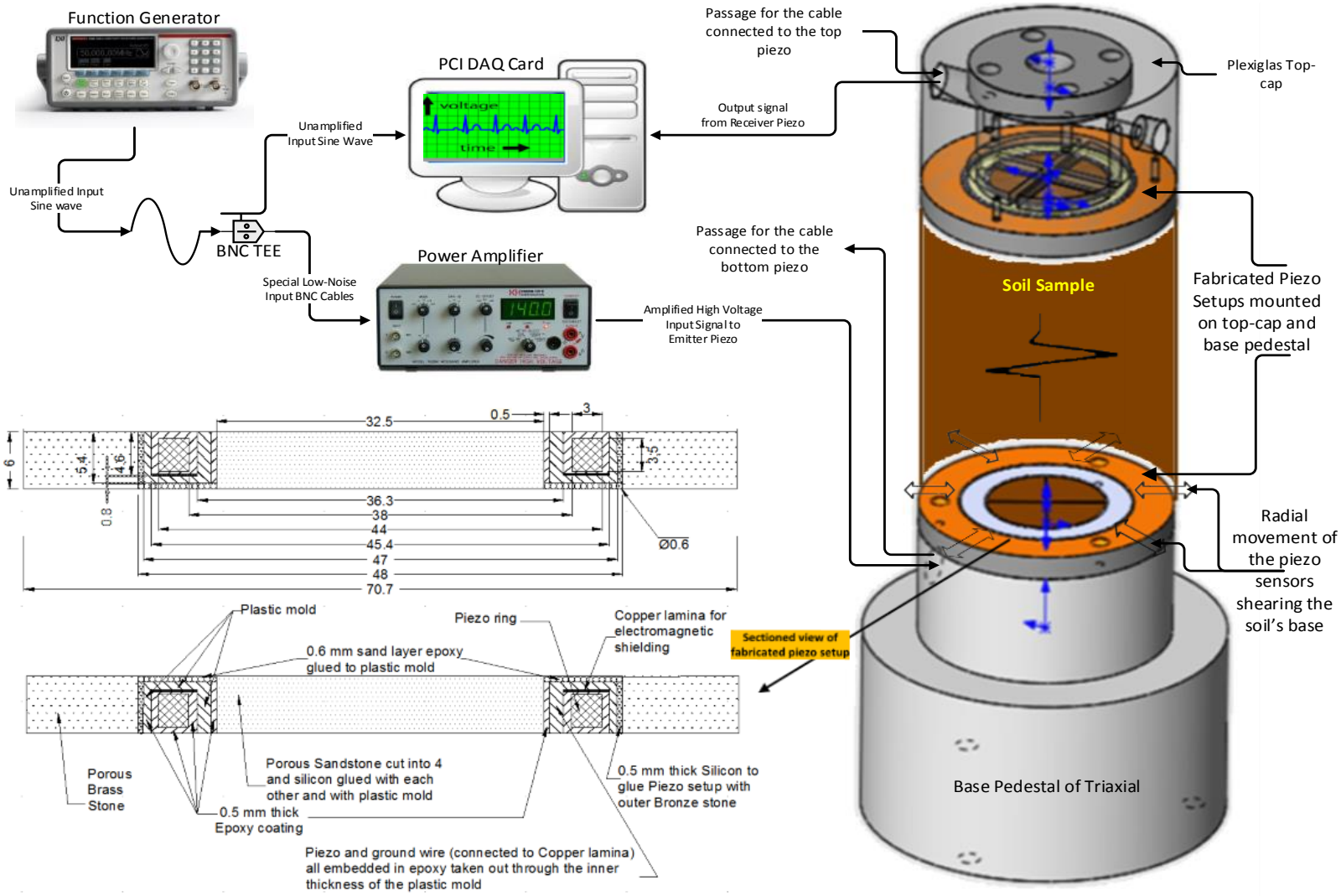

Figure 5-2. Details of the Fabricated Triaxial Setup

It is important to protect the piezoelectric elements from the harsh environment, especially water. Therefore, several layers of protections were applied to the piezoelectric elements. This was achieved by coating the elements first with conformal spray and then with high performance epoxy to make them waterproof. After the epoxy cured, another layer of conformal was sprayed and a thin layer of silicone coating was applied so seal the epoxy coating.

In order to achieve a smooth and uniform coating of epoxy on the piezoelectric rings, a Delrin mold was used to house the piezoelectric rings. This mold also ensured the vertical and horizontal alignment (centering) of the piezoelectric transducers inside the porous stones as centering especially in horizontal direction is very important to for the performance of the PRA setup. This mold also acts as an additional insulation giving more protection to the piezoelectric rings. The mold is 5.4 mm high, which is 0.6 mm less than the height of the inner and outer metallic porous stones as noted on Fig.5-2. The height difference between the mold and porous stones allowed gluing a 0.6 mm uniform layer of sand, which ensured a rough contact surface between the specimen and the setup for a stronger shear wave.

"Crosstalk" is a phenomena that takes place due to electromagnetic coupling between the source (emitter) and receiver piezoelectric elements (Lee and Santamarina, 2005; Leong et al., 2009). It can appear on the output signal as a duplicate of the input sine-wave (Fig.5-3a). Crosstalk can be very significant in conductive soils such as wet clays. Leong et al. (2009) observed the crosstalk during their studies and attributed this to the improper grounding. Crosstalk can interfere with the output signal and can mask the arrival of the shear wave, especially when testing short specimens at low frequencies and/or at high pressures. In such cases, the shear wave arrival time, t_s, is either very close or less than the period of the input wave.

To eliminate the crosstalk in the developed device, proper shielding and grounding was provided to the piezoelectric elements. Fig.5-3 shows that the output signal with cross-talk (duplicate) when grounding is cut-off on purpose. On the other hand, Fig.3-4b shows the typical signal from the fabricated PRA oedometric device devoid of cross-talk (no duplicate of the input sine-wave) when the ground wires are connected to the appropriate ground resulting in a clean signal making the fabricated device very reliable for measuring V_s for different soil types under different loading

conditions and different specimen sizes. The grounding was accomplished by using copper lamina, cut into circular shape and placed inside the plastic mold and connected to a ground wire. Insulation was applied to the small metal surfaces exposed at the connection of ground wire and copper lamina and at the connection of the wires to the inner and outer electrodes of the piezoelectric elements.

During the initial trials of device fabrication, a metallic mold was used to shield the piezoelectric actuator elements from the electromagnetic coupling as a Faraday's cage in order to eliminate the cross-talk. The metallic mold actually eliminated the cross-talk, but resulted in an output voltage signal with multiple major peaks of the same amplitude, which was attributed to possible resonance or shorting. Even though epoxy with high dielectric resistance was applied between the mold and the piezoelectric elements to eliminate shorting, it appears one or both piezo elements somehow touched the metallic mold sides causing such an output. Therefore, the metallic mold was replaced with a Delrin mold and copper lamina to shield the actuators to prevent cross-talk.

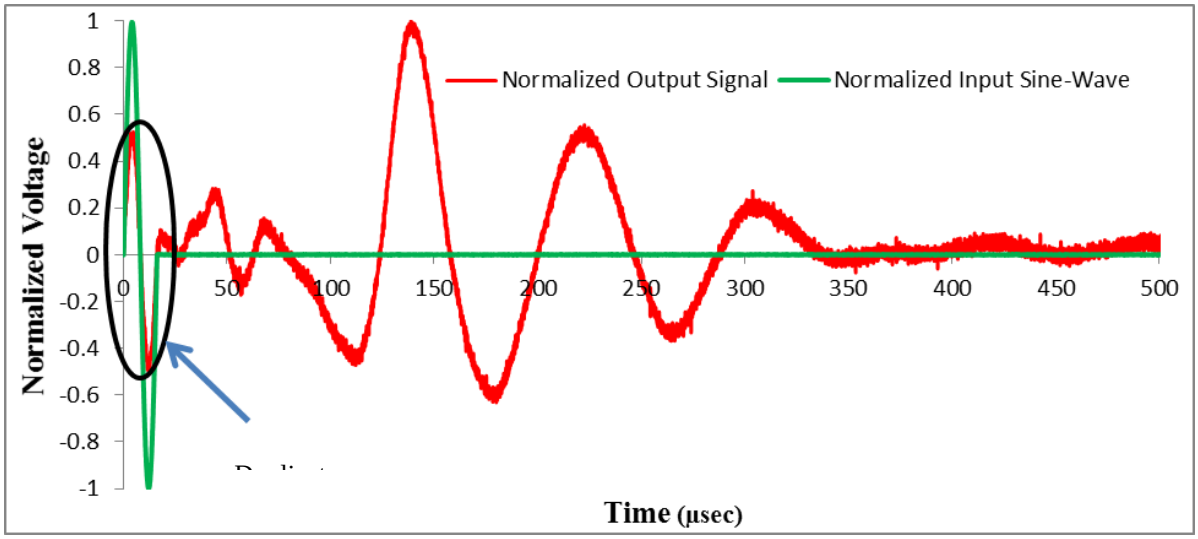

Figure 5-3. Normalized Output Signal showing Cross-Talk (duplicate) when ground cut's-off

Some of the steps of fabrication are summarized in Fig.5-4. After completing the insulation and shielding, the inner metallic porous stone was epoxied to the Delrin mold (Fig.5-4c). Epoxy was preferred over soft bonding agents like silicone so that the assembly strictly behaves as one unit

and the deformations of the piezoelectric rings are transmitted to the inner porous stone causing it to vibrate the same way as the piezoelectric elements. The inner stone before epoxied to Delrin mold (Fig.5-4c) was cut into four pieces (Fig.5-4a), and these pieces were then glued together (Fig.5-4b) using soft material (silicone) in order to facilitate uniform distribution of shear deformations to the specimen surface. The entire inner setup (piezoelectric element in Delrin mold and the inner metallic stone glued to it) was then glued to the outer metallic porous stone using silicone (Fig.5-4d). The silicone was preferred because of its flexibility, which allows the entire inner setup to vibrate easily creating a strong signal.

Extreme caution was exercised when applying the epoxy and silicone for gluing the different components together so that the porous stones don't get clogged. This is necessary to facilitate back-pressure saturation and drainage through these porous stones during sample preparation and testing. The few of the many different stages of fabrication are presented in Fig.5-4.

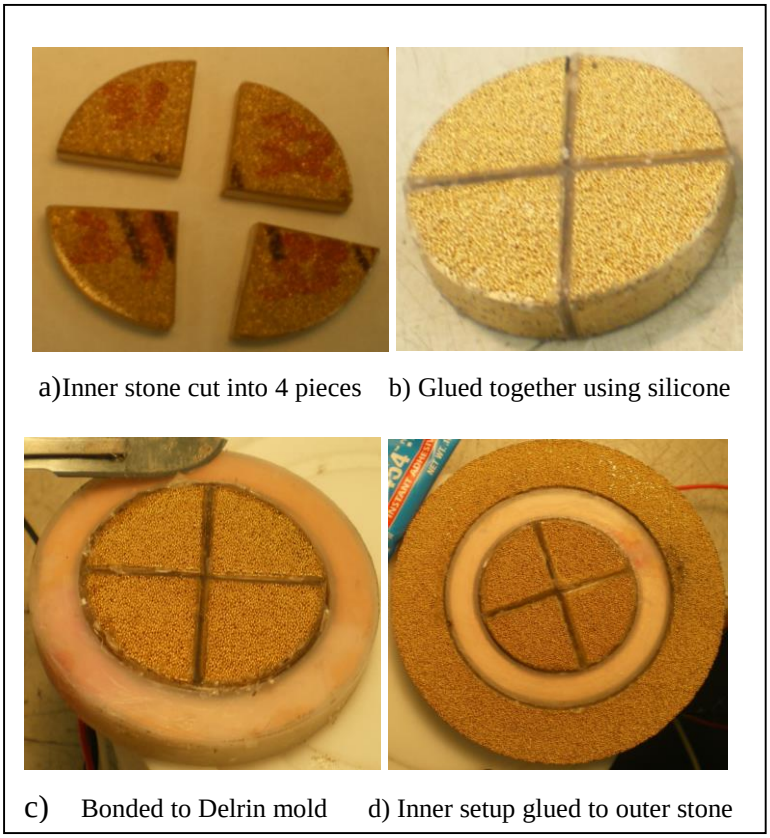

Figure 5-4. Different stages of cutting and bonding of inner porous stones

The base pedestal of the triaxial cell was fabricated from Aluminum while its top cap was made with Plexiglas. The top cap and base pedestal of the triaxial cell were fabricated in such a way to ensure the regular triaxial operations (i.e. Back-pressure saturation and pore-pressure measurement) are not hindered and also to ensure that both parts provide safe and water-tight passage to cables and ground wires connected to the piezoelectric rings. Thick (as compared to oedometer setup) and right size (diameter) cables were connected to the piezoelectric elements in triaxial setup to ensure a snug fitting through the base (annular ring) and the top cap as shown in Figs.5-5 and 5-6. This is important to prevent leakage through the base also known as annular ring of the triaxial cell. Finally, the fabricated parts were screwed to the base pedestal and top cap of triaxial setup.

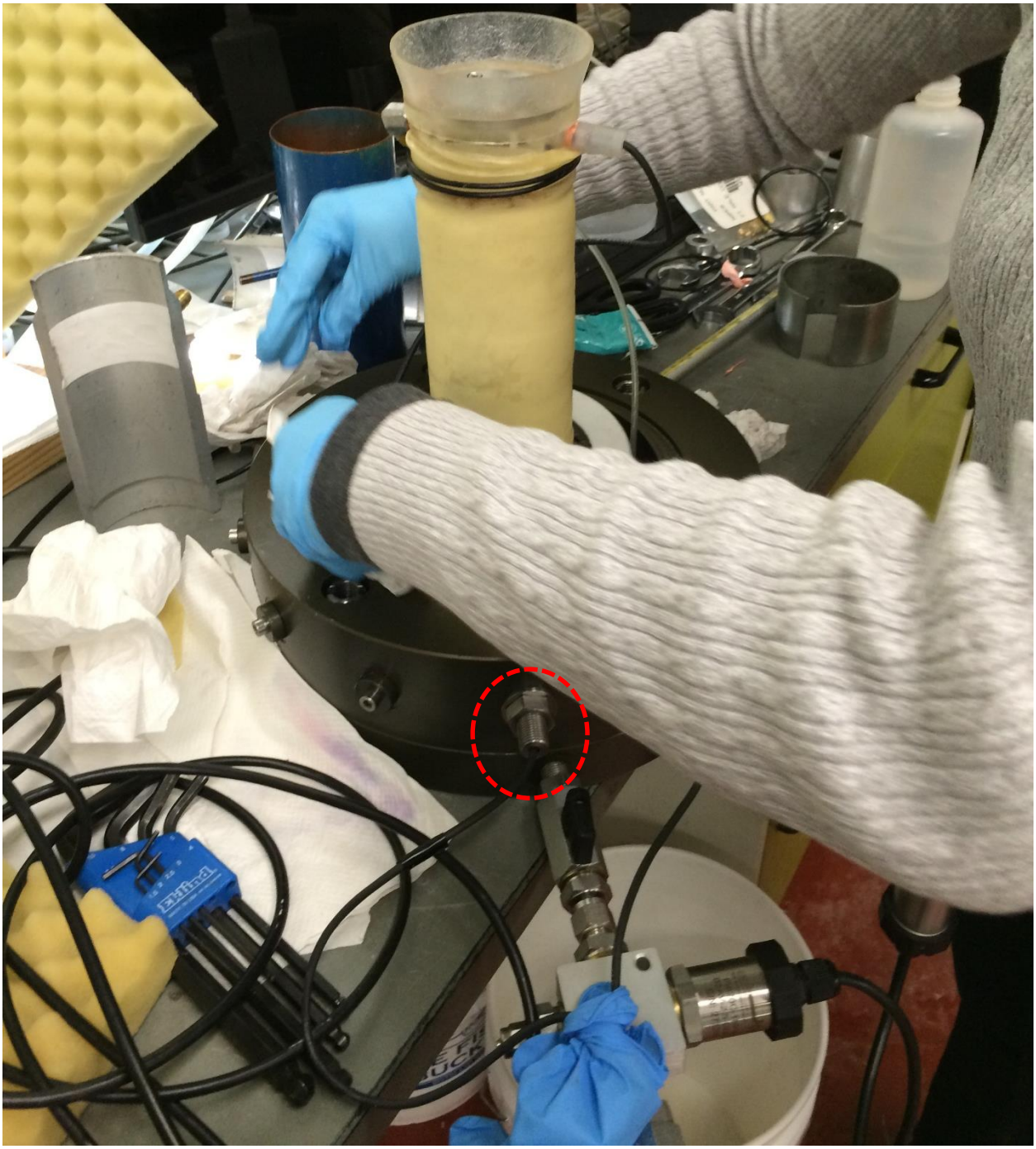

Figure 5-5. Sample setup showing the cables connecting to the PRA coming out of annular ring

Figure 5-6. Connection of the bottom PRA installed in the triaxial base

Sample preparation and set up for triaxial testing is far more complicated as compared to the oedometer test. For example, the consolidation pressure in triaxial chamber is achieved by applying isotropic cell pressure through a combination of air and water as opposed to applying direct loading to the specimen in oedometer testing. Because of such complexity, the fabricated triaxial setup went through several modifications to accommodate the requirements for triaxial testing and to achieve functional piezoelectric setup.

Numerous trial tests were conducted with real soil and dummy (rubber) specimens to identify any issues with the fabricated PRA setup, and to evaluate its performance and output signals. During these trials, the regular cyclic triaxial test phases (i.e. saturation, consolidation and cyclic shearing) were conducted to ensure all the device functions can be performed successfully. Eventually, a PRA was successfully fabricated, and was demonstrated to operate as expected and provide consistent repeatable results.

During the initial trials, a number of problems occurred. For example, water leaked through the cables connecting to the piezoelectric elements. The water leaked through the spot shown in Fig.5-7, then travelled along the cables and finally came out through the BNC connectors affixed to the cables attached to the piezoelectric elements. The leakage was pronounced in the bottom piezoelectric setup since it has much more intricacies than the top cap setup. The leakage was also aggravated by the high water pressure inside the triaxial chamber, as would be expected. These type of leakage have been seen even with the factory made bender element devices.

Several solutions were applied to prevent water leakage inside and outside the triaxial cell. Initially, small diameter O-rings were used with tight connectors, and were taped with Teflon. In addition, silicone was injected into the cables at few critical spots, which created silicone plug and hence reduced water leakage significantly. Furthermore, silicone was injected along with the liquid electric tape into all fittings and connections, which stopped the leakage. The chamber pressure inside the triaxial cell then was raised in the final trials to the maximum pressure of 1000 kPa (1MPa) to check whether the developed device can withstand the highest pressure possible and to test the performance of water proofing at this pressure level. The device continued to operate satisfactorily at the maximum pressure.

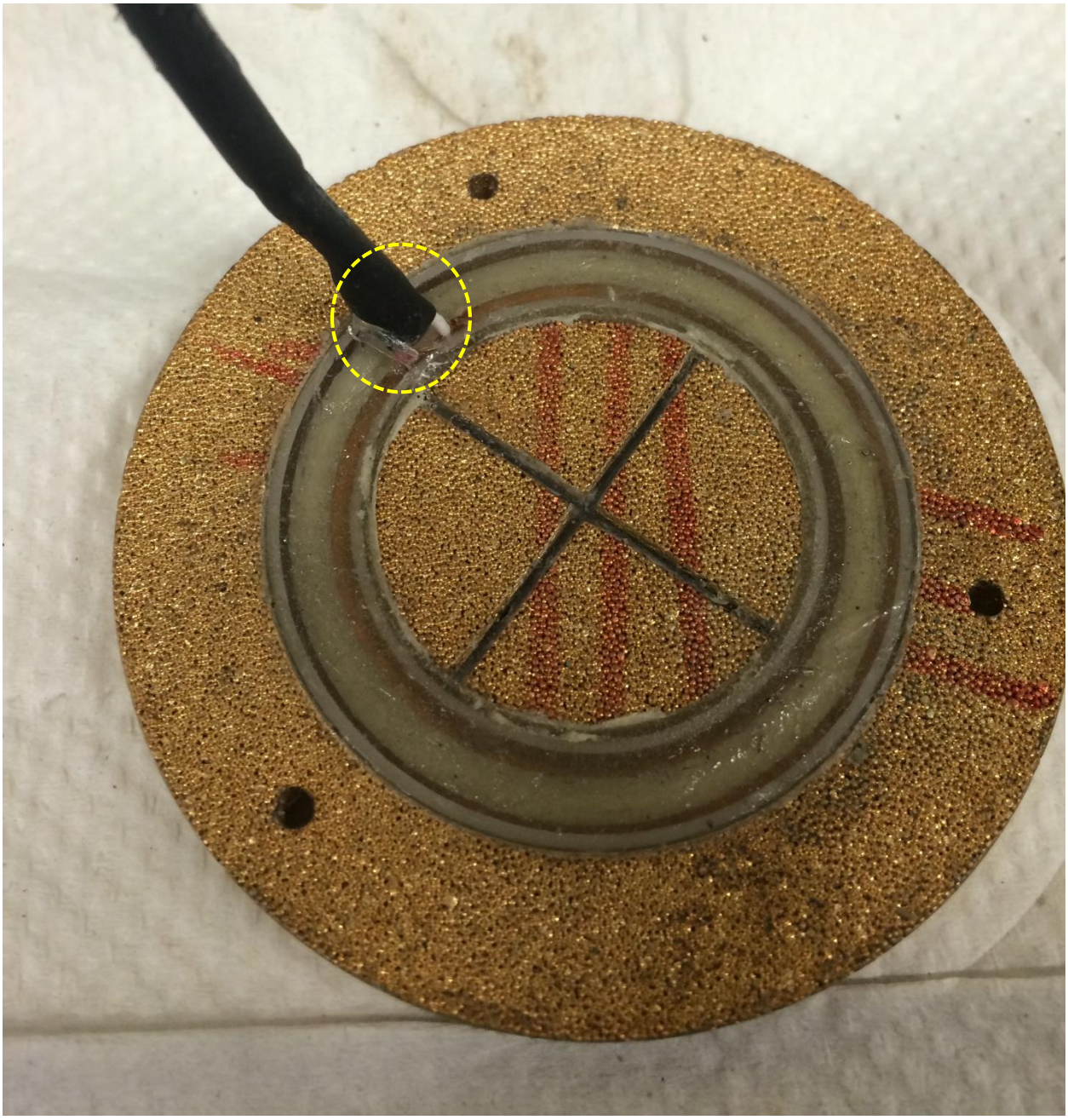

Figure 5-7. Piezo-setup showing the suspected point for the water leakage

Since high voltage input signals are utilized to activate the piezoelectric elements, it was necessary to apply multiple precautions to ensure safe operation of the system. First, the piezoelectric elements were grounded using cables extending outside the triaxial device. Second, the triaxial system itself was grounded. Finally, ground fault interrupter (GFI) was utilized to shut down the equipment in case of any short-circuiting.

5.6 Tested Soils

Six different cohesive soils tested in the present study including one artificial clay and five undisturbed natural cohesive soils. The natural clay soils are: Sombra, Ottawa I, Ottawa II, Cayuga, and Port-Alma. The artificial clay soil is Kaolin-silt clay (K-S), which is commonly used in geotechnical centrifuge studies to represent the behaviour of clay. The K-S specimens were reconstituted in the laboratory by mixing kaolin and silt at equal proportions (i.e. each 50% by weight) in a slurry consistency. The slurry was consolidated under one-dimensional conditions by applying a vertical effective pressure of 300 kPa. After completion of primary consolidation, the specimen was extruded. The index properties of the tested soils were determined based on ASTM specifications. The Atterberg Limits were measured following ASTM D4318 procedure (ASTM 2010). The measure index properties are presented in Table.5-1.

Sombra and Ottawa I clays have the highest plasticity among the tested soils indicating medium plastic clay (plasticity index, PI or I_p = 25-28%). Ottawa II, K-S, Cayuga and Port-Alma soils had low plasticity (I_p, in the range of 15%). The average water content of the Sombra clay was found to be close to its liquid limit, which explains its soft consistency. For the Ottawa soils, the water content was higher than its liquid limit giving it very soft consistency and a liquidity index of slightly more than unity indicating the soils were slightly sensitive.

Cayuga and Port-Alma are very stiff soils with natural water content close to or slightly lower than their plastic limits indicating overconsolidation.

All the tested natural soils were trimmed from high quality undisturbed Shelby tube samples. The PRA setup is suitable for a variety of height to diameter ratio (H/D) including the conventional H/D = 2. In the current investigation, H/D was kept $\geq$ 1. Using H/D $\geq$ 1 is consistent with

investigations conducted by Wichtmann et al. (2012), Dirgeliene et al. (2007), Schanz and Gussman (1994), and Jacobson (1967).

Table 5-1. Index Properties of the tested soils

Soil Type	Avg. Initial Void Ratio, e_0	Specific Gravity, G_s	Avg. Natural Water Content, w_N (%)	Liquid Limit, w_L (%)	Plasticity Index, I_P (%)
Sombra	1.20	2.70	46	50	25
Ottawa I	2.10	2.75	71	48	28
Ottawa II	1.10	2.74	39.8	32	14
K-S	0.80	2.63	30	38	15.7
Cayuga	0.65	2.8	22.2	34.4	14.8
Port-Alma	0.45	2.68	18	33.5	13.5

5.7 Results and Discussions

5.7.1 Characteristics of the obtained signals and analysis technique

Fig.5-8 shows the typical output signal obtained from the fabricated triaxial setup. It can be seen that the output signal is very clear with one single major peak (shear-wave), with a high signal-to-noise ratio (SNR). The clarity of the output signals can be attributed to the fact that the PRA setup shears the entire soil sample cross-section because the ends of tested samples were in direct contact with the PRA setup unlike bender elements that shear the soil at a certain point. Thus, the PRA setup excites a larger soil mass, which represents better representation of the in-situ condition than the conventional bender elements in measuring V_s.

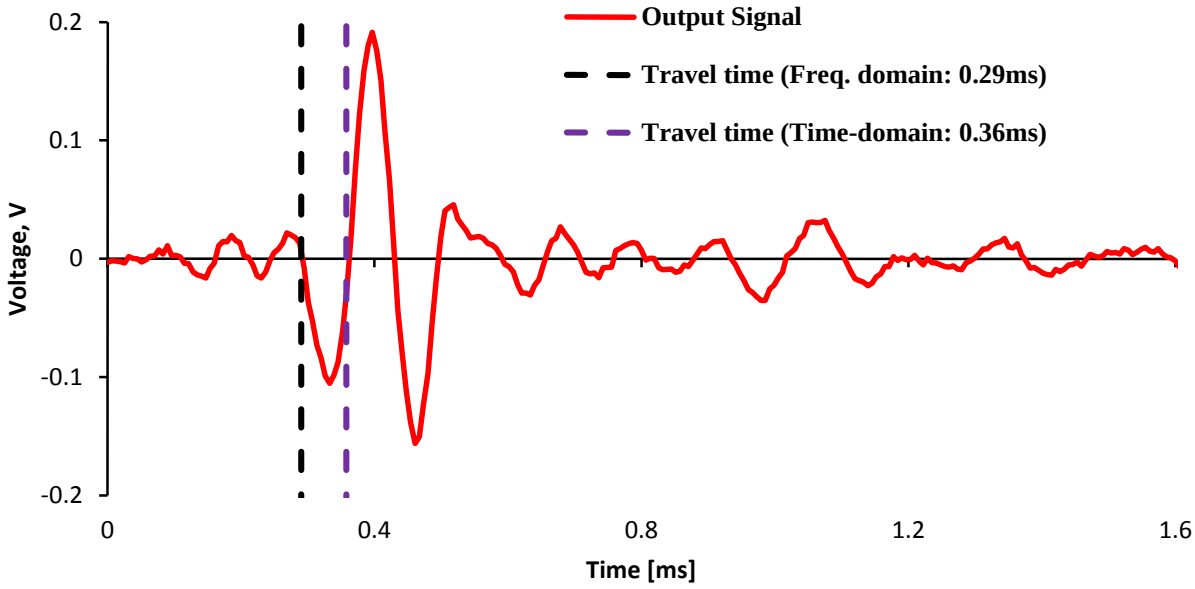

a) Travel Time Interpratation using Time and Frequency Domain Analysis

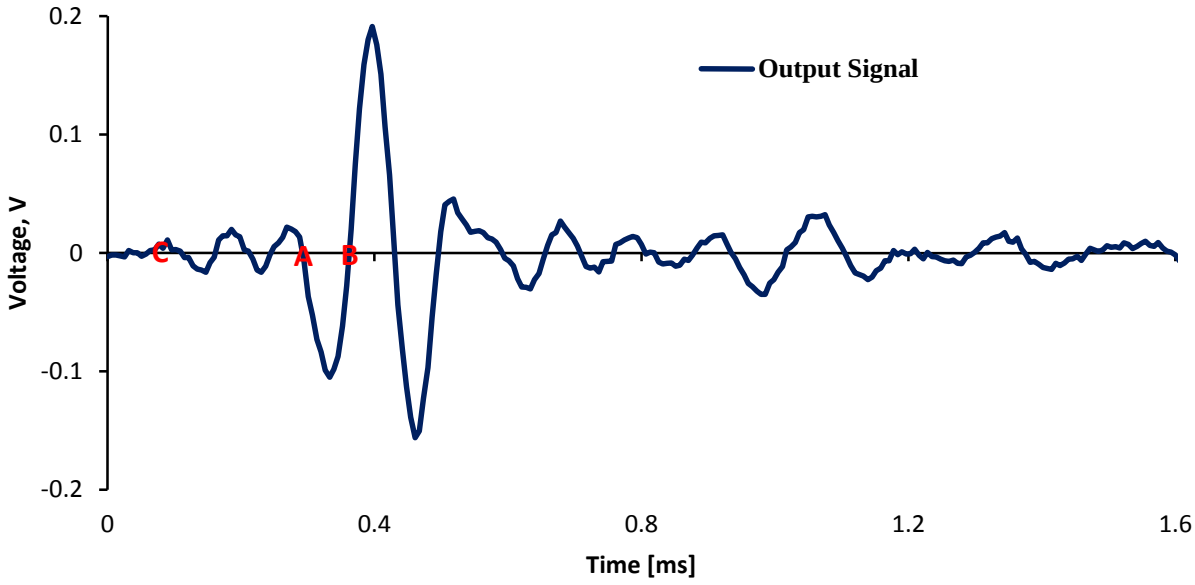

b) Travel Time Interpratation using Direct Arrival Method

Figure 5-8. Typical signal obtained by the fabricated triaxial setup from the K-S soil and travel time interpretation

The output signal shown in Fig.5-8 is obtained by using high voltage input sine wave. The input voltage and frequency used along with the current piezoelectric setup can be varied over a wide range. The input voltage in this study varied between 50-100 $V_{p\text{-}p}$, which can be further increased if required up to 300 $V_{p\text{-}p}$ safely without depolarizing the PRA owing to the bigger dimensions of the chosen PRA. The input frequency was varied between 1 to 15 kHz. Also, the input signal can have a variety of patterns including sine, square or white (random) noise signals. Such flexibility of input voltage, frequency and shape can facilitate measuring shear wave velocity of a wide range of specimen stiffness and allow different methods of interpretation of test results. This may not be the case for conventional BE testing.

It is important to mention that the typical frequency range selected for V_s measurement during 1D consolidation testing was around 15-40 kHz, while for the triaxial setup it was between 1-15 kHz and this is related to the sample height. The sample height for the triaxial testing is three times the sample height during oedometer testing (i.e. $H_{triaxial} \geq 3\ H_{oedometer}$), which allows lower input frequency.

The output signals are analyzed using both the time and frequency domain and using direct arrival method (first zero crossing before the major peak) and the results of the analyses are presented in Figs.5-8a and b and Fig.5-9. Fig. 5-8a shows the time history of the output signal and the interpretation of the shear wave travel time using cross-correlation (time domain) and cross-power spectrum analysis aka group velocity method (frequency domain). The cross-power spectrum phase diagram (Fig.5-9) is required to find the group travel time and hence group velocity (frequency domain analysis) as shown in Fig.5-8a. The slope of cross-power spectrum phase diagram (Fig.5-9) is used to determine the group travel time. The group travel time $\boldsymbol{t_g}$ determined from the frequency domain analysis (Viggiani and Atkinson, 1995), which is shown in Fig.5-8a, is calculated as $t_g = \eta/2\pi$, where η is the slope of the straight line (cross-power spectrum phase diagram) in Fig.5-9. A broad range of frequencies and a high correlation of a linear fit in the cross-power spectrum phase diagram are key for reliable evaluation of arrival time (group travel time $\boldsymbol{t_g}$) and hence group velocity using the frequency domain analysis technique (e.g. Ferreira and Fonseca, 2005). A very high correlation ($R^2 \approx 1$) for the linear fit can be observed in the cross-power spectrum phase diagram (Fig.5-9) along with the broad range of frequencies considered

confirms the reliable estimate of shear wave arrival time. The arrival time established from the frequency domain analysis was consistent with the arrival time using direct arrival method established by testing well documented Ottawa sand in addition to a variety of cohesive soils during oedometer testing as reported in Chapters 3 and 4. Using direct arrival method, the shear wave arrival time is at or close to the first zero crossing before the major event/peak presented as Pt **A** in Fig.5-8b. As seen in Fig.5-8a and Fig. 5-8b, the shear-wave arrival time using the frequency domain analysis was similar to the first zero crossing before the major peak (i.e. Pt ***A*** in Fig.5-8b) and hence validated the developed consistency between the frequency domain analysis and the direct arrival technique, while the arrival time established by the cross-correlation/time domain analysis (i.e. Pt ***B*** in Fig.5-8b) underestimates V_s. If the very first movement (indicated by Pt C in Fig.5-8b) is considered a P-wave arrival, travel times using Pt ***A*** and Pt ***C*** can be used to evaluate the dynamic Poisson's ratio, i.e.:

$$\nu = \frac{1}{2}\frac{\left(V_p/V_s\right)^2 - 2}{\left(V_p/V_s\right)^2 - 1} \tag{5.13}$$

where V_s is shear wave velocity and V_p is the P-wave velocity

Using Eq.5.13, Poisson's ratio was found to be around 0.44 for the K-S soil, which falls within the range of Poisson ratio expected for cohesive soils (Chapter 4.). This further supports using Pt ***A*** as the arrival point for the shear wave.

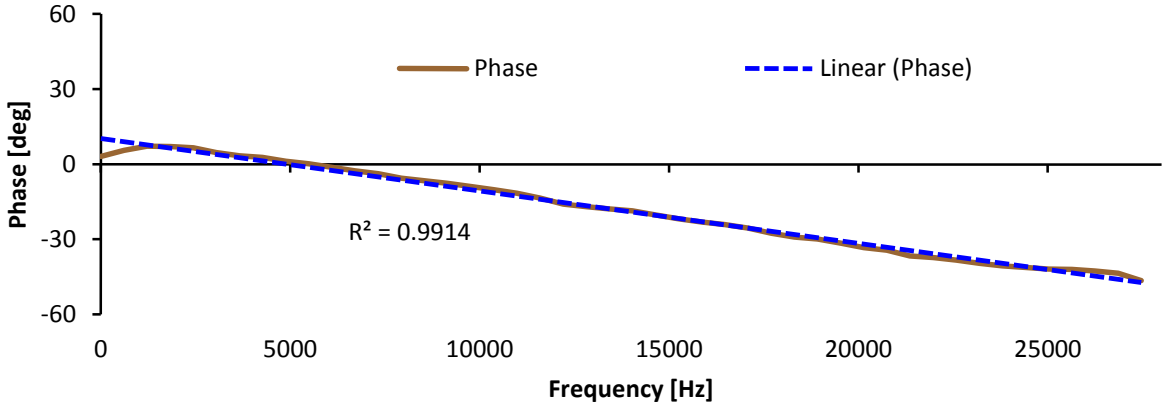

Figure 5-9. Cross-power spectrum phase diagram

5.7.2 V_s - σ_m' relationships and performance evaluation of the fabricated PRA setup

Some of the soils tested during the present study (i.e. Ottawa II, Sombra and K-S soils) were also tested under 1D consolidation) and their results were used to obtain the curve fitting parameters of Eqs.5.10 - 5.12). Fig.5-10 presents the relationship between the shear wave velocity and the mean effective pressure, V_s - σ_m', for the specimens tested using the triaxial PRA setup. For the purpose of comparison, the results obtained from the oedometer PRA setup are also included in Fig.5-10. As can be noted from Fig.5-10, there is an excellent comparison between the measured V_s values from the two PRA setups, which confirms the performance and reliability of both PRA setups as well as the analysis technique. Similarly, excellent agreement between V_s values obtained from the oedometer and triaxial PRA setups was observed for Sombra and K-S soils. The repeatability of the results was also confirmed throughout the measurement of the shear wave velocity during the present study.

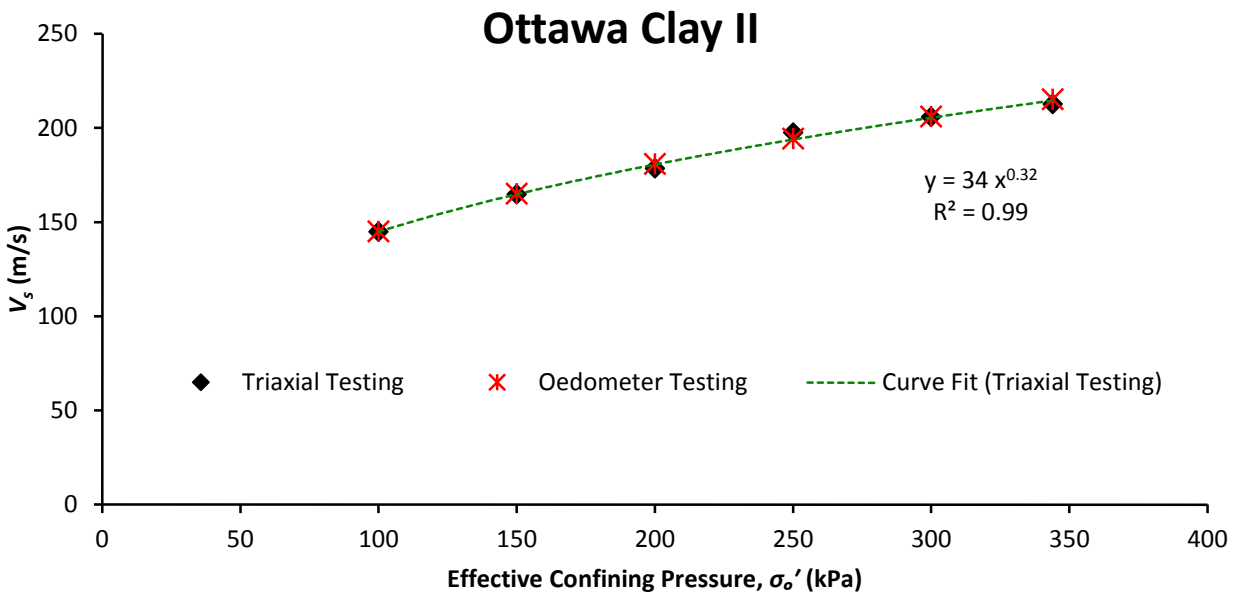

Figure 5-10. V_s vs. effective confining pressure for Ottawa II clay

Figs.5-11 and 5-12 present the V_s - σ_o' results for Port-Alma and Cayuga clays, respectively. The curve fitting parameters α and β for these soils are also presented in Figs.5-11 and 5-12. In addition, α and β back figured from V_s measurements, along with the measured C_c of both soils, are

summarized in Table.5-2. In addition, Table.5-2 shows α and β values predicted employing Eqs. 5.10 and 5.11 using the measured C_c of each soil as an input. Table.5-2 shows that the curve fittings parameters obtained from the current tests are similar to those obtained using Eqs.5.10 and 5.11, which verifies the applicability of Eqs.5.10 and 5.11 for a variety of soils. This also verifies the consistency of results obtained from both the oedometer and triaxial PRA setups. Moreover, α and β values obtained in the current testing satisfy the inverse relationship given as Eq.5.12, which was proposed based on the V_s measurements obtained utilizing the oedometer PRA setup.

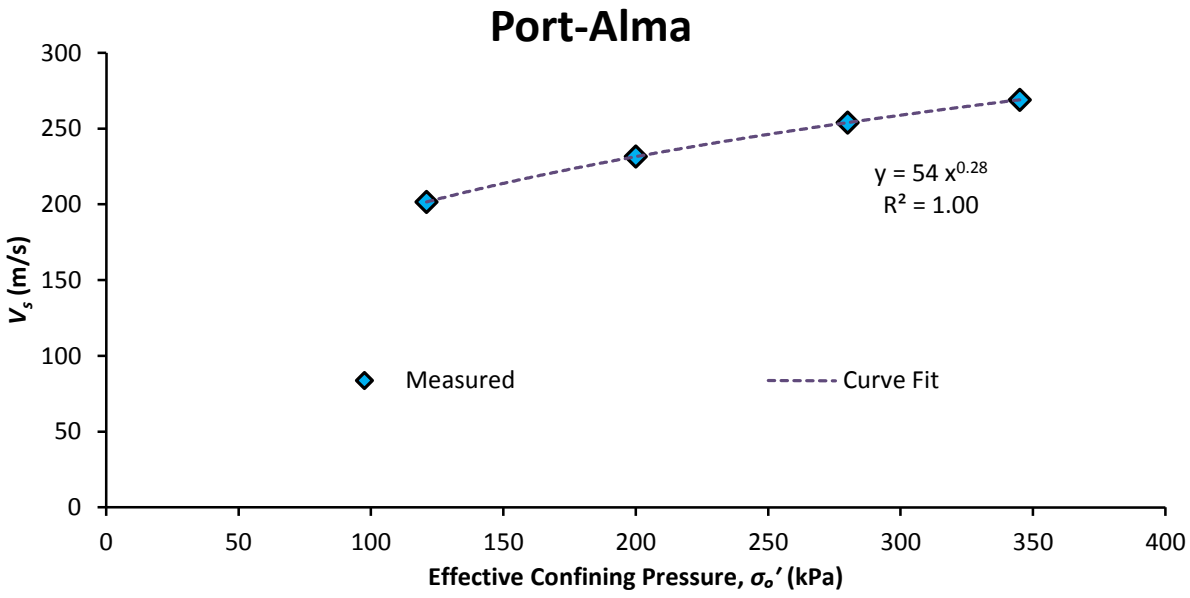

Figure 5-11. V_s versus effective confining pressure for Port-Alma soil

Table 5-2. Measured and predicted fitting parameters along with C_c

Soil Type	C_c Measured	α Measured	α Predicted	β Measured	β Predicted
Cayuga	0.16	41.65	43.44	0.295	0.303
Port-Alma	0.115	53.75	55.42	0.276	0.278

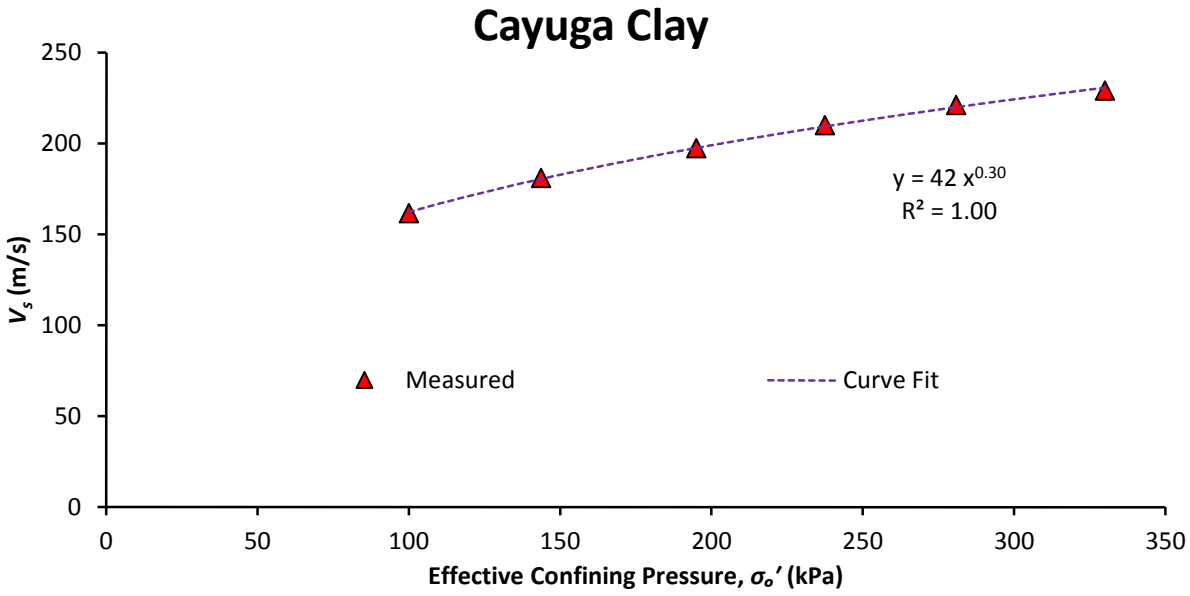

Figure 5-12. V_s versus applied effective confining pressure for Cayuga clay

5.7.3 Shear modulus reduction and damping ratio curves

The soil's secant shear modulus can be determined from the results of the cyclic triaxial test as the slope of the hysteretic loop (i.e. the curve representing the shear stress- shear strain over one complete cycle of loading). The area of the hysteretic loop is a manifestation of the energy dissipated through this load cycle, which indicates the material damping of the test soil. Fig.5-13 shows a typical hysteresis loop obtained during the present study. The slope of the straight line between the tips of the stress-strain curves gives the secant shear modulus (G_{sec} or simply G). The area of the hysteretic loop normalized by the elastic strain energy gives the damping ratio (Kramer, 1996), i.e.

$$\xi = \frac{1}{2\pi}\frac{A_{Loop}}{G_{sec}\,\gamma_c^2} \tag{5.14}$$

For each soil sample, values of G and ξ were determined at each applied cyclic strain increment in order to plot the shear modulus reduction and damping ratio curves. The area of hysteretic loop was calculated using MATLAB (2015).

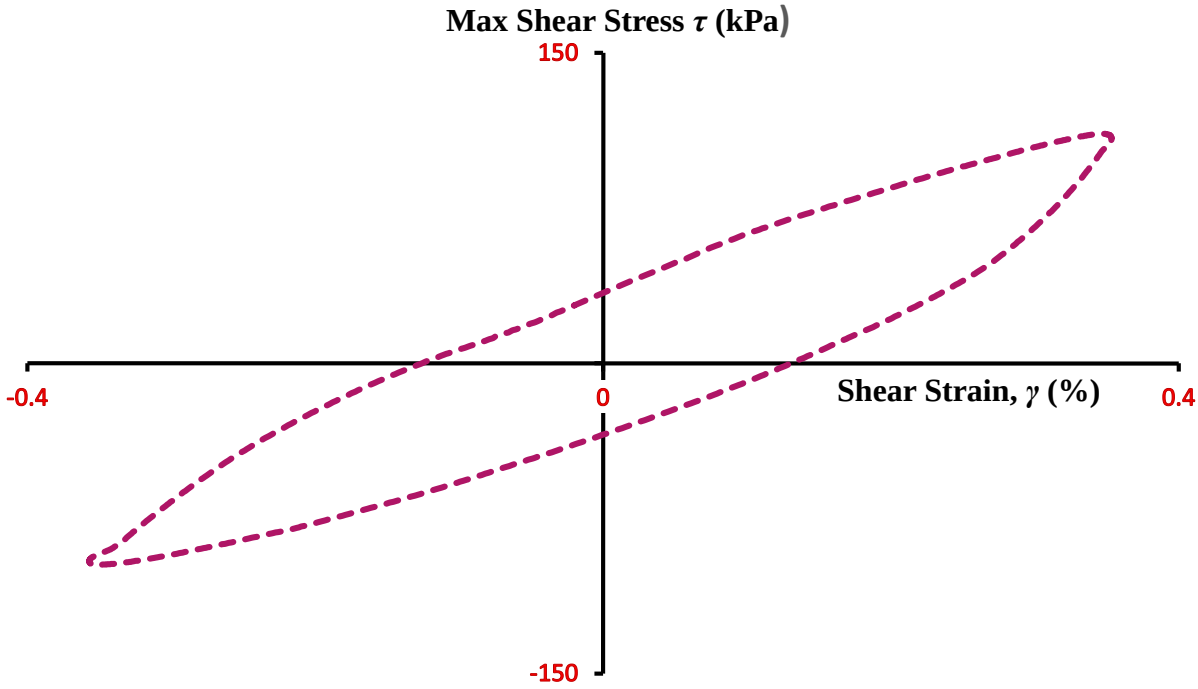

Figure 5-13. Typical Hysteresis loop (Cayuga clay)

All test specimens were saturated at an effective confining pressure of around 7-10 kPa. Applied cell pressure during the saturation phase was usually in excess of 200 kPa and both the cell and the back pressures were increased in a ramp manner to reach the target pressures. Saturation was ensured by measuring the Skempton's (1954) pore pressure parameter **B** to be at least 0.96.

To consolidate the specimen at a certain target confining pressure, the back pressure was kept constant and the cell pressure was increased in a ramp manner until it reached the target pressure. The shear wave velocity for each soil sample was measured using the PRA at several effective consolidation stress increments up to the final target effective confining pressure of ≈ 350 kPa. Knowing the shear wave velocity V_s and the bulk density (ρ) of the sample, G_{max} was determined using Eq.5.1. The average values of V_s, ρ and G_{max} for each tested soil at the final target effective confining pressure before the cyclic shearing was performed are summarized in Table.5-3.

Table 5-3. Measured V_s, ρ and G_{max} values for tested soil at confining pressure of 350 kPa

Soil	Average Effective Confining Pressure σ'_o (kPa)	Avg. V_s (m/s)	Avg. ρ (kg/m^3)	Avg. G_{max} (MPa)
Sombra		161.2	1811	47.3
Ottawa I		179.5	1810	58.3
Ottawa II		212.6	2027	91.6
K-S	350	261.2	2100	143.3
Cayuga		226.6	2160	110.9
Port-Alma		268.9	2375	171.7

In the final stage of the test, the cyclic shear strain was applied to the soil specimens under undrained conditions. The cyclic shear strain amplitude was varied between 0.08% and 3-5% and was applied in several increments. At each strain level, both G and ξ were measured as described above. The shear modulus reduction curve, defined as variation of G/G_{max} with cyclic shear strain level, is obtained. Also the damping ratio curve, defined as variation of damping ratio with applied cyclic shear strains was plotted.

Fig.5-14 shows the shear modulus reduction curves for the tested soils. All test soils, except the sensitive Ottawa clays, exhibited the same trend with regard to effect of PI on the shear modulus reduction curve. That is, for the same confining pressure, loading frequency, number of cycles and a given shear strain amplitude, as the plasticity index of the soil, PI, increases the ordinates of G/G_{max} increases (i.e. small reduction in shear modulus). Several researchers reported the same trend. For example, Zhang et al. (2005) reported the findings of several researchers to characterize the factors that affect G/G_{max} and D (damping) of soils. This includes the work of Zen et al. (1978);

Kokusho et al. (1982); Sun et al. (1988); Vucetic and Dobry (1991); Ishibashi and Zhang (1993); Vucetic et al. (1998). These studies demonstrated that the most important factors, which affect G/G_{max} include: Shear strain amplitude, γ, mean effective confining stress, σ'_m and soil type and plasticity index (PI). These researchers reported the same trend of increase in G/G_{max} with the increase in PI. Iwasaki et al. (1978) and Kokusho et al. (1982) concluded that the soils with low PI are more affected by σ'_m than the soils with high PI. On the other hand, Zhang et al. (2005) and Darendeli (2001) reported that other factors can affect G/G_{max}, but are less important, such as: loading frequency, number of loading cycles, OCR, *e*, degree of saturation, and grain characteristics.

Vucetic and Dobry (1991) reported that sensitive clays may have quite different shear modulus reduction curves independent of PI, which was observed in the results obtained in the current study. For example, PI of sensitive Ottawa clay I is closer to that of Sombra clay, which is not sensitive, but the reduction in the shear modulus of the Ottawa clay was much less in comparison with Sombra clay. Among the two sensitive clays tested during the present study they followed the PI rule i.e. the Ottawa clay I, with PI = 28%, exhibited higher G/G_{max} (or less reduction in shear modulus) in comparison with Ottawa clay II, which had PI = 14%.

It should be noted that ordinates of the shear modulus reduction curves at shear strain less than 0.1% are expected to be less accurate due to the limitation of the triaxial test device. This is demonstrated in Fig.5-14, where it shows lower slope of the curve compared with ordinates at higher shear strain levels. This is attributed to the compliance effect, i.e. the minimum strain that can be measured using a particular triaxial apparatus under given test conditions.

Fig.5-15 shows the damping ratio curves of the tested soils. Again, the curves of damping ratios for all soils, except for sensitive Ottawa clays, exhibited the same trend with regard to PI. That is, at a given cyclic shear strain amplitude, the soil with higher PI displayed lower damping ratio. Same behavior was observed for the sensitive Ottawa clays relative to each other, the damping ratio decreased as PI increased. However, at high strains (>3%), the damping ratio dropped significantly and the effect of PI on damping was reversed. For Ottawa clay I with PI = 28, the damping ratio was higher than that of Ottawa II, which had PI = 14.

The damping ratio values obtained in the current study, especially at small strains, are generally slightly lower than the values reported in the literature (e.g. Vucetic and Dobry, 1991), which may be attributed to the accuracy of the triaxial results at lower strain.

Fig.5-15 also shows that the damping ratio decreases significantly at shear strains higher than 2% for all tested clays. Ardoino et al. (2015) performed resonant column tests (involving small to moderate strains) and cyclic simple shear tests (involving high strains) on sandy and clayey soils and noted that for sandy soils, damping ratios rapidly decreasing for cyclic shear strain amplitudes higher than about 1%. This observation is consistent with the findings of Matasovic & Vucetic (1993) who concluded that at large strains sand tends to display a dilative behavior, the hysteresis loop is no longer elliptical and the so-called "S shaping" tendency of the stress-strain curve yields to rapid drop of hysteretic damping. Brennan et al. (2004) reported similar behavior of marked drop in hysteretic damping of saturated sands at high strains and attributed this to change in soil behavior as it approaches liquefaction.

El-Takch (2014) reported significant reduction of the damping ratio of silts as the strain level exceeded 1%. He attributed this behavior to development of a shear band and sliding of particles, hence reducing the energy dissipation. Similarly, Kim and Novak (1981) performed resonant column tests on seven different cohesive soils at very low to intermediate strain levels. Their results showed that the damping ratio of some of the tested soils decreased slightly at shear strains slightly higher than 0.2% (which is still low compared to strain levels considered in the current study). However, they did not discuss the reason for such behavior.

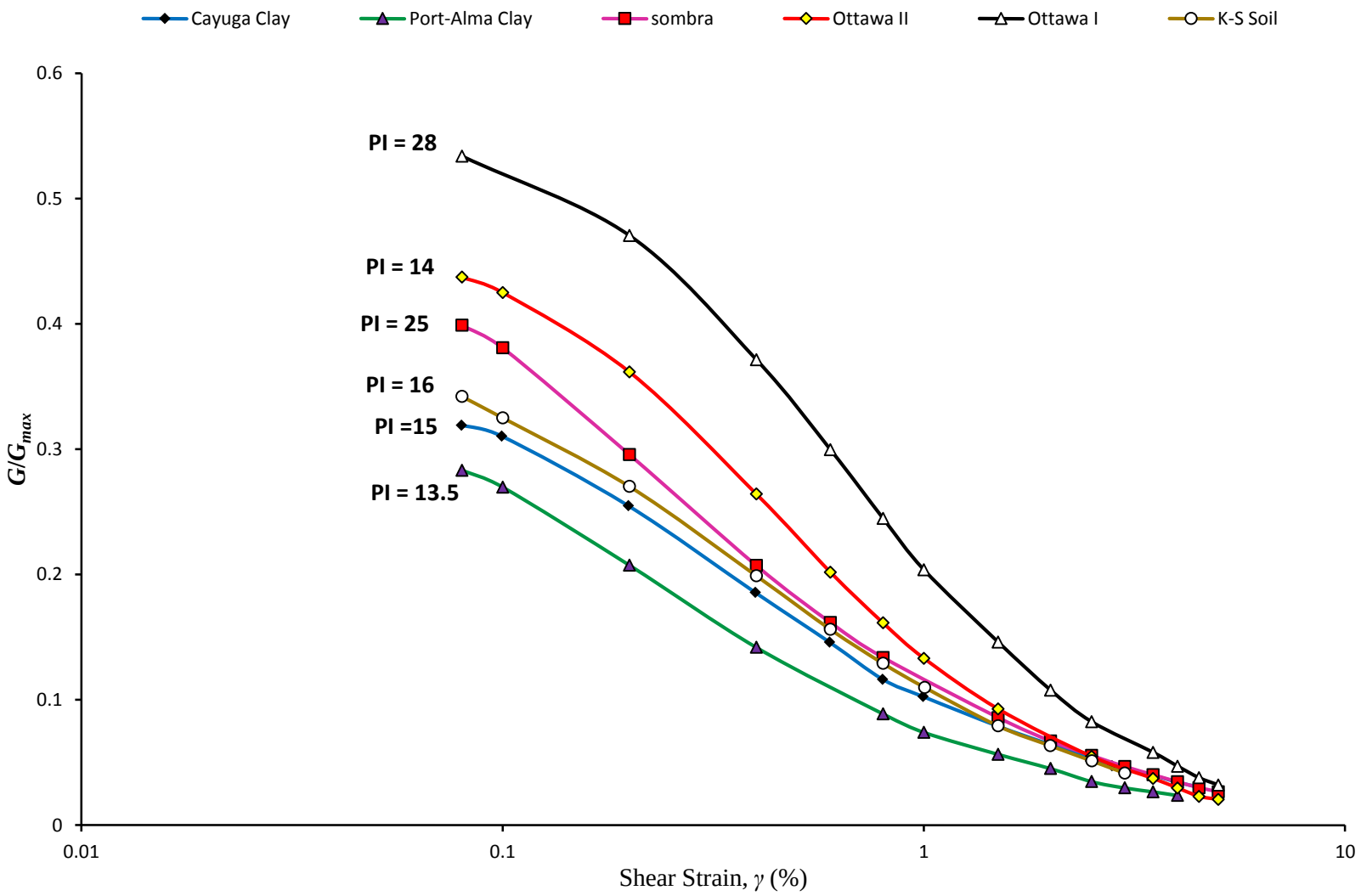

Figure 5-14. Modulus reduction curves for the tested soil

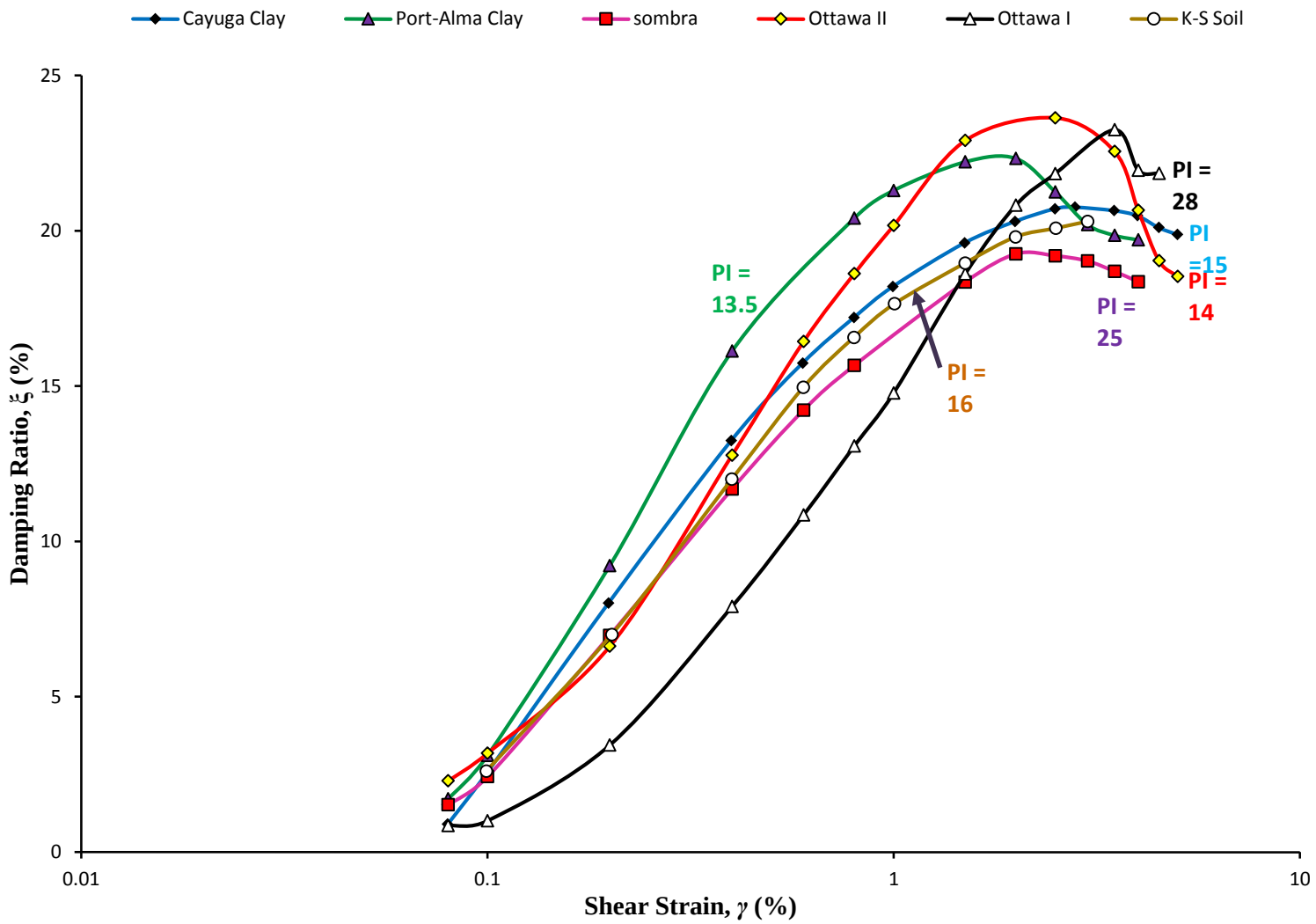

Figure 5-15. Damping ratio curves for the tested soils

5.7.4 Comparison of obtained modulus reduction curves with published results

Depending upon the availability of soil samples, two to three tests were performed on specimens of each soil type, and the results presented here are the average of the G/G_{max} values obtained from the different specimens. Fig.5-16 shows the comparison of the shear modulus reduction curves obtained in the present study with the predictions of Vardanega and Bolton (2011, 2013) given by Equations 5.2 to 5.8. At low strains, the predicted G/G_{max} values were found to be higher than the measured values. This discrepancy is attributed to the limitations of the triaxial device at low strains (compliance effect) as explained previously. As the strain level increased, the agreement between the measured and predicted G/G_{max} values improved significantly. For example, at intermediate to high strains (0.2-3%), the measured values are in excellent agreement with the predicted values, which verify the results from the current testing program. Even for the sensitive Ottawa clays, the percentage difference between the measured and predicted G/G_{max} at the intermediate to high strain levels is less than 5%. At high strains (≥3%) the predicted G/G_{max} values are slightly higher than the measured ones. It should be noted that Vardanega and Bolton (2011, 2013) reported the inability of Eqs. 5.2 to 5.4 to accurately estimate G/G_{max} at high strains. Some of these differences may be attributed to the fact that these equations, especially for γ_{ref}, were not highly correlated with the data set used for their developing (i.e. R^2 = 0.75), which may explain the observed differences. In addition, the frequency of the input sine wave was found to have some effect on the measured V_s and hence G_{max}. However, the measured and predicted reduction curves are, in general, agree well confirming the performance of the fabricated device.

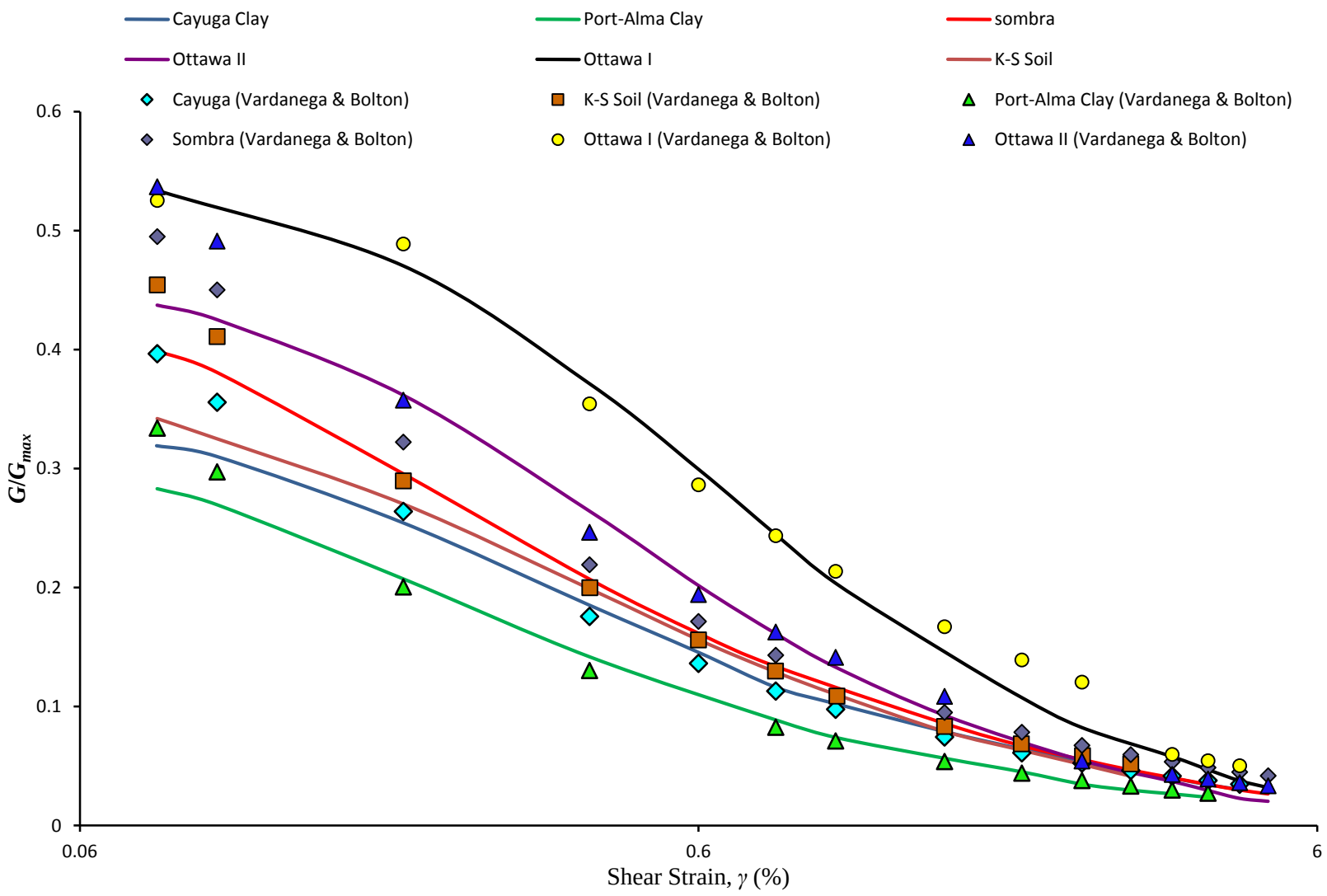

Figure 5-16. Comparison between the measured and the predicted reduction curves

It is important to note that Fig.5-16 compares the results from all tested soils, including the sensitive Ottawa clays. Similarly, the data used to develop Eqs.5.3 and 5.4 for γ_{ref} also included results from testing Leda clay; however, the points representing Leda clay do not fit well Eqs.5.3 and 5.4. Therefore, the modulus reduction curves do not agree as well as the other soils with the predictions of Eqs.5.3 and 5.4.

5.7.5 Empirical correlations between V_s, γ and G

As preliminary investigations, the shear wave velocity V_s was measured during the cyclic shearing at each strain amplitude employing several input sine wave frequencies. The measured V_s values are then correlated with the measured G, G_{max}, Vs_{max} and γ. The input sine wave frequency utilized for V_s measurements used in these correlations was 5 kHz.

All the terminologies used in these correlations are defined as follows:

Vs_{max} = the maximum shear wave velocity at zero cyclic shear strain amplitude (Vs_{max} is measured pre cyclic shearing using PRA). It was measured using the developed PRA setup after reaching the target confining pressure of 350 kPa.

Vs = the maximum shear wave velocity at a given applied cyclic shear strain amplitude (Vs is measured post cyclic shearing using PRA). The Vs is measured at each applied cyclic strain amplitude using the developed PRA setup, while the cyclic shear strains are applied using the cyclic triaxial apparatus.

G_{max} = the maximum shear modulus at zero applied cyclic shear strain amplitude. It was calculated using $G_{max} = \rho\ (Vs_{max})^2$. Where Vs_{max} is the measured velocity as discussed above.

G = the measured secant shear modulus at each applied cyclic shear strain amplitude. At a given applied shear strain amplitude, G is determined from the slope of hysteresis loop.

γ = the applied cyclic shear strain. It was applied using the cyclic triaxial apparatus during a strain controlled cyclic test.

Figures 5-17 to 5-20 present the relationship between V_s, Vs_{max}, γ, G and G_{max}, respectively. These relationships are produced by subdividing the tested soils into two main groups, i.e. sensitive and non-sensitive soils. These relationships have the potential to eliminate the need for conducting a cyclic test as the high strain soil stiffness can be obtained without actually performing the cyclic test.

First, V_s/Vs_{max} is correlated with shear strain, γ, as shown in in Figs. 5-17and 5-18, i.e.

$$V_s/V_{s_{max}} = Se^{J\gamma} \tag{5.15}$$

where: S and J are curve fitting parameters.

Fig.5-17 displays this correlation (i.e. Eq.5.15) for the tested sensitive clays, while Fig.5-18 presents the same correlation for the tested non-sensitive clays. The obtained curve fitting parameters from Figs. 5-17 and 5-18 are summarized in Table.5-4.

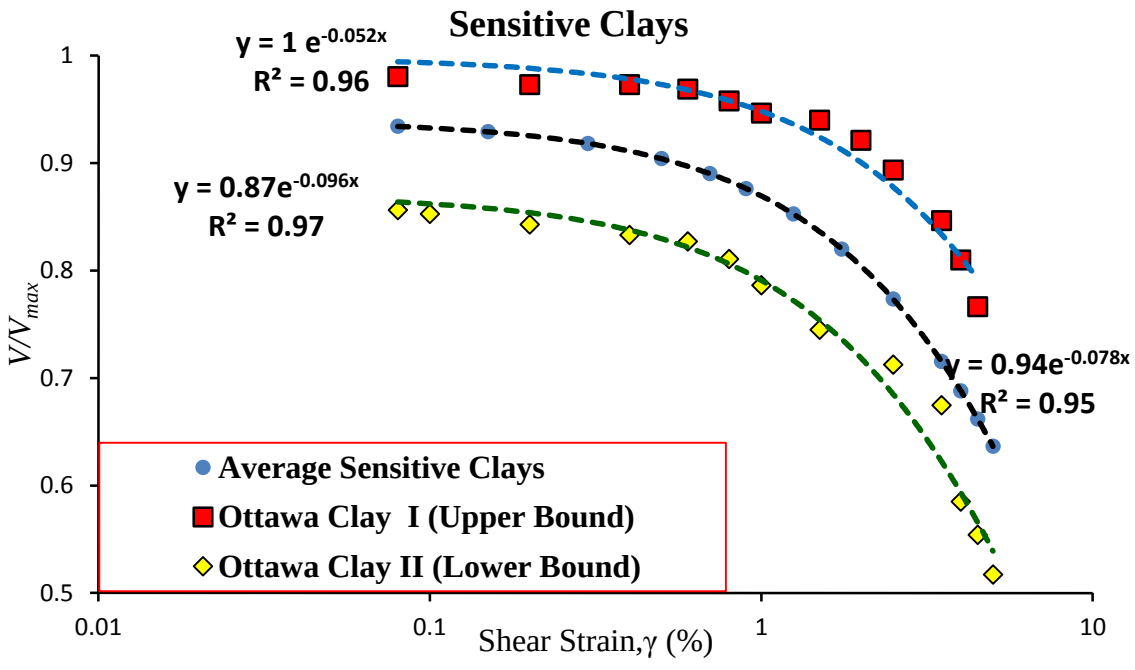

Figure 5-17. γ - $Vs/(V_s)_{max}$ relationships for tested sensitive soils

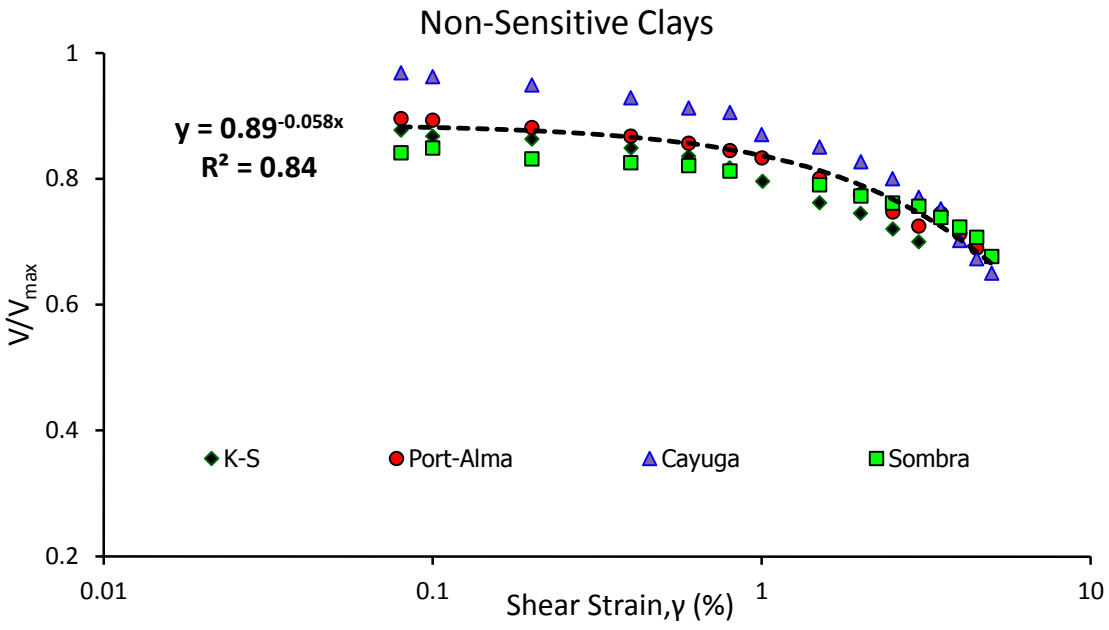

Figure 5-18. γ - $Vs/(V_s)_{max}$ relationship for the tested non-sensitive soils

It can be seen from Fig.5-17 that the response of the sensitive soils was different than that of non-sensitive clays. Similar observations were made by Vucetic and Dobry (1991). Ottawa clay I with medium PI (28) showed less degradation than Ottawa clay II, which has lower PI (14). Considering the available data, Ottawa clays represents a range of expected behavior where Ottawa I represents the upper bound of this range and Ottawa clay II represents its lower bound. The average of this range is presented in Fig.5-17, and is proposed to represent behavior of sensitive clays in Ontario. On the other hand, Fig.5-18 shows that the variation of V_s/Vs_{max} with strain, γ, is similar for all tested non-sensitive clays.

Table 5-4. γ-$Vs/(V_s)_{max}$ relationships for the tested soils

Soil Group	Soil Type	Correlation $V_s/(V_s)_{max} = S\, e^{J\gamma}$ S	J	R^2
SENSITIVE CLAYS	Upper Bound (Ottawa I)	1	-0.052	0.96
	Lower Bound (Ottawa II)	0.87	-0.096	0.97
	Average for Sensitive Clays	0.94	-0.078	0.95
NON-SENSITIVE SOILS		0.89	-0.058	0.84

Fig.5-19 and Fig.5-20 presents the relationship between V_s/Vs_{max} and G/G_{max} for sensitive and non-sensitive clays, respectively. As can be noted from Figs. 5-19 and 5-20, this relationship is almost a straight line. The data can be fitted with Eq.5.16 represents this dimensionless correlation i.e.

$$\frac{V_s}{V_{s_{max}}} = \mathrm{K}\left(\frac{G}{G_{max}}\right)^{\mathrm{L}} \tag{5.16}$$

where K and L are the curve fitting parameters. Table.4-5 summarizes the obtained curve fitting parameters for both the tested groups.

Since all the K values in Table.4-5 are close to unity, Eq.5.16 can be further simplified by forcing a K value equal to 1 and the corresponding new/updated values of exponent L are obtained and are summarized in Table.5-6.

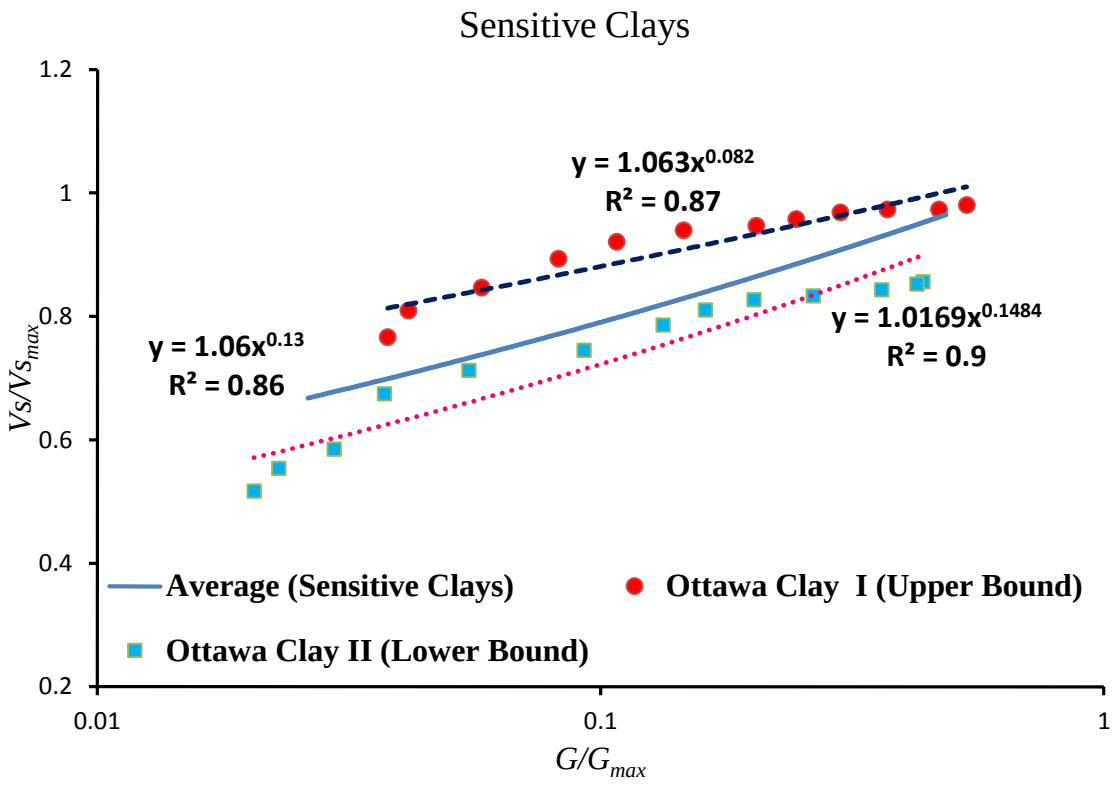

Figure 5-19. $Vs/(V_s)_{max}$ –G/G_{max} relationship for the tested sensitive soils

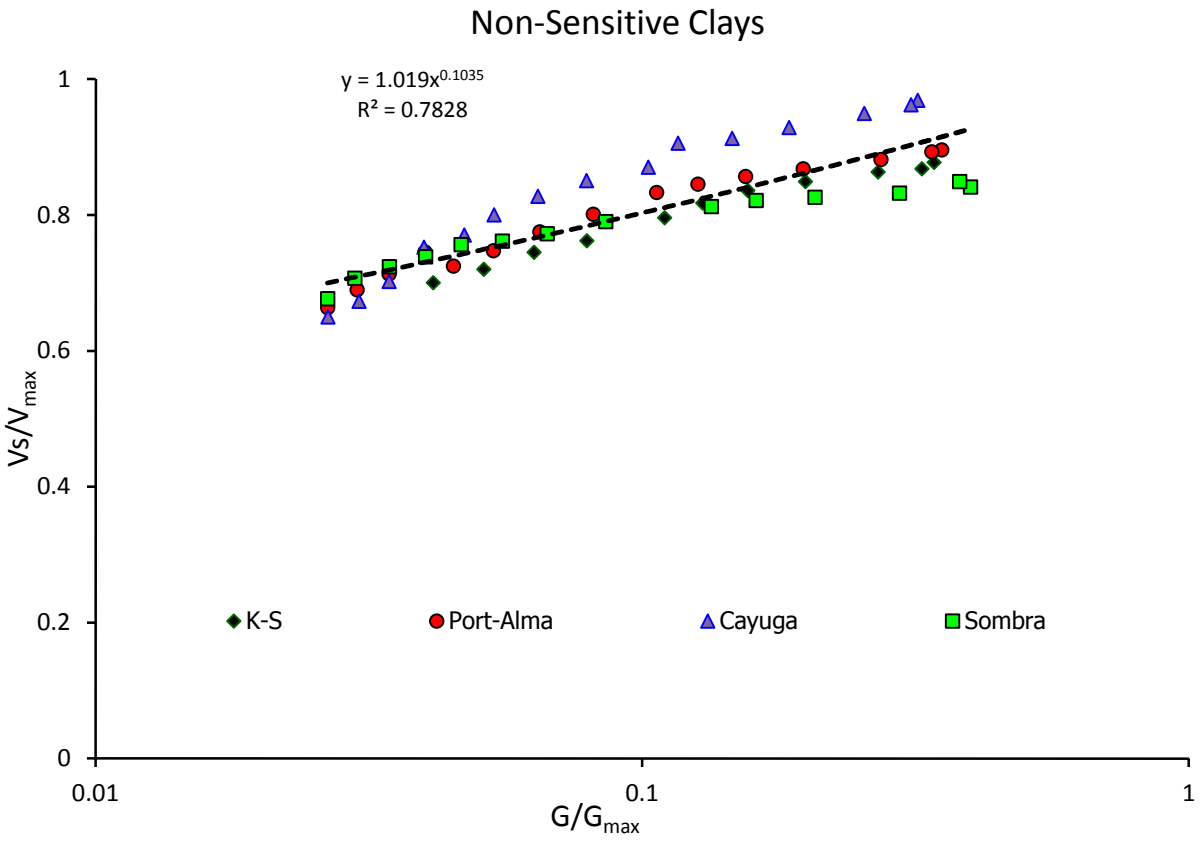

Figure 5-20. $Vs/(V_s)_{max}$ –G/G_{max} relationship for the tested non-sensitive soils

Fig.5-17 to Fig.5-20, Eq.5.15 and Eq.5.16, Tables 5-4 to 5-6 along with Eqs. 5.10-5.12 can be used to define the soil's shear wave velocity profile both under dynamic and static conditions, covering a range of shear strain from very low strains to very high as explained below.

Table 5-5. $Vs/(V_s)_{max} - G/G_{max}$ relationships for the tested soils

Soil Group	Soil Type	Correlation $V_s/(V_s)_{max} = K\,(G/G_{max})^L$		R^2
		K	**L**	
SENSITIVE CLAYS	Upper Bound (Ottawa I)	1.063	0.082	0.87
	Lower Bound (Ottawa II)	1.06	0.13	0.86
	Average for Sensitive Clays	1.017	0.1484	0.90
NON-SENSITIVE SOILS		1.019	0.1035	0.78

The compression index (C_c) of the soil can be determined experimentally from 1D consolidation (Oedometer) testing or from triaxial testing. It is well correlated with the index properties of soils, namely: the Atterberg limits (liquid limit I_L, plastic limit I_P, and plasticity index PI), initial void ratio (e_o), in-situ porosity (n_o), natural water content (W_N) and the specific gravity (G_s). Many studies have correlated C_c with these basic soil properties (e.g. Terzaghi and Peck, 1967; Azzous et al., 1976; Park and Koumoto, 2004; and Nagaraj and Murthy, 1986). The compression index can easily be determined analytically using empirical correlations established from the aforementioned studies for disturbed and undisturbed natural soils. Knowing the soil compression index (C_c), Eq. 5.10

and Eq.5.11 can be used to determine the curve fitting parameters α and $\boldsymbol{\beta}$ for a giving confining pressure, then Eq.5.9 can be used to predict V_s.

Table 5-6. $V_s/(V_s)_{max} - G/G_{max}$ relationships for the tested soils (Modified with K = 1)

Soil Group	Soil Type	Correlation $V_s/(V_s)_{max} = 1*(G/G_{max})^L$	
		K	**L**
SENSITIVE CLAYS	Upper Bound (Ottawa I)	**1**	**0.0533**
	Lower Bound (Ottawa II)	**1**	**0.1023**
	Average for Sensitive Clays	**1**	**0.1395**
NON-SENSITIVE SOILS		**1**	**0.0953**

The calculated V_s and the soil bulk density (ρ) can then be used in Eq.5.1 to calculate G_{max} at the specified confining pressure. This procedure can be repeated to calculate V_s and G_{max} at low strains and any applied confining pressure. The shear wave velocity of sensitive and non-sensitive clays for higher values of shear strain amplitudes may then be easily determined. Employing Eq.5.15 and Table. 5-4, the ratio V_s/V_{smax} can be obtained for a given strain amplitude, γ. Knowing the ratio V_s/V_{smax} for the given shear strain amplitude (γ), the corresponding G/G_{max} can be calculated from Eq.5.16 and Table.5-5.

The above procedure takes advantage of the empirical correlations developed in the current study to evaluate variation of *Vs* and *G* with strain level, employing the basic soil property, C_c. This may be appropriate for preliminary design and/or small jobs where accurate determination of soil nonlinearity is not critical. However, for final design and relatively important projects, the shear wave velocity can be measured at different levels of shear strain using the conventional triaxial test, eliminating the need for the more expensive and often not available, cyclic triaxial testing. This can be achieved by using the PRA device mounted on a triaxial cell and making V_s readings at different levels of shear strain. These readings can then be used along with Eq.5.16 and Table.5- 5 to determine the variation of G/G_{max} with the strain level. The measured Vs_{max} (at low strain), bulk density, ρ, and calculated G/G_{max} can be used to find the secant shear modulus *G*.

It should be noted that this study is exploratory investigation to obtain the dynamic nonlinear soil properties without actually conducting the cyclic loading (i.e. cyclic triaxial test). The proposed correlations can be applied within the range of the investigated soils or soils that have similar characteristics. On the other hand, it is important to expand this beneficial work in future to include testing a variety of soil types to increase the data points, which can be used to further enhance/refine the proposed correlations. In addition, the cyclic tests performed in the present study were carried out for a constant load frequency (1 Hz), maximum confining pressure (350 kPa). These parameters may alter the soil response. For example, Zhang et al. (2005) reported from Ishibashi and Zhang (1993) and Stokoe et al. (1999) that G/G_{max} shows less reduction with the applied γ as the mean effective pressure/confining pressure increases. Therefore, it is important to consider a wider range of confining pressure, and possibly different loading frequencies.

5.8 Conclusions.

Based on the obtained results, the conclusions can be drawn as follows:

1. The fabricated PRA triaxial device provided clear output signals with one major peak and high SNR, which confirms the high performance of the developed device.
2. The fabricated device performed well for all test conditions considered in this study, including: soil type, range of applied effective confining pressure, voltage, shape and frequency of the input signal.
3. The fitting parameters obtained from V_s measurements using the fabricated device matched well with those developed in Chapter 4, thus verifying consistent performance of the PRA setups developed for the oedometer and triaxial devices.
4. The shear modulus reduction curves G/G_{max} obtained in the current study are in good agreement with the findings of published shear modulus reduction curves for cohesive soils, further verifying the results and performance of the fabricated PRA setup.
5. An exploratory relationship between V_s, Vs_{max} and shear strain, γ, (Eq.5.15) is proposed to evaluate V_s at any strain level for both sensitive and non-sensitive soils. Furthermore, a correlation between V_s, Vs_{max} and G and G_{max} is proposed (Eq.5.16) for sensitive and non-sensitive soils. Eqs. 5.15 and 5.16 along with Eqs, 5.10-5.12 may be used to develop the shear modulus reduction curves from the measured shear wave velocity using the PRA device.

References

Airey, D., and Mohsin, A. K. M. (2013). "Evaluation of shear wave velocity from bender elements using cross-correlation". *ASTM Geotechnical Testing Journal*, 36 (4), 506-514.

Anderson, D. G., and Richart, F. E. (1976). "Effect of straining on shear modulus of clays." *Journal of Geotechnical Engineering Division*, 102(9), 975–987.

Ardoino, F., Bertalot, D., Piatti, C., & Zanoli, O. "Effect of pore pressure build-up on the seismic response of sandy deposits." Matasović, N., & Vucetic, M. (1993). "Cyclic characterization of liquefiable sands." *Journal of Geotechnical Engineering*. 119(11), 1805-1822

ASTM Standard D4318, 2010, "Standard Test Methods for Liquid Limit, Plastic Limit, and Plasticity Index of Soils," *ASTM International*, West Conshohocken, PA, www.astm.org.

Atkinson, J. H. and Sallfors, G. (1991). "Experimental determination of stress-strain-time characteristics in laboratory and in situ tests" *Proceedings of the 10th European Conference on Soil Mechanics and Foundation Engineering*, Florence, Italy, 915-956.

Azzous, A.S., Krizek, R.J., and Corotis, R.B. (1976), "Regression Analysis of Soil Compressibility", *Soils and Foundations*, 16(2), 19-29

Ben Romdhan, M., Hussien, M.N., Karray, M. (2015). "Correlation between elastic modulus and shear wave velocity at large strain level", *Conférence Canadienne de Géotechnique, Geoquebec* 2015.

Cha, M., Santamarina, J., Kim, H., and Cho, G. (2014). Technical Note. "Small-Strain Stiffness, Shear-Wave Velocity, and Soil Compressibility." *Journal of Geotechnical and Geoenvironmental Engineering.*, 140 (10), 06014011.

da Fonseca Ferreira, C. M., & da Fonseca, A. J. P. V. (2005). "International Parallel Tests on Bender Elements at the University of Porto, Portugal."

Darendeli, M. B. (2001). "Development of a new family of normalized modulus reduction and material damping curves." Ph.D. thesis, Univ. of Texas at Austin, Austin, TX.

Dirgėlienė, N.; Amšiejus, J.; Stragys, V. 2007a. Effect of Ends Restraint on Soil Shear Strength Parameters during Triaxial Testing, in *Polish-Ukrainian-Lithuanian Transactions of Theoretical Foundations of Civil Engineering*. Warsaw, Poland, 2007. Warszawa: Wydawnictwo Politechniki Warszawskiej, 151–156

Doroudian, M., and Vucetic, M. (1999). "Results of geotechnical laboratory tests on soil samples from the UC Santa Barbara campus." *UCLA Research Rep. No. ENG-99-203*, Civil and Environmental Engineering Dept., Univ. of California, Los Angeles

d'Onofrio, A., Silvestri, F., and Vinale, F. (1999). "Strain-rate dependent behaviour of a natural stiff clay." *Soils and Foundations*. 39(2), 69–82

El Takch, Ali, (2013). "Cyclic and Post-Cyclic Response of Silt and Sandy Silt Soils" MESc Thesis. Western University, London, ON, Canada

Georgiannou, V. N., Rampello, S., and Silvestri, F. (1991). "Static and dynamic measurements of undrained stiffness on natural overconsolidated clays." *Proc., 10th European Conf. on Soil Mechanics and Foundation Engineering*, A. A. Balkema, Rotterdam, Netherlands, 91–95

Ishibashi, I., and Zhang, X. J. (1993). "Unified dynamic shear moduli and damping ratios of sand and clay." *Soils and Foundations*, 33(1), 182–191

Ismail, M.A., and Rammah K.I. (2005). "Shear-plate Transducers as a Possible Alternative to Bender Elements for Measuring Gmax." *Géotechnique* 55 (5), 403–407.

Iwasaki, T., Tatsuoka, F., and Takagi, Y. (1978). "Shear moduli of sands under cyclic torsional shear loading." *Soils and Foundations*, 18 (1), 39–56.

Jacobsen, M. (1968). “The undrained shear strength of preconsolidated boulder clay.”

Karray, M.,Ben Romdhan, M., Hussien M. N., Éthier Y. (2015), Measuring shear wave velocity of granular material using the Piezoelectric Ring Actuator Technique (P-RAT), *Canadian Geotechnical Journal*. 52: 1–16.

Kim, T. C., and Novak, M. (1981). “Dynamic properties of some cohesive soils of Ontario”. *Canadian Geotechnical Journal*, 18(3), 371-389.

Kokusho, T., Yoshida, Y., and Esashi, Y. (1982). “Dynamic properties of soft clay for wide strain range.” *Soils and Foundations*. 22(4), 1–18.

Kramer, S. L. (1996). “Geotechnical Earthquake Engineering” (Vol. 80). Upper Saddle River, NJ: Prentice Hall.

Lee, J-S., and Santamarina, J.C. (2005). “Bender Elements: Performance and Signal Interpretation.” *Journal of Geotechnical and Geoenvironmental Engineering* 131 (9), 1063–1070.

Leong, E. C., Cahyadi, J., and Rahardjo, H. (2009). “Measuring Shear and Compression Wave Velocities of Soil Using Bender–extender Elements.” *Canadian Geotechnical Journal* 46 (7), 792–812.

Lo Presti, D. C. F., Jamiolkowski, M., Pallara, O., Cavallaro, A., and Pedroni, S. (1997). “Shear modulus and damping of soils.” *Geotechnique*, 47(3), 603–617.

Mair, R. J. (1993), “Developments in Geotechnical Engineering Research: Application to Tunnels and Deep Excavations,” Unwin Memorial Lecture 1992, *Proceedings of the Institution of Civil Engineers-Civil Engineering*, 97(1), 27-41.

MATLAB by Mathworks [Computer software]. (2015). Retrieved from http://www.mathworks.com/products/matlab/ <Accessed on August 14th, 2015>

Nagaraj, T. S., & Murthy, B. S. (1986). “A critical reappraisal of compression index equations.” Géotechnique, 36(1), 27-32.

Park, J. and Koumoto, T. (2004). "New Compression Index Equation." Journal of Geotechnical and Geoenvironmental Engineering, 130:2(223), 223-226

Rampello, S., and Silvestri, F. (1993). “The stress-strain behaviour of natural and reconstituted samples of two overconsolidated clays.” Geotechnical engineering of hard soils-soft rocks, A. Anagnostopoulos et al., eds., Balkema, Rotterdam, Netherlands, 769–778

Rees, S. (2015a). What is Triaxial Testing? Part 1 of 3. GDS Advanced Triaxial Testing. 1–4. www.gdsinstruments.com. <Accessed on September 30th, 2015>

Rees, S. (2015b). What is Triaxial Testing? Part 2 of 3. GDS Advanced Triaxial Testing. 1–5. www.gdsinstruments.com. <Accessed on September 30th, 2015>

Rees, S. (2015c). What is Triaxial Testing? Part 3 of 3. GDS Advanced Triaxial Testing. 1–5. www.gdsinstruments.com. <Accessed on September 30th, 2015>

Sawangsuriya, A. (2012). Wave Propagation Methods for Determining Stiffness of Geomaterials. INTECH Open Access Publisher.

Schanz, T., & Gussman, P. (1994). “The influence of geometry and end restraint on the strength in triaxial compression in numerical simulation.” Proc. of the 3rd Eur. Conference on Numerical Methods in Geotechnical Engineering, 129-133.

Shibuya, S., and Mitachi, T. (1994). “Small strain modulus of clay sedimentation in a state of normal consolidation.” *Soils and Foundations*, 34(4), 67–77

Skempton, A. W. (1954). “The pore pressure coefficients A and B.” *Geotechnique*, 4, 143–147

Stokoe, K. H., II, Darendeli, M. B., Andrus, R. D., and Brown, L. T. (1999). "Dynamic soil properties: Laboratory, field and correlation studies." *Proc., 2nd Int. Conf. on Earthquake Geotechnical Engineering*, Vol. 3, Lisbon, Portugal, 811–845

Sun, J. I., Goleskorkhi, R., and Seed, H. B. (1988). "Dynamic moduli and damping ratios for cohesive soils." *Rep. No. UCB/EERC-88/15*, Univ. of California at Berkeley, Berkeley, Calif

Teachavorasinskun, S., Thongchim, P., and Lukkunaprasit, P. (2002). "Shear modulus and damping of soft Bangkok clays." *Canadian Geotechnical Journal*, 39(5), 1201–1208

Terzaghi, K. and Peck, R.B. (1967), "Soil Mechanics in Engineering Practice", John Wiley & Sons Inc. New York.

Wichtmann, T., Andersen, K. H., Sjursen, M. A., & Berre, T. (2013). "Cyclic tests on high-quality undisturbed block samples of soft marine Norwegian clay." *Canadian Geotechnical Journal*, 50(4), 400-412.

Viggiani, G and Atkinson, JH (1995). Interpretation of bender element tests. *Géotechnique*: 45: 1: 149–154.

Vardanega, P. J., & Bolton, M. D. (2011). "Practical methods to estimate the non-linear shear stiffness of fine grained soils". In *Deformation Characteristics of Geomaterials: Proceedings of the Fifth International Symposium on Deformation Characteristics of Geomaterials, I*S-Seoul 2011, 1-3 September 2011, Seoul, Korea (p. 372). IOS Press.

Vardanega, P. J., & Bolton, M. D. (2013). "Stiffness of clays and silts: Normalizing shear modulus and shear strain". *Journal of Geotechnical and Geoenvironmental Engineering*. 139 (9), 1575-1589.

Vucetic, M., and Dobry, R. (1991). "Effect of soil plasticity on cyclic response." *Journal of Geotechnical and Geoenvironmental Engineering*. 117(1), 89–107.

Vucetic, M., Lanzo, G., and Doroudian, M. (1998). "Damping at small strains in cyclic simple shear test." *Journal of Geotechnical and Geoenvironmental Engineering*, 124(7), 585–594

Vucetic, M. and Tabata, K., (2003). "Influence of soil type on the effect of strain rate on small-strain cyclic shear modulus." *Soils and Foundations*. 43(5), 161-173.

Zen, K., Umehara, Y., and Hamada, K. (1978). "Laboratory tests and in situ seismic survey on vibratory shear modulus of clayey soils with various plasticities." *Proc., 5th Japanese Earthquake Engineering Symp*osium, Japan, 721–728

Zhang, J., Andrus, R. D., and Juang, C. H. (2005). "Normalized shear modulus and material damping ratio relationships." J. *Geotech. Geoenviron. Eng*., 131(4), 453–464.

Chapter 6

6 Conclusions and Recommendations

6.1 General

A fair amount of experience and knowledge on measurement of shear wave velocity as well as other soil properties was gained throughout this study. The literature review provided necessary and relevant information on different laboratory techniques employed for measuring soil shear wave velocity and interpretation methods for shear wave travel time in test specimens. In addition, procurement, fabrication, testing and refinement of the PRA devices and their incorporation in oedometer and triaxial apparatus provided valuable engineering design experience. Finally, the extensive experimental testing program on different cohesionless and cohesive soils under variety of testing conditions and apparatuses provided broad understanding of the factors that affect the soil dynamic properties.

This chapter summarizes the key outputs and conclusions reached during this study. It also presents a number of recommendations based on the experience gained during this study. Finally, it provides a few of the many potential uses of the developed PRA setup/technique.

6.2 Conclusions

The key conclusions of the current study are summarized below.

1. The fabricated PRA setup was incorporated in the top cap and base pedestal of both oedometer and triaxial devices. This technique allows performing these conventional tests (1D consolidation and triaxial testing) along with the simultaneous measurements of V_s of the tested soils. The design of the PRA devices ensured the regular test operation such as consolidation (drainage) and back-water saturation.
2. The piezoelectric elements of the fabricated device do not penetrate the test specimen, hence reducing the sample disturbance compared to Bender element

tests. In addition, this allows using the PRA at higher levels of shear strain as the piezoelectric element would not be damaged.

3. The device was successfully used to measure the shear wave velocity for a variety of tested soils including sands, silts, and clays, and varying consistency from dense and hard soils to loose and soft soils.
4. This device is quite slim as compared to other devices e.g. shear-plate transducers, and transfers the kinetic energy to the soil specimen by friction. Unlike BE and shear-plate transducers, it conveys high energy to the soil over a large area. The PRA device performs in in-plane radial shearing mode of excitation with large excitation and reception areas, which makes it a superior V_s measuring technique.
5. Unlike BE, the PRA device shears the entire soil base (soil as a mass), resulting in a clear output signal with a single major peak and high SNR. These strong and clear output signals are a result of good coupling and contact (adhesion/friction) between the soil and the PRA. The fabricated device performed well for all testing conditions considered in this study, including: soil type, range of applied effective vertical and confining pressures, input voltage, shape and frequency of the input signal.
6. The fabricated PRA technique overcame many reported issues related to soil testing using the existing pulse devices, including, reflection/refraction of the signals at specimen boundaries (ends and sides), overall sample disturbance, weak shear coupling between soil and testing device as well as fixation problems. Unlike other pulse devices the output signals from the fabricated PRA were clear and strong and did not need any signal stacking, amplification or conditioning.
7. The strains applied by the ring actuators are small to ensure the soil behaves as a linear elastic material during V_s measurement to capture the true very low stiffness. When, used to measure V_s at higher strain, the applied shear strain is due to the applied loading, not induced through the PRA device.
8. The performance and output of the developed PRA setups was validated by comparing the obtained results with the published literature, and good match was observed for all tested soils.

9. Performance evaluation was further authenticated by performing bender element testing. The results presented in Chapter 4 and Chapter 5 confirm the device reliability with the repeatability of the results and robustness of the presented empirical correlations.
10. The developed technique is fairly simple, robust and very flexible. A variety of input signal shapes from basic shapes (sine, square or ramp pulse) to sophisticated and user defined signals can be applied. It is capable of measuring V_s over a wide range of applied pressure (low to very high stress) using relatively low input voltages.
11. Relatively wide range of input frequencies could be utilized when measuring the shear wave velocity. The optimal frequency of excitation depends on many factors including the rigidity and dimensions (especially height) of the tested materials, soil type (sand vs. clay), and type of piezoceramic transducers and applied stress/confining pressure. Therefore, many input frequencies should be tried beginning at low frequencies. It was observed that the input frequency that gives $L/\lambda = t_s * f$ between 2 and 4 generally yields good output signals with reliable V_s values. Low to medium input frequencies were found to yield clear output signals (high amplitude and high SNR). Very high frequencies yielded low amplitude outputs signals and/or signal distortions. The range of reasonable input frequencies depends upon the sample height and typically ranged between 3-40 kHz. Bigger height samples can be tested with lower input frequencies. The PRA performed well over a wide range of input frequencies.
12. The cross-correlation technique (time domain analysis) for travel time interpretation was found to underestimate the measured shear wave velocity. It was found that using the direct arrival method the shear wave arrival time is close to the first zero crossing before the most significant peak. The frequency domain analysis (group velocity method) resulted in the same conclusion as direct arrival method.
13. The base shear excitation (i.e. mode of operation of the PRA setup) is expected to reduce/eliminate the side and end reflections and hence direct arrival method can be used with the fabricated device by using low to medium input frequencies.

However, small amplitude waves can be observed in the output signals before the shear wave arrival. This may be the P-wave arrival, even though the base excitation is purely shear. This may be attributed to the Poisson's effect/ratio. The radial expansion and contraction results in the longitudinal contraction and expansion of the piezoelectric actuator setup that can produce a P-wave. However this P-wave amplitude is very small as compared to the shear wave. It can be further minimized using excitation with medium frequency and hence they can be easily segregated.

14. The overall shape of the output signal depends on many factors, including: the physical dimensions, properties and consistency of the tested soil specimens; the used input frequency, the amplitude of the input voltage; and geometric, rigidity, physical and mechanical properties of the piezoelectric ring actuators. Though not checked in details during this study, the shape of the used input signal may also considerably affect the characteristics of the output signal.
15. "Cross-talk" can be significantly reduced/eliminated by using proper grounding and shielding. The magnitude (amplitude) of the cross-talk on the output signal depends upon the soil type and is usually more on wet clays as compared to the dry sands. Cross-talk in general may not affect the shear wave measurement unless testing the soils of very small height, and/or using very low input frequencies, and/or testing very dense and stiff soils. In all such cases, the shear wave arrival time can be less than the period of the input wave and hence the cross-talk can affect the measurements.
16. For clean Ottawa sand, at constant e, V_s increases by increasing σ_m' with a stress exponent, β, of 0.25-0.26.
17. For a given e, and σ_m', V_s of the clean Ottawa sand was found to be independent of mean particle size (D_{50}).
18. For the tested Ottawa sand, G_{max} decreased significantly (by almost 25-40%) due to adding a small percentage (10-15%) of non-plastic fines.
19. The dynamic Poisson's ratio for clean Ottawa sand as preliminary investigations was evaluated and an average value of 0.29 was found.

20. The proposed correlations in Chapter 4, can be used to predict the V_s using the readily measured soil parameter, C_c without direct measurement for V_s. The obtained correlations were examined with the available data in literature and strong matching was observed. Inverse correlations are suggested for the fitting parameters α and β for both the mean and vertical effective stress concepts.
21. Soil specific empirical correlations are proposed to be used for the estimation of G_{max} from measured S_u for cohesive soils. In general, the low strain shear modulus, G_{max} was found to vary from 400 to 1400 times the soil's undrained shear strength, S_u.
22. The ratio $G_{dynamic}/G_{static}$ i.e. the ratio of the stiffness from the V_s measurement to the one obtained from static triaxial test, was found to be in between 5 and 13 for the tested cohesive soil specimens and this ratio was found to decrease with increasing confining pressure.
23. As a preliminary estimate, the average dynamic Poisson's ratio for the tested cohesive soils was found to be around 0.42.
24. Based on the conducted small and large strain measurements, the stiffness ratios E_{dyn}/E_{oed}, $E_{dynamic}/E_{static}$, E_{stat}/E_{oed} were found to be around 40, 8 and 5, respectively (Chapter 4)
25. The fitting parameters obtained from V_s measurements using the fabricated triaxial device (Chapter 5) matched very well with those developed for oedometer setup (Chapter 4), thus verifying the efficiency and performance of the PRA setups developed for both the oedometer and triaxial devices and also validated the presented empirical correlations.
26. The shear modulus reduction curves G/G_{max} obtained in the current study with the fabricated triaxial device are in good agreement with the published literature, further verifying the results and performance of the fabricated PRA setup.
27. Dimensionless empirical relationship between V_s, Vs_{max} and shear strain, γ, is proposed to evaluate V_s at any strain level for both sensitive and non-sensitive soils. Furthermore, another dimensionless correlation between V_s, Vs_{max} and G and G_{max}

is proposed for sensitive and non-sensitive soils. These correlations can be used to develop the shear modulus reduction curves from the measured shear wave velocity.

6.3 Recommendations and Suggested Improvements for Future Development of PRA Device

1. Centering the piezoceramic rings along with their inner stones both in the horizontal and vertical directions is crucial to achieve the desired performance. As discussed in Chapter 3 and Chapter 5, a Delrin mold was used for this purpose and also to serve few other purposes. However, during the initial trials of device fabrication, a metallic (Brass/Bronze) mold was used instead of the later used Delrin mold. It was thought that using such mold should completely shield the piezo actuator elements from the electromagnetic coupling and should act as a better Faraday's cage to completely eliminate the cross-talk. It was found that it actually served the purpose of eliminating the cross-talk; however, using metallic mold caused some other issues. It resulted in an output voltage signal with multiple major peaks of the same amplitude. This may be attributed to resonance or short circuit. It was, therefore, decided to use Delrin mold instead of the metallic mold. Nevertheless, it can be reconsidered for future investigations as an improvement to the fabricated device to replace the plastic/Delrin mold and the copper lamina, which was employed to provide the shielding to avoid cross-talk.
2. Further refinements can be applied to the used cables/wires, mold material and material and roughness of the metallic porous stones. The contact between the sample and the setup should be as rough as possible. This can be achieved by using very rough/coarse porous stones along with gluing coarser angular sand to the mould housing the piezo setup. The final finished product should be uniform, and the final finished surface of the emitter and receiver piezoelectric elements should be as even as possible.
3. Depending upon the desired size (especially diameter) of the test specimens, the dimensions of the piezoelectric elements can be optimized. Larger piezoelectric elements dimensions are generally preferred. In addition, low-noise and high performance cables should be used to have clearer output signals. The length of

these cables should not be too long as it may cause a loss of amplitude in the output signal and can also create unwanted noise on output signals.

4. The posterior side of the piezoceramic ring actuator unit should be even and smooth for better performance. Grounding the entire piezoelectric setup along with all other connected metallic parts/devices/apparatus is very important for eradicating electromagnetic interactions (Cross-talk) in the output signals. Centering of the piezo rings with the metallic porous stones in both directions (especially in the horizontal direction) is essential to optimize the performance of the PRA setup.
5. The snapshot of the tailored LabVIEW program used for capturing input and output signals is given below in Fig.6-1. The sampling rate and number of points as shown in the figure should be kept high to improve the resolution. A clear shear wave can be seen between 250 and 500 μ-sec, but the time axis is extended up to 1683.3 μ-sec. It is necessary to keep the time axis broad enough to have a better understanding of the characteristics of the output signal. E.g. if a second arrival exists in the output signal, it will only be visible if the time axis is broad enough and beyond the mean event (main shear wave arrival).

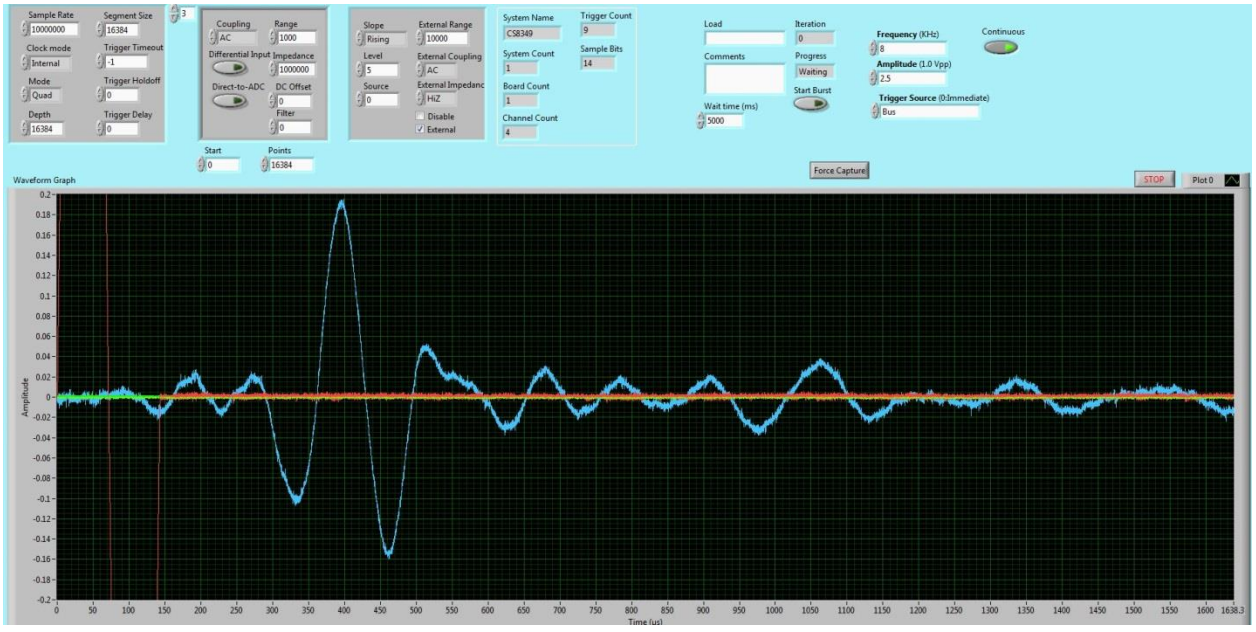

Figure 6-1. Snapshot of the used LabVIEW program during the present study

6. As shown in the Fig.6-1, it is important to select the right impedance for the selected channel. The input sine wave to emitter is the output of a function generator. The impedance of output from function generator is 50 Ω while the output signal from receiver piezo has an impedance of 1MΩ. It is therefore, important to select the right impedance for each used channel to view both signals without causing any electrical damage to the data acquisition system.
7. The voltage range shown in Fig. 6-1 was also found to affect the clarity of output signals. Voltage range for each channel should be kept as low as possible but ensuring that it is slightly more than the expected voltage amplitudes of both the input and output signals.
8. The input and output signals can be captured in the two extreme channels of the data acquisition system. Doing so may reduce the amplitude of the cross-talk on the output captured signals.

6.4 Future Research

The significance of shear wave velocity in geotechnical applications is discussed in details in Chapter 1. Therefore, the developed PRA device can be applied on a broader scale for numerous geotechnical investigations. A few suggested applications are given below.

1. Effect of sample dimension (especially diameter), and the effect of height-to-diameter ratio (H/D) on measured shear wave velocity should be investigated.
2. The developed PRA device can be used to accurately measure V_s of very stiff cemented soil specimens.
3. Using the PRA setup, the shear wave velocity of different soils can be measured during both loading and unloading and hence some new correlations can be suggested from such study incorporating the effect of stress history (OCR).
4. A number of empirical correlations have been suggested in the present study utilizing the fabricated device on a variety of soils**.** These correlations can be further refined by adding more data points. Natural and reconstituted, normally and overconsolidated, dense and loose, stiff and soft soils can be tested and the new data

can be combined with the existing results to refine and polish the suggested correlations.

5. The fabricated PRA setup can be incorporated in other devices to yield some new and practical correlations by correlating the results and parameters from these devices with the shear wave velocity measurements through the fabricated setup. E.g. PRA setup has a potential to be installed in the large CPT triaxial cell (190 mm tall) developed at Western University. If successfully installed, this study can yield very practical outcomes utilizing the results of CPT and V_s data. The PRA setup may also be installed in other devices e.g. the direct shear apparatus.
6. The fabricated technique has the potential to study soil's anisotropy. This can be achieved by measuring the horizontal shear wave velocity (speed of the horizontally propagating vertically polarized waves) along with conventionally measured velocity (speed of vertically propagating horizontally polarized waves).
7. As discussed earlier, the amplitude of the output signal was found to change significantly with changing the frequency. Increasing the frequency, decreased the output amplitude. This may be attributed partly to transfer function (response of piezo sensors to a certain frequency) and partly due to damping ratio of soils and its highly dispersive nature. High frequency or low period waves easily get damped as compared to low frequency waves. Thus, an interesting study can be made utilizing the PRA's to estimate the damping ratio of the tested soils.

Curriculum Vitae

Name: **Saeed Ahmad**

Post-secondary Education and Degrees:

University of Engineering and Technology, Peshawar
Peshawar, Khyber Pakhtunkhwa, Pakistan
2000-2005 Bachelors in Civil Engineering

University of Engineering and Technology, Peshawar
Peshawar, Khyber Pakhtunkhwa Pakistan
2005-2008 Master in Civil Engineering

Honours and Awards:

Recipient of the prestigious **Milos Novak Memorial Award**
Geotechnical Research Centre (GRC) Awards
The University of Western Ontario, 2013

Position Holder Award (2004)
Department of Civil Engineering
University of Engineering and Technology, Peshawar, Pakistan

Best Teacher Award (2007)
Department of Civil Engineering
University of Engineering and Technology, Peshawar, Pakistan

Related Work Experience

Lecturer (2005-2008)
Department of Civil Engineering
University of Engineering and Technology, Peshawar
Khyber Pakhtunkhwa, Pakistan

Research Assistant (2009-2015) and Teaching Assistant (2009-2013)
Department of Civil and Environmental Engineering
The University of Western Ontario
London, Ontario, Canada

Publications:

Ahmad. S., Alnuaim. A., El Naggar., M (2015). "Dynamic Shear Modulus of Kaolin-Silt Clay Using a Novel Technique" *The Six International Symposium on Deformation Characteristics of Geomaterials, At Buenos Aires, Argentina*, Volume: 6. DOI: 10.3233/978-1-61499-601-9-331